

**The role of tetraspanins in the regulation  
of the A Disintegrin And Metalloprotease 10  
(ADAM10)**

Dissertation

In fulfilment of the requirement for the degree “Dr. rer. nat.”  
of the Faculty of Mathematics and Natural Sciences  
at the Christian-Albrechts University of Kiel

submitted by  
Lisa Seipold

Kiel, February 2017



Referee: Prof. Dr. Paul Saftig

Co-Referee: Prof. Dr. Eric Beitz

Date of oral presentation: 21.04.2017

Approved for publication: 21.04.2017

Prof. Dr. Natascha Oppelt  
(The dean)



# Table of Contents

<b>List of Abbreviations .....</b>	<b>V</b>
<b>Summary .....</b>	<b>IX</b>
<b>Zusammenfassung .....</b>	<b>XI</b>
<b>1 Introduction .....</b>	<b>1</b>
1.1 Proteases.....	1
1.1.1 Zinc-dependent metalloproteases .....	1
1.1.2 A Disintegrin and Metalloproteases (ADAMs) .....	2
1.1.3 A Disintegrin and Metalloprotease 10 (ADAM10) .....	4
1.1.4 ADAM10 substrates in the central nervous system.....	6
1.2 Alzheimer's Disease .....	10
1.2.1 Processing of the amyloid precursor protein.....	11
1.3 Regulation of ADAM10 activity.....	14
1.4 Tetraspanins.....	17
1.4.1 Functions of tetraspanins.....	20
1.4.2 Tetraspanins as regulators of ADAM10 .....	22
<b>2 Objectives .....</b>	<b>25</b>
<b>3 Material and Methods.....</b>	<b>27</b>
3.1 Materials .....	27
3.1.1 Chemicals .....	27
3.1.2 Antibodies .....	27
3.1.3 Cell culture media and additives.....	28
3.1.4 Kits.....	29
3.1.5 DNA and protein standards.....	29
3.1.6 Enzymes.....	29
3.1.7 Oligonucleotides.....	29
3.1.8 siRNA .....	31
3.1.9 Plasmids and expression constructs .....	31
3.1.10 Cell lines.....	32
3.1.11 Transgenic mouse lines .....	32
3.1.12 Frequently used buffers and solutions.....	32
3.2 Molecular biological methods .....	33
3.2.1 Generation of chemically competent <i>E. coli</i> .....	33
3.2.2 Transformation of chemically competent <i>E. coli</i> .....	34
3.2.3 Amplification and isolation of plasmid DNA from <i>E. coli</i> .....	34
3.2.4 Determination of nucleic acid concentration .....	34

---

3.2.5	Polymerase chain reaction (PCR) .....	35
3.2.5.1	Generation of Tspan3 <sub>Y243A</sub> -myc by mutagenesis PCR.....	35
3.2.6	Agarose gel electrophoresis .....	36
3.2.7	Sequence analysis .....	36
3.2.8	Split-Ubiquitin yeast two-hybrid interaction screen.....	36
3.2.9	Total RNA extraction .....	37
3.2.10	cDNA synthesis .....	37
3.2.11	Quantitative real-time PCR (qRT-PCR) .....	37
3.3	Cell biological methods.....	38
3.3.1	Maintenance of cell lines .....	38
3.3.2	Determination of cell number.....	38
3.3.3	Cryo-preservation of cell lines.....	39
3.3.4	Transient transfection of cells.....	39
3.3.5	siRNA-mediated knockdown .....	39
3.3.6	Inhibitor treatment of cells .....	40
3.3.7	Indirect immunofluorescence staining .....	40
3.3.8	Flow cytometric analysis .....	41
3.4	Biochemical methods.....	42
3.4.1	Protein extraction from cells.....	42
3.4.2	Preparation of tissue homogenates.....	42
3.4.3	Co-immunoprecipitation experiments.....	43
3.4.4	Biotinylation of cell surface proteins .....	43
3.4.5	Determination of protein concentrations.....	44
3.4.6	SDS polyacrylamide gel electrophoresis (SDS-PAGE).....	45
3.4.7	Western blotting and immunodetection .....	46
3.4.8	Reprobing of immunoblots .....	48
3.5	Histological methods .....	49
3.5.1	Preparation of semi-thin cryosections .....	49
3.5.2	Immunofluorescence staining of cryosections .....	49
3.5.3	Diaminobenzidine (DAB) staining.....	50
3.5.4	Ultra-structural analysis of hippocampal sections.....	50
3.6	Animal experimentation .....	50
3.6.1	Generation of Tspan3 and Tspan15 knockout mice .....	50
3.6.2	Animal housing.....	51
3.6.3	Breeding strategy .....	52
3.6.4	Tail biopsy and isolation of genomic DNA.....	53
3.6.5	PCR for genotyping of mice.....	53
3.6.6	Euthanasia of mice .....	53

---

3.7	Analysis of human brain samples .....	54
3.8	Statistical analysis .....	54
<b>4</b>	<b>Results .....</b>	<b>55</b>
4.1	Characterisation of tetraspanin-3 as an ADAM10 interaction partner .....	55
4.1.1	Identification of tetraspanin-3 as an ADAM10 interaction partner in yeast .....	55
4.1.2	Tetraspanin-3 interacts with ADAM10 in mammalian cells.....	57
4.1.3	Tetraspanin-3 does not exert an apparent effect on the maturation of ADAM10	59
4.1.4	Tetraspanin-3 does not affect the surface expression of ADAM10.....	61
4.1.5	Overexpression of tetraspanin-3 affects APP but not N-cadherin processing .....	63
4.1.6	Tetraspanin-3 increases the appearance of the APP-CTF which is generated by ADAM10.....	64
4.1.7	Overexpression of tetraspanin-3 promotes $\alpha$ -secretase cleavage, but does not influence $\beta$ - and $\gamma$ -secretase cleavage of APP.....	67
4.1.8	Immunofluorescence analysis of the subcellular localisation of tetraspanin-3 .....	71
4.1.9	How does tetraspanin-3 modulate ADAM10-dependent APP processing? .....	74
4.1.9.1	Tetraspanin-3 interacts with APP and presenilin-1 .....	74
4.1.9.2	Tetraspanin-3 overexpression increases the surface level of the APP-CTF ...	75
4.1.9.3	Mutation of the tetraspanin-3 endocytic motif modulates the surface level of APP.....	77
4.1.10	Downregulation of tetraspanin-3 expression does not affect APP processing .....	81
4.2	Analysis of the <i>in vivo</i> function of tetraspanin-3 .....	84
4.2.1	Tetraspanin-3 is glycosylated and highly expressed in the murine brain.....	84
4.2.2	Tetraspanin-3 is predominantly expressed in neurons of the murine brain .....	86
4.2.3	Tetraspanin-3 interacts with ADAM10 and APP in mouse brain .....	88
4.2.4	Does tetraspanin-3 deficiency alter ADAM10-mediated shedding? .....	89
4.2.4.1	The knockout of tetraspanin-3 has no apparent effect on ADAM10 and APP .....	93
4.2.4.2	Loss of tetraspanin-3 is possibly compensated by tetraspanin-5 and -7 .....	95
4.2.4.3	Overexpression of tetraspanin-7 increases the appearance of the APP-CTF. 96	
4.2.5	Tetraspanin-3 expression is elevated in the brains of Alzheimer's Disease patients.....	98
4.3	Characterisation of the <i>in vivo</i> function of tetraspanin-15 .....	99
4.3.1	Generation of tetraspanin-15 knockout mice.....	99
4.3.2	Tetraspanin-15 is predominantly expressed in lung and intestine.....	102
4.3.3	Tetraspanin-15 knockout impairs ADAM10 maturation and shedding activity ...	103
4.3.4	Loss of Tspan15 increases the appearance of perforated postsynaptic densities	106

---

<b>5 Discussion .....</b>	<b>109</b>
5.1 Identification of tetraspanin-3 as a novel ADAM10 interaction partner .....	109
5.1.1 Tetraspanin-3 has no apparent effect on ADAM10 maturation and surface trafficking .....	111
5.1.2 The role of tetraspanin-3 in the proteolytic processing of APP .....	112
5.1.3 Tetraspanin-3 acts as a scaffold for non-amyloidogenic APP processing .....	115
5.1.4 The potential function of tetraspanin-3 in endocytic processes .....	119
5.1.5 The influence of tetraspanin-3 on the production of ADAM10-CTFs .....	122
5.2 Tetraspanin-3 deficiency is likely compensated by other tetraspanins .....	124
5.3 Tetraspanin-3 in Alzheimer's Disease .....	127
5.4 Characterisation of the physiological function of tetraspanin-15 .....	128
5.4.1 Loss of tetraspanin-15 affects ADAM10 substrates in the brain .....	129
5.4.2 The role of tetraspanin-15 in dendritic spine morphology .....	133
5.5 Tetraspanin-3 and -15 as potential therapeutic targets .....	136
5.6 Conclusions and Outlook .....	139
<b>6 References .....</b>	<b>141</b>
<b>7 List of Figures and Tables .....</b>	<b>169</b>
<b>8 Declaration .....</b>	<b>173</b>
<b>9 Curriculum Vitae .....</b>	<b>175</b>
<b>10 Publications and scientific participations .....</b>	<b>177</b>
<b>11 Acknowledgement .....</b>	<b>179</b>



---

## List of Abbreviations

A $\beta$	Amyloid-beta
AD	Alzheimer's Disease
ADAM	A Disintegrin and Metalloprotease
AML	Acute myelogenous leukaemia
AMPA	Amino-3-hydroxy-5-methyl-4-isoxazolepropionic acid
ANOVA	Analysis of variance
AP-2	Adaptor protein-2
APP	Amyloid precursor protein
BACE1	$\beta$ -site APP cleaving enzyme 1
CAM	Cell adhesion molecule
CaMKII $\alpha$	Calcium/calmodulin-dependent protein kinase II $\alpha$
cKO	Conditional knockout
CNS	Central nervous system
CTF	C-terminal fragment
Cub	C-terminal part of ubiquitin
DAPI	4-,6-diamidino-2-phenylindole
DMEM	Dulbecco's modified Eagle Medium
DNA	Deoxyribonucleic acid
<i>E. coli</i>	<i>Escherichia coli</i>
EDTA	Ethylenediaminetetraacetic acid
EEA1	Early endosomal antigen 1
EGF	Epidermal growth factor
ER	Endoplasmic reticulum
ERK	Extracellular signal-regulated kinase
ESCRT	Endosomal sorting complex required for transport
FCS	Fetal calf serum
fl	Full length
FwrD	Forward
GAPDH	Glyceraldehyde 3-phosphate dehydrogenase
GPI	Glycosylphosphatidylinositol
ICD	Intracellular domain

ILVs	Intraluminal vesicles
kDa	Kilo Dalton
ko	Knockout
KPI	Kunitz-type protease inhibitor
LAMP-2	Lysosome-associated membrane protein-2
LB	Lysogeny broth
LEL	Large extracellular loop
LIMP-2	Lysosomal integral membrane protein-2
LTD	Long-term depression
LTP	Long-term potentiation
MAPK	Mitogen-activated protein kinase
mRNA	Messenger RNA
MT-MMP	Membrane-type matrix metalloproteinase
MVB	Multi vesicular body
NaCl	Sodium chloride
NeuN	Neuronal nuclei
Nogo	Neurite outgrowth inhibitor
NP-40	Nonidet P-40
Nub	N-terminal part of ubiquitin
OAP1	OSP-associated protein 1
OSP	Oligodendrocyte-specific protein
PBS	Phosphate-buffered saline
PC7	Proprotein convertase 7
PCR	Ploymerase chain reaction
PDI	Protein disulfide-isomerase
PEI	Polyethylenimine
PFA	Paraformaldehyde
PI4K	Phosphatidylinositol 4-kinase
PKC	Protein kinase C
PMA	Phorbol-12-myristat-13-acetat
PMEL	Premelanosome protein
PNGase F	Peptide N-Glycosidase F

---

PrP	Prion protein
PSD	Post-synaptic density
qRT-PCR	quantitative real-time PCR
Rab5	Ras-related protein Rab5A
rev	Reverse
RIP	Regulated intramembrane proteolysis
RNA	Ribonucleic acid
S1PR2	Sphingosine-1-phosphate receptor 2
SAP97	Synapse-associated protein 97
sAPP	Soluble APP
siRNA	Small interfering RNA
SD	Standard deviation
SDS	Sodium dodecyl sulfate
SDS-PAGE	Sodium dodecyl sulfate-polyacryl amide electrophoresis
SDF1	Stromal cell-derived factor-1
SEL	Short extracellular loop
SH3	Src homology 3
Swe	Swedish
TEM	Tetraspanin-enriched microdomain
TIMP	Tissue inhibitor of metalloprotease
TNF $\alpha$	Tumour necrosis factor $\alpha$
Tris	Tris(hydroxymethyl)aminomethane
Tspan	Tetraspanin
Wt	Wild-type



## Summary

The A Disintegrin and Metalloprotease 10 (ADAM10) is responsible for the ectodomain shedding of multiple cell surface proteins and is involved in important physiological processes in the brain and other organs. As the responsible  $\alpha$ -secretase of the amyloid precursor protein (APP), ADAM10 counteracts amyloid-beta liberation, which is the main component of amyloid plaques in Alzheimer's Disease patients.

Tetraspanins were identified as potent regulators of ADAM10 activity. In particular, members of the TspanC8 subgroup of tetraspanins (Tspan5, Tspan10, Tspan14, Tspan15, Tspan17, Tspan33) promote ADAM10 maturation and surface trafficking.

In the present work, the function of tetraspanin-3 (Tspan3) as a novel ADAM10 interaction partner was characterised. In murine tissues, Tspan3 was detected in almost all tissues and was highly expressed in the brain. Interestingly, Tspan3 expression was enhanced in the brains of Alzheimer's Disease patients. In cells, Tspan3 was mainly detected in endosomal-lysosomal compartments. Co-immunoprecipitation experiments confirmed Tspan3 as an ADAM10 interaction partner and additionally revealed its interaction with APP and presenilin-1, which is the catalytic active subunit of the  $\gamma$ -secretase complex. Overexpression of Tspan3 in cells promotes ADAM10-mediated APP processing, without affecting ADAM10 maturation or trafficking to the cell surface. Decreasing Tspan3 internalisation by mutation of a cytosolic endocytic sorting motif increased the surface levels of its partner proteins APP and ADAM10. In contrast to overexpression, downregulation of Tspan3 expression did not alter APP proteolytic processing in cells and mice. Further analysis revealed increased levels of Tspan7 and Tspan5 transcripts in Tspan3-deficient brains, which possibly compensate for the loss of Tspan3.

Moreover, the *in vivo* importance of tetraspanin-15 (Tspan15), as an ADAM10 regulator was investigated. Tspan15 expression was detected in several murine tissues and was also abundantly expressed in the brain. Tspan15-deficient mice showed a reduction of mature ADAM10 in the brain. Additionally, a decreased proteolytic cleavage of N-cadherin and the cellular prion protein (PrP<sup>C</sup>) was observed. The ultrastructural analysis of hippocampal neurons revealed alterations of synaptic structures, which are related to ADAM10-dependent functions.

In conclusion, Tspan3 is a novel regulator of ADAM10-mediated shedding, which promotes APP processing by acting as a scaffold and stabiliser for its partner proteins at the plasma membrane. Additionally, analysis of Tspan15 knockout mice validated the important role of Tspan15 as a regulator of ADAM10 activity and substrate cleavage *in vivo*.

## Zusammenfassung

Die *A Disintegrin and Metalloprotease 10* (ADAM10) hat ein breites Substratspektrum. Durch proteolytische Spaltung setzt ADAM10 die Ektodomäne seiner Substrate frei und ist an einer Vielzahl von physiologischen Prozessen beteiligt. Als hauptverantwortliche  $\alpha$ -Sekretase für die Spaltung des amyloiden Vorläuferproteins (APP) verhindert ADAM10 die Freisetzung von Amyloid-beta Peptiden, deren extrazelluläre Ablagerung ein Hauptmerkmal der Alzheimer'schen Erkrankung ist.

Tetraspanine wurden als wirkungsvolle Regulatoren von ADAM10 identifiziert. Im Besonderen, Mitglieder der TspanC8 Tetraspanine (Tspan5, Tspan10, Tspan14, Tspan15, Tspan17, Tspan33) zeigten einen fördernden Einfluss auf die ADAM10 Maturierung und den Transport von ADAM10 zur Zelloberfläche.

Im Verlauf dieser Arbeit wurde die Funktion von Tetraspanin-3 (Tspan3) als ein neuer ADAM10 Interaktionspartner charakterisiert. In murinen Geweben zeigte Tspan3 ein breites Expressionsmuster, wobei die stärkste Expression im Gehirn auftrat. Eine erhöhte Tspan3 Expression konnte auch in den Gehirnen von Alzheimer Patienten beobachtet werden. Auf subzellulärer Ebene wurde Tspan3 überwiegend in endosomal-lysosomalen Kompartimenten detektiert. Neben ADAM10 wurde Tspan3 auch als Interaktionspartner von APP und der katalytisch aktiven Untereinheit des  $\gamma$ -Sekretase Komplexes, Präsenilin-1, identifiziert. Überexpression von Tspan3 in Zellen führte zu einer verstärkten ADAM10-vermittelten Spaltung von APP, hatte jedoch keinen Einfluss auf die ADAM10 Maturierung und Oberflächenexpression. Eine Verzögerung der Tspan3 Internalisierung, durch Mutation eines zytosolischen Endozytosemotivs, erhöhte die Oberflächenexpression von APP und ADAM10. Eine Verringerung der Tspan3 Expression hatte keinen offensichtlichen Einfluss auf die APP-Prozessierung in Zellen und in Tspan3-defizienten Mäusen. Weitere Untersuchungen zeigten eine verstärkte Transkription von Tspan7 und Tspan5 in Tspan3-defizienten Gehirnen, die wahrscheinlich den Verlust von Tspan3 kompensieren.

Des Weiteren wurde die Bedeutung von Tetraspanin-15 (Tspan15) als ADAM10 Regulator *in vivo* untersucht. Tspan15 wurde in verschiedenen murinen Geweben detektiert und zeigte ebenfalls eine prominente Expression im Gehirn. Tspan15-defiziente Mäuse zeigten eine Reduktion der maturen Form von ADAM10 im Gehirn. Darüber hinaus wurde eine verringerte proteolytische Spaltung von N-Cadherin und der zellulären Form des Prion-

Proteins (PrP<sup>c</sup>) beobachtet. Die ultrastrukturelle Analyse von hippocampalen Neuronen zeigte morphologische Veränderungen der Synapsen Struktur, die auf ADAM10-abhängige Funktionen zurückzuführen ist.

Zusammengefasst wurde Tspan3 als Regulator der ADAM10-vermittelten APP-Prozessierung identifiziert. Dabei moduliert Tspan3 nicht die Maturierung oder den Transport von ADAM10 zur Plasmamembran, sondern fungiert als Gerüst und Stabilisator für seine Partnerproteine. Des Weiteren konnte mit Hilfe eines Tspan15 *Knockout*-Mausmodells die wichtige Rolle von Tspan15 als Regulator für ADAM10-vermittelte Sheddingprozesse validiert werden.



# 1 Introduction

## 1.1 Proteases

Proteases are enzymes that catalyse the breakdown of proteins by hydrolysis of peptide bonds. Proteases are broadly distributed and are found in all living organisms. In human and mouse more than 500 proteases, with several orthologues in other organisms, have been identified (López-Otín and Matrisian, 2007). Depending on their catalytic mechanism and the key amino acid or ion in the active centre, proteases are classified as aspartate, cysteine, glutamate, metallo, serine, threonine or asparagine proteases (Fujinaga et al., 2004; Rawlings and Barrett, 1995; Seemüller et al., 1995). Protein substrates are cleaved by proteases at specific sites located at the amino- or carboxy-terminal ends (exopeptidases) or within the peptide chain (endopeptidases). Initially, proteases were thought to be primary responsible for the unspecific degradation of proteins during digestion and for intracellular protein catabolism. More recently, research revealed that proteolytic cleavage is a highly specific event and limited to distinct substrates.

Proteolytic processing is a regulatory mechanism that modifies the function of certain proteins. For example, inactive precursor proteins (zymogens) can be activated by proteolytic cleavage and the localisation of proteins can be modified by proteolytic removal of signal peptides. Thus, proteases play an important role in a large number of biological processes, such as DNA replication, neuronal outgrowth, tissue remodelling, wound healing, angiogenesis, apoptosis and many others (López-Otín and Bond, 2008). Dysregulation of protease activity is associated with several pathological events. Therefore, proteases became interesting targets for the development of novel drugs in several human diseases like cancer, neurodegeneration, inflammation, bacterial and viral infections (Turk, 2006).

### 1.1.1 Zinc-dependent metalloproteases

Zinc-dependent metalloproteases make use of  $Zn^{2+}$ -ions to catalyse peptide bond cleavage and are subdivided according to the zinc-binding motif within their active centre. A prominent subgroup of metalloproteases are the metzincins, which are further split into astacins, serralytins, matrix metalloproteases and adamalysins. The catalytic site of metzincins is characterized by a common HExxHxxGxxH (x can be any amino acid) zinc-binding motif and a

conserved methionine-containing 1,4- $\beta$ -turn, which is an unique feature of this superfamily (Bode et al., 1993; Gomis-Rüth, 2003; Stöcker and Bode, 1995).

### **1.1.2 A Disintegrin and Metalloproteases (ADAMs)**

A Disintegrin and Metalloproteases (ADAMs) are a family of transmembrane proteases. ADAMs derived their name from their structural similarity to the disintegrin and metalloprotease domain of snake venom proteases (Wolfsberg et al., 1995). According to the MEROPS protease database, ADAMs are categorised as MP12B adamalysin metalloproteases, which also include the family of snake venom metalloproteases and A disintegrin and metalloproteases with a thrombospondin motif (ADAMTS). ADAMs were detected in various species ranging from yeast (*Schizosaccharomyces pombe*), nematodes (*Caenorhabditis elegans*) to vertebrates (*Mus musculus*, *Homo sapiens*) and most of them are broadly distributed. In the mammalian system, 40 different ADAM proteases were identified. 37 of them were found in the mouse and 21 in the human genome (Puente and Lo, 2004). Of the human ADAMs only ADAM8, 9, 10, 12, 15, 17, 19, 20, 21, 28, 30, 33 contain the HExxHxxGxxH zinc-binding motif and are catalytically active (Bode et al., 1993).

Members of the ADAM family share a similar modular domain structure. They contain a N-terminal signal peptide, which is followed by a prodomain, the catalytic active metalloprotease domain, a cysteine-rich, an EGF-like, a transmembrane domain and a short C-terminal cytoplasmic tail (Fig. 1.1A). Exceptions are ADAM10 and ADAM17 (Fig. 1.1B), which miss the EGF-like domain and contain a membrane proximal domain (MPD) instead of the cysteine-rich domain (Düsterhöft et al., 2013; Janes et al., 2005; Takeda et al., 2006). The N-terminal signal peptide guides the ADAM proteases to the Golgi apparatus and to the secretory pathway after their synthesis in the endoplasmic reticulum (ER). The prodomain inhibits protease activity during intracellular transport and is removed by proprotein convertases or an autocatalytic mechanism in the Golgi apparatus (Howard et al., 2000; Lum et al., 1998; Schlomann et al., 2002). Furthermore, the prodomain functions as an intramolecular chaperone, controlling correct protein folding and transport of ADAM proteases (Roghani et al., 1999). The metalloprotease domain of catalytic active ADAMs is responsible for the substrate cleavage at the plasma membrane.

By cleaving their substrates close to the plasma membrane, ADAM proteases release the ectodomain of type I and type II integral proteins, which is referred to as ectodomain

shedding. Substrate recognition and proteolytic activity are mainly regulated by the disintegrin domain, in concert with the cysteine-rich and the EGF-like domain, which is thought to assist substrate binding to the cysteine-rich domain (Janes et al., 2005; Smith et al., 2002; Takeda, 2009). Additionally, the disintegrin domain is described to be responsible for the function of several ADAMs in cell-cell adhesion, due to its interaction with integrin molecules (White, 2003). Analogous to the cysteine rich and EGF-like domain, the MPD of ADAM10 and ADAM17 is responsible for substrate recognition, protein multimerisation and regulation of their activity (Düsterhöft et al., 2013; Lorenzen et al., 2011, 2012). The length and sequence of the cytoplasmic domain of ADAMs is highly variable and it takes part in the regulation of their proteolytic activity, intracellular localisation and signalling by binding to specific cytosolic proteins or phosphorylation (Seals and Courtneidge, 2003).

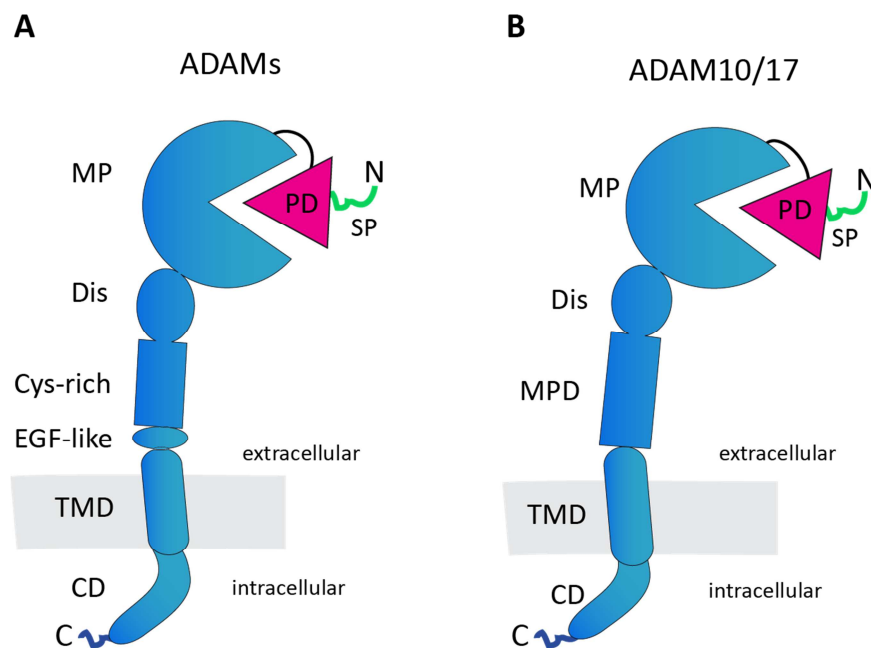


**Fig. 1.1: Structure of A Disintegrin and Metalloproteases (ADAMs).**

Domain structure of classical ADAMs (A), ADAM10 and ADAM17 (B). Abbreviations N: N-terminus, SP: Signal peptide, PD: Prodomain, MP: Metalloprotease domain, Dis: Disintegrin domain, Cys-rich: Cysteine-rich domain, EGF-like: EGF-like domain, TMD: Transmembrane domain, CD: C-terminal domain, C: C-terminus

Upon ectodomain shedding, the extracellular domain of a protein is released and can take part in autocrine and paracrine signalling events. Additionally, shedding is a prerequisite for further intramembrane proteolysis of the membrane remaining part, which is also known as regulated intramembrane proteolysis (RIP). Intramembrane cleaving proteases (iCLiPs) release the cytoplasmic part of a protein, which can further take part in intracellular signalling or translocates to the nucleus, where it regulates gene transcription. The ability of ADAMs to

modulate protein functions by ectodomain shedding, in combination with their broad expression pattern, involves ADAMs in a multitude of physiological and pathophysiological processes such as fertilisation, inflammation and developmental processes (reviewed in Weber and Saftig, 2012).

### **1.1.3 A Disintegrin and Metalloprotease 10 (ADAM10)**

ADAM10 is, together with its close relative ADAM17, one of the best-described members of the ADAM family. ADAM10 expression is described in several mammalian cell lines and in a wide variety of human organs, including the brain (Howard et al., 1996; Kärkkäinen et al., 2000; Marcinkiewicz and Seidah, 2000). As a type I transmembrane protein, ADAM10 is synthesized in the ER as an inactive proform with a molecular weight of about 100 kDa (Fig. 1.2). During transport to the plasma membrane, ADAM10 is N-glycosylated at four positions and undergoes maturation by removal of the prodomain through the proprotein convertase furin and the proprotein convertase 7 (PC7) (Anders et al., 2001; Escrevente et al., 2008; Lopez-Perez et al., 1999). The resulting mature and active form of ADAM10 has a molecular weight of about 70 kDa and mediates substrate cleavage in late secretory compartments and at the plasma membrane (Fig. 1.2) (Lammich et al., 1999).

The substrate spectrum of ADAM10 comprises more than 40 validated substrates, including adhesion molecules (e.g. cadherins), chemokines (e.g. CX3CL1), growth factors (e.g. EGF, TNF $\alpha$ ), signalling receptors and ligands (e.g. Notch receptor, Fas ligand) (Kuhn et al., 2016; Reiss and Saftig, 2009; Weber and Saftig, 2012). For most of these substrates, ADAM10-mediated shedding initiates RIP, which is mediated by intramembrane proteases, such as the multiprotein  $\gamma$ -secretase complex (Fig. 1.2). A prominent example for this process and a key substrate of ADAM10 is the Notch receptor. Signal transduction by the Notch receptor plays a pivotal role in cell fate decisions during embryonic development and in adult tissue homeostasis (Gordon et al., 2009). Upon binding of Notch ligands, from the Delta or Jagged family, to the Notch receptor ADAM10 sheds the Notch receptor and releases its extracellular domain (van Tetering et al., 2009). This step initiates intramembrane proteolysis of the membrane bound part by the  $\gamma$ -secretase complex, which releases the Notch intracellular domain (NICD) into the cytosol (De et al., 1999). The NICD contains a nuclear localisation sequence and translocates into the nucleus, where it activates transcription of Notch responsive genes. These include *hes* (*hairy/enhancer of Split*) and *hey* (*hairy/enhancer of Split*

related with *YRPW motif*) genes, which are involved in cell proliferation, differentiation and stem cell self-renewal (Hitoshi, 2002; Imayoshi et al., 2010; Jarriault et al., 1998; Ohtsuka et al., 1999; Schroeter et al., 1998).

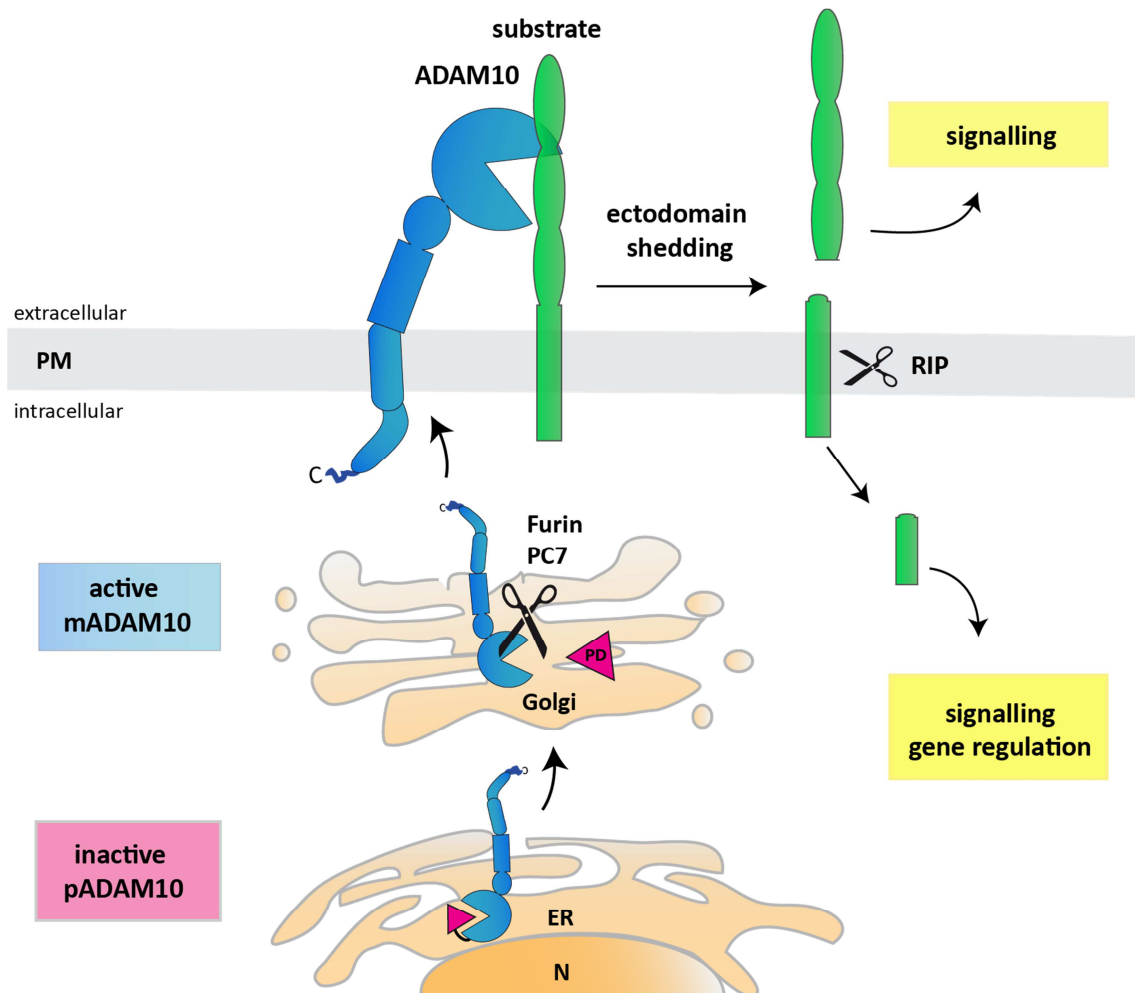


**Fig. 1.2: ADAM10 maturation and ectodomain shedding.**

ADAM10 is synthesised as an inactive proform (pADAM10) in the endoplasmic reticulum (ER). During transport to the plasma membrane (PM) ADAM10 is activated by the removal of its prodomain (PD). The PD is cleaved by furin or the proprotein convertase 7 (PC7) in the Golgi apparatus (Golgi), which reveals the mature and active form of ADAM10 (mADAM10). At the plasma membrane ADAM10 cleaves the ectodomain of its substrates close to the plasma membrane, which is described as ectodomain shedding. The soluble ectodomain can take part in autocrine or paracrine signalling. The remaining membrane-bound part is further substrate for regulated intramembrane proteolysis (RIP). Following, the intracellular domain (ICD) is released into the cytosol and can take part in intracellular signalling pathways or modulates gene expression after translocation into the nucleus.

The importance of ADAM10 in Notch signalling is supported by the phenotype of classical ADAM10 knockout mice, which is similar to the phenotype of Notch-deficient mice. Classical ADAM10 knockout mice are not viable and die at an early embryonic stage (embryonic day 9.5) with severe developmental defects in the central nervous system, somitogenesis and the vascular system (Hartmann et al., 2002). Reduced Notch signalling was also identified as a

major cause for the late embryonic lethality, a disrupted organization of the cortex and a reduced ganglionic eminence in mice with a conditional Nestin-Cre-driven ADAM10 deletion in neuronal progenitor cells (Jorissen et al., 2010). In the same study, ADAM10 was identified as the *in vivo*  $\alpha$ -secretase for proteolytic processing of the amyloid precursor protein (APP) (Jorissen et al., 2010). APP is another prominent ADAM10 substrate and became of special interest due to its involvement in the development of Alzheimer's disease (AD) (Hardy and Selkoe, 2002; O'Brien and Wong, 2011).

Further conditional knockout mouse models, knockdown and inhibitor studies led to the identification of several other ADAM10 substrates and demonstrated the central role of ADAM10 in developmental processes, skin homeostasis, cancer development, inflammation and neurodegeneration (Kuhn et al., 2016; Weber and Saftig, 2012)

In addition to its function as a protease, ADAM10 itself is subject to ectodomain shedding by ADAM9 and ADAM15, which initiates intramembrane proteolysis of the remaining, membrane-bound part of ADAM10 by the  $\gamma$ -secretase complex (Parkin and Harris, 2009; Tousseyn et al., 2009). It is also speculated that ADAM10 itself initiates RIP by an autocatalytic mechanism (Suh et al., 2013). The released ADAM10 intracellular domain was found in nuclear speckles, where it is possibly involved in transcriptional regulation (Tousseyn et al., 2009). The soluble ADAM10 ectodomain can still contribute to proteolytic events (Cissé et al., 2005). Moreover, ADAM10 acts as a receptor for the  $\alpha$ -toxin of *Staphylococcus aureus* and contributes to bacterial infections through increased shedding of epithelial cadherin (E-cadherin), which disrupts the epithelial barrier function (von Hoven et al., 2016; Inoshima et al., 2011; Wilke and Wardenburg, 2010).

#### **1.1.4 ADAM10 substrates in the central nervous system**

The phenotype of classical and Nestin-Cre-driven conditional knockout mice revealed ADAM10 as an essential protease in the developing central nervous system. However, the early lethality of these mice hampered further functional analysis. To overcome this problem ADAM10-deficient mice with a postnatal calcium/calmodulin-dependent protein kinase II  $\alpha$  (CaMKII $\alpha$ )-Cre-driven conditional ADAM10 knockout in neurons were generated (Prox et al., 2013). These mice displayed epileptic seizures, severe learning deficits and an altered spine morphology, which confirmed the important role of ADAM10 also in the adult brain. Although an increased postnatal lethality still indicated a disturbed Notch signalling, the

phenotype of these mice is also related to impaired shedding of other ADAM10 substrates in the brain (Prox et al., 2013). Besides a decreased proteolytic processing of APP, knockout of ADAM10 in neurons reduced the shedding of neuronal adhesion molecules such as the neuronal cadherin (N-cadherin), Nectin-1 and neuronal cell adhesion molecule (NCAM)(Kuhn et al., 2016; Prox et al., 2013). N-cadherin is an adhesion molecule that has also functions outside the brain. It is associated with  $\beta$ -catenin signalling pathway and is involved in neurulation, heart tube formation, tissue remodelling and wound healing (Ko et al., 2001; Radice et al., 1997). In the brain, ADAM10-mediated N-cadherin shedding is involved in neurite outgrowth, remodelling of the postsynaptic structures and synaptic plasticity (Malinverno et al., 2010; Paudel et al., 2013). Nectin-1 and NCAM are also adhesion molecules with important functions in synapse formation, axon growth and synaptic plasticity (see Tab. 1.1)(Brenneman et al., 2014; Maness and Schachner, 2007; Mizoguchi et al., 2002). Additional neuronal cell adhesion molecules that are shed by ADAM10 are listed in Tab. 1.1. Furthermore, ephrins and their receptors, which have important functions in axon repulsion and cell-cell communication, are also subject to ADAM10-mediated shedding (Hattori et al., 2000; Janes et al., 2005; Litterst et al., 2007).

In addition to APP, the cellular prion protein and Bri2 have emerged as ADAM10 substrates that are involved in neurodegenerative diseases (Altmepfen et al., 2011, 2015; Martin et al., 2008; Vincent et al., 2001). The cellular prion protein ( $\text{PrP}^{\text{C}}$ ) is a glycosylated, glycosylphosphatidylinositol (GPI)-anchored membrane protein. Misfolding of  $\text{PrP}^{\text{C}}$  leads to a conformational conversion into a pathologic isoform named scrapie PrP ( $\text{PrP}^{\text{Sc}}$ ).  $\text{PrP}^{\text{Sc}}$  is the principal component of the infectious particles in prion disease, which are referred to as prions. By cleaving  $\text{PrP}^{\text{C}}$  ADAM10 has a dual role in prion disease. On the one hand ADAM10 cleavage reduces the available substrate for the conversion into  $\text{PrP}^{\text{Sc}}$ . On the other hand shedding of  $\text{PrP}^{\text{Sc}}$  and conversion of already cleaved  $\text{PrP}^{\text{C}}$  into soluble  $\text{PrP}^{\text{Sc}}$  accelerates prion spreading (Altmepfen et al., 2011, 2015; Taylor et al., 2009).

Bri2 is a type II transmembrane protein that undergoes intramembrane proteolysis by signal peptide peptidase-like 2a (SPPL2a) after shedding by ADAM10. Accumulation of a mutant form of Bri2 is associated with the development of British and Danish dementia. However, the functional consequences of ADAM10 shedding are not yet clear. Further ADAM10 substrates in the CNS, including the metalloproteases MT4-MMP, the low-density lipoprotein receptor (LDLR), Klotho and other proteins, are described in Tab. 1.1 (Kuhn et al., 2016; Saftig and

Lichtenthaler, 2015). Moreover, proteomic analysis of ADAM10-deficient neurons using ‘secretome protein identification with click sugars’ (SPECS) identified 91 novel substrate candidates, which highlights the essential role of ADAM10 as a sheddase for proteins in the central nervous system (Kuhn et al., 2016).

**Tab. 1.1: List of selected ADAM10 substrates and their function in the CNS.**

<b>Substrate</b>	<b>Function</b>	<b>Reference</b>
APP	<ul style="list-style-type: none"> <li>Involved in cell and synaptic adhesion</li> <li>Putative functions in synapse formation and synaptic plasticity</li> <li>Source of A<math>\beta</math> peptides, which are involved in Alzheimer’s Disease</li> </ul>	(Abraham et al., 1988; Aydin et al., 2012; Dawkins and Small, 2014; Hardy and Selkoe, 2002)
Bri2	<ul style="list-style-type: none"> <li>Associated with British and Danish dementia</li> <li>biological function unknown</li> </ul>	(Lashley et al., 2008; Martin et al., 2008; Vidal et al., 1999, 2000)
PrP <sup>c</sup>	<ul style="list-style-type: none"> <li>Putative functions in neurogenesis, myelin maintenance and the immune system</li> <li>PrP<sup>c</sup> converts into the pathological isoform PrP<sup>sc</sup>, which is involved in prion disease</li> <li>ADAM10 cleavage promotes prion spreading, but reduces prion pathology</li> </ul>	(Altmeppen et al., 2011, 2015; Bremer et al., 2010; Isaacs et al., 2006; Steele et al., 2006)
N-cadherin	<ul style="list-style-type: none"> <li>Neuronal adhesion molecule</li> <li><math>\beta</math>-catenin signalling</li> <li>Synaptic adhesion, regulation of dendritic spine morphology and synaptic plasticity</li> </ul>	(Mendez et al., 2010; Prox et al., 2013; Reiss et al., 2005; Togashi et al., 2002; Xie et al., 2008)
Nectin-1	<ul style="list-style-type: none"> <li>Cell migration and adhesion, synapse formation</li> <li>Linked to the actin cytoskeleton via afadin</li> <li>Functions together with the cadherin/catenin system</li> </ul>	(Kim et al., 2010; Mizoguchi et al., 2002; Prox et al., 2013; Shukla et al., 2006; Togashi et al., 2002)
L1 family (L1/CHL1/Neurofascin/NRCAM)	<ul style="list-style-type: none"> <li>Cell adhesion and signalling molecules</li> <li>Axon targeting, cell migration, synaptic plasticity</li> <li>Reduced L1 shedding impairs neurite outgrowth and cell migration</li> </ul>	(Gutwein, 2002; Hortsch, 1996; Kuhn et al., 2016; Maness and Schachner, 2007; Maretzky et al., 2005)
NCAM	<ul style="list-style-type: none"> <li>Cell adhesion molecule</li> <li>Axon growth, synaptic plasticity, GABAergic interneuron arborisation</li> <li>Inhibition of ADAM10 causes growth cone collapse</li> </ul>	(Brenneman et al., 2014; Maness and Schachner, 2007)
Ephrin A2, A5	<ul style="list-style-type: none"> <li>Ligands for Eph receptors</li> <li>Axon repulsion</li> <li>Cell-cell communication</li> </ul>	(Hattori et al., 2000; Janes et al., 2005)



Substrate	Function	Reference
$\gamma$ -protocadherin (C3)	<ul style="list-style-type: none"> <li>• Adhesion and signalling molecule</li> <li>• Neuronal survival, dendrite arborisation</li> <li>• Synapse formation and maturation</li> </ul>	(Garrett and Weiner, 2009; Garrett et al., 2012; Reiss et al., 2006; Wang et al., 2002)
Neurologin-1, -3, -4	<ul style="list-style-type: none"> <li>• Postsynaptic adhesion molecules, form trans-synaptic complexes with neurexins</li> <li>• Involved in synapse formation, maturation and synaptic transmission</li> <li>• Associated with schizophrenia and autism spectrum disorders</li> <li>• Increased shedding of NLG-1 decreases dendritic spine number</li> </ul>	(Bang and Owczarek, 2013; Kuhn et al., 2016; Südhof, 2008; Suzuki et al., 2012)
Neurexin-2, -3	<ul style="list-style-type: none"> <li>• Localised at the presynaptic membrane</li> <li>• Function together with neuroligins (see above)</li> </ul>	(Bang and Owczarek, 2013; Kuhn et al., 2016)
NG2	<ul style="list-style-type: none"> <li>• Expressed on oligodendrocyte precursor cells (OPC)</li> <li>• OPC migration and oligodendrocyte differentiation</li> <li>• Neuronal network formation</li> </ul>	(Biname et al., 2013; Sakry et al., 2014)
Fractalkine (CX3CL1)	<ul style="list-style-type: none"> <li>• Chemokine</li> <li>• Involved in microglial activation</li> <li>• Soluble CX3CL1 has neuroprotective functions</li> </ul>	(Kuhn et al., 2016; Lyons et al., 2009; Morganti et al., 2012)
Klotho	<ul style="list-style-type: none"> <li>• anti-aging functions</li> <li>• Involved in oligodendrocyte maturation and myelination</li> </ul>	(Bloch et al., 2009; Chen et al., 2007, 2013; Kuro-o et al., 1997)
MT4-MMP	<ul style="list-style-type: none"> <li>• GPI-anchored metalloprotease</li> <li>• Neural regulation of thirst</li> </ul>	(Kuhn et al., 2016; Rikimaru et al., 2007; Srichai et al., 2011)
LDLR	<ul style="list-style-type: none"> <li>• Receptor for apolipoprotein E</li> <li>• Regulates A<math>\beta</math> deposition in Alzheimer's Disease mouse models</li> </ul>	(Fryer et al., 2005; Katsouri and Georgopoulos, 2011; Kim et al., 2009a; Kuhn et al., 2016)

CHL1: Close homolog of L1; CX3CL1: C-X3-X motif chemokine 1; Eph: Erythropoietin-producing human hepatocellular; GABA: gamma-Aminobutyric acid; LDLR: Low-density lipoprotein receptor; MT4-MMP: Membrane-type-4 matrix metalloprotease; NCAM: Neural cell adhesion molecule; NLG: Neurologin, NG2: Neuron/glia antigen 2; NRCAM: Neuronal cell adhesion molecule.

## 1.2 Alzheimer's Disease

Alzheimer's Disease (AD) is one of the most prevalent forms of Dementia. It accounts for 60 to 80% of dementia cases and is the most common neurodegenerative disease worldwide (Alzheimer's Association). According to the latest data from the Alzheimer's Association, AD affects more than 5 million US Americans in the age of 65 years and is the 6<sup>th</sup> leading cause of death in the USA (Alzheimer Association, 2016). Since, aging is a critical factor for the development of AD and given the fact that in the coming years the number of individuals surviving to an age of 60-65 will almost double, its prevalence will be drastically increased to estimated 13 million AD cases by mid of the century (Brookmeyer et al., 2007; Ortman et al., 2014).

AD is characterised by the degeneration and loss of neurons in the hippocampal and cortical region of the brain, which causes a gradual deterioration of the memory function, cognitive decline and behavioural changes. Progression of the disease is accompanied by a drastic atrophy of the brain tissue and leads in its final stage to a complete loss of the ability to perform everyday activities (Hubbard and Anderson, 1981). The life expectancy of Alzheimer's Disease patients lies within 3-8 years after diagnosis (Brookmeyer et al., 2002).

Histological analysis of post-mortem brains of AD patients revealed lesions in the cortical and hippocampal regions as the main pathological hallmark of AD. These lesions are composed of amyloid plaques and neurofibrillary tangles. Neurofibrillary tangles are formed by accumulation of hyperphosphorylated, microtubule-associated tau proteins in neurons. Amyloid plaques consist of extracellular deposits of a pathological form of the amyloid-beta peptide ( $A\beta$ ). Additionally, brains of AD patients showed increased levels of neuroinflammatory molecules and an enhanced activity of immune cells (McGeer and McGeer, 2007).

According to genetic risk factors and the onset of AD symptoms, two forms of AD are distinguished. Early-onset Alzheimer's Disease (EOAD) is diagnosed before an age of 65 and first symptoms can already appear at an age of 40-50. It is related to mutations in the genes coding for presenilin-1, -2 (*PSEN1/2*) and APP (*APP*) (Rovelet-Lecrux et al., 2006). EOAD is a rather uncommon form of AD and accounts only for around 5% of all AD cases (Zhu et al., 2015). The more widespread form of AD is late-onset Alzheimer's Disease (LOAD), which occurs at an age of more than 65. Aging is one of the most striking risk factors for the development of LOAD. However, the presence of the  $\epsilon 4$  allele of the Apolipoprotein E (APOE)

was identified as an additional, genetic risk factor (Corder et al., 1993). Furthermore, epidemiological factors, such as traumatic brain injury, heart diseases, stroke, obesity and diabetes are critical factors for the development of AD (Citron, 2010).

Despite the increasing understanding of the pathological processes that drive AD pathology, efficient therapeutics are still not available.

### 1.2.1 Processing of the amyloid precursor protein

The A $\beta$  peptide is assumed to be the key factor in AD (Hardy and Selkoe, 2002). It is generated by sequential proteolytic processing of the amyloid precursor protein (APP), which is a secreted type I transmembrane protein with a short cytoplasmic tail, one transmembrane domain and a large extracellular domain (Chow et al., 2010; O'Brien and Wong, 2011). Due to their ability to release soluble fragments from the full length APP molecule, the APP cleaving enzymes are described as secretases. APP proteolytic processing is divided into two major processing pathways, the amyloidogenic processing pathway, which gives rise to the A $\beta$  peptide and the non-amyloidogenic processing pathway (Fig. 1.3)(summarised in Chow et al., 2010; Haass et al., 2012).

The amyloidogenic processing pathway (Fig. 1.3) is initiated by  $\beta$ -secretase cleavage, which releases the APP ectodomain as soluble APP $\beta$  (sAPP $\beta$ ). The membrane remaining C-terminal stub has a length of 99 (C99) or 89 (C89) amino acids. The latter of them results from an alternative  $\beta$ -secretase cleavage site. The C-terminal fragments are further processed by the  $\gamma$ -secretase complex, which liberates A $\beta$  peptides with a length ranging from 38-43 amino acids. At the same time the APP intracellular domain (AICD) is released into the cytosol. While A $\beta_{40}$  peptides are the most abundantly released A $\beta$  species, in particular A $\beta_{42}$  species are prone to form neurotoxic oligomers and further aggregate to amyloid plaques (Younkin, 1998).

In contrast to the amyloidogenic processing pathway, the non-amyloidogenic processing is initiated by  $\alpha$ -secretase cleavage of APP (Fig. 1.3). Upon cleavage, the ectodomain is released as soluble APP $\alpha$  fragment (sAPP $\alpha$ ). The membrane bound C-terminal stub (C83) is again substrate for the  $\gamma$ -secretase complex, which releases the AICD into the cytosol. In this case, A $\beta$  liberation is prevented, due to the fact that the  $\alpha$ -secretase cleavage site lies within the A $\beta$  domain. Instead of A $\beta$ , intramembrane proteolysis of the C83 fragment releases a short, non-toxic p3 fragment with a yet unknown biological function (Chow et al., 2010).

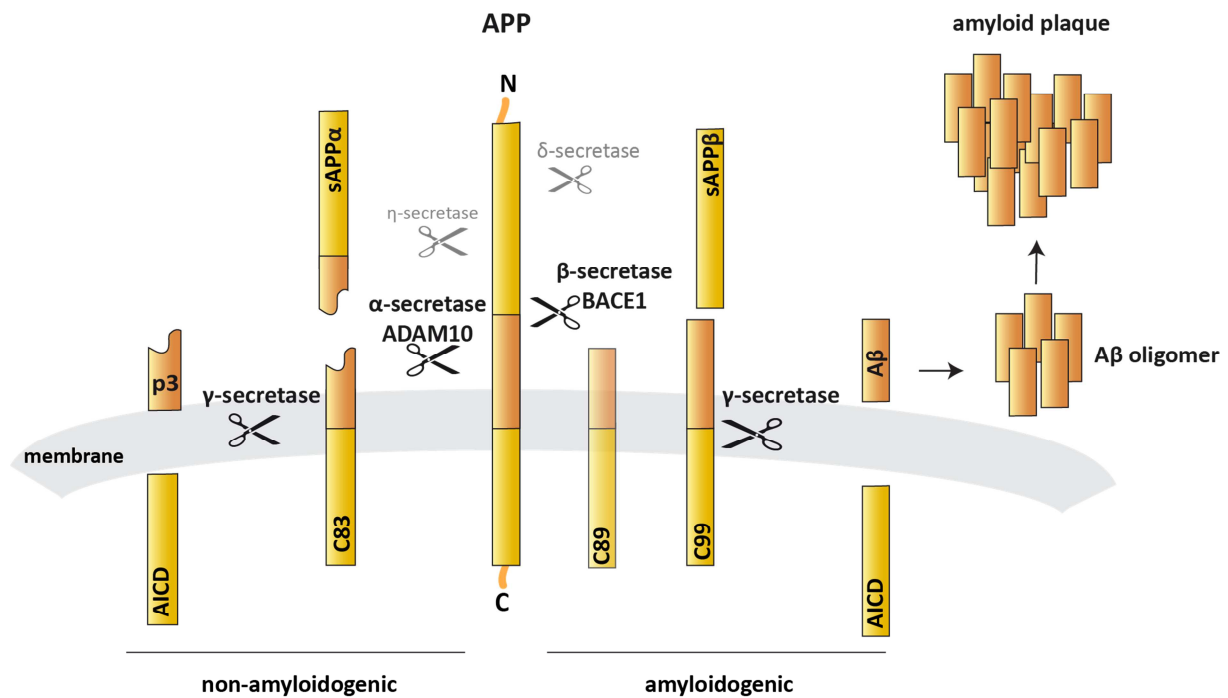


**Fig. 1.3: Processing of the amyloid precursor protein.**

The amyloid precursor protein (APP) is processed in two different ways. Amyloidogenic processing is initiated by  $\beta$ -secretase cleavage. The ectodomain is released as soluble APP $\beta$  (sAPP $\beta$ ) fragment. The C-terminal fragment has a length of 99 (C99) or 89 (C89) amino acids, when an alternative cleavage site is used. The C-terminal fragments are further processed by the  $\gamma$ -secretase complex, which releases A $\beta$  peptides and the APP intracellular domain (AICD). Distinct A $\beta$  peptides are prone to form neurotoxic oligomers and further accumulate to amyloid plaques. Non-amyloidogenic processing of APP is initiated by  $\alpha$ -secretase (ADAM10) cleavage. The  $\alpha$ -secretase cleaves APP within the A $\beta$  domain and releases the ectodomain as soluble APP $\alpha$  (sAPP $\alpha$ ). The membrane remaining 83 amino acid long C-terminal stub (C83) is subject to intramembrane proteolysis by the  $\gamma$ -secretase complex. This results in the liberation of the p3 peptide and the AICD. In addition to  $\alpha$ -,  $\beta$ -secretase cleavage, APP can be cleaved by a  $\delta$ - and a  $\eta$ -secretase. The resulting cleavage products are further subjected to proteolytic processing by the  $\alpha$ - and  $\beta$ -secretase.

Initially, the identity of the  $\alpha$ -secretase was controversially discussed. Several proteases were suggested as possible  $\alpha$ -secretases, including members of the membrane type matrix metalloproteases (MT-MMP) and the ADAM proteases ADAM10, ADAM17, ADAM8, ADAM9 and ADAM19 (Ahmad et al., 2006; Koike et al., 1999; Lammich et al., 1999; Naus et al., 2006; Slack et al., 2001). Although overexpression of ADAM9 promoted APP  $\alpha$ -secretase cleavage, knockdown of ADAM9 in cells and knockout in mice did not alter  $\alpha$ -secretase cleavage of APP and precluded it as  $\alpha$ -secretase (Koike et al., 1999; Kuhn et al., 2010; Weskamp et al., 2002). ADAM17 displayed  $\alpha$ -secretase activity upon stimulation with the phorbol ester phorbol-12-myristat-13-acetat (PMA) in murine fibroblasts (Buxbaum et al., 1998). However, ADAM17 was excluded as the constitutive active  $\alpha$ -secretase, since its expression pattern in the brain is very restricted (Kärkkäinen et al., 2000). Moreover, knockdown of ADAM17 in primary

neurons did not show significant alterations in APP processing (Kuhn et al., 2010). Finally, the conditional neuronal knockout of ADAM10 and knockdown studies in primary neurons identified ADAM10 as the physiological relevant and constitutively active  $\alpha$ -secretase in the brain (Jorissen et al., 2010; Kuhn et al., 2010).

The identity of the  $\beta$ -secretase was unclear for a long time. Several groups suggested the aspartyl protease  $\beta$ -site APP cleaving enzyme 1 (BACE1) as responsible APP cleaving  $\beta$ -secretase (Hussain et al., 1999; Sinha et al., 1999; Vassar, 1999; Yan et al., 1999). Later, analysis of BACE1-knockout mice led to the final proof and revealed BACE1 as the exclusively responsible  $\beta$ -secretase in the brain (Cai et al., 2001; Luo et al., 2001). The knockout of BACE1 prevented A $\beta$  production and improved memory function in an AD mouse model (Munro et al., 2016; Ohno et al., 2006, 2007).

The  $\gamma$ -secretase complex is a multiprotein enzyme. It is composed of four proteins, presenilin-1 or-2, presenilin enhancer-2 (Pen2), anterior pharynx defective 1 (Aph1) and nicastrin. While Aph1, Pen2 and nicastrin are responsible for complex assembly and substrate recognition, the proteolytic activity of the  $\gamma$ -secretase complex is mediated by presenilin-1 or presenilin-2. Correct assembly of the four proteins is necessary for its activity (Wolfe, 2008).

According to the enrichment of active ADAM10 at the cell surface,  $\alpha$ -secretase cleavage of APP is mainly localised at the plasma membrane (Lammich et al., 1999; Parvathy et al., 1999). In contrast, BACE1 is mainly found in late secretory compartments and in endosomes, which provide an acidic pH that is favourable for BACE1 activity (H. Hook et al., 2002). This correlates with the fact that A $\beta$  production was mainly found in the endocytic pathway (Koo and Squazzo, 1994).

Despite a different cellular localisation of ADAM10 and BACE1, there is increasing evidence that the  $\alpha$ - and  $\beta$ -secretase compete for the initial APP cleavage step. This is supported by the finding that upregulation of ADAM10 activity in an AD mouse model increased sAPP $\alpha$  production, while at the same time reducing  $\beta$ -secretase-mediated A $\beta$  liberation and amyloid plaque formation (Postina et al., 2004). The other way around expression of catalytic inactive ADAM10 mutants reduced  $\alpha$ -secretase activity and shifted APP processing towards the  $\beta$ -secretase-mediated processing pathway, which increased A $\beta$  generation in AD mouse models (Postina et al., 2004; Suh et al., 2013).

In addition to the above described  $\alpha$ -,  $\beta$ - and  $\gamma$ -secretase cleavage events, recent studies reported the presence of further APP cleavage products, which are generated by a  $\delta$ - and a  $\eta$ -secretase (Fig. 1.3)(Willem et al., 2015; Zhang et al., 2015).

The asparagine endopeptidase (AEP) was identified as  $\delta$ -secretase and cleaves the ectodomain of APP at positions 585 and 373 (Zhang et al., 2015). Although both cleavage products can be further processed by the  $\alpha$ - and  $\beta$ -secretase, AEP cleavage at position 585 favours  $\beta$ -secretase-dependent APP processing and increases A $\beta$  liberation. Since an increased AEP expression and activity was observed during ageing and in AD brains, AEP is supposed to contribute to age-dependent mechanisms in AD development (Zhang et al., 2015).

The  $\eta$ -secretase cleavage of APP is mediated by membrane-bound matrix metalloproteinases, such as the membrane-type-5 matrix metalloproteinase (MT5-MMP), and occurs primarily at positions 504-505 of APP (Willem et al., 2015). The resulting  $\eta$ -CTF is also subject to  $\alpha$ - or  $\beta$ -secretase cleavage, resulting in the release of A $\eta$ - $\alpha$  and A $\eta$ - $\beta$  peptides, respectively. Interestingly, it was shown that  $\eta$ -secretase cleavage exceeds amyloidogenic APP processing in human neurons. Moreover, accumulation of  $\eta$ -CTFs in dystrophic neurites close to amyloid plaques was observed in the brains of AD patients and indicated its potential involvement in AD pathology (Willem et al., 2015).

### **1.3 Regulation of ADAM10 activity**

ADAM10 has a wide substrate spectrum, it is broadly expressed and shares several substrates with its close relative ADAM17 (Saftig and Reiss, 2011). ADAM10 and ADAM17 lack a definable consensus cleavage motif, but favour different amino acid residues at positions surrounding their cleavage sites. While ADAM10 prefers aromatic amino acid residues, ADAM17 favours cleavage sites with small aliphatic amino acids, in particular valine (Caescu et al., 2009; Tucher et al., 2014). Additionally, positioning of the cleavage site with regard to its distance to the plasma membrane influences substrate specificity for ADAM10 and ADAM17 (Riethmueller et al., 2016).

The regulation of ADAM10's proteolytic activity and substrate specificity plays an important role in physiological processes and decides about its function in health or disease. This is exemplified by the fact that an increased ADAM10 activity has beneficial effects in an AD

mouse model, whereas such an increased activity promotes cancer progression and prion spreading.

The functional analysis of the ADAM10 promoter region, revealed several transcription factor binding sites including retinoic acid response elements (RXR) and a X-box binding protein 1 (XBP1) binding site (Fig. 1.4)(Prinzen et al., 2005). Treatment with all-trans retinoic acid and a spliced variant of XBP-1 increased ADAM10 expression and substrate cleavage (Endres et al., 2005; Reinhardt et al., 2014; Tippmann et al., 2009). The retinoic acid derivate *acitretin* stimulates ADAM10 expression by releasing all-trans retinoic acid from the cellular retinoic acid binding protein (CRABP). It is used as a therapeutic drug in psoriasis (Olsen et al., 1989; Sue Lee and Koo, 2005). *Acitretin* is also currently tested in clinical trials for the treatment of Alzheimer's Disease (Endres et al., 2014; Tippmann et al., 2009).

In the nascent ADAM10 protein, the prodomain acts as an intrinsic inhibitor and prevents substrate and autocatalytic cleavage during transport. Interestingly, also expression of the prodomain alone inhibits ADAM10 activity (Moss et al., 2007). Moreover, proteins from the tissue inhibitor of metalloprotease (TIMP) family are natural occurring inhibitors for metalloproteases (Fig. 1.4). While TIMP-3 inhibits a broad range of ADAM proteases, TIMP-1 is more specific to ADAM10 (Amour et al., 2000). To date no inhibitor was found that exclusively inhibits ADAM10. A synthetic hydroxamate based inhibitor (GI254023X) selectively inhibits ADAM10 with a 100-fold higher affinity for ADAM10 than for ADAM17 (Fig. 1.4)(Hoettecke et al., 2010).

Trafficking of ADAM10 to the plasma membrane is another essential factor that determines ADAM10 activity by regulating access to its substrates. Within the cytosolic C-terminus of ADAM10 an arginine-rich sequence (RRR, Fig. 1.4) was found to limit ADAM10's exit from the ER. Mutating this sequence promotes trafficking to the cell surface (Marcello et al., 2010). Additionally, ADAM10 contains a proline-rich sequence in its cytoplasmic C-terminal domain, which can bind to the Src homology 3 (SH3) domain of proteins that are involved in membrane trafficking (Ebsen et al., 2014; Marcello et al., 2007). For example, ADAM10 interacts with the SH3 domain of the synaptic associated protein 97 (SAP97), which promotes trafficking of ADAM10 to synaptic membranes and increases APP  $\alpha$ -secretase activity (Fig. 1.4) (Marcello et al., 2007). Internalisation of ADAM10 from the plasma membrane represents another mechanism to control ADAM10 activity and is initiated by interaction of the ADAM10 C-terminal domain with the clathrin adaptor protein AP-2 (Fig. 1.4). Blocking ADAM10

endocytosis by expression of a dynamin-dominant negative mutant increases ADAM10 surface levels and APP shedding (Carey et al., 2005). Interestingly, in brains of AD patients an increased association of ADAM10 with AP-2 was observed (Marcello et al., 2013).

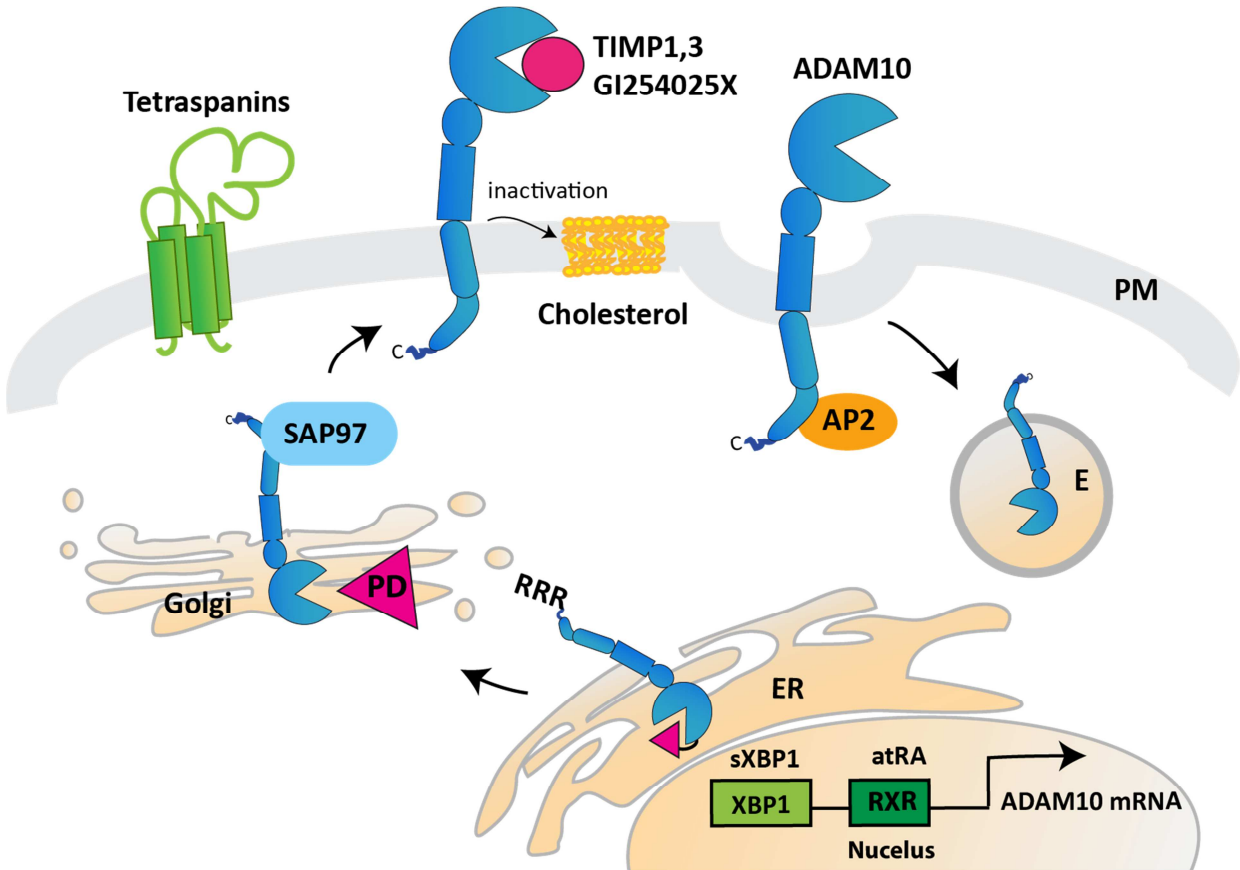


**Fig. 1.4: Regulation of ADAM10.**

Schematic representation of mechanisms that regulate ADAM10 transcription, trafficking and activity. The promoter region of ADAM10 in the nucleus (N) contains a X-box binding protein-1 (XBP1) binding motif and a retinoic acid response motif (RXR). Binding of spliced XBP1 (sXBP1) and all-trans retinoic acid (atRA) stimulates ADAM10 transcription. ADAM10 transport to the cell surface is limited by an ER retention motif (RRR). SAP97 interacts with ADAM10 via its Src homology 3 (SH3) domain and promotes ADAM10 surface trafficking. ADAM10 activity is inhibited by its prodomain (PD), the tissue inhibitor of metalloproteinase-1, -3 (TIMP-1, -3) and the synthetic hydroxamate-based inhibitor GI254025X. Internalisation of ADAM10 by association with the adaptor protein-2 (AP2) reduces ADAM10 activity and targets ADAM10 to clathrin-dependent endocytosis (E, endosome). Targeting ADAM10 to cholesterol-rich domains at the plasma membrane (PM), reduces its activity. Tetraspanins interact with ADAM10 and regulate its activity and substrate specificity (see section 1.4.2).

The activity of ADAM10 is also influenced by its membrane environment. Depletion of cholesterol stimulated ADAM10-mediated APP shedding in peripheral and neural cell lines (Kojro et al., 2001, 2010). On the contrary, targeting ADAM10 to lipid rafts, which are rich in cholesterol, by addition of a glycosylphosphatidylinositol (GPI)-anchor reduced its  $\alpha$ -secretase activity (Fig. 1.4)(Harris et al., 2009; Kojro et al., 2010).



Tetraspanins were discovered to associate with ADAM10 and to regulate ADAM10 activity and substrate specificity (Fig. 1.4) (Dornier et al., 2012; Haining et al., 2012; Prox et al., 2012). The regulation of ADAM10 by tetraspanins will be described in more detail in the next section.

## 1.4 Tetraspanins

Tetraspanins are a group of evolutionary conserved transmembrane proteins with a sequence length of 200-350 amino acids. They are characterised by four membrane spanning domains and form a small (SEL) and a large extracellular loop (LEL). The amino- and carboxyl-terminal ends remain in the cytosol (Fig. 1.5). Another structural characteristic of tetraspanins is the formation of 2-4 disulfide bonds in the LEL. This involves 4-8 cysteines with two of them located in a highly conserved CCG motif (Fig. 1.5A). Structure and sequence analysis of the LEL revealed a constant region, which was conserved among tetraspanins and a variable region. While the constant region contains a potential dimerisation interface, the variable region is important for the interaction of tetraspanins with other transmembrane proteins (Kitadokoro, 2001; Seigneuret et al., 2001; Yauch, 2000). The transmembrane domains also facilitate protein-protein interactions and stabilise the overall structure (Bienstock and Carl Barrett, 2001; Bassani and Cingolani, 2012).

Moreover, tetraspanins are subject to two major post-translational modifications. Tetraspanins contain N-glycosylation sites and are glycosylated at one or more positions in their large extracellular region (Boucheix and Rubinstein, 2001). Interestingly, all tetraspanins that were studied so far undergo palmitoylation at cytosolic cysteine residues close to the membrane (Fig. 1.5A). The covalent attachment of palmitate is critical for protein-protein interactions, in particular for interactions among different tetraspanins (Berditchevski et al., 2002; Charrin et al., 2002; Yang, 2002). Within the C-terminal tail, tetraspanins contain PDZ domain binding motifs, which can link them to PDZ domain containing proteins in the cytosol. Recently the first crystal structure of a human full length tetraspanin, CD81, was reported (Fig. 1.5B)(Zimmerman et al., 2016). It revealed a cone-like structure, where the transmembrane domains form an intramembrane cavity by converging close to the cytoplasmic site of the plasma membrane (Fig. 1.5B). The intramembrane cavity is capped by the large extracellular loop and is supposed to act as a cholesterol binding pocket (Fig. 1.5B)(Zimmerman et al., 2016). It was further shown that the presence of cholesterol led

to conformational changes in the CD81 structure, which modified the ability of CD81 to bind to its partner protein CD19 (Zimmerman et al., 2016).

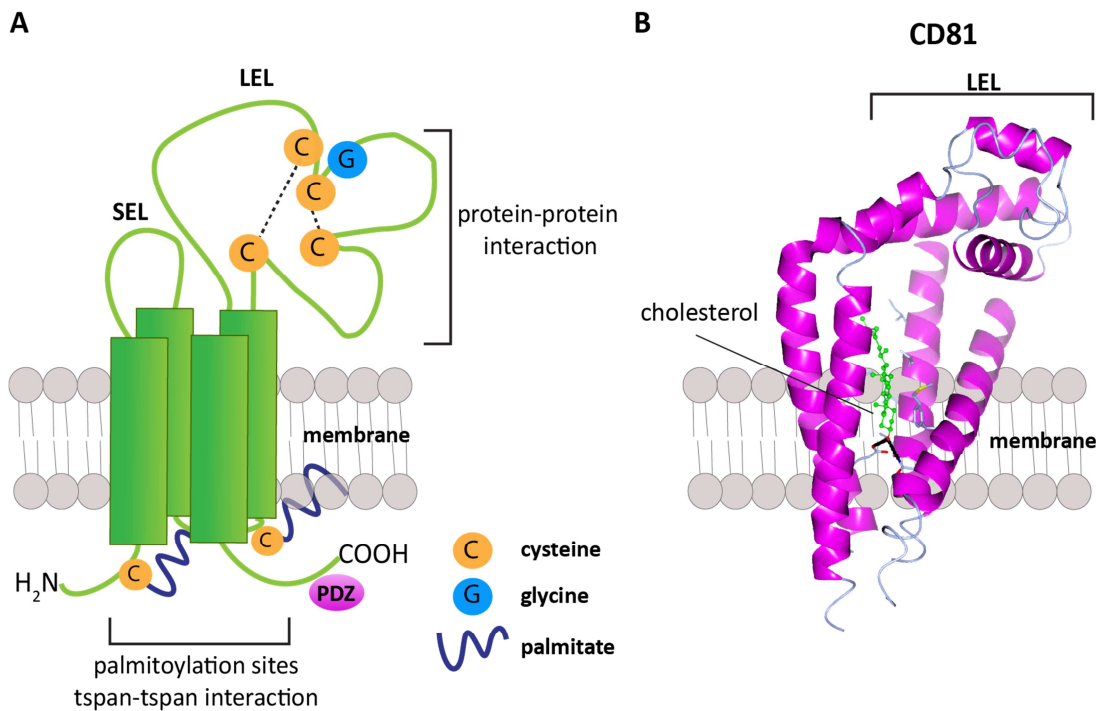


**Fig. 1.5: The structure of tetraspanins.**

**A)** Schematic drawing of the tetraspanin overall structure. Tetraspanins are characterised by four transmembrane domains and the formation of a small (SEL) and a large extracellular loop (LEL). The amino- and carboxyl terminus remain in the cytosol. The large extracellular loop contains a conserved CCG motif. Together with additional 2-8 cysteines, the CCG motif forms disulfide bonds (dashed lines), which gives the LEL a specific structure. The LEL and the transmembrane domains mediate protein-protein interactions. Intracellular cysteine residues are palmitoylated and are important for the interaction of tetraspanins with each other. Abbreviations: C, Cysteine; G, Glycine. **B)** Crystal structure of human CD81 (PDB entry: 5TXC). The four transmembrane domains form an intramembrane cavity, which contains a cholesterol molecule and is capped by the LEL. No electron density was observed for the SEL (Zimmerman et al., 2016).

Tetraspanins are widely distributed and were found in vertebrates, insects, plants, fungi and also in amoeba (Huang et al., 2005). In human, 33 members of the tetraspanin family were identified (Fig. 1.6). Tetraspanins were discovered in almost all cell and tissue types, ranging from 30,000 to 100,000 copies per cell (Hemler, 2005). However, the expression pattern of individual tetraspanins is very diverse. While some of them, such as CD81 and CD151, are present in almost all tissues, others have a restricted expression. For example CD37 and CD53 are only found in lymphoid cells, whereas Peripherin-2 (PRPH2) and ROM1 (rod outer segment membrane protein 1) are exclusively expressed in photoreceptors (Bascom et al., 1992; Boucheix and Rubinstein, 2001; Hemler, 2005; Van Soest et al., 1999). At a cellular level tetraspanins are mainly found at the plasma membrane and on endosomal/lysosomal

membranes. Additionally, tetraspanins are enriched in extracellular vesicles (exosomes), which are formed in multivesicular bodies and released upon fusion with the plasma membrane (Charrin et al., 2009; van Niel, 2006).

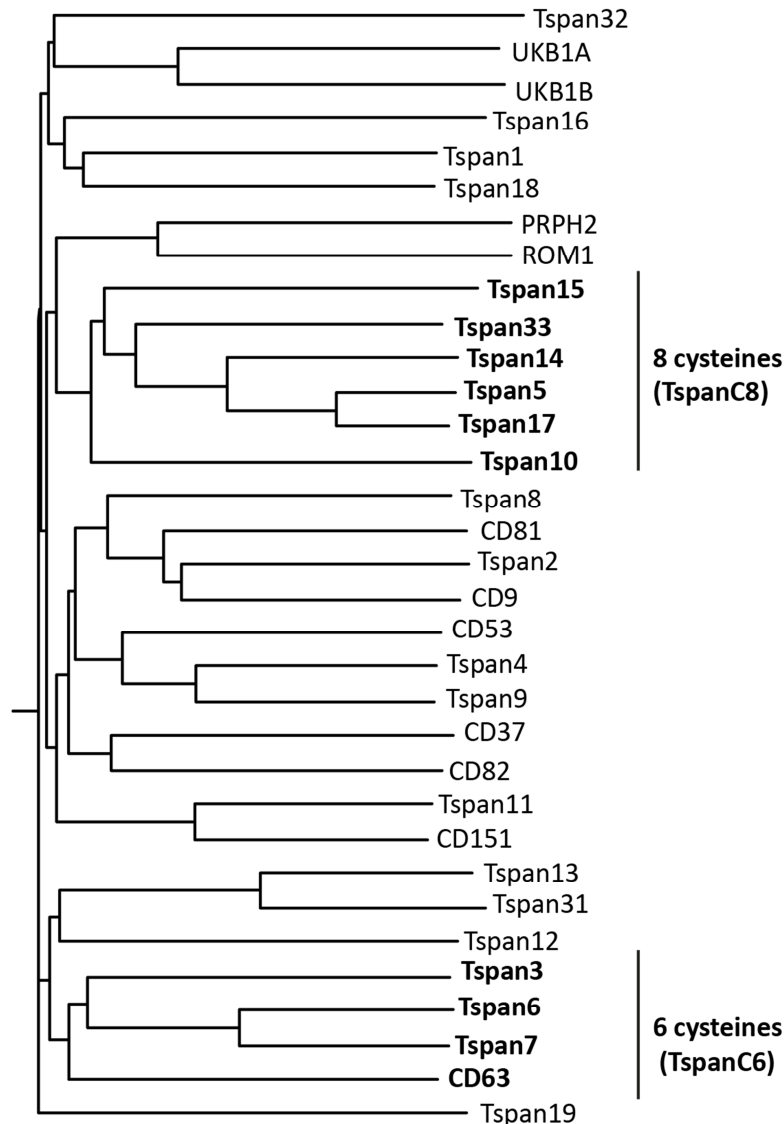


**Fig. 1.6: Phylogenetic tree of the 33 human tetraspanins.**

Sequence alignment of the 33 human tetraspanin amino acid sequences was performed with the multiple sequence alignment tool ClustalOmega (<http://www.ebi.ac.uk/Tools/msa/clustalo/>). Data is shown as dendrogram. Divergence of the human tetraspanins is indicated by the relative branch length. Tetraspanin subgroups with eight (C8) and six cysteines (C6) in their large extracellular region are highlighted in bold.

Through a wide-ranging network of interactions, including interactions with other tetraspanins and other integral membrane proteins, tetraspanins form tetraspanin-enriched microdomains (TEMs) within the membrane. TEMs represent platforms, where tetraspanins organise their partner proteins in functional complexes. Typical tetraspanin partner proteins are integrins, members of the immunoglobulin superfamily, signalling receptors and

ectoenzymes (Charrin et al., 2009). Similar to lipid rafts, TEMs contain lipids such as cholesterol and gangliosides (Charrin et al., 2003; Odintsova et al., 2006). Nevertheless, TEMs are physically and functionally different from lipid rafts and are regarded as a different type of microdomain (Hemler, 2005).

#### **1.4.1 Functions of tetraspanins**

One of the first identified, and in the meanwhile best-studied tetraspanins, is CD81. It was initially discovered as a tumour marker on human leucocytes (Takagi et al., 1995). Later, several other tetraspanins were identified and associated with cancer progression, invasion and metastasis (e.g. CD9, CD82 and CD151). This is mainly due to their ability to regulate cell migration and adhesion of cancer cells (Hemler, 2003; Tsai and Weissman, 2011; Wang et al., 2011). Increasing understanding of the tetraspanin biology in the recent years revealed further roles of tetraspanins in immune response, fertilization, pathogen infection and synapse formation (Hemler, 2005).

A striking feature of tetraspanins is their ability to interact with many different integral membrane proteins and their cellular function largely depends on the type of their partner protein. To regulate the function of their partner proteins, tetraspanins use two major mechanisms. (1) Tetraspanins regulate the cellular trafficking of their partner proteins either by modulating trafficking to the plasma membrane or internalisation from the plasma membrane by endocytosis. (2) Tetraspanins coordinate and stabilise their partner proteins in functional complexes at the plasma membrane (e.g. enzyme-substrate or ligand-receptor).

The interaction of tetraspanins with integrins is critical for cell adhesion and the strengthening of adhesion. For example, tetraspanin CD151 controls integrin-dependent cell migration by promoting the surface expression of the laminin receptor  $\alpha3\beta1$  integrin. CD151 also stabilizes  $\alpha3\beta1$  at the plasma membrane in an activated conformation and thereby contributes directly to integrin-dependent adhesion and cell motility (Nishiuchi et al., 2005).

In addition to integral membrane proteins, tetraspanins interact with intracellular signalling enzymes such as protein kinase C (PKC) and phosphoinositol 4-kinase (PIK4) and link extracellular molecules to intracellular signalling pathways. This is also exemplified by studies analysing the function of CD151, which links integrins to intracellular signalling by interaction with PKC and PIK4. Both, PKC and PIK4 are implicated in the regulation of the cytoskeleton architecture and contribute to the regulation of integrin-dependent cell morphology.

Similarly, CD81 overexpression, stimulates cell proliferation by activation of the extracellular signal-regulated kinase (ERK)/mitogen-activated protein kinase (MAPK) signalling pathway through increased association with PI4K in an integrin-dependent manner (Carloni et al., 2004).

Tetraspanins also directly coordinate receptor-ligand binding at the cell surface. Tspan3 facilitates binding of Nogo-A to the G-protein coupled receptor sphingosine-1-phosphate-receptor-2 (S1RP2) and stabilises this complex, which controls neurite outgrowth and cell spreading (Thiede-Stan et al., 2015). CD81 regulates B-cell activation and signalling by controlling surface expression of CD19, which is an important costimulatory molecule for B-cell receptor activation. In this context, a mutation of CD81 is directly linked to decreased surface levels of CD19 and was identified as the cause for immunodeficiency in a human patient with a defective humoral response (van Zelm et al., 2010; Vences-Catalán et al., 2015). An example for a PDZ domain interacting protein is Tspan7. Tspan7 interacts via its PDZ binding motif with protein interacting with C kinase 1 (PICK1). By limiting PICK1 accessibility for  $\alpha$ -amino-3-hydroxy-5-methyl-4-isoxazolepropionic acid (AMPA) receptors, which is necessary for AMPA receptor internalisation and recycling, Tspan7 regulates AMPA receptor trafficking and maturation of dendritic spines (Bassani et al., 2012).

Several tetraspanins contain potential sorting motifs in the C-terminus that can recruit intracellular adaptor proteins for clathrin dependent endocytosis (Berditchevski and Odintsova, 2007). A prominent example for this is CD63, which is one of the few, yet identified tetraspanins that is mainly found in endosomal/lysosomal compartments (Pols and Klumperman, 2009). By initiating internalisation of the membrane type-1 matrix metalloproteinase (MT1-MMP) and targeting it to lysosomal degradation, CD63 modulates the activity of MT1-MMP (Takino et al., 2003). In melanocytes, CD63 is involved in the endosomal sorting complex required for transport (ESCRT)-independent formation of intraluminal vesicles (ILVs). Furthermore, CD63 targets the luminal domain of the premelanosome protein (PMEL) to ESCRT-independent ILVs, which is important for melanosome biogenesis (van Niel et al., 2011). Moreover, loss of CD63 in mice caused an accumulation of lamellar bodies in cells of the collective duct and led to an impaired water balance (Schroder et al., 2009).

Besides MT1-MMP, also other membrane proteases are regulated by tetraspanins, including members of the matrix metalloproteases, members of the ADAM family and the  $\gamma$ -secretase

complex. Through direct and indirect interactions tetraspanins regulate the activity of membrane proteases by modulating their surface expression and accessibility to specific substrates at the cell surface (Yáñez-Mó et al., 2011).

The physiological function of tetraspanins was addressed by loss-of-function studies. In mice, CD151 is critical for lymphocyte proliferation and platelet clotting. CD9 knockout mice displayed defective sperm-egg fusion, brain and peripheral nerve defects. CD81 is associated with immune regulation, brain enlargement and malaria infection. Despite these findings most tetraspanin loss-of-function studies remained less conclusive, due to functional redundancy and possible compensation by other tetraspanins (Hemler, 2005).

In human, mutations in the Tspan7 gene are associated with X-linked retardation and Peripherin-2 and ROM1 mutations are frequently found in retinal disorders (Kajiwara et al., 1994; Kohl et al., 1997; Zemni et al., 2000). Moreover, CD151 is associated with skin, kidney and platelet malfunctions, deafness and  $\beta$ -thalassemia (Crew et al., 2004; Kagan et al., 1988).

#### **1.4.2 Tetraspanins as regulators of ADAM10**

Several tetraspanin have been identified to associate with ADAM10 and came into focus as potent regulators for ADAM10-mediated shedding processes.

Initially, CD9, CD53, CD81, CD82 and CD151 were identified to associate with ADAM10 under mild detergent conditions. Specific antibodies directed against these tetraspanins stimulated ADAM10 activity towards tumour necrosis factor  $\alpha$  (TNF $\alpha$ ) and epidermal growth factor (EGF) (Arduise et al., 2008a). Tspan12 was also discovered as an ADAM10-interacting tetraspanin (Xu et al., 2009). Overexpression of Tspan12 promoted ADAM10 maturation and  $\alpha$ -secretase cleavage of APP most likely by accelerating ADAM10 activation through proprotein convertases and stabilisation of mature ADAM10 at the cell surface (Xu et al., 2009).

Under stringent detergent conditions, the interaction of ADAM10 with CD9, CD81, CD82 CD63 and CD151 could not be validated (Dornier et al., 2012). Therefore the previous reported interactions were considered as indirect interactions, which are mediated by the tetraspanin-tetraspanin network (Dornier et al., 2012). However, these studies also revealed a certain subgroup of conserved tetraspanins as direct interaction partners of ADAM10 (Dornier et al., 2012; Haining et al., 2012; Prox et al., 2012). This subgroup comprises six members (Fig. 1.6), Tspan5, Tspan10, Tspan14, Tspan15, Tspan17 and Tspan33, which share the feature of

containing eight cysteines in their large extracellular loop. They are therefore referred to as TspanC8 tetraspanins (TspanC8, see Fig. 1.6).

Overexpression of Tspan5, Tspan14, Tspan15, Tspan33 led to an increased maturation of ADAM10 in *Drosophila melanogaster*, human and murine cells (Dornier et al., 2012; Haining et al., 2012; Prox et al., 2012). Additionally, all of these tetraspanins increased the surface expression of ADAM10. Tspan15 promoted ADAM10 maturation and trafficking by accelerating ADAM10's ER exit (Prox et al., 2012). In contrast to the other TspanC8 members, Tspan10 and Tspan17 overexpression had no or only a moderate effect on ADAM10 maturation, but initiated a redistribution of surface ADAM10 into endosomal compartments (Dornier et al., 2012).

In correlation with the increased maturation and surface trafficking of ADAM10, expression of TspanC8 tetraspanin also enhanced the shedding of certain substrates such as N-cadherin, APP and Notch (Dornier et al., 2012; Jouannet et al., 2015; Prox et al., 2012). Interestingly, it became evident that TspanC8 tetraspanins differentially regulate cleavage of ADAM10 substrates in a cell type-dependent manner. The diverse effects of TspanC8 tetraspanins on ADAM10-mediated substrate cleavage, observed by overexpression and knockdown experiments in different cell lines, are summarised in the following table (Tab. 1.2).

Although tetraspanins came into focus as potent regulators for ADAM10 activity and substrate specificity, the mechanism how tetraspanins regulate ADAM10 activity and shedding of different substrates is largely unknown.

**Tab. 1.2: Diverse effects of TspanC8 tetraspanins on ADAM10-mediated substrate cleavage.**

<b>TspanC8</b>	<b>Effect on ADAM10 substrate</b>	<b>Cellular system</b>	<b>Reference</b>
<b>Tspan5</b>	• promotes CD44 shedding	PC3	(Jouannet et al., 2015)
	• Stimulates Notch activity	HeLa/U2OS-1/PC3 Osteoclasts	(Dornier et al., 2012; Jouannet et al., 2015) (Zhou et al., 2014)
<b>Tspan10</b>	• Increases Notch activity	Osteoclasts	(Zhou et al., 2014)
<b>Tspan14</b>	• Reduces glycoprotein VI (GPVI) shedding	HEK293T	(Noy et al., 2016)
	• Slightly reduces APP shedding	U2OS-N1	(Jouannet et al., 2015)
	• Increases Notch activity	HeLa/U2OS-N1	(Dornier et al., 2012)

<b>TspanC8</b>	<b>Effect on ADAM10 substrate</b>	<b>Cellular system</b>	<b>Reference</b>
<b>Tspan15</b>	<ul style="list-style-type: none"> <li>Increases APP shedding</li> <li>Promotes N-cadherin cleavage</li> <li>Reduces APP shedding</li> <li>Negative regulator of Notch activity</li> </ul>	N2a/HEK293T Cos7/HEK293/PC3 U2OS-N1 U2OS-N1/PC3	(Prox et al., 2012) (Jouannet et al., 2015; Noy et al., 2016; Prox et al., 2012) (Jouannet et al., 2015) (Jouannet et al., 2015)
<b>Tspan17</b>	<ul style="list-style-type: none"> <li>Not characterised</li> </ul>	-	-
<b>Tspan33</b>	<ul style="list-style-type: none"> <li>Negative regulator of Notch activity</li> <li>(slightly) reduces APP shedding</li> </ul>	U2OS-N1	(Jouannet et al., 2015)



## 2 Objectives

Despite a rapidly growing substrate spectrum and the increasing understanding of ADAM10 functions, the mechanisms that regulate its activity towards specific substrates are still elusive. Tetraspanins came into focus as important regulators of ADAM10 activity and substrate specificity. However, their mode of action and their physiological function for ADAM10-mediated shedding events are barely understood.

In a yeast two-hybrid interaction screen the tetraspanin proteins Tspan3 and Tspan15 were identified as two novel ADAM10 interaction partners. The function of Tspan15 for ADAM10 was further described in cell-based experiments and revealed it as a potent regulator of ADAM10 activity (Prox et al., 2012). The function of Tspan3 as an ADAM10-interacting protein is not yet described.

The central aim of the present thesis was to characterise the function of Tspan3 as a novel ADAM10 interaction partner. To unravel the role of Tspan3 as ADAM10 interaction partner, the Tspan3-ADAM10 interaction should first be verified in a mammalian cell system. Furthermore, overexpression and knockdown approaches were used to analyse the possible influence of Tspan3 on ADAM10 and ADAM10-mediated shedding processes. In addition, the function of Tspan3 was investigated *in vivo*. Therefore, a Tspan3 knockout mouse model was generated and analysed using biochemical and histological methods.

Another objective of this project was the characterisation of Tspan15 as an ADAM10 regulator *in vivo*. To gain insight into the physiological function of Tspan15, Tspan15-deficient mice should be generated and phenotypic alterations assessed with special regards to ADAM10-related functions.

By giving further insight into the function of Tspan3 and Tspan15 as interaction partner of ADAM10, this thesis aims to improve the understanding how tetraspanins modulate ADAM10-mediated shedding events. Moreover, loss-of-function studies should reveal the physiological importance of Tspan3 and Tspan15 and provide insight into the role of Tspan3 and Tspan15 as potential therapeutic targets.



## 3 Material and Methods

### 3.1 Materials

#### 3.1.1 Chemicals

If not stated differently, all chemicals were purchased from AppliChem, Carl Roth, Sigma-Aldrich or Merck with the purity grade *pro analysi* (p.a.).

#### 3.1.2 Antibodies

Tab. 3.1: List of primary antibodies

Antigen	Host	Application (dilution)	No.	Reference
Actin	Rabbit	IB (1:2500)	A2066	Sigma-Aldrich
ADAM10 (C-term.)	Rabbit	IB (1:1000)	EPR5622	Abcam
ADAM10 (C-term.)	Rabbit	IP (1:500)	Pin-1	Pineda
ADAM10 (N-term.)	Rat	FACS (1:500)	MAB946	R&D Systems
ADAM17	Mouse	IB (1:1000)	A300D	(Trad et al., 2011)
APP (C-term.)	Rabbit	IB (1:1000)	A8717	Sigma-Aldrich
A $\beta$ /sAPP $\alpha$ (9E10)	Rabbit	IB (1:500)	SIG-39151	Covance
APP (C-term.)	Rabbit	IB (1:5000)	B63.2	Wim Aennert, Leuven, Belgium
EEA1	Rabbit	IF (1:200)	Ab6319	Cell Signaling Technology
GAPDH	Rabbit	IP (1:2500)	FL-335	Santa Cruz Biotechnology
KDEL	Mouse	IF (1:500)	10C3	Enzo
LAMP-2	Mouse	IF (1:300)	H4B4	DSHB
LIMP-2	Rabbit	IF (1:500)	L2T2	(Trad et al., 2011)
Myc	Mouse	IB (1:2500) IF (1:300)	9B11	Santa Cruz
Myc	Goat	IP (1:500)	GTX30518	GeneTex
NeuN	Mouse	IHC (1:500)	MAB377	Millipore
N-Cadherin	Mouse	IB (1:1000)	610921	BD Transduction Laboratories
PDI (A6)	Rabbit	IF (1:500)	ab11432	Abcam

Antigen	Host	Application (dilution)	No.	Reference
Prion Protein (PrP <sup>c</sup> )	Mouse	IB (1:2500)	POM1	<i>Prof. Dr. A. Aguzzi, Zürich, Switzerland</i>
Shed PrP <sup>c</sup> (shPrP <sup>c</sup> )	rabbit	IB (1:500)	shPrP	<i>Prof. Dr. M. Glatzel, Hamburg</i>
Presenilin-1 NTF	Rat	IB (1:500)	D39D1	Millipore
Rab5	Mouse	IB (1:1000) IF (1:100)	18258	Synaptic Systems
Tspan15	Rabbit	IB (1:2500) IF (1:300)	1-92540	Novusbio
Tspan3 (C-term.)	Rabbit	IB (1:1000)	-	Pineda antibody service
Beta-Tubulin	Mouse	IB (1:2500)	E7	DSHB

Dilution factors refer to usage for immunoblot (IB), immunoprecipitation (IP), immunofluorescence staining (IF) or fluorescence activated cell sorting (FACS)

**Tab. 3.2: List of secondary antibodies**

Antibody	Conjugated to	Host	No.	Reference
Anti-mouse	Horseradish peroxidase	Sheep	515-035-062	Dianova
Anti-rabbit		Goat	111-035-144	
Anti-rat		Goat	112-035-143	
Anti-rabbit	ALEXA Fluor®-488	Goat	A11034	Thermo Fischer Scientific
		Donkey	A21206	
Anti-mouse		Goat	A11029	
Anti-rabbit	ALEXA Fluor®-594	Goat	A11037	
		Donkey	A21207	
Anti-mouse		Goat	A11032	
		Donkey	A21203	

### 3.1.3 Cell culture media and additives

Dulbecco's Modified Eagle Medium (DMEM)	Life Technologies
Fetal calf serum (FCS)	Biochrom
Penicillin/Streptomycin	Life Technologies
Trypsin/ Ethylenediaminetetraacetic acid (EDTA)	Sigma-Aldrich
G418 (Geneticin, 100mg/ml)	Invivo Gen

Polyethylenimine Max MW 40000 (PEI)	Polysciences
INTERFERin®	Polyplus
Trypan blue	Life Technologies
GI254023X	Iris Biotech
InSolution™ Inhibitor X	Calbiochem
β-secretase inhibitor IV (C3)	Calbiochem
Marimastat	Sigma-Aldrich

### 3.1.4 Kits

PureYield™ Midiprep	Promega
NucleoSpin® RNA plus kit	Machery-Nagel
RevertAid First Strand cDNA Synthesis Kit	Thermo Fisher Scientific
Pierce™ BCA Protein Assay Kit	Thermo Fisher Scientific
Lumigen® ECL Ultra (TMA-6)	Lumigen Inc.

### 3.1.5 DNA and protein standards

GeneRuler 100 bp DNA ladder	Thermo Fisher Scientific
GeneRuler 1 kB DNA ladder	Thermo Fisher Scientific
PageRuler Plus Prestained Protein Ladder	Thermo Fisher Scientific
Spectra™ Multicolor Low Range Protein Ladder	Thermo Fisher Scientific

### 3.1.6 Enzymes

DpnI (10 U/l)	Thermo Fisher Scientific
<i>Pfu</i> DNA polymerase (2.5 U/l)	Thermo Fisher Scientific
Proteinase K	Roche
DreamTaq™ DNA Polymerase (5U/l)	Thermo Fisher Scientific

### 3.1.7 Oligonucleotides

**Tab. 3.3: Oligonucleotides used for genotyping, mutagenesis PCR and sequencing**

Name	Oligonucleotide sequence 5'-3'
Tspan3 exon2 forward	GGGACTCAAACCAAGTGTTTC
Tspan3 exon2 reverse	CCAAGACATCTACATCTACAG

Name	Oligonucleotide sequence 5'-3'
Tspan15 exon2 forward	AAGCTTGGGCTATAGGCATACACC
Tspan15 exon2 reverse	GGATCCCCAGCATCTCTGTGACAGC
Tspan3 Y243A forward	CAGTGATGAGGAGCTCAGCGGCAGGATCTCTACTCC
Tspan3 Y243A reverse	GGAGTAGAGATCCTGCCGCTGAGCTCCTCATCACTG
pFrog3_seq forward	GAGACTCCATTTCGGGTGTTCT

**Tab. 3.4: Oligonucleotides and hydrolysis probes (UPL, Roche) used for qRT-PCR**

Gene	Species		Oligonucleotide sequence 5'-3'	UPL
<i>Adam10</i>	murine	left	GGGACACTCCCTTTTATAGTA	47
		right	ACCCATGACTAAAGCTTCCTTCT	
<i>Tspan3</i>	human	left	CTGTGGACTTGCCACGTTTGCA	15
		right	ATGCTGCGATCAACCTCATT	
<i>TSPAN5</i>	human	left	GGGAAAACACTTTCCTTCTCAAG	1
		right	CTTTGAAAACAAATGCTAGAACTCC	
<i>Tspan5</i>	murine	left	TGCACAGATTCCAATGCAAG	18
		right	CCTGGCATCATAGCCACAC	
<i>TSPAN6</i>	human	left	CTTTGGAGTTGCTTGCTTCC	34
		right	TTGGGTTACACTATCTCATACTGGTT	
<i>Tspan6</i>	Murine	left	ACACGGGCTCATATCTCCTC	58
		right	GCTTTTCAGGCTAAGCAGATG	
<i>TSPAN7</i>	human	left	CATCTACTCCTTCGTCTTCTGGA	18
		right	AGTAAGTTTGCCCCAGACTCC	
<i>Tspan7</i>	murine	left	ACCAGTTTTATGGAGACTAACATGG	67
		right	AGCAGCATGCCAATCAACT	
<i>TSPAN12</i>	human	left	TCTCACTTTAACTGCAGAAACGA	38
		right	TCATGACCGGATGAACCAC	
<i>Tspan12</i>	murine	left	TGTGTGTCCCCGACTGTTC	51
		right	CCCATCCTCTCACCACATTC	
<i>CD63</i>	human	left	GAATGAAATGTGTGAAGTTCTTGC	18
		right	GCAATCAGTCCCACTGCAC	
<i>Cd63</i>	murine	left	TGAAGTGTGTCAAGTTTTTGCTC	2
		right	ACCAATGGCGATCAATCC	

### 3.1.8 siRNA

**Tab. 3.5: List of used siRNAs**

siRNA target	Name	No.	Source
Human ADAM10	Stealth RNAi™ siRNA	#1320001	Thermo Fisher Scientific
Human Tspan3	ON-TARGETplus® smart pool	#10099	GE Healthcare Dharmacon

### 3.1.9 Plasmids and expression constructs

In this work, the eukaryotic expression vectors pcDNA3.1+ (Thermo Fisher Scientific), pfrog3 (*Prof. Dr. Dr. T. J. Jentsch*, ZMNH, Hamburg) and pcl-neo (Promega) were used. The pcDNA3.1 and pcl-neo vector have a size of 5.4 kb and contain a multiple cloning site and a CMV-promotor for strong, constitutive expression. Both vectors contain an ampicillin resistance gene for prokaryotic selection and the sequence of a neomycin resistance gene for selection of stable transfected eukaryotic cell lines. The pFrog3 vector was generated by modification of the pcDNA3.1 vector and contains the 5'- and 3'-untranslated region of the  $\beta$ -globin gene (*Xenopus laevis*) and the coding sequence for a myc-tag.

**Tab. 3.6: List of plasmids and expression constructs**

Plasmids	Insert	Reference
pcDNA3.1+	-	Thermo Fisher Scientific
pFrog3	-	(Gunther et al., 1998)
pcDNA3.1-mADAM10	Murine ADAM10	(Reiss et al., 2005)
pFrog3-mTspan3-myc	Murine Tspan3 C-terminal myc-Tag	(Seipold et al., 2017)
pFrog3-mTspan3 <sub>Y243A</sub> -myc	Murine Tspan3 <sub>Y243A</sub> C-terminal myc-Tag	(Seipold et al., 2017)
pFrog3-mTspan15-myc	Murine Tspan15 C-terminal myc-Tag	(Prox et al., 2012)
pcl-neo-hAPP695	Human APP695	(Choy et al., 2012)

### 3.1.10 Cell lines

**Tab. 3.7: List of used cell lines and bacteria strains**

Cell line	Description	Reference
HeLa	Human cervix carcinoma cells (Henrietta Lachs, HeLa)	DMSZ, Braunschweig, Germany
HEK293	Human embryonic kidney cells	DKFZ, Heidelberg, Germany
HEK293 APP-wt	HEK293 cells overexpressing human APP695	(Haass et al., 1993)
HEK293 APP-swe	HEK293 cells overexpressing Swedish mutant human APP695-swe	(Citron et al., 1992)
HEK293 ADAM10 <i>-/-</i>	ADAM10 deficient HEK293 cells	(Riethmueller et al., 2016)
HEK293 ADAM17 <i>-/-</i>	ADAM17 deficient HEK293 cells	(Riethmueller et al., 2016)
Neuro2a (N2a)	Murine neuroblastoma cells	(Olmsted et al., 1970)
SH-SY5Y	Human neuroblastoma cells	(Biedler et al., 1978)
<i>E. coli</i> XL-1 blue	<i>Escherichia coli</i> XL1-blue	Agilent Technologies

### 3.1.11 Transgenic mouse lines

**Tab. 3.8: List of transgenic mouse lines**

Mouse strain	Mutation	Reference
Tspan3X46	Insertion of 26 bp in <i>Tspan3</i> exon2	(Seipold et al., 2017)
Tspan15 $\Delta$ 104	Deletion of 104 bp in <i>Tspan15</i> exon2	-

### 3.1.12 Frequently used buffers and solutions

**Tab. 3.9: List of frequently used buffers and solutions**

Buffer	Ingredients
Lysogeny broth (LB) medium	1% Trypton/Pepton (w/v) 1% NaCl (w/v) 0.5% Yeast extract pH 7.0
LB agar	1.5% Agar-agar in LB medium



Buffer	Ingredients
Mounting solution	PBS pH 7.4 17% (w/v) Mowiol 4-88 33% (v/v) Glycerol 20 mg/ml DAPCO (1,4-Diaza-bicyclo-[2,2,2]-octane)
Phosphate buffered solution (PBS)	137 mM NaCl 2.7 mM KCl 4.3 mM Na <sub>2</sub> HPO <sub>4</sub> 1.4 mM KH <sub>2</sub> PO <sub>4</sub> pH 7.4
Phosphate buffer (PB)	10% (v/v) 0.2 M NaH <sub>2</sub> PO <sub>4</sub> 81% (v/v) 0.2 M Na <sub>2</sub> HPO <sub>4</sub> pH 7.4

## 3.2 Molecular biological methods

### 3.2.1 Generation of chemically competent *E. coli*

Tris-buffered saline (TBS)                      0.2 M Glycine  
0.1% (w/v) SDS  
1% (v/v) Tween® 20  
pH 2.2

CaCl<sub>2</sub> solution                                    0.1 M CaCl<sub>2</sub>  
5 mM Tris  
5 mM MgCl<sub>2</sub>  
pH 7.0

To facilitate transformation of plasmid DNA into *E. coli* XL-1 blue bacteria, chemically competent bacteria cells were generated. *E. coli* XL-1 blue bacteria were grown in 5 ml LB media, supplemented with the selection antibiotic tetracycline (20 mg/ml), at 37°C overnight. The next day, 50 ml of LB media, containing 50 µl tetracycline, were inoculated with 500 µl of the bacteria suspension and cultivated for 3 h at 37°C under continuous shaking. Afterwards, the bacteria suspension was chilled on ice for 20 minutes and cells were collected by

centrifugation at 5000 x g and 4°C for 15 minutes. The cell pellet was washed with 20 ml sterile TBS followed by another washing step with 20 ml of ice-cold CaCl<sub>2</sub> solution. After 20 minutes on ice, the cells were again pelleted by centrifugation at 5000 x g for 10 minutes and resuspended in 2 ml CaCl<sub>2</sub> solution, containing 20% (v/v) glycerol. Finally, 50 µl aliquots were prepared and bacteria stored at -80°C.

### **3.2.2 Transformation of chemically competent *E. coli***

Transformation of plasmid DNA into *E. coli* XL-1 blue was conducted by heat-shock treatment of chemically competent *E. coli* XL-1 blue bacteria (see 3.2.1). Therefore, 50 µl of *E. coli* XL-1 blue bacteria were thawed and incubated with 1 µl plasmid DNA for 5 minutes on ice. To enable uptake of the plasmid DNA into the bacteria, the cells were subjected to heat-shock for 30 seconds at 42°C, followed by incubation for 5 minutes on ice. The bacteria cells were incubated with 300 µl LB media for 30 minutes at 37°C and 20-100 µl of the suspension were plated on LB agar plates, containing the respective selection antibiotic (ampicillin, 50 µg/ml). Growth of bacteria was monitored after incubation at 37°C overnight.

### **3.2.3 Amplification and isolation of plasmid DNA from *E. coli***

To obtain large amounts of plasmid DNA for transfection of mammalian cells, expression plasmids were transformed into *E. coli* XL-1 blue bacteria (see 3.2.2). Single bacteria clones were picked from the LB agar plate and transferred into 200 ml LB media supplemented with the appropriate selection antibiotic (ampicillin, 50 µg/ml). The suspension was incubated at 37°C overnight under continuous shaking and plasmid DNA was purified by using the DNA isolation PureYield™ Plasmid Midiprep system according to the manufacturer's instructions.

### **3.2.4 Determination of nucleic acid concentration**

The concentration of DNA and RNA in aqueous solutions was determined by measurement of the absorbance (A) at a wavelength of 260 nm using a Synergy HT (BioTek) microplate reader. To control for protein contaminations the absorbance at a wavelength of 280 nm was measured and the A<sub>260</sub>/A<sub>280</sub> ratio was calculated. At a value of 1.8 for DNA and around 2.0 for RNA, the nucleic acid solution was assumed as pure.

### 3.2.5 Polymerase chain reaction (PCR)

The polymerase chain reaction (PCR) is a technique used for sequence specific amplification of DNA fragments *in vitro*. The starting point for DNA amplification is defined by oligonucleotides (primers) that are complementary to the 3' end of the sense (forward) and antisense (reverse) strand of the targeted DNA region. A mixture of template DNA, a thermostable DNA polymerase, reaction buffer and deoxynucleotides (dNTPs) is prepared. After an initial denaturation step, exponential DNA amplification is achieved by repetitive cycles of denaturation, annealing and elongation. Thereby, the DNA double strands are separated by heating at 95°C (denaturation), which enables primers to hybridize with the single stranded template DNA (annealing) at a primer specific temperature. Following, the DNA polymerase synthesizes the complementary DNA strands in 5' to 3' direction by extension of primer sequences (Elongation). The PCR is then finished by a final elongation step and cooling to 10°C.

#### 3.2.5.1 Generation of Tspan3<sub>Y243A</sub>-myc by mutagenesis PCR

To introduce a mutation in the Tspan3 DNA sequence, which results in an amino acid exchange of tyrosin<sub>243</sub> to alanine, a primer pair (Tab. 3.3) containing the required nucleic acid changes (TA<sub>728</sub>GC) was designed with the aid of the QuickChange Primer Design Tool (Agilent Technologies). Using the pFrog3-mTspan3-myc plasmid as a template, the PCR reaction mix was prepared according to the pipetting scheme (Tab. 3.10).

Tab. 3.10: Pipetting scheme for mutagenesis PCR

	Volume (µl)
Primer forward [20 µM]	1.13
Primer reverse [20 µM]	1.13
10x <i>Pfu</i> buffer (10x)	10
dNTPs [2 mM]	6.3
<i>Pfu</i> Polymerase	1
DMSO	2.5
Plasmid DNA	500 ng
Add H <sub>2</sub> O	50

Tab. 3.11: Program for mutagenesis PCR

Step	t (min)	T (°C)	Cycles
Initial denaturation	3	96	1
Denaturation	1	96	
Annealing	1	55	12
Elongation	15	68	
End	∞	10	1

Whole plasmid PCR amplification was performed using the mutagenesis PCR program (Tab. 3.11). Thereafter, the remaining template DNA was degraded by incubation with 1 µl of the restriction enzyme DpnI for 1 h at 37°C. The newly synthesised pFrog3-Tspan3<sub>Y243A</sub>-myc

plasmid DNA was transformed into *E. coli* (see 3.2.2) and subjected to sequence analysis (see section 3.2.7).

### 3.2.6 Agarose gel electrophoresis

<u>50x Tris-acetate-EDTA (TAE) buffer</u>	2 M Tris/ HCl pH 8.0
	5.5% (v/v) Acetic acid
	50 mM EDTA

To analyse DNA fragments according to their length, agarose gel electrophoresis was performed. Therefore, DNA samples were mixed with 6x DNA loading dye (Thermo Fisher Scientific) and loaded onto an agarose gel. Depending on the expected size of DNA fragments, 1-2% (w/v) agarose was dissolved in 1x TAE buffer supplemented with 333 ng/ml ethidium bromide. DNA samples were separated for 30 minutes at a voltage of 120 V and visualised under UV light ( $\lambda=312$  nm). The length of DNA fragments was estimated by comparison to the distinct signals of a 100 bp or 1 kb DNA standard ladder (see 3.1.5).

### 3.2.7 Sequence analysis

To analyse the sequence of DNA samples, sequencing was performed by GATC Biotech (Konstanz, Germany) using the Sanger chain-termination method (Sanger et al., 1977). The starting point was defined by appropriate primers, covering the desired sequence (Tab. 3.3). Sequencing results were further analysed with the sequence alignment tool SerialCloner 2.6.1 (SerialBasics).

### 3.2.8 Split-Ubiquitin yeast two-hybrid interaction screen

To screen for novel ADAM10 interaction partner a split-ubiquitin yeast two-hybrid interaction screen (MoBiTec) was performed by *Dr. Johannes Prox* as previously described (Prox et al., 2012). According to the manufacturer's instructions, murine ADAM10 cDNA was C-terminal fused to the C-terminal part of Ubiquitin (Cub) and an artificial transcription factor LexA-VP16. The ADAM10-Cub-LexA-VP16 was cloned into a yeast expression vector (pTMBV4) and expression in NMY51 yeast was monitored on selective media plates using a positive (Nubl) and a negative control (NubG) as supplied by the manufacturer. As prey constructs, cDNAs from a murine brain library (MoBiTec) N-terminally fused to N-terminal part of mutated Ubiquitin (NubG) were used. The ADAM10 bait construct was co-transfected with

prey constructs into NMY51 yeast and seeded onto selective media plates lacking leucine, tryptophan and histidine. After incubation for 3-5 days at 30°C clones were selected and expanded. Prey plasmids were isolated and subjected to sequence analysis.

### 3.2.9 Total RNA extraction

For the extraction of total RNA from cells and organs, the NucleoSpin® RNA kit (Macherey Nagel) was used. Cells were washed twice with PBS, detached from the cell culture dish and harvested by centrifugation at 3000 x g for 10 minutes. The cell pellet was resuspended in 350 µl of the kit's lysis buffer and further processed according to the manufacturer's protocol. For RNA isolation from organs, 350 mg of the organ were taken and disrupted with 350 µl lysis buffer together with 3-4 porcelain beads using a Precellys® homogenizer (Bertin Corp.) for two times 30 seconds at 6000 rpm. Further steps were performed according to the manufacturer's instructions.

### 3.2.10 cDNA synthesis

To transcribe the isolated RNA (see 3.2.9) into complementary DNA (cDNA) the RevertAid™ First Strand cDNA Synthesis Kit (Thermo Fisher Scientific) was used. Following the manufacturer's protocol, 0.5-1 µg of extracted RNA were subjected to reverse transcription using random hexamer primer.

### 3.2.11 Quantitative real-time PCR (qRT-PCR)

The expression levels of certain genes were analysed by quantitative real-time PCR (qRT-PCR) using the Universal ProbeLibrary Technology System (UPL, Roche). The UPL system makes use of small hydrolysis probes, consisting of a short oligonucleotide, which hybridizes with the target sequence and is fused to a reporter fluorescein at the 5' end and to a dark quencher dye at the 3' end. Due to the 5' to 3' exonuclease activity of the DNA polymerase, the reporter is released from the quencher during PCR-based sequence amplification and emits fluorescence light. The fluorescence signal can be detected and correlates with the number of transcripts.

To design gene specific assays, primer pairs were designed with the UPL Assay Design Centre (Roche) and appropriate UPLs were used (Tab. 3.4). The samples were prepared as triplicates in a reaction volume of 10 µl using 0.5 µL cDNA, 0.1 µM UPL, 0.3 µM of each primer (left and

right) and 1x LightCycler® 480 Probes Master (Roche), containing reaction buffer, a Taq polymerase, dNTPs and MgCl<sub>2</sub>. After mixing, samples were measured on a LightCycler® 480 real-time PCR instrument (Roche). Additionally, primer efficiency ( $E=10^{-1/\text{slope}}$ ) was determined by analysis of serial cDNA dilutions.  $\Delta C_t$  were calculated by normalisation of sample  $C_t$  values to  $C_t$  values of stably expressed housekeeping genes (*GAPDH*, *actin*) and relative mRNA levels calculated taking the primer efficiency ( $E^{-\Delta C_t}$ ) into account. Statistical analysis was performed on  $E^{-\Delta C_t}$  values.

### 3.3 Cell biological methods

#### 3.3.1 Maintenance of cell lines

##### Cell culture media

DMEM only

10% (v/v) FCS

1% (v/v) penicillin/streptomycin

All cells were cultured in DMEM (Life Technologies) with 10% fetal calf serum (FCS) supplemented with 1% penicillin/streptomycin at 37°C, 5% CO<sub>2</sub> atmosphere and 95% relative humidity. HEK293 cells stably overexpressing human APP695-wt or APP695-swe were additionally supplemented with 200 µg/ml of the antibiotic Geneticin (G418).

Cells were cultured on 10 cm cell culture dishes and passaged two times per week at 80% confluency. Therefore, cells were rinsed once with sterile PBS and incubated with 1 ml Trypsin/EDTA (0.5 mg/ml / 0.22 mg/ml in PBS) at 37°C until the cells detached from the cell culture dish. Then, cells were gently resuspended in 10 ml cell culture media and seeded onto new cell culture dishes in a 1:5 or 1:10 dilution. To prevent contaminations, all steps were performed under a laminar flow clean bench with sterile materials.

#### 3.3.2 Determination of cell number

To determine the number of viable cells, cells were detached (see 3.3.1) and dead cells visualised by trypan blue staining. To this end, cells were mixed with trypan blue in a 1:2 ratio. 10 µl of the cell suspension was loaded onto a Neubauer improved counting chamber (Hecht Assistent) and unstained cells were counted. The final cell number was calculated according to the manufacturer's instruction taking relevant dilutions into account.

### 3.3.3 Cryo-preservation of cell lines

For preservation of cell lines, cells were washed once with sterile PBS and detached by Trypsin/EDTA treatment (see 3.3.1). Cells were centrifuged for 5 minutes at 300 x g and the cell pellet was dissolved in 1 ml DMEM complete supplemented with 10% (v/v) sterile DMSO. The cell suspension was transferred into a cryo-tube and frozen at -80°C. The next day, cryo-tubes were transferred into liquid nitrogen for long-term storage.

For thawing, cells were briefly incubated in a 37°C water bath. Together with nine parts of culture media, cells were centrifuged for 5 minutes at 300 x g in a falcon tube to remove the remaining DMSO. Afterwards, the supernatant was removed and cells resuspended in pre-warmed DMEM complete (see 3.3.1). Following, cells were transferred into new cell culture dishes and maintained according to section 3.3.1. Stably transfected cell lines were cultured for 24 hours before the selection antibiotic was added.

### 3.3.4 Transient transfection of cells

For the transient transfection of cells, the transfection reagent polyethylenimine (PEI) was used. Cells were seeded into cell culture dishes 24 h before transfection. Depending on the cell line, 2-4 µg DNA were diluted in 200 µl DMEM without FCS and antibiotic and mixed with the transfection reagent in a 1:3 (w/v) DNA to PEI ratio. The solution was incubated for 15 minutes at room temperature and drop by drop added to the cells. Following, cells were incubated for 6 h at 37°C in one third of the total cell culture media. After transfection was completed, the media was exchanged by the appropriate volume of pre-warmed cell culture media. Cells were harvested at confluency of around 80-100%, which was typically 48 h after transfection.

### 3.3.5 siRNA-mediated knockdown

For the siRNA-mediated downregulation of protein expression, cells were seeded in 6 cm cell culture dish plates and transfected with 5 nM of targeting siRNA or a non-targeting control siRNA. Therefore, 100 µl DMEM only were supplemented with 5 nM siRNA and 5 µl of the transfection reagent INTERFERin® (Polyplus). After brief mixing, the solution was incubated for 10 minutes at room temperature and added to the cells. The procedure was repeated 48 h after the first transfection and cells were harvested additional 24 hours later.

### 3.3.6 Inhibitor treatment of cells

For inhibitor treatment of cells, 24 hours after transfection the cell culture media was replaced and inhibitors (see 3.1.3) were added in respective dilutions to achieve a final concentration of 1 to 10  $\mu\text{M}$ . After 24 hours, cells were harvested and further analysed.

### 3.3.7 Indirect immunofluorescence staining

<u>Fixation solution</u>	4% (w/v) Paraformaldehyde (PFA) in PBS
<u>Permeabilisation/wash buffer</u>	0.2% (v/v) Saponin in PBS
<u>Quenching buffer</u>	0.2% (w/v) Saponin 0.12% Glycine PBS, pH 7.4
<u>Blocking buffer</u>	0.2 % (w/v) Saponin 10% (v/v) FCS PBS, pH 7.4

The subcellular localisation of proteins was analysed by indirect immunofluorescence staining. Marker proteins for subcellular compartments and proteins of interest were labelled with primary antibodies and visualised by fluorophore-coupled secondary antibodies. Cells were cultured on coverslips in six-well cell culture dishes. 48 h past transfection, cells were three times washed with sterile PBS and fixed by incubation with 4% PFA (w/v) in PBS for 20 minutes. To make intracellular proteins accessible for antibody binding, cell membranes were permeabilised by incubation for 5 minutes in permeabilisation buffer, followed by incubation with quenching buffer for 10 minutes. To saturate unspecific binding sites, cells were incubated with blocking solution for 1 hour at room temperature. The primary antibodies were diluted in blocking solution and the coverslips incubated with 50  $\mu\text{L}$  of the appropriate antibody overnight at 4°C in a wet chamber. After five times washing with wash buffer, cells were incubated for 1 hour with ALEXA<sup>®</sup>-fluorophore-coupled secondary antibodies (Tab. 3.2) diluted in 30  $\mu\text{L}$  blocking solution. The coverslips were rinsed five times with wash buffer and additionally two times with double-distilled water (ddH<sub>2</sub>O). Coverslips



were mounted on object slides using mounting solution supplemented with 1 µg/ml DAPI (4',6-diamidino-2-phenylindole) for nuclear staining. Confocal pictures were acquired with an Olympus FV1000 (Olympus) confocal laser scanning microscope.

### 3.3.8 Flow cytometric analysis

<u>FACS buffer</u>	PBS
	0.5% BSA
	2 mM EDTA

To quantify cell surface expression of proteins, flow cytometric activated cell sorting (FACS) analysis was performed. Cells were washed with ice-cold PBS and were gently detached from the cell culture dish by incubation with 2 ml accutase (PAA Laboratories) for 5 minutes at 37°C. Cells were centrifuged for 5 minutes at 300 x g and resuspended in 100 µl FACS buffer. The cell number was determined by using a Neubauer improved counting chamber. A total cell number of  $5 \times 10^5$  cells per sample were added to 100 µl FACS buffer and incubated with respective primary antibodies (Tab. 3.1) for 1 hour at 4°C. Following, cells were washed once with 100 µl FACS buffer and incubated with an ALEXA<sup>®</sup>-488 conjugated secondary antibody (Tab. 3.2) for 1 hour at 4°C in the dark. Omitting the primary antibody was used as control for unspecific binding of the secondary antibody. After another washing step, cells were resuspended in 200 µl FACS buffer and fluorescence measured using the BD FACS Canto<sup>™</sup> II system (BD Biosciences). Evaluation of the collected data was performed with the FlowJo (FlowJo LLC) analysis software.

### 3.4 Biochemical methods

#### 3.4.1 Protein extraction from cells

<u>ADAM10 lysis buffer</u>	1 mM EGTA
	5 mM Tris/HCl, pH 7.4
	250 mM Sucrose
	1% Triton X-100
	1x cOmplete protease inhibitor (Roche)

Cells were washed three times with cold PBS and replaced from the cell culture dish with a cell scraper in the presence of 500 µl PBS supplemented with protease inhibitor cocktail. Cells were centrifuged for 20 minutes at 4000 x g and 4°C. The cell pellet was resuspended in an appropriate amount of ADAM10 lysis buffer. Following, the cells were two times sonicated for 15 seconds at 60 Hz, incubated for 1 hour on ice and repeatedly sonicated. Cell lysates were centrifuged for 10 minutes at 14000 x g and 4°C to pelletize cellular debris and protein concentration was determined (see 3.4.5).

#### 3.4.2 Preparation of tissue homogenates

<u>RIPA lysis buffer</u>	20 mM Tris/HCl pH 7.5
	150 mM NaCl
	1 mM EDTA
	1 mM EGTA
	2.5 mM sodium deoxycholate
	1% (v/v) NP-40
	1x cOmplete protease inhibitor (Roche)

For protein extraction from organs, tissues were homogenised with 3-4 porcelain beads in radioimmunoprecipitation assay (RIPA) lysis buffer, using the Precellys® homogenisation system (Bertin Corp.) two times for 30 seconds at 6000 x g. Thereafter, homogenates were sonicated two times for 15 seconds at 60 Hz and were incubated for 1 hour on ice. To separate cellular debris, homogenates were centrifuged for 10 minutes at 14000 x g and 4°C and protein concentration was determined (see 3.4.5).

### 3.4.3 Co-immunoprecipitation experiments

<u>EBC lysis buffer</u>	120 mM NaCl
	50 mM Tris-HCl, pH 7.4
	0.5% (v/v) NP-40
	1x cOmplete protease inhibitor (Roche)

To analyse protein-protein interactions, co-immunoprecipitation experiments were performed. Cell or tissues lysates were prepared as described above (see 3.4.1; 3.4.2), using 500  $\mu$ l EBC lysis buffer containing 0.05% (v/v) Nonidet P-40 (NP-40). 60  $\mu$ L of the total lysates were kept to control for protein expression. Equal amounts of the residual lysates were incubated with respective primary antibodies (Tab. 3.1) overnight at 4°C under continuous rotation. Meanwhile, magnetic Protein G coupled Dynabeads (Thermo Fisher Scientific) were three times washed with EBC lysis buffer and incubated with SEA-blocking buffer (Thermo Fisher Scientific, 1:1 diluted with lysis buffer) overnight at 4°C to saturate unspecific binding sites. The next day, Dynabeads were once washed with EBC lysis buffer and 50  $\mu$ l per sample were used for precipitation of antibody labelled proteins. Thereafter, Dynabeads were added to the lysate-antibody complexes and were incubated for 30 minutes at room temperature under continuous rotation. The supernatant was removed and the Dynabeads were three times washed with EBC lysis buffer. Proteins were eluted by heating the Dynabeads for 20 minutes at 65°C together with 50  $\mu$ L of reducing SDS-PAGE loading buffer. Immunoprecipitates and total lysate controls were further analysed by SDS-PAGE and immunoblotting (see 3.4.6, 3.4.7).

### 3.4.4 Biotinylation of cell surface proteins

<u>Biotin solution</u>	1 mg/ml EZ-Link™ Sulfo-NHS-SS-Biotin (Thermo Fisher Scientific) in PBS-CM
<u>PBS-CM</u>	0.1 mM CaCl <sub>2</sub> 1 mM MgCl <sub>2</sub> in PBS

<u>Quenching buffer</u>	50 mM Tris/HCl in PBS-CM pH 8.0
<u>EBC-lysis buffer (Biotin)</u>	50 mM Tris/HCl pH 7.4 150 mM NaCl 1% (v/v) Triton-X100 1x cComplete protease inhibitor cocktail

To quantify the cell surface expression of proteins by biotinylation, 48 h after transfection surface proteins were labelled with biotin and precipitated using streptavidin-coupled agarose beads. To minimize endocytosis of surface proteins all steps were performed at 4°C. Cells were cooled on ice and three times washed with ice-cold PBS-CM. Following, cells were covered with 3-4 ml biotin solution and incubated for 30 minute. To remove unreacted biotin, cells were incubated with 10 ml quenching buffer for 10 minutes. After another three times washing with PBS-CM, cells were harvested with 500 µl EBC lysis buffer (biotin) and directly subjected to cell lysis (see 3.4.1). The protein concentration of total cell lysates was determined (see 3.4.5) and a small part (50 µl) was taken to control for protein expression. Equal amounts (1-2 mg) of the residual lysates were subjected to precipitation of biotin-labelled proteins using 70 µL Pierce™ Streptavidin Agarose beads (Thermo Fisher Scientific) per sample. After 1 hour incubation at 4°C under continuous rotation, agarose beads were five times washed with lysis buffer and bound proteins eluted by incubation with 50 µl of reducing 5x SDS-PAGE loading buffer for 20 minutes at 65°C. Finally, precipitates and total lysates were analysed by SDS-PAGE (see 3.4.6) and immunoblotting (see 3.4.7).

### **3.4.5 Determination of protein concentrations**

The total protein concentration of cell and tissue lysates was measured with the aid of the Pierce™ BCA Protein Assay Kit. The bicinchoninic acid (BCA) assay makes use of the capacity of peptide bonds to reduce  $\text{Cu}^{2+}$  cations to  $\text{Cu}^{+}$  in an alkaline solution. In the presence of bicinchoninic acid, the  $\text{Cu}^{+}$  cations form chelate complex, which can be photometrical measured at a wavelength of 562 nm and is proportional to the protein concentration. According to the manufacturer's protocol, diluted samples were incubated for 30 minutes at

37°C with the assay mixture and the absorbance was measured with a Synergy HT (BioTek) microplate reader. To calculate the protein concentration, the sample absorption values were correlated to a standard curve, which was generated from measured absorption values of defined albumin solutions with concentrations ranging from 0 to 2 mg/ml.

### 3.4.6 SDS polyacrylamide gel electrophoresis (SDS-PAGE)

<u>SDS-PAGE sample buffer (5x)</u>	625 mM Tris/HCl pH 6.8 10% (w/v) SDS 50% Glycerol 200 mM DTT Bromophenol blue
<u>Separating gel buffer</u>	1.5 M Tris/HCl pH 8.8 0.4% (w/v) SDS
<u>Stacking gel buffer</u>	0.5 M Tris/HCl pH 6.8 0.4% (w/v) SDS
<u>SDS-PAGE running buffer (10x)</u>	1.92 M Glycin 250 mM Tris/HCl 35 mM SDS

To analyse the composition of protein mixtures, cell or tissue lysates were separated by discontinuous sodium dodecyl sulphate polyacrylamide gel electrophoresis (SDS-PAGE) as described by Laemmli (Laemmli, 1970). Protein samples were prepared by heating for 5 min at 95°C together with reducing SDS-PAGE loading buffer. Thereby, proteins are coated with the anionic SDS, which is proportional to their molecular mass and results in a uniform negative charge. Furthermore, secondary and tertiary structures are disrupted and protein-protein disulfide bonds are reduced in the presence of dithiotreitol (DTT). Thus, allowing separation of proteins according to their molecular weight in an electrical field. For the electrophoretic separation of proteins, a 4.5 % stacking gel and a 10% separation gel (Tab. 3.12) were used in combination with the Mini-PROTEAN™ Electrophoresis System (Biorad). Equal protein amounts were loaded onto the SDS gel and electrophoresis performed using 1x SDS-PAGE

running buffer and a constant voltage of 80 V for 30 minutes followed by 120 V for 1 hour. The running behaviour of proteins was compared to the known molecular weights of a standard marker (PageRuler Plus).

**Tab. 3.12: Composition of SDS gels**

	10% separation gel	4.5% stacking gel
Separating gel buffer	2.6 ml	-
Stacking gel buffer	-	1.35 ml
30% (w/v) Acrylamide/bisacrylamide Rotiphorese® gel 30 (37.5:1)	3.3 ml	1.75 ml
H <sub>2</sub> O	4 ml	6.85 ml
10% (w/v) Ammonium persulphate	60 µl	60 µl
TEMED	30 µl	30 µl

Separation of APP C-terminal fragments was performed on precast NuPAGE™ Novex™ 4-12% Bis-Tris protein gels (Thermo Fisher Scientific) using the XCell SureLock™ Mini-Cell Electrophoresis System (Thermo Fisher Scientific) together with MES-running buffer (Thermo Fisher Scientific) according to the manufacturer's protocol. Separation of APP C-terminal fragments on 16% tris-tricine gels was performed by *Dr. Barry Boland* (University College Cork, Ireland) as described in Boland et al., 2010.

### 3.4.7 Western blotting and immunodetection

#### Transfer buffer (10x)

100 mM Glycine  
20 mM Mg(CH<sub>3</sub>COOH)<sub>2</sub>  
pH 2.2, HCl

#### Transfer buffer (1x)

10% (v/v) 10x Transfer buffer  
20% (v/v) Methanol  
70% (v/v) ddH<sub>2</sub>O

---

<u>TBS with Tween<sup>®</sup>20 (TBST)</u>	20 mM Tris/HCl, pH 7.5 150 mM NaCl 0.1% (v/v) Tween <sup>®</sup> 20
<u>Blocking buffer</u>	5% (w/v) dry milk in TBST
<u>Detection solution A</u>	0.1 M Tris/HCl pH 8.6 0.025% (w/v) Luminol
<u>Detection solution B</u>	0.11% (w/v) p-Coumaric acid in DMSO

The western blot method is used to detect specific proteins in lysates or tissue homogenates after separation by SDS-PAGE (see 3.4.6). The proteins are transferred to a nitrocellulose membrane and labelled with a specific primary antibody. A Horseradish peroxidase (HRP)-coupled secondary antibody, which detects the Fc-part of the primary antibody, is used to detect proteins on the membrane. In the presence of H<sub>2</sub>O<sub>2</sub>, HRP oxidises luminol, which results in a detectable chemiluminescence signal.

To transfer proteins from a SDS gel onto a nitrocellulose membrane the Criterion<sup>™</sup> (Biorad) wet blotting system was used. The SDS gel, two sheets of Whatman<sup>®</sup> Blotting paper and one nitrocellulose membrane were equilibrated in 1x transfer buffer and placed onto the anode side of a blotting cassette in the following order: fibre pad, Whatman<sup>®</sup> Blotting Paper, nitrocellulose membrane, SDS gel, Whatman<sup>®</sup> blotting paper, fibre pad. The blotting cassette was inserted into the blotting chamber according to the manufacturer's instructions and proteins were transferred at a constant current of 800 mA for 2 hours at 4°C. For detection of smaller proteins (<20 kDa) a current of 250 mA was applied for 2 hours at 4°C.

To reduce background and unspecific antibody signals, blotting membranes were incubated for 1 hour at room temperature with blocking buffer. Appropriate primary antibodies (see Tab. 3.1) were diluted in blocking buffer and were incubated with the membranes overnight at 4°C in gentle agitation. Following three times washing with TBST for 15 minutes, the membranes were incubated for 1 hour at room temperature with HRP-conjugated secondary antibodies, diluted in blocking solution. Again, membranes were washed thrice in TBST for 15 minutes and HRP activity was analysed. Therefore, a solution containing 1 ml detection solution A, 100 µl detection solution B, 2 µl H<sub>2</sub>O<sub>2</sub> and 100 µl of the Lumigen<sup>®</sup> ECL

Ultra solutions A and B was prepared. The membrane was covered with the detection solution and chemiluminescence signals were detected with the ImageQuant™ Las 4000 (GE Healthcare). Quantification of chemiluminescence signals was performed with the ImageJ software.

### 3.4.8 Reprobing of immunoblots

<u>Stripping buffer (mild)</u>	0.2 M Glycin 0.1% (w/v) SDS 1% (v/v) Tween® 20 pH 2.2
<u>Stripping buffer (strong)</u>	62.5 mM Tris/HCl pH 6.8 2% (w/v) SDS 0.83% (v/v) 2-Mercaptoethanol

To reuse a blotting membrane for the detection of another protein, previously bound antibodies were removed by incubation with reducing stripping buffers. Membranes were incubated for 30 min at room temperature under gentle shaking with a mild stripping buffer to remove secondary antibodies. Afterwards the membranes were four times washed with TBST. To remove strongly bound primary antibodies membranes were incubated for 30 min at 80°C with a strong stripping buffer containing 2-mercaptoethanol. The membrane was washed with TBST, until residual 2-mercaptoethanol was washed away. After removal of antibodies, membranes were again subjected to immunodetection (see 3.4.7).



### 3.5 Histological methods

#### 3.5.1 Preparation of semi-thin cryosections

<u>Fixation buffer</u>	0.4% Paraformaldehyde (PFA) in 0.1 M PB, pH 7.4
------------------------	--

To prepare semi-thin cryosections from organs, mice were anaesthetised with Ketamin/Rompun® (see 3.6.6) and transcardial perfusion performed with PBS followed by perfusion with 4% (w/v) PFA in phosphate buffer. Organs were removed and post-fixed in fixation buffer for 1-2 hours at room temperature. Afterwards the fixation buffer was replaced by 30% sucrose in 0.1 M phosphate buffer (pH 7.4) and tissues stored for 24 hours at 4°C. Semi-thin sections of 35 µm were cut with a Leica SM 2000 R sliding microtome (Leica Microsystems) under dry ice cooling. Prepared sections were stored in 0.1 M phosphate buffer.

#### 3.5.2 Immunofluorescence staining of cryosections

<u>Blocking solution</u>	0.1 M PB, pH 7.4 0.5% (v/v) Triton-X100 4% (v/v) Goat-Serum
<u>Wash buffer</u>	0.1 M PB, pH 7.4 0.25% (v/v) Triton-X100

For immunofluorescence analysis of semi-thin cryosections, indirect immunofluorescence labelling was performed. Tissue sections were incubated for 2 hours at room temperature in blocking solution to saturate unspecific binding sites. Respective primary antibodies (Tab. 3.1) were diluted in blocking solution and incubated with the sections overnight at 4°C. The next day, sections were three times rinsed with wash buffer and were incubated for 2 hours at room temperature with ALEXA®-fluorophore-coupled secondary antibodies (Tab. 3.2). Thereafter, the sections were three times washed with wash buffer for 10 minutes under gentle agitation and mounted on microscope slides using mounting solution supplemented with 1 µg/ml DAPI for nuclear staining.

### **3.5.3 Diaminobenzidine (DAB) staining**

For DAB staining of brain sections was performed by *Dr. Hermann Altmeyen* (University Medical Centre Hamburg-Eppendorf). Brain tissue was fixed with fixation buffer and 3 µm thick sagittal sections of paraffin-embedded brain hemispheres were prepared. Sections were stained with a respective primary antibody and DAB solution according to common protocols of the University Medical Centre Hamburg-Eppendorf, using a Ventana Benchmark XT staining system.

### **3.5.4 Ultra-structural analysis of hippocampal sections**

For ultra-structural analysis of dendritic spines in brains of *Tspan3* and *Tspan15*-deficient mice, electron microscopy was performed by *Dr. Michaela Schweizer* (University Medical Centre Hamburg-Eppendorf). Animals were anaesthetised with Ketamin/Rompun® and transcardially perfused with 0.9% (w/v) NaCl followed by tissue fixation with 4% PFA and 1% glutaraldehyde in phosphate buffer (pH 7.4). Sections of the hippocampal region were cut and postfixed in 1% OsO<sub>4</sub>. After dehydration, sections were embedded in Epon. Ultra-thin sections were prepared and stained with uranyl acetate and lead citrate and ultra-structural pictures of the hippocampal CA1 region taken with a Zeiss EM902 transmission-electron microscope.

## **3.6 Animal experimentation**

### **3.6.1 Generation of *Tspan3* and *Tspan15* knockout mice**

To generate transgenic mice that are deficient for *Tspan3* or *Tspan15*, respectively, transcription activator-like effector nucleases (TALEN)-mediated genome editing was used. TALENs consist of gene specific TALEN-repeat DNA recognition sequences fused to an effector nuclease. The DNA recognition sequence is defined by a pair of variable amino acids in the TALEN repeat sequence, also named as repeat variable di-residues (NI, ND, NG, NN), which preferentially associate with different nucleotides (A, C, T; G). For the gene specific knockout of *Tspan3* and *Tspan15*, TALENs were designed to target exon2 of the *Tspan3* and *Tspan15* gene locus, respectively (Tab. 3.13).

Tab. 3.13: List of TALEN target sequences

Target	TALEN sequence
<i>Tspan3</i> exon2	left: NN NG NN NG NI HD NI HD NN HD NG HD NG NG HD HD HD NG NN HD right: NN NI NI NI NI NN HD NI NI NN NN HD NG HD HD NG NI HD NI
<i>Tspan15</i> exon2	left: NN HD HD NG NG HD HD NG NN NN HD HD HD HD HD NN right: NN NI NI HD NI NG NN NI HD HD NI HD HD HD HD HD NI NN NN NI

Coding: Abbreviations: N: asparagine, I: isoleucine, D: aspartate, G: Glycine; Coding: NI= A, ND= C, NG=T, NN= A or G, NS= A, C, G, T; A: Adenine, G: Guanine: Cytosine: Cytosine; T: Thymine.

The TALEN RNA precursors were designed, generated and microinjected into male nucleoli of zygotes isolated from C57BL/6N mice by Dr. Petr Kasperek and Prof. Radislav Sedlacek (Czech Centre for Phenogenomics and Laboratory of Transgenic Models of Diseases, Vestec, Czech Republic) as previously described in Kasperek et al., 2014. The *Tspan3* TALEN mRNA was co-injected with a single stranded synthetic 46 bp long oligodeoxynucleotide, bearing three stop codons and one XbaI restriction site.

#### X46 ssOligodeoxynucleotide sequence:

5'-ACGACTATGACCACTTCTTCGAGGATGTGTACACGCTCTAACCTGCCGTGGTGATAGCATAGTAGTATGAGTC  
TAGATTTTCATCATTGGCCTGATCGGCTGCTGTGC-3'

Offspring mice were screened for TALEN-mediated frameshift mutations using genotyping PCR and sequence analysis (see sections 3.6.5 and 3.2.5.1). Heterozygous mice, carrying a 27 bp insertion mutation in the *Tspan3* exon2 (*Tspan3X46*) and a 104 bp deletion mutation in the *Tspan15* exon2 (*Tspan15Δ104*), were identified and used for further breeding (see 3.6.3).

### 3.6.2 Animal housing

Housing of experimental animals was approved by the guidelines of the ministry of Energy, Agriculture, the Environment and Rural Areas of Schleswig Holstein. To ensure a pathogen free environment animals were housed in individual ventilated cages (IVC). The room was kept at a temperature of 19-20°C and 12 h light-dark cycles were applied. Animals were provided with water and standardised laboratory animal food (Sniff) *ad libitum*. All animal works were approved by the Animal welfare committee of the Christian-Albrechts University

of Kiel and were performed according to the guidelines of the Federation of European Laboratory Animal Science Associations (FELASA).

### 3.6.3 Breeding strategy

For the breeding of mice, animals with an age of around nine weeks were matched in one-to-one or one-to-two (male/female) mating. To obtain mice with the desired genotypes the following breeding schemes (Fig. 3.1) were applied. Offspring were weaned three weeks after birth and a tail biopsy was taken to determine the genotype.

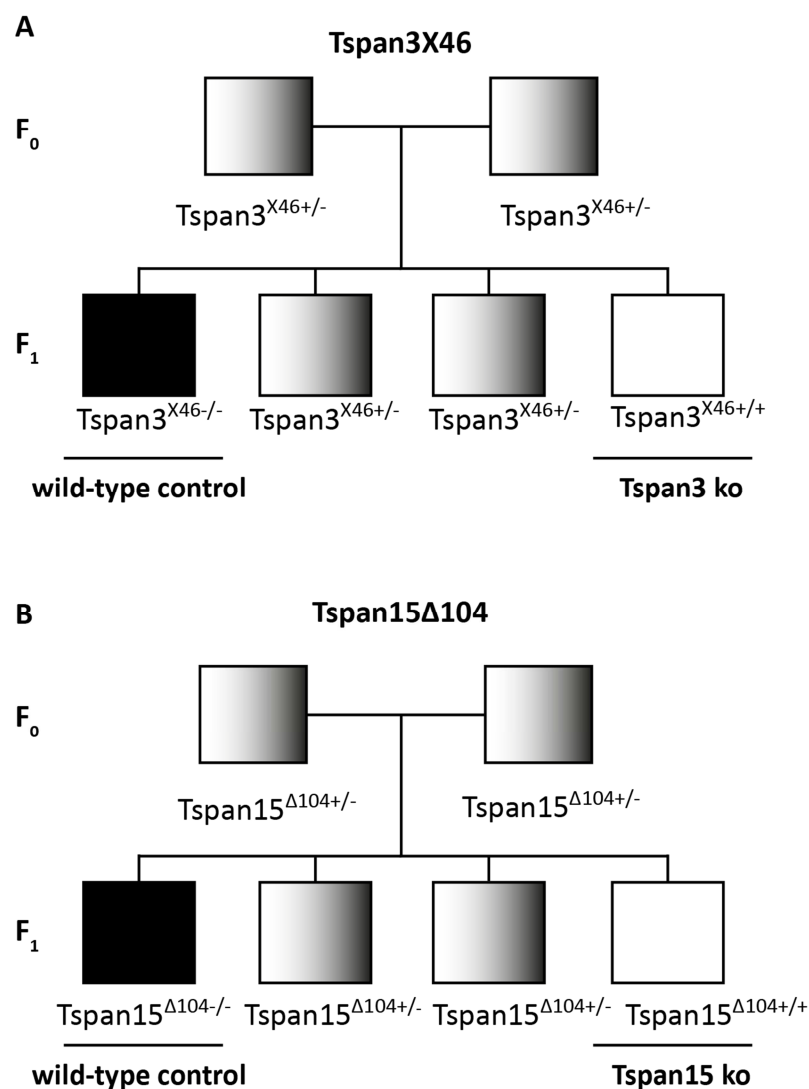


**Fig. 3.1: Breeding strategy for Tspan3 and Tspan15 knockout**

Schematic drawing showing representative mating for the breeding of **A**) Tspan3<sup>X46</sup> and **B**) Tspan15<sup>Δ104</sup> mouse strains. Heterozygous Tspan3<sup>X46+/-</sup> (A) and Tspan15<sup>Δ104+/-</sup> (B) mice were mated (F<sub>0</sub>) and the underlined genotypes of the F<sub>1</sub> generation were used for further analysis.

### 3.6.4 Tail biopsy and isolation of genomic DNA

To obtain genomic DNA for genotyping of experimental animals a tail biopsy was taken from three to four weeks old mice. The tail was subjected to digestion with DirectPCR® Lysis Reagent Tail (PepqLab) supplemented with 0.3 mg/ml proteinase K and incubated overnight at 55°C under continuous shaking. After heat-inactivation of the enzyme for 45 minutes at 85°C, the samples were centrifuged and applied to genotyping PCR (see section 3.6.5).

### 3.6.5 PCR for genotyping of mice

For genotyping of experimental animals, the presence of mutated and wild-type alleles in Tspan3X46 and Tspan15Δ104 mice was analysed by PCR. Genomic DNA was isolated as described in section 3.6.4 and subjected to PCR using gene specific primers (Tab. 3.3). The reaction mixture was prepared (Tab. 3.14) and amplification performed using an appropriate PCR program (Tab. 3.15). Afterwards, PCR products were analysed by agarose gel electrophoresis (see section 3.2.6)

**Tab. 3.14: Pipetting scheme for genotyping PCR**

	µl
Primer forward [10 µM]	1
Primer reverse [10 µM]	1
10x DreamTaq™ buffer	5
dNTPs [2 mM]	5
DreamTaq™	0.3
DNA	1
Add H <sub>2</sub> O	50

**Tab. 3.15: Genotyping PCR program**

step	t	T (°C)	cycles
Initial denaturation	5 min	95	1
Denaturation	30 s	95	
Annealing	30 s	48	30
Elongation	36 s	72	
Final elongation	7 min	72	1
End	∞	10	1

### 3.6.6 Euthanasia of mice

To remove organs from mice, animals were sacrificed by cervical dislocation. Anaesthesia of mice was performed by intra peritoneal injection of 10 mg/ml Ketamin and 6 mg/ml Rompun® in 0.9% (w/v) NaCl, if necessary. The mice were weighed and a dosage of 10 µl/g body weight was injected.

### 3.7 Analysis of human brain samples

Post-mortem samples from the cortical region of Caucasian Alzheimer's Disease (AD) patients and healthy controls were kindly provided by the group of *Prof. Markus Glatzel* (University Medical Centre Hamburg-Eppendorf). The samples were used for preparation of tissue homogenates (see 3.4.2) and subjected to immunoblot analysis as described in section 3.4.7. Clinical characteristic of Alzheimer's Disease (AD) patients and control subjects, are given below (Tab. 3.16, Tab. 3.17). AD pathology was classified by Consortium to Establish a Registry for AD (CERAD) criteria and Braak stage.

**Tab. 3.16: Clinical characteristics of AD patients**

	Age at death	Gender	CERAD	Braak stage
1	69	m	C	4-5
2	88	m	C	4-5
3	74	m	C	3-4
4	79	m	B	5
5	63	m	C	4-5
6	88	f	B	4
7	82	m	B	4
8	83	f	B	3

**Tab. 3.17: Characteristics of control subjects**

	Age at death	Gender
1	68	m
2	68	f
3	63	m
4	86	m
5	61	m
6	69	f
7	70	m

M: male, f: female; CERAD, neuritic plaque appearance B: moderate, C: frequent; Braak stage neurofibrillary tangles restricted in the limbic system (III/IV), abundant distribution in the isocortex (IV/V).

### 3.8 Statistical analysis

All statistical analyses were performed with GraphPad Prism5 (GraphPad Software, Inc.) using the unpaired, two-tailed Student's t-test or analysis of variance (ANOVA) in combination with the Bonferroni's post-hoc test.

## 4 Results

### 4.1 Characterisation of tetraspanin-3 as an ADAM10 interaction partner

The metalloprotease ADAM10 is responsible for the ectodomain shedding of several cell surface proteins. ADAM10 is involved in a multitude of physiological and cellular processes. It has attracted attention due to its key role as an  $\alpha$ -secretase in APP proteolytic processing and its requirement for early developmental processes (Jorissen et al., 2010; Kuhn et al., 2010; Weber and Saftig, 2012). Despite an increasing understanding of the functions of ADAM10, there is still limited knowledge about the mechanisms that regulate its tissue and substrate-specific activity. Previous studies, addressing the question how ADAM10 activity is regulated, have identified members of the tetraspanin protein family as modulators of ADAM10-mediated shedding processes (Arduise et al., 2008b; Charrin et al., 2014; Dornier et al., 2012; Haining et al., 2012; Noy et al., 2016; Prox et al., 2012; Xu et al., 2009).

A yeast based interaction screen led to the identification of tetraspanin-15 (Tspan15) as an ADAM10 interactor. Tspan15 turned out to act as a potent regulator of ADAM10 maturation and trafficking in cell based studies (Prox et al., 2012). Using a similar approach, another member of the tetraspanin family, tetraspanin-3 (Tspan3), was found as a putative interaction partner of ADAM10. The function of Tspan3 as an ADAM10 interaction partner is unknown. In order to elucidate its role in the possible regulation of the protease the Tspan3-ADAM10 interaction was first addressed by using cell-based experiments.

#### 4.1.1 Identification of tetraspanin-3 as an ADAM10 interaction partner in yeast

In order to identify novel interaction partners and putative regulators of ADAM10, a split-ubiquitin yeast two-hybrid interaction screen was performed. This screen was part of the preliminary work of *Dr. Johannes Prox* and is the basis for the following studies.

The cDNA sequence of murine ADAM10 was C-terminal fused to the C-terminus of ubiquitin (Cub) and the artificial transcription factor LexA-VP16. Proteins encoded by a murine brain cDNA library, N-terminal fused to the mutated N-terminal moiety of ubiquitin (NubG), were used as prey proteins. The mutated NubG prevents reconstitution of ubiquitin halves, unless the Cub and NubG were brought into close proximity. To control specificity of the screen, the yeast transmembrane ER protein Alg5 was fused to wild-type Nub (Nubl) as a positive control and to mutated NubG as a negative control, respectively. ADAM10 bait and prey constructs,

positive and negative controls were transformed into NMY51 yeast, a competent *Saccharomyces cerevisiae* reporter strain (MoBiTec, Göttingen, Germany), and growth of yeast cells was monitored on selective media plates.

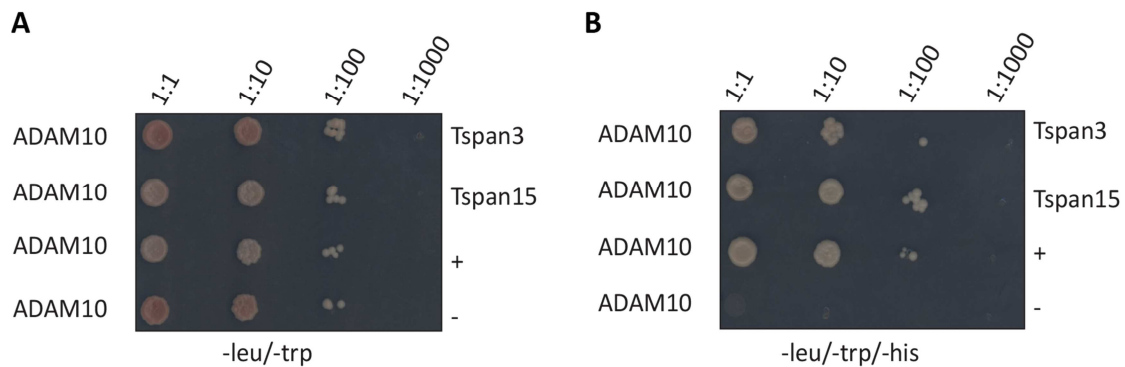


**Fig. 4.1: Identification of Tspan3 as an ADAM10 interaction partner in a split-ubiquitin yeast two-hybrid screen.**

Yeast cells were transformed with ADAM10 bait and Tspan3 or Tspan15 prey constructs. Co-expression of Nubl (+) or NubG (-) served as positive or negative control. Yeast cells were seeded on media plates in different dilutions (1:1, 1:10, 1:100, 1:1000). **A**) Expression of ADAM10 bait and Tspan3, Tspan15 prey constructs, “+” and “-” control was verified by growth of yeast clones on leucine/tryptophan (leu/trp)-deficient media. **B**) Interaction of ADAM10 with Tspan3, Tspan15 and the positive control allowed yeast clones to grow under selective pressure on leucine/tryptophan/histidine (leu/trp/his)-deficient media plates (Prox et al., 2012).

The successful expression of prey, bait and Nubl (+) and NubG (-) control proteins was observed by growth of yeast cells on leu/trp-deficient media plates up to a dilution of 1:100 of the yeast culture (Fig. 4.1A). Close proximity of bait and prey proteins lead to the release of an artificial transcription factor, which allows yeast cells to grow under selective pressure on leu/trp/his-deficient media plates. This was observed after co-expression of ADAM10 with Tspan3, Tspan15 or the Nubl (+) positive control (Fig. 4.1B). No yeast cells grew after co-expression of ADAM10 bait protein with the NubG (-) negative control confirming specificity of the screen.

The yeast screen therefore identified Tspan3 and Tspan15 (Prox et al., 2012) as ADAM10 interaction partner.



#### 4.1.2 Tetraspanin-3 interacts with ADAM10 in mammalian cells

It was required to independently confirm the data from the yeast screen in a mammalian cell system. Therefore, co-immunoprecipitation experiments were performed in human cervix carcinoma cells (HeLa).

HeLa cells were transiently transfected with a murine C-terminal myc-tagged Tspan3 (Tsp3) construct, together with an empty vector (V) or a murine ADAM10 (A10) expression plasmid. To compare the interaction of Tspan3 and ADAM10 with an already described ADAM10 interaction partner, murine Tspan15-myc (Tsp15) was expressed alone or together with ADAM10. The cells were lysed and 50  $\mu$ l of the total lysate was taken to control protein expression (Input). The residual lysate was used for precipitation of ADAM10 or myc-tagged proteins (Tsp3, Tsp15) using an anti-ADAM10 (IP anti-ADAM10) or anti-myc (IP anti-myc) antibody, respectively. Total cell lysates (Input) and precipitates were analysed by immunoblotting (Fig. 4.2). The immunoblot analysis of ADAM10 immunoprecipitates (Fig. 4.2A, IP anti-ADAM10) using a C-terminus specific anti-ADAM10 antibody, revealed prominent signals at 100 kDa and 70 kDa, corresponding to the pro- (pADAM10) and mature form of ADAM10 (mADAM0), in all samples, but not in the antibody (ab ctrl) and bead control (beads). Compared to mock, Tsp3/V and Tsp15/V transfected samples, the signal intensity for pro- and mature ADAM10 was increased in the immunoprecipitates of Tsp3/A10, Tsp15/A10 transfected cells. After staining with an anti-myc antibody, signals at around 45 kDa and 25 kDa, corresponding to myc-tagged Tspan3 (45 kDa) and Tspan15 (25 kDa) were observed in Tsp3V, Tsp3/A10, Tsp15/V and Tsp15/A10 immunoprecipitates, respectively (Fig. 4.2A, IP anti-ADAM10). Comparable amounts of Tspan3-myc and Tspan15-myc were co-immunoprecipitated in Tsp3/V, Tsp3/A10 and Tsp15/V transfected samples. In contrast, an increased co-precipitation of Tspan15-myc was observed in the Tsp15/A10 immunoprecipitate (Fig. 4.2A, IP anti-ADAM10). Probing the total lysates (Fig. 4.2A, Input) for expression of ADAM10 confirmed sufficient expression of pro- and mature ADAM10 in all samples. Signal intensities of pro- and mature ADAM10 were increased in Tsp3/A10 and Tsp15/A10 transfected samples, confirming the successful overexpression of ADAM10. Using an anti-myc antibody (Fig. 4.2A, Input), expression of Tspan3- and Tspan15-myc was confirmed by prominent signals around 45 kDa (Tspan3-myc) and 25 kDa (Tspan15-myc) in Tsp3/V, Tsp3/A10 and Tsp15/V, Tsp15/A10, respectively.

Overall, the presence of Tspan3-myc in ADAM10 immunoprecipitates verified the Tspan3-ADAM10 interaction in mammalian (HeLa) cells.

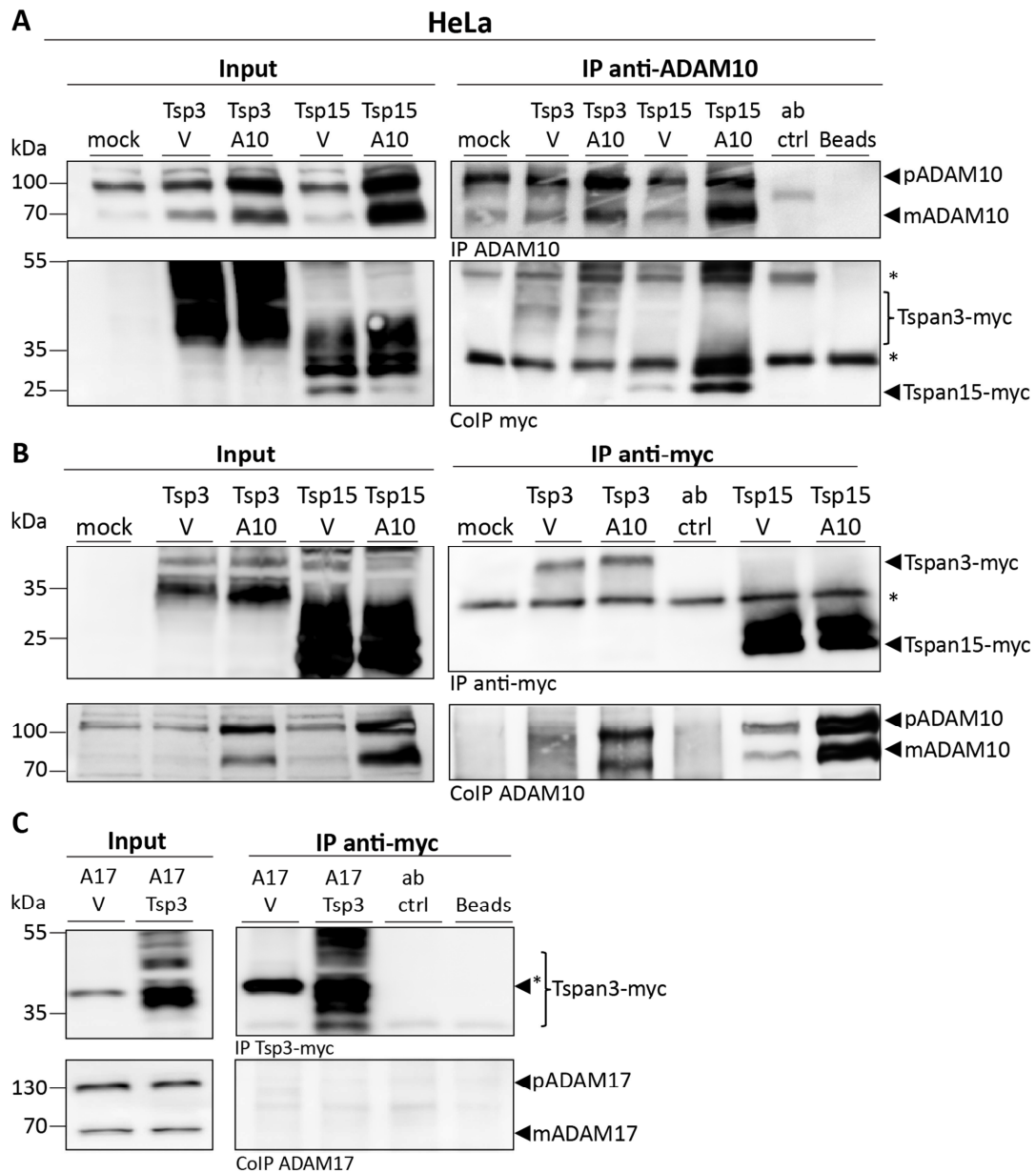


**Fig. 4.2: Transiently expressed Tspan3 interacts with ADAM10 but not with ADAM17 in HeLa cells.**

HeLa cells transiently transfected with Tspan3-myc (Tsp3) or Tspan15-myc (Tsp15) together with an empty vector (V), ADAM10 (A10) or ADAM17 (A17), were lysed in the presence of 0.5% TritonX-100. Total cell lysates were taken as expression control (Lysate) and ADAM10 (**A**) or Tsp3, Tsp15 (**B**, **C**) precipitated, using a specific anti-ADAM10 or anti-myc antibody. A lysate-free sample containing lysis buffer and the anti-ADAM10 (**A**) or anti-myc (**B**, **C**) antibody served as control (ab ctrl). Unspecific protein binding to the beads was controlled by incubation of beads with lysate (beads). After immunoblotting the expression of Tsp3, Tsp15, ADAM10 and ADAM17 was verified in lysates (**A**, **B**, **C**). Using the same antibodies co-immunoprecipitation (CoIP) of Tsp3 and Tsp15 (**A**) or ADAM10 (**B**) was analysed in ADAM10 (**A**) and anti-myc (**B**, **C**) immunoprecipitates (IP). Unspecific signals at 35 and 55 kDa (\*), correspond to denatured immunoglobulin fragments (heavy and light chain) and protein G eluted from the beads used for immunoprecipitation. p: pro, m: mature, \*: unspecific signal.

In a different experimental setup where Tspan3- and Tspan15-myc were precipitated (Fig. 4.2B, C), co-precipitation of overexpressed pro- and mature ADAM10 was observed in Tsp3/A10 and Tsp15/A10 transfected samples (Fig. 4.2B). Precipitation of Tspan15-myc (Fig. 4.2B) also co-precipitated endogenous ADAM10 (Tsp15/V), whereas Tspan3-myc precipitated only pro-ADAM10, but no mature ADAM10 (Tsp3/V). In contrast to ADAM10, the immunoprecipitation of Tspan3-myc did not co-precipitate pro- (p, 130 kDa) or mature (m, 70 kDa) ADAM17 (Fig. 4.2C).

In summary, reciprocal co-immunoprecipitation of Tspan3-myc and ADAM10 under overexpression conditions confirmed Tspan3 as an ADAM10 interacting protein. Moreover, the extent of this interaction was comparable with the Tspan15-myc/ADAM10 interaction. In contrast, Tspan3-myc did not co-precipitate ADAM17, which is closely related to ADAM10.

#### **4.1.3 Tetraspanin-3 does not exert an apparent effect on the maturation of ADAM10**

Having confirmed Tspan3 as an ADAM10 interacting protein, the next question was what the function of this interaction could be. Several tetraspanins have already been described to associate with ADAM10 and to function as regulators of ADAM10-mediated shedding events (Dornier et al., 2012; Haining et al., 2012; Prox et al., 2012; Xu et al., 2009). Especially members of the TspanC8 tetraspanins, including Tspan15, have attracted attention due to their role in promoting ADAM10 maturation and surface trafficking, which in turn modulated cleavage of certain substrates (Dornier et al., 2012; Haining et al., 2012; Prox et al., 2012). However, sequence analysis of 33 human tetraspanins revealed that Tspan3 does not belong to the TspanC8 subgroup. With only six cysteines in its extracellular loop it belongs to the TspanC6 tetraspanins. To address the question, whether Tspan3 could have a similar impact on ADAM10 maturation as described for TspanC8 tetraspanins, the effect of Tspan3 expression on the pro- and the mature form of ADAM10 was analysed.

To this end, HeLa and murine neuroblastoma N2a cells were transiently transfected with Tspan3-myc (Tsp3) or an empty vector as control (mock) in triplicates. Additionally, Tspan15-myc (Tsp15), which increases ADAM10 maturation (Prox et al., 2012), was used as a positive control. The transfected cells were lysed and ADAM10 maturation was analysed by immunoblot (Fig. 4.3). After staining with an anti-ADAM10 antibody, prominent signals of endogenous pro- and mature ADAM10 were detected in HeLa (Fig. 4.3A) and N2a (Fig. 4.3B)

cells. Overexpression of Tspan3-myc (40 kDa) did not alter signal intensities of pro- or mature ADAM10, compared to the mock control. In contrast, expression of Tspan15-myc significantly increased the mature form of ADAM10 and decreased the proform in HeLa and N2a cells (Fig. 4.3A, B). Increased signal intensities of ADAM10 C-terminal fragments (CTFs) (Suh et al., 2013; Tousseyn et al., 2009) at about 12 kDa and 15-18 kDa (Fig. 4.3A, B) were detected in cells expressing Tspan3-myc, but not Tspan15-myc (Fig. 4.3A, B). Equal protein loading was verified by similar signal intensities in all samples after beta-tubulin (Fig. 4.3A) and glyceraldehyde-3 phosphate dehydrogenase (GAPDH) staining (Fig. 4.3B). Unlike Tspan15-myc, the expression of Tspan3-myc did not alter ADAM10 maturation, but significantly increased the generation of ADAM10-CTFs, which are either generated by autocatalytic ectodomain shedding of ADAM10 (Suh et al., 2013) or by other ADAM proteases and regulated intramembrane proteolysis (Tousseyn et al., 2009).

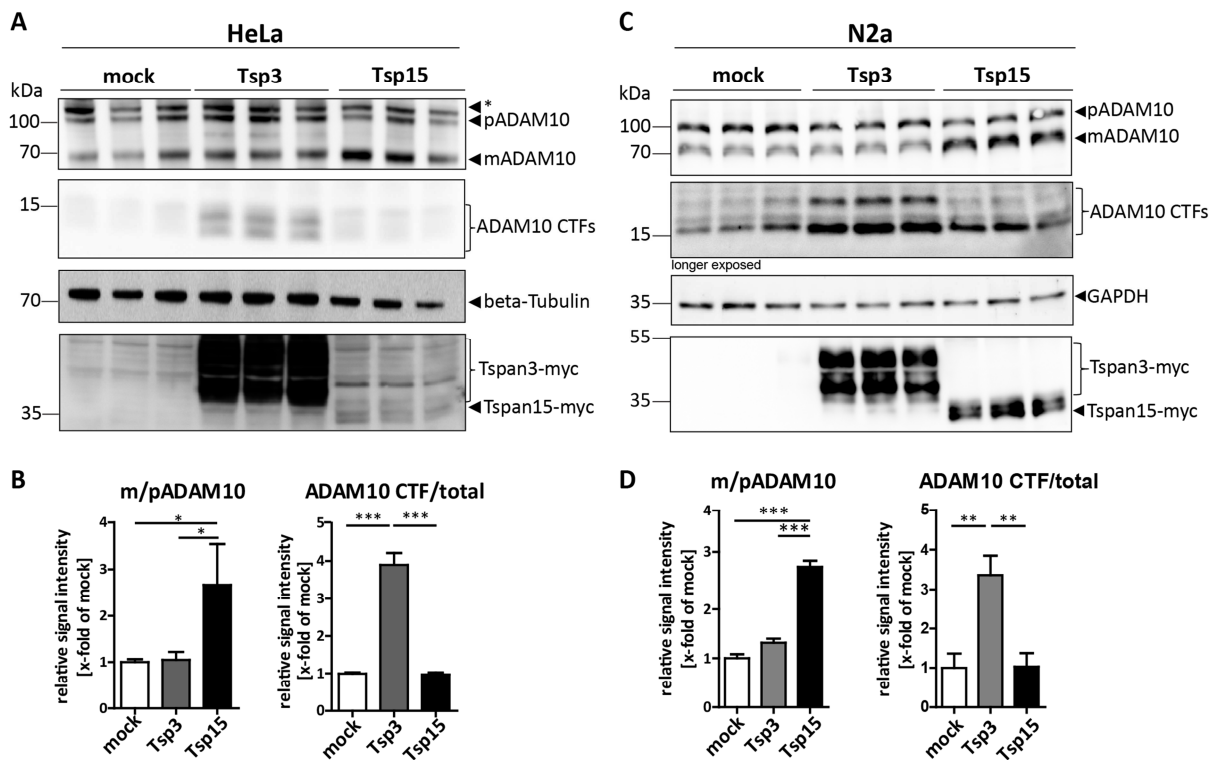


**Fig. 4.3: Tspan3 overexpression does not affect ADAM10 maturation.**

Immunoblot analysis of **A**) HeLa and **B**) N2a cells transfected with an empty vector (mock), Tspan3-myc (Tsp3) or Tspan15-myc (Tsp15) expression plasmids. Endogenous pro- (p) and mature (m) ADAM10 generation of ADAM10 C-terminal fragments (CTFs) was detected with an antibody specific for the C-terminus of ADAM10 (**A**, **B**). Expression of Tspan3-myc and Tspan15-myc was analysed with an anti-myc antibody. Equal protein loading was controlled by detection of beta-tubulin (**A**) and GAPDH (**B**). Quantification of signal intensities p/m and CTF/total (m+p) ADAM10 are shown below (**A**, **B**). Data is shown as mean values  $\pm$ SD. For statistical analysis, a one-way ANOVA followed by Bonferroni's multiple comparisons test was performed (\*  $p < 0.05$ , \*\*  $p < 0.005$ , \*\*\*  $p < 0.001$ ).

#### 4.1.4 Tetraspanin-3 does not affect the surface expression of ADAM10

To analyse whether Tspan3 affects the cell surface expression of ADAM10, ADAM10 cell surface levels were analysed by cell surface biotinylation (Fig. 4.4). N2a cells expressing Tspan3-myc (Tsp3) or Tspan15-myc (Tsp15) were incubated with a Biotin solution (+Biotin) to label surface proteins or left untreated (-Biotin). Non-transfected (UT) and mock transfected cells (mock) served as negative controls. Cells were lysed and biotinylated proteins precipitated using streptavidin-coupled beads. To control for protein expression a small amount of the total lysate was kept. Subsequently, an immunoblot analysis of total lysates and pull-down fractions was performed (Fig. 4.4A).

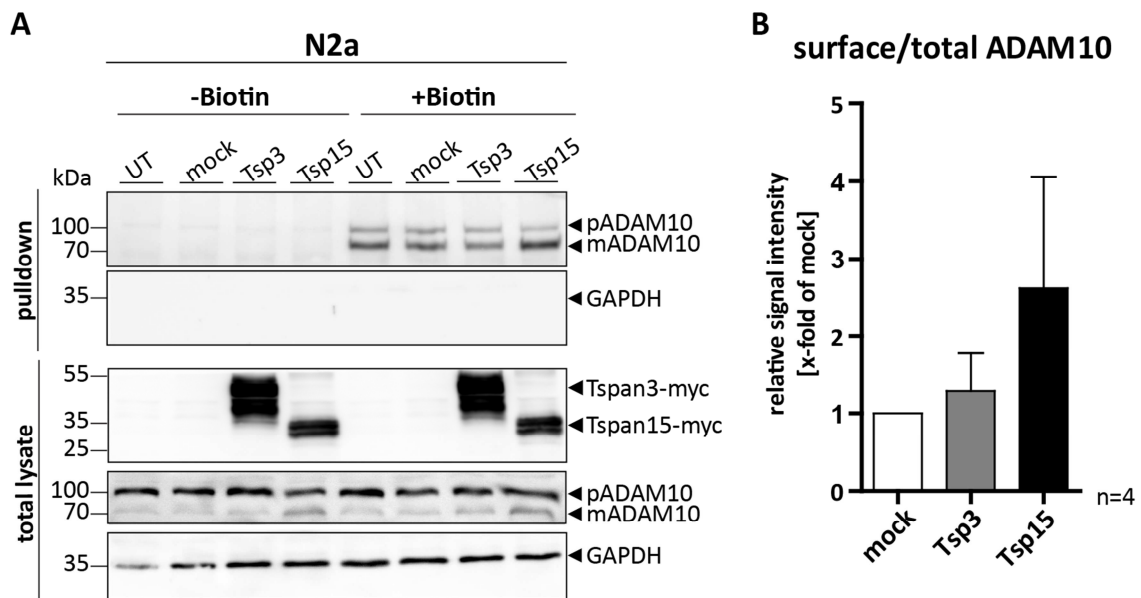


**Fig. 4.4: Analysis of the cell surface expression of ADAM10 using cell surface biotinylation.**

N2a cells were transiently transfected with Tspan3-myc (Tsp3) or Tspan15-myc (Tsp15). Non-transfected (UT) or mock transfected (mock) cells were used as negative control. Following, surface biotinylation of N2a cells was performed and ADAM10 cell surface expression analysed. **A**) Immunoblot showing the cell surface expression of pro- (p) and mature (m) ADAM10 in pull-down fractions of biotin labelled (+Biotin), but not in untreated (-Biotin) samples. GAPDH was not detected in the pull-down fraction confirming that no cytosolic proteins were present in the pull-down fraction (pull-down). Expression of Tsp3, Tsp15 and endogenous mADAM10 was detected in total lysates. **B**) Densitometric analysis of signal intensities of surface and total ADAM10 of four (n=4) independent experiments. Data is shown as mean values  $\pm$ SD.

After immunoblotting, surface levels of pro- and mature ADAM10 were detected in the pull-down fractions of biotin treated (+Biotin) samples. No signals were observed in untreated (-Biotin) samples, confirming specificity of the streptavidin pull-down (Fig. 4.4A). In comparison to untransfected and mock transfected cells, the expression of Tspan3-myc did not alter ADAM10 surface levels. On the contrary, Tspan15-myc expression clearly increased the surface level of mature ADAM10. Using an anti-GAPDH antibody, GAPDH was detected in total

lysates of untreated (-Biotin) and biotinylated (+Biotin) samples, but not in the respective pulldown fractions, confirming that only cell surface proteins were precipitated. Detection of Tspan3-myc, Tspan15-myc and endogenous pro- and mature ADAM10 confirmed sufficient protein expression in total lysates.

As an independent approach, ADAM10 surface expression was analysed by fluorescence activated cell sorting (FACS). N2a cells were transiently transfected with Tspan3-myc (Tsp3), Tspan15-myc (Tsp15) or an empty vector (mock) and incubated with an N-terminal anti-ADAM10 primary antibody. Using a fluorophore-coupled secondary antibody (ALEXA-488) surface ADAM10 was detected and directly analysed by FACS (Fig. 4.5).

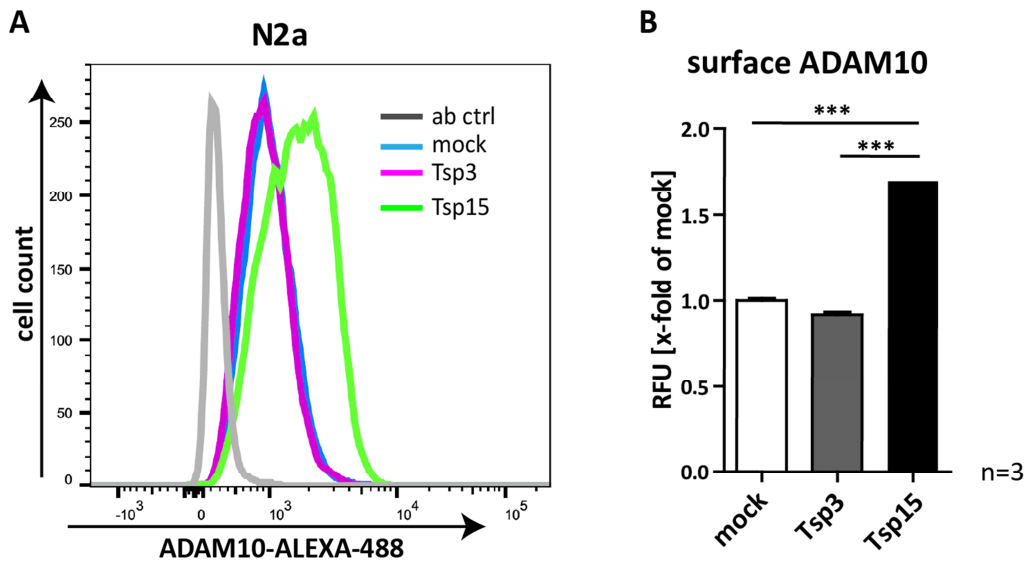


**Fig. 4.5: FACS analysis of ADAM10 cell surface levels.**

N2a cells were transiently transfected with Tspan3-myc (Tsp3) or Tspan15-myc (Tsp15). Cells transfected with an empty vector were used as mock control. **A**) Histogram of one representative FACS measurement showing the number of counted cells (cell count) against the measured relative fluorescence (ADAM10-ALEXA-488) which corresponds to the relative amount of surface ADAM10, labelled with a N-terminal ADAM10 primary and a fluorophore coupled secondary antibody. Omitting the primary antibody was used as control specificity of the secondary antibody (ab ctrl). **B**) Quantification of ADAM10 surface levels from three independent experiments (n=3). Data are shown as mean values  $\pm$ SD of relative fluorescence units (RFU) related to mock samples (\*\* $p < 0.001$ , according to one-way ANOVA and Bonferroni's post hoc test).

After FACS measurements, Tspan3-myc and mock transfected cells showed similar fluorescence signal intensities, which corresponded to the surface expression of ADAM10 (ADAM10-ALEXA-488). The expression of Tspan15-myc significantly increased fluorescence signal intensities (Fig. 4.5B). No fluorescence signal was detected in cells treated only with the secondary antibody (ab ctrl), validating specificity of the secondary antibody.

In conclusion, cell surface biotinylation and FACS analysis showed that in contrast to Tspan15-myc, overexpression of Tspan3-myc had no obvious effect on the cell surface expression of ADAM10.

#### 4.1.5 Overexpression of tetraspanin-3 affects APP but not N-cadherin processing

To this point, no overt effects of Tspan3 on ADAM10 maturation or surface expression were observed. In order to elucidate if Tspan3 influences ADAM10-mediated substrate shedding, cleavage of the two well-described ADAM10 substrates, N-cadherin and the amyloid precursor protein (APP) was analysed (Lammich et al., 1999; Reiss et al., 2005).

Tspan3-myc (Tsp3) and Tspan15-myc (Tsp15) were expressed in HeLa cells. Cells transfected with an empty vector (mock) served as negative control. Following cell lysis, the generation of APP and N-Cadherin C-terminal cleavage products (C-terminal fragments, CTFs) was analysed by immunoblot (Fig. 4.6).

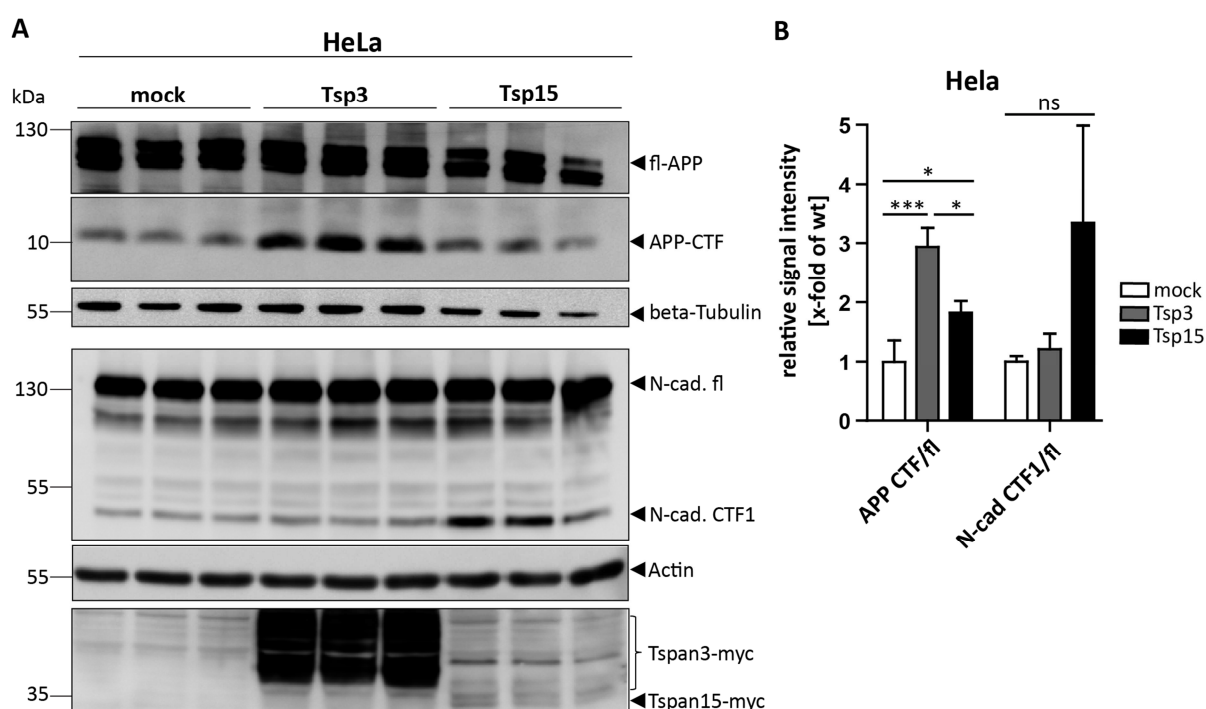


**Fig. 4.6: Tspan3 expression increases the APP-CTF, but has no effect on N-cadherin shedding.**

**A)** HeLa cells transiently transfected with an empty vector (mock), Tspan3-myc (Tsp3) and Tspan15-myc (Tsp15) were lysed and APP and N-cadherin cleavage was analysed by immunoblot. Full length (fl-) APP (immature 126 kDa, mature 130 kDa) and the APP-C-terminal fragment (CTF, 10 kDa) were detected with a C-terminal anti-APP antibody. Using a C-terminal anti-N-cadherin antibody full length N-cadherin (N-cad. fl) and the ADAM10 generated cleavage product N-cadherin CTF1 (N-cad. CTF1) were analysed. Equal protein loading was confirmed by anti-beta-tubulin and anti-actin staining, respectively. **B)** Quantitative analysis of APP and N-cadherin signal intensities. The ratio of cleavage product to respective full length protein (CTF/fl) was calculated and statistical significance was tested using one-way analysis of variance (ANOVA, \* $p < 0.05$ , \*\*\* $p < 0.001$ , ns: not significant). Values are shown as means  $\pm$  SD.

Detection of APP using a C-terminal anti-APP antibody resulted in strong signals at 130 kDa and 126 kDa, corresponding to the mature and immature form of full length (fl-) APP (Fig. 4.6A). The APP C-terminal cleavage product (APP-CTF) was observed at 10 kDa. The expression of Tspan3-myc caused a threefold increase of the APP-CTF compared to mock transfected cells, whereas signal intensities of fl-APP remained unchanged (Fig. 4.6A, B). Furthermore, the expression of Tspan3-myc had no apparent effect on the signal intensities of full length N-cadherin (N-cad. fl, 130 kDa) and the N-cadherin C-terminal fragment 1 (N-cad. CTF1, 40 kDa). In contrast, Tspan15-myc expression led to a modest increase of the APP-CTF (1.5-fold), but clearly increased the generation of the N-cadherin CTF1 (Fig. 4.6A, B). The signal intensities of actin and beta-tubulin confirmed equal protein loading in all samples (Fig. 4.6A).

In conclusion, the analysis of APP and N-cadherin processing demonstrated that the expression of Tspan3 increases the appearance of the APP-CTF, but does not affect N-cadherin processing. This indicates that Tspan3 could have a substrate specific function in ADAM10-mediated shedding events.

#### **4.1.6 Tetraspanin-3 increases the appearance of the APP-CTF which is generated by ADAM10**

Although Tspan3 was found as an ADAM10 interacting protein, the increased appearance of the APP-CTF could also result from increased  $\beta$ - or inhibited  $\gamma$ -secretase processing. While ADAM10-mediated APP processing generates the APP- $\alpha$ CTF, which consists of 83 amino acids (C83), the  $\beta$ -secretase (BACE1) cleavage generates the  $\beta$ CTF, consisting of 99 amino acids (C99). Both APP-CTFs have a similar molecular weight and are further processed by the  $\gamma$ -secretase complex.

To answer the question whether Tspan3 expression affects ADAM10-mediated APP processing, the influence of a hydroxamate-based ADAM10 inhibitor (GI254023X) (Hoettecke et al., 2010) on the Tspan3 induced increase of the APP-CTF was analysed. HeLa cells were transiently transfected with Tspan3-myc (Tsp3) or a mock control. The cells were treated with 10  $\mu$ M GI254023X for 24 h, lysed and APP proteolytic processing analysed by immunoblot (Fig. 4.7). Compared to mock transfected cells, the expression of Tspan3-myc led to a 10-fold increase of the APP-CTF, which was significantly decreased upon treatment with the ADAM10 inhibitor GI254023X (Tsp3+GI254023X) (Fig. 4.7A), indicating that the Tspan3-myc induced



increase in the APP-CTF is related to ADAM10-mediated APP processing. Staining with an anti-myc antibody confirmed comparable expression of Tspan3-myc in Tspan3-myc transfected, untreated (Tsp3) and GI254023X-treated (Tsp3+GI254023X) samples. Equal protein loading was verified by actin staining.

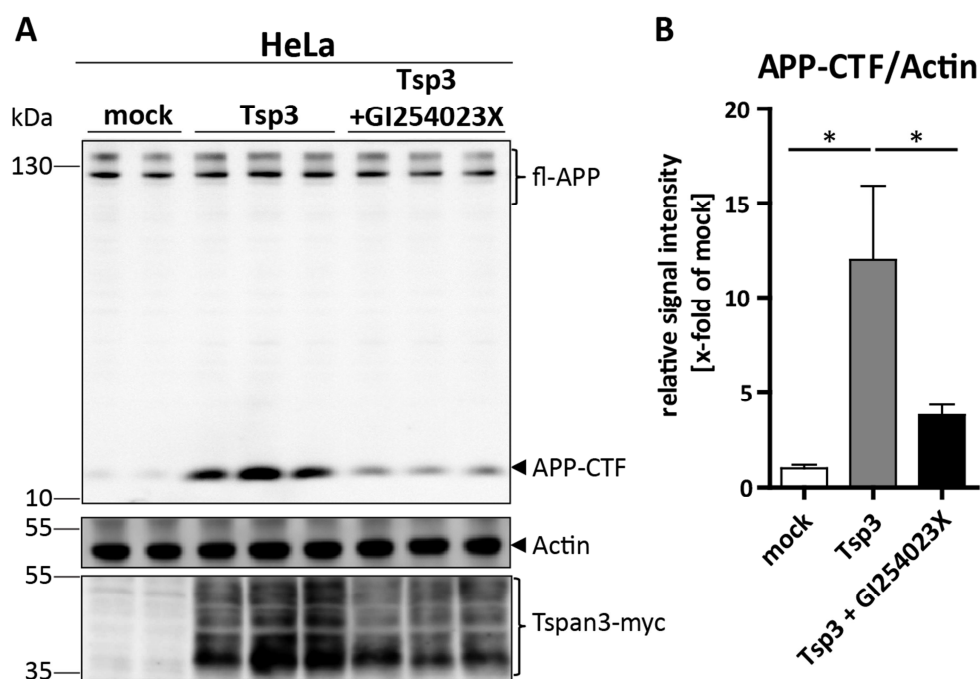


**Fig. 4.7: Inhibition of ADAM10 counteracts the Tspan3-induced increase of the APP-CTF.**

**A)** Immunoblot analysis of Tspan3-myc (Tsp3) expressing HeLa cells, which were incubated with 10  $\mu$ M GI254023X (Tsp3+GI254023X) or left untreated for 24 h. Cells transfected with an empty vector (mock) were used as negative control. Expression of full length (fl)-APP and the APP-C-terminal fragment (CTF) were analysed using a C-terminal anti-APP antibody. Equal protein loading was confirmed by anti-actin staining and expression of Tsp3 was detected with an anti-myc antibody. **B)** Quantitative analysis of APP-CTF signal intensities. The graph depicts the calculated mean values  $\pm$ SD of APP-CTF/Actin normalised to the mock control. Statistical significance was analysed by one-way ANOVA followed by Bonferroni's post-hoc test (\* $p$ <0.05).

To verify this finding by another approach not relying on pharmacological inhibition, the Tspan3 induced generation of the APP-CTF was monitored after siRNA-mediated knockdown of ADAM10 in N2a cells. Mock transfected and Tspan3-myc (Tsp3) expressing N2a cells were treated with a non-targeting control siRNA (Ctrl siRNA) or an ADAM10-specific siRNA (A10 siRNA). Cells were lysed and an immunoblot analysis of APP, ADAM10 and Tspan3-myc was performed (Fig. 4.8). Tspan3-myc expression led to a significant increase (12.5-fold) of the APP-CTF in control siRNA (Ctrl siRNA, Tsp3) transfected cells (Fig. 4.8A, B). Likewise, APP-CTF signal intensities increased in Tspan3-myc expressing, ADAM10 siRNA transfected cells (A10 siRNA, Tsp3), but this effect was less pronounced compared to Tspan3-myc transfected, control siRNA treated (Ctrl siRNA, Tsp3) samples (Fig. 4.8A, B). Efficiency of the siRNA-

mediated knockdown was confirmed by a considerable decrease of pro- and mature ADAM10 after treatment with ADAM10 siRNA (A10 siRNA), compared to control siRNA (Ctrl siRNA) treated samples (Fig. 4.8A). This data further indicates, that the increased appearance of the APP-CTF after Tspan3-myc expression is related to ADAM10-mediated APP processing.

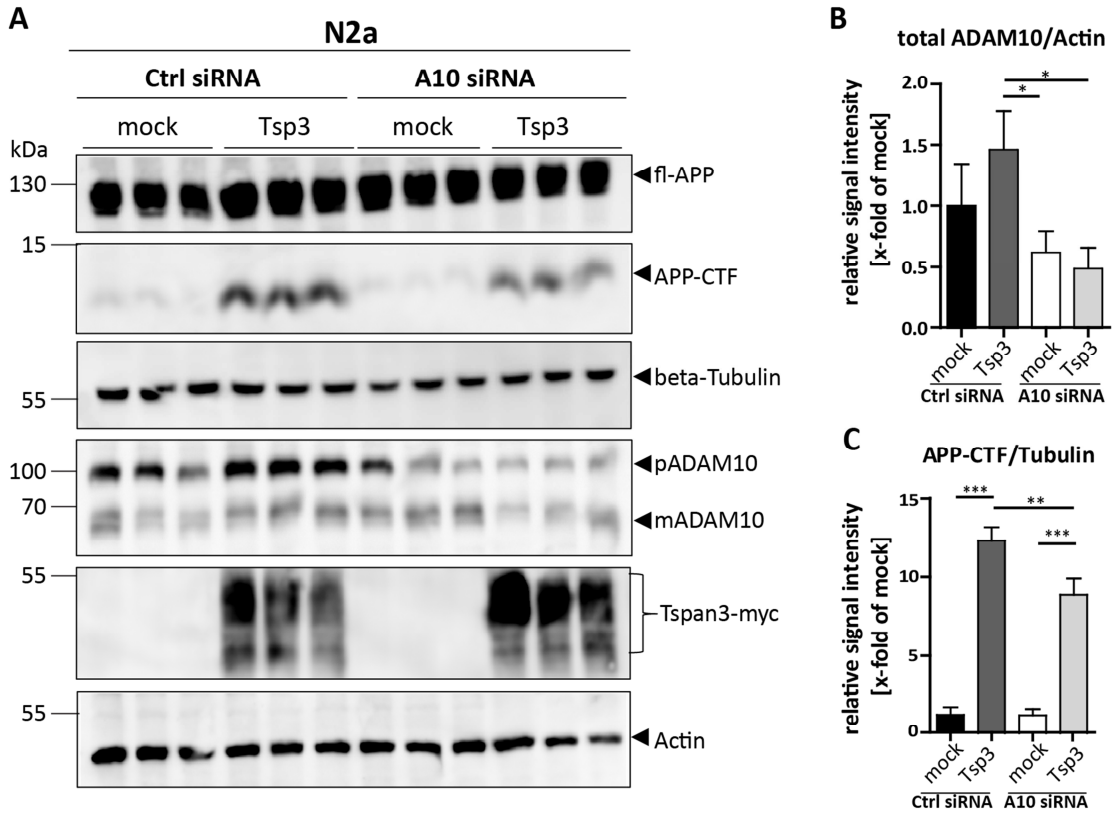


**Fig. 4.8: siRNA-mediated ADAM10 knockdown diminishes the Tspan3 induced increase of the APP-CTF.**

**A)** N2a cells were transiently transfected with Tspan3-myc (Tsp3) or a mock control. For siRNA-mediated knockdown of ADAM10, cells were additionally treated with an unspecific control (ctrl siRNA) or ADAM10-specific siRNA (A10 siRNA). Following lysis and immunoblotting, full length (fl-) APP and the APP-C-terminal fragment (CTF) were detected. Successful knockdown of pro- (p) and mature (m) ADAM10 was observed with a C-terminal anti-ADAM10 antibody in A10 siRNA transfected samples. Tsp3 expression was verified by anti-myc staining. **B-C)** Quantitative analysis of total ADAM10 (pro + mature)/Actin and APP-CTF/Tubulin signal intensities shown as mean values  $\pm$ SD. Ctrl siRNA, mock transfected samples were set to one. For statistical analysis, a one-way ANOVA followed by Bonferroni's multiple comparisons test was performed (\*  $p < 0.05$ , \*\*  $p < 0.005$ , \*\*\*  $p < 0.001$ ).

Similar to the previous experiments, the heterologous expression of Tspan3-myc (Tsp3) in ADAM10-deficient (A10<sup>-/-</sup>) human embryonic kidney (HEK293) cells clearly diminished the appearance of the APP-CTF (Fig. 4.9A, B) compared to wild-type (wt) and ADAM17-deficient (A17<sup>-/-</sup>) cells.

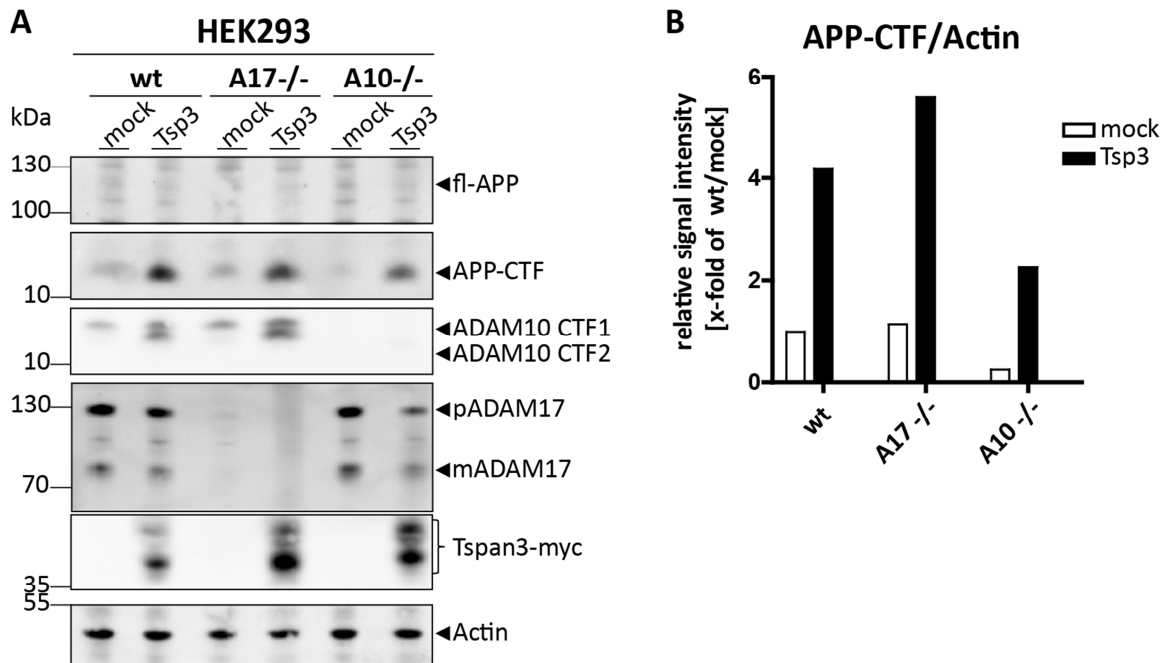


**Fig. 4.9: Analysis of APP processing in ADAM10- and ADAM17-deficient HEK293 cells.**

**A)** Wild-type (wt), ADAM10 (A10<sup>-/-</sup>) and ADAM17 (A17<sup>-/-</sup>) deficient human embryonic kidney (HEK293) cells were transiently transfected with Tspan3-myc (Tsp3) and analysed by immunoblot. Full length (fl-) APP and the APP-C-terminal fragment (CTF) were detected with a C-terminal anti-APP antibody. Tspan3-myc expression was confirmed by anti-myc staining. ADAM10-CTFs, pro- (p) and mature (m) ADAM17 were detected with an anti-ADAM10 and anti-ADAM17 antibody, respectively. **B)** The ratio of the APP-CTF/actin signal intensity was calculated and normalised to HEK293 wt mock transfected cells (wt/mock).

Taken together, the downregulation of ADAM10 activity or expression, using inhibitor or siRNA treatment, reduced the Tspan3-induced increase of the APP-CTF. Additionally, expression of Tspan3 in ADAM10<sup>-/-</sup>, but not in ADAM17-deficient HEK293 cells, attenuated the increase of the APP-CTF compared to wild-type HEK293 cells.

#### 4.1.7 Overexpression of tetraspanin-3 promotes $\alpha$ -secretase cleavage, but does not influence $\beta$ - and $\gamma$ -secretase cleavage of APP

The previous experiments indicate that Tspan3 expression increases the generation of the APP-CTF, which is related to ADAM10. To further analyse this, the influence of Tspan3 on the appearance of the ADAM10-generated, soluble counterpart of the APP-CTF C83, soluble APP $\alpha$  (sAPP $\alpha$ ), was analysed.

HEK293 cells stably overexpressing human wild-type APP695 (APP-wt) were mock or Tspan3-myc (Tsp3) transfected, cell culture supernatants (SN) were collected and cells were lysed. The supernatants and lysates were subjected to immunoblot and generation of APP cleavage products was observed (Fig. 4.10). In the cell lysates, full length (fl-) APP and the APP-CTF

were detected. The expression of Tspan3-myc did not alter signal intensities of fl-APP but led to a significant increase of the APP-CTF as compared to mock transfected samples (Fig. 4.10A, B). Similar, a considerable increase of sAPP $\alpha$  was observed in cell culture supernatants of cells expressing Tspan3-myc.

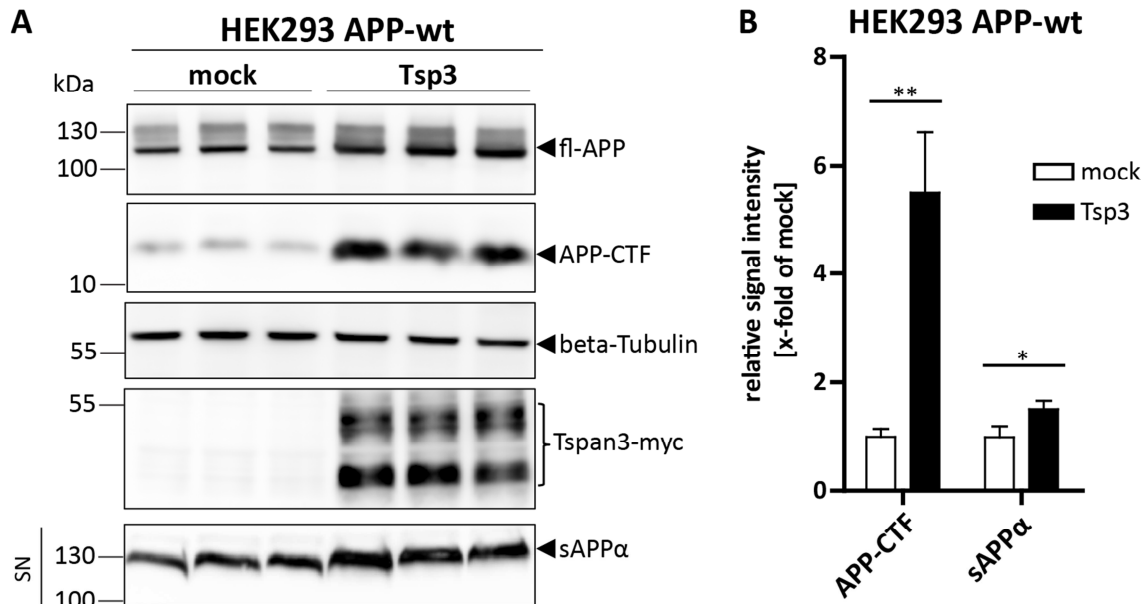


**Fig. 4.10: Expression of Tspan3 in HEK293 APP-wt cells increases APP-CTF and sAPP $\alpha$  levels.**

**A)** HEK293 cells stably overexpressing human APP695 (APP-wt) were transiently transfected with Tspan3-myc (Tsp3) or a mock control (mock). Cell culture supernatants (SN) were collected and cells were lysed. After immunoblotting, full length (fl-) APP and APP-C-terminal fragments (CTFs) were detected in cell lysates. Using an APP antibody raised against an epitope N-terminal to the ADAM10 cleavage site, sAPP $\alpha$  was detected in the cell culture supernatants (SN). Equal protein loading and expression of Tsp3 was confirmed by anti-tubulin and anti-myc staining in cell lysates. **B)** Quantification of APP-CTF and sAPP $\alpha$  signal intensities. Data is presented as mean values  $\pm$ SD normalised to mock transfected samples. Statistical significance was tested using the Student's t-test. (\* $p$ <0.05, \*\* $p$ <0.005).

In most non-neuronal cell lines, APP processing is predominantly mediated by ADAM10 (Saftig and Lichtenthaler, 2015) and the  $\beta$ -secretase generated  $\beta$ CTF (C99) is rarely detectable. In order to evaluate whether Tspan3 has an impact on  $\beta$ -secretase cleavage of APP, APP processing was assessed in HEK293 cells, which stably overexpress human APP695, harbouring the Swedish mutation (Citron et al., 1992; Mullan et al., 1992). Due to an amino acid substitution KM670/671NL, the Swedish mutant APP695 (APP-swe) favours  $\beta$ -secretase cleavage and generates increasing amounts of the  $\beta$ CTF C99 and soluble A $\beta$  (Citron et al., 1992; Felsenstein et al., 1994; Scheuner et al., 1996).

HEK293 APP-swe cells were transfected with Tspan3-myc (Tsp3) or a mock control, supernatants were collected and cell lysates were prepared. APP cleavage was then assessed by immunoblot analysis (Fig. 4.11). After immunoblotting, fl-APP and APP-CTFs, C99 and C83

were detected in the cell lysates (Fig. 4.11A). The expression of Tspan3-myc increased the signal intensity of the lower molecular weight APP-CTF (10 kDa), which corresponds to the APP-C83 fragment, but did not alter the signal intensity of the APP-CTF C99 (12 kDa). In the supernatants (SN), sAPP $\alpha$  and A $\beta$  were detected with an anti-APP antibody raised against the first N-terminal amino acids of the A $\beta$  domain. In contrast to the previous finding, Tspan3-myc expression in HEK293 APP-swe cells did not alter sAPP $\alpha$  levels, but significantly decreased A $\beta$  levels. This discrepancy might be explained by the finding that increased  $\alpha$ -secretase activity reduced the release of A $\beta$  by conversion of the  $\beta$ CTF APP-C99 to  $\alpha$ CTF APP-C83 in HEK293 APP-swe cells (Kuhn et al., 2010). Hence, Tspan3 could increase ADAM10-dependent generation of the APP-C83, while sAPP $\alpha$  levels remain unchanged. This further supports the finding that Tspan3 specifically promotes ADAM10-mediated APP processing, but does not influence  $\beta$ -secretase activity.

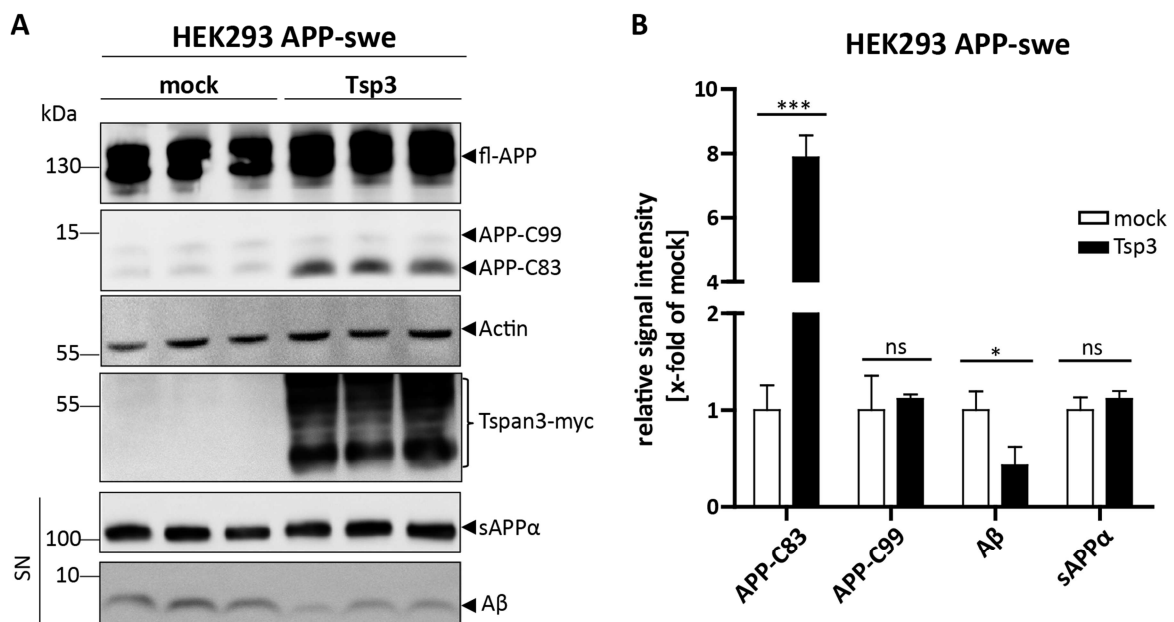


**Fig. 4.11: Tspan3 increases the appearance of the APP fragment C83 and reduces A $\beta$ -levels.**

**A)** HEK293 cells stably overexpressing APP-swe were transfected with Tspan3-myc (Tsp3). Cells were lysed and full length (fl-) APP and APP C-terminal fragments C99 and C83 were detected. **B)** Quantification of APP-C83, APP-C99, A $\beta$  and sAPP $\alpha$  signal intensities. Values were related to mock transfected cells and are shown as means  $\pm$ SD. Statistical significance was analysed using Student's t-test (\* $p$ <0.05, \*\*\* $p$ <0.001, ns: not significant).

Following  $\alpha$ - and  $\beta$ -secretase cleavage, the  $\gamma$ -secretase complex further degrades APP-CTFs. Thus, the increased appearance of the APP-C83 due to Tspan3 expression could also result from decreased  $\gamma$ -secretase cleavage. To address this issue, the effects of a  $\gamma$ -secretase

inhibitor and Tspan3 expression on the generation of APP-C-terminal fragments were compared.

N2a cells were mock or Tspan3-myc (Tsp3) transfected and treated with 1  $\mu$ M of the  $\gamma$ -secretase inhibitor X or left untreated for 24 h. To distinguish the different APP-CTF species, cells were treated with 1  $\mu$ M of the broadband metalloprotease inhibitor marimastat, which inhibits  $\alpha$ -secretase activity, or the  $\beta$ -secretase inhibitor C3, respectively. Cell lysates were separated on a 16% tris-tricine gel and APP-CTF generation was analysed by immunoblot analysis (Collaboration with *Dr. Barry Boland*, University College Cork, Ireland, Fig. 4.12).

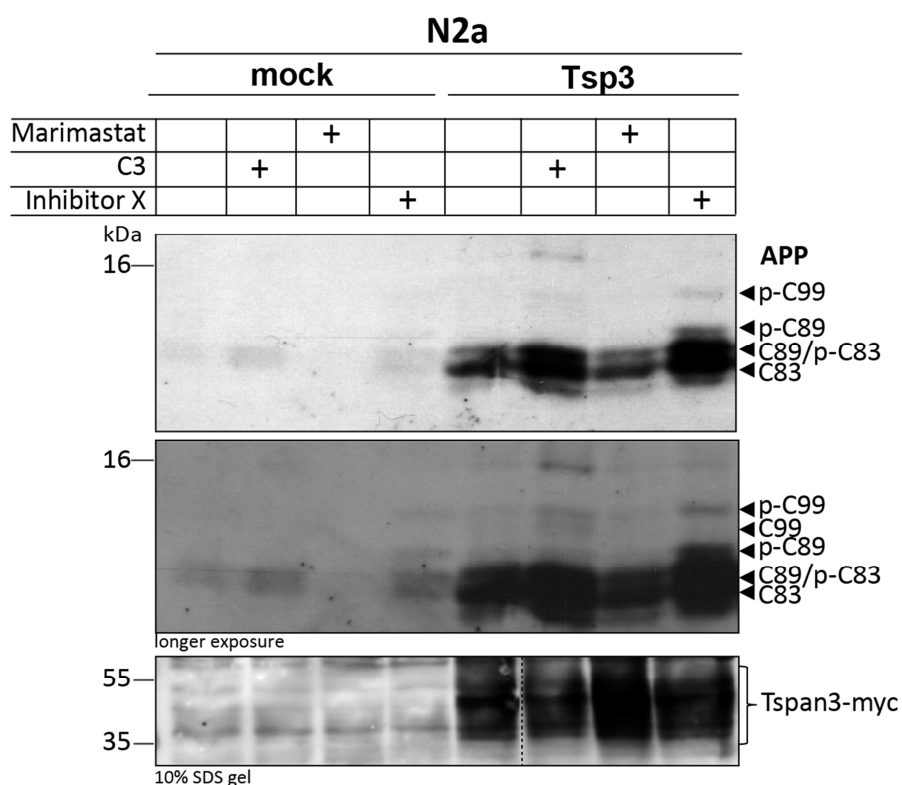


**Fig. 4.12: Tspan3 expression does not inhibit  $\gamma$ -secretase activity.**

N2a cells were transiently transfected with a mock control (mock) or Tspan3-myc (Tsp3). 24 h before lysis cells were treated with 1  $\mu$ M marimastat,  $\beta$ -secretase inhibitor C3,  $\gamma$ -secretase inhibitor X or left untreated. Cell lysates were separated on a 16% tris-tricine gel, immunoblotted and APP-C-terminal fragments C99, C89, C83 and respective phosphorylated (p) C-terminal fragment species detected with a C-terminal anti-APP antibody (C1/6.1). Tsp3 expression was confirmed by staining with an anti-myc antibody. (Collaboration with *Dr. Barry Boland*, University College Cork, Ireland).

After staining with an anti-APP antibody, phosphorylated (p) and non-phosphorylated APP-CTF species, C83, C99 and the alternative  $\beta$ -secretase cleavage product C89 were detected (Fig. 4.12). In mock transfected cells,  $\beta$ -secretase inhibition increased the appearance of the C83 and p-C83, whereas  $\alpha$ -secretase inhibition (marimastat) almost abolished the appearance of both fragments, compared to untreated cells (Fig. 4.12). This was

even clearer after a longer exposure time (Fig. 4.12, longer exposure). In the same mock transfected samples, treatment with the  $\gamma$ -secretase inhibitor X resulted in a clear increase of C83, p-C83, p-C99 and p-C89 signal intensities. Compared to such a treatment, Tspan3-myc (Tsp3) expression in untreated cells increased signal intensities of the  $\alpha$ CTFs C83 and the pC83, but did not alter the appearance of  $\beta$ CTFs, pC89, pC99 as observed in mock transfected, inhibitor X treated cells. Tspan3-myc expression in combination with  $\beta$ -secretase inhibitor treatment reinforced the appearance of  $\alpha$ CTFs and led to the appearance of a faint, higher molecular weight signal. Incubation of Tspan3-myc expressing cells with inhibitor X increased the appearance of  $\beta$ CTFs, p-C99 and p-C89, and enhanced the appearance of the C83 and p-C83 compared to Tspan3-myc transfected, untreated cells.

Altogether, these experiments demonstrated that overexpression of Tspan3 increases  $\alpha$ -secretase-mediated APP cleavage and does not influence  $\beta$ -secretase activity or inhibit  $\gamma$ -secretase cleavage. Moreover, by increasing  $\alpha$ -secretase-mediated APP processing, Tspan3 overexpression also reduced the amyloidogenic release of A $\beta$ .

#### 4.1.8 Immunofluorescence analysis of the subcellular localisation of tetraspanin-3

In correlation with the localisation of the active form of ADAM10, APP  $\alpha$ -secretase cleavage is supposed to take place at the cell surface and to a minor extent in late secretory compartments (Lammich et al., 1999). In contrast, amyloidogenic  $\beta$ -secretase processing is supposed to occur in the trans-Golgi network and endosomal compartments, where BACE1 is mainly localised (Koo and Squazzo, 1994; Vassar, 1999).

To gain more insight into the role of Tspan3 in ADAM10-mediated APP processing, the subcellular localisation of Tspan3 was analysed by indirect immunofluorescence.

Heterologously expressed Tspan3-myc (Tsp3-myc) or endogenous Tspan3 (Tsp3) was visualised in HeLa cells using an anti-myc or a C-terminal anti-Tspan3 primary antibody followed by incubation with a fluorophore-coupled secondary antibody. Marker proteins of endosomal and lysosomal compartments were co-stained and co-localisation with Tspan3 analysed by confocal microscopy (Fig. 4.13).

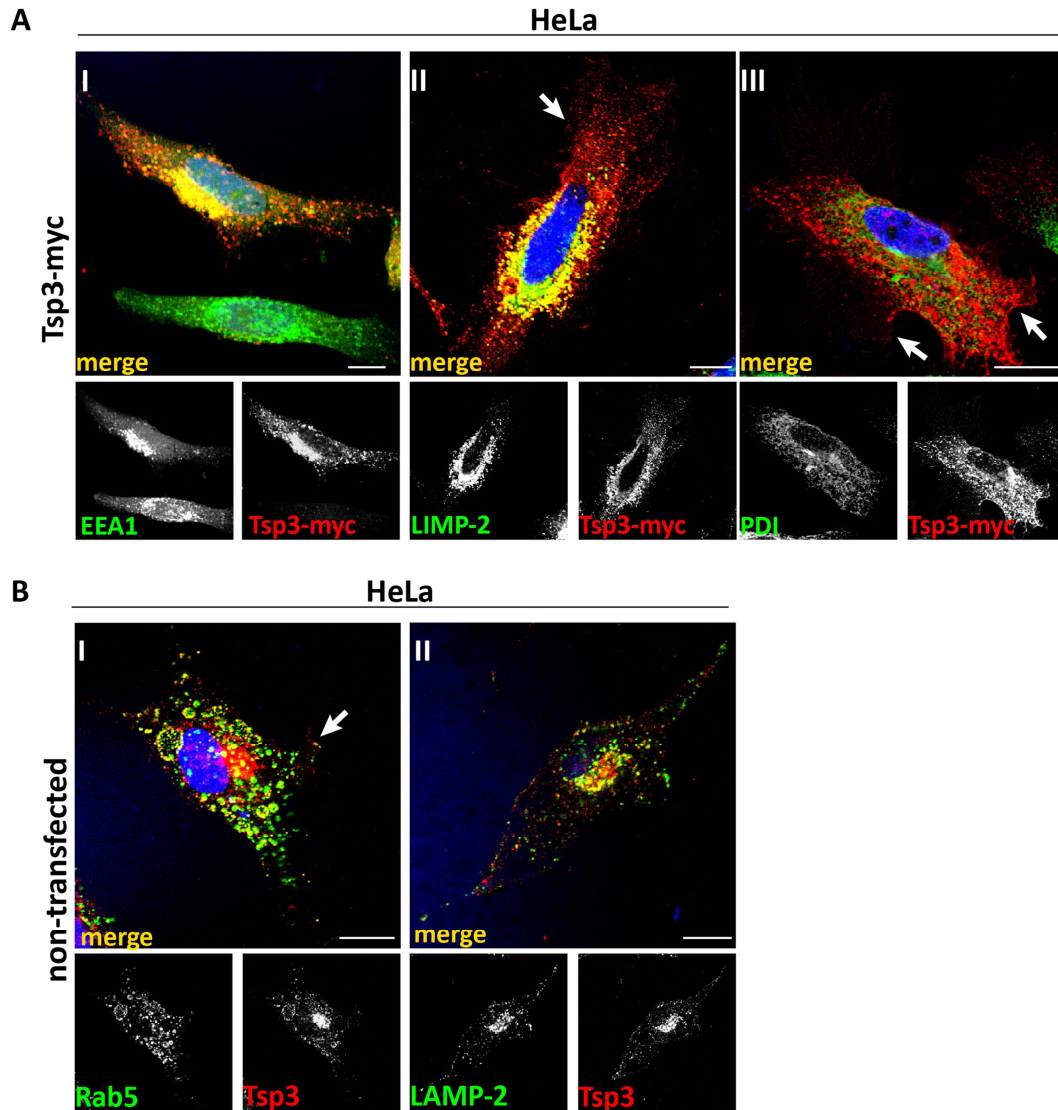


**Fig. 4.13: Tspan3 is mainly localised in endosomal compartments.**

**A)** HeLa cells were transfected with Tspan3-myc (Tsp3-myc). After fixation, Tsp3-myc was visualised using an anti-myc primary antibody and a fluorophore-coupled secondary antibody. Co-localisation with the endosomal marker EEA1 (I), lysosomal LIMP-2 (II) and the ER-marker protein PDI (III) was then analysed by confocal microscopy. White arrows indicate localisation of Tspan3-myc at the plasma membrane. **B)** Endogenous Tspan3 (Tsp3) was visualised in HeLa cells using a C-terminal anti-Tspan3 antibody and co-localisation with the early endosomal marker protein Rab5 (I) and the lysosomal protein LAMP-2 (II) was observed. White arrows indicate localisation of endogenous Tspan3 at the plasma membrane. Scale bars represent 10  $\mu\text{m}$  (**A, B**). EEA1: early endosomal antigen 1, LIMP-2: lysosomal integral membrane protein 2, PDI: protein disulfide isomerase, LAMP2: lysosomal associated membrane protein-2, Rab5: Ras-related protein Rab5A.

Detection of Tspan3-myc (red) revealed a predominant intracellular and vesicular fluorescence staining (Fig. 4.13A, I-III). Minor amounts were also found at the cell surface, indicated by white arrows (Fig. 4.13A, II-III). The co-staining of Tspan3-myc (red) with the early endosomal marker protein early endosomal antigen 1 (EEA1, green) resulted in a strong overlap of Tspan3-myc and EEA1 fluorescence signals (yellow) in the merged picture (Fig. 4.13A, I). A partial co-localisation of Tspan3-myc was also observed with the lysosomal



integral membrane protein-2 (LIMP-2, Fig. 4.13A, II). No co-localisation was detected with the ER-marker protein disulfide-isomerase (PDI, Fig. 4.13A, III). Likewise, endogenous Tspan3 (Tsp3, Fig. 4.13B) predominantly co-localised with the early endosomal marker Ras-related protein Rab5A (Rab5, Fig. 4.13B, I) and with the lysosome-associated membrane protein-2 (LAMP-2, Fig. 4.13B, II). Only a small quantity of endogenous Tspan3 was found at the cell surface (Fig. 4.13, I, white arrow).

Further immunofluorescence studies aiming to analyse the localisation of APP revealed that heterologous expressed Tspan3-myc (Tsp3) co-localised with endogenous APP in HeLa cells. Similar to the observed cellular distribution of Tspan3-myc, co-localisation with APP was observed in intracellular vesicular-like structures and at the cell periphery close to the plasma membrane, as indicated by white arrows (Fig. 4.14, I). The overexpression of APP-wt together with Tspan3-myc (Tsp3+APP-wt) increased the overall staining of APP (Fig. 4.14, II). This further increased the overlap of APP and Tspan3-myc signals at the plasma membrane, but also in intracellular vesicular-like structures (Fig. 4.14, II, indicated by white arrows).

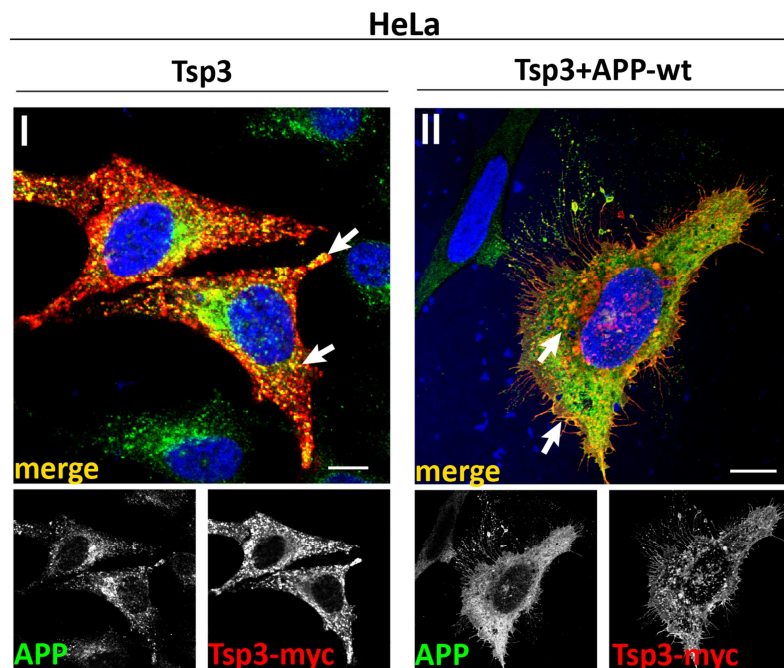


**Fig. 4.14: Tspan3 co-localises with endogenous and overexpressed APP in HeLa cells.**

HeLa cells were transfected with (I) Tspan3-myc alone or (II) together with human APP695 (APP-wt) and analysed by indirect immunofluorescence. Endogenous (I) and overexpressed (II) APP was visualised with a C-terminal anti-APP antibody (green). Heterologous expressed Tspan3-myc (I, II) was visualised with an ALEXA-594 antibody (red). White arrows indicate co-localisation of Tspan3-myc and endogenous (I) or overexpressed APP (II). Scale bars=10  $\mu$ m.

In conclusion, under steady state conditions, Tspan3 is predominantly localised in endosomal and lysosomal compartments. Not much Tspan3 was found at the cell surface. Interestingly, the co-staining of Tspan3 with APP revealed a close proximity between both proteins at the plasma membrane and in vesicular-like intracellular structures. Thus, indicating that APP could be another interaction partner of Tspan3.

#### **4.1.9 How does tetraspanin-3 modulate ADAM10-dependent APP processing?**

The previous experiments identified Tspan3 as a novel ADAM10 interaction partner, which increases ADAM10-mediated APP cleavage. Unlike most, already described, ADAM10-interacting tetraspanins, e.g. TspanC8, Tspan3 did not affect ADAM10 maturation or trafficking to the cell surface, which raised the question how Tspan3 modulates ADAM10-dependent APP processing.

Tetraspanins are capable of multiple interactions to organise their partner proteins in functional complexes at the plasma membrane (Boucheix and Rubinstein, 2001; Mattila et al., 2013; Rubinstein et al., 1996). Since the previous experiments indicated a close proximity of Tspan3 and APP, it was of interest whether Tspan3 modulates APP-processing by directly interacting with APP.

##### **4.1.9.1 Tetraspanin-3 interacts with APP and presenilin-1**

To examine if Tspan3 could act as a scaffold for APP cleavage, its possible interaction with APP and presenilin-1, the catalytic active subunit of the  $\gamma$ -secretase complex, was analysed.

Using stringent lysis conditions heterologous expressed Tspan3-myc was precipitated from HEK293 APP-wt cells transfected with Tspan3-myc (Tsp3) alone or together with ADAM10 (Tsp3/A10). A small amount of the lysate was kept to control for protein expression. Lysates and immunoprecipitates were subjected to immunoblot analysis and expression of Tspan3-myc, APP and presenilin-1 was analysed (Fig 4.15). After immunoblotting (Fig 4.15), anti-myc staining showed prominent signals of Tspan3-myc (IP Tspan3-myc) in Tsp3 and Tsp3/A10 precipitates, confirming successful immunoprecipitation (IP anti-myc). In the same samples, prominent signals of co-precipitated fl-APP and APP-CTFs (CoIP APP) were observed. Surprisingly, probing the precipitates for presenilin-1 revealed the N-terminal fragment (NTF) of presenilin-1 (PS1) as another Tspan3 associated protein (CoIP PS1). The co-expression of Tsp3 and ADAM10 (Tsp3/A10) did not alter the signal intensities of co-precipitated fl-APP, APP-CTFs and PS1, compared to Tsp3 single transfected cells. Immunoblot analysis of

respective total lysates (Input) confirmed the expression of Tspan3-myc, APP and presenilin-1 in HEK293 APP-wt cells.

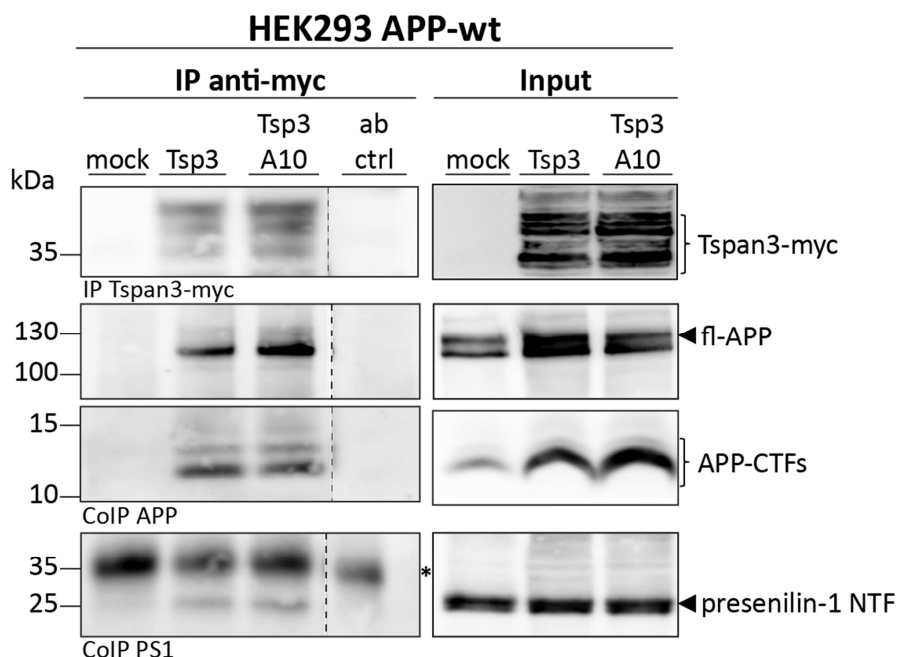


**Fig 4.15: Tspan3-myc interacts with APP and presenilin-1.**

Heterologously expressed Tspan3-myc (Tsp3) was immunoprecipitated from Tsp3 and Tsp3/ADAM10 (A10) transfected HEK293 APP-wt cells using an anti-myc antibody (IP Tspan3-myc). Co-immunoprecipitation of fl-APP, APP-CTFs (CoIP APP) and presenilin-1 (CoIP PS1) was observed after staining with an anti-APP or a N-terminal anti-presenilin-1 antibody, respectively. Using the same antibodies, expression of proteins was verified by immunoblot analysis of total lysates (Input). Fl: full length, CTF: C-terminal fragment, NTF: N-terminal fragment, \*: unspecific signal.

This experiment revealed APP and presenilin-1 as additional Tspan3-associated proteins. This further supports the idea that Tspan3 could act as a scaffold for the proteolytic processing of APP by connecting and stabilising APP together with some of its cleaving enzymes.

#### 4.1.9.2 Tetraspanin-3 overexpression increases the surface level of the APP-CTF

Recent studies demonstrated that APP processing can be regulated by modulation of its surface presence and endocytosis. While inhibition of endocytosis increased the generation of APP  $\alpha$ -secretase cleavage products and decreased A $\beta$  liberation, enhanced endocytosis increased the generation of  $\beta$ -secretase cleavage products (Grbovic et al., 2003; Koo and Squazzo, 1994; Neumann et al., 2006; Schöbel et al., 2006).

The finding, that Tspan3 interacts with APP and localises to early endosomes led to the assumption that Tspan3 could modulate APP processing by affecting its endocytosis. To address this issue, the influence of Tspan3 on the surface presence of APP was analysed.

APP cell surface expression was assessed by surface biotinylation of N2a cells transfected with Tspan3-myc (Tsp3) or Tspan15-myc (Tsp15). Non-transfected (UT) and mock transfected cells were used as negative controls. The cells were incubated with biotin (+Biotin) or left untreated (-biotin). A small amount of the total lysates was kept and biotin-labelled cell surface proteins were precipitated. Total lysates and pulldown fractions were analysed by immunoblot (Fig. 4.16).

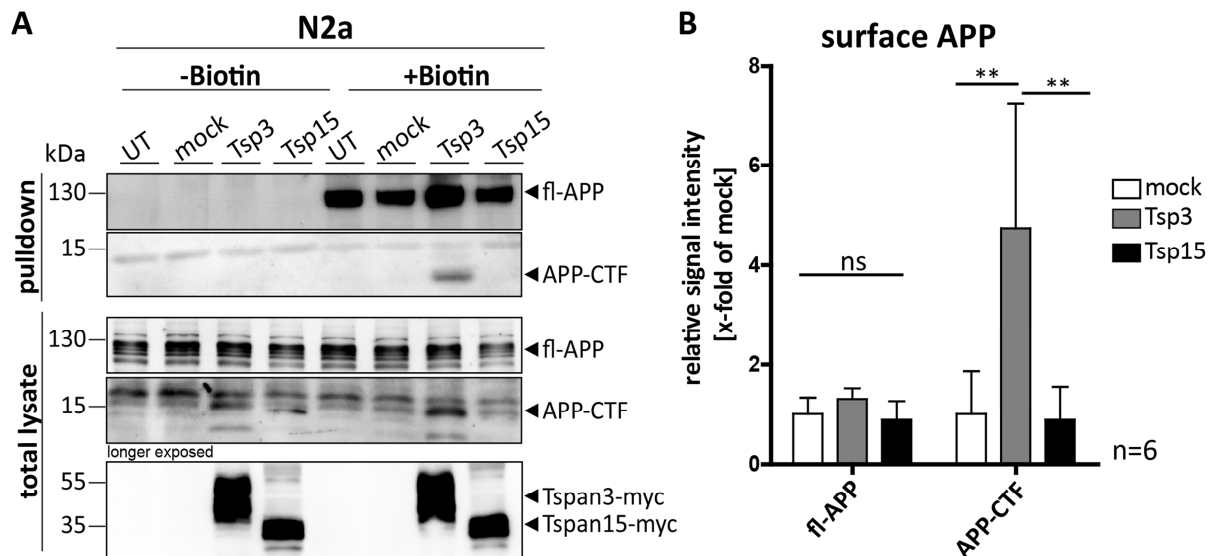


**Fig. 4.16: Overexpression of Tspan3 increases the surface levels of fl-APP and the APP-CTF.**

**A)** APP surface levels were analysed by surface biotinylation of N2a cells expressing Tspan3-myc (Tsp3) and Tspan15-myc (Tsp15). Untreated (UT) and mock transfected cells were used as negative controls. Biotinylated surface proteins were precipitated using streptavidin coupled beads (+Biotin, pulldown) and subjected to immunoblot. Full length (fl-) APP and APP-C-terminal fragment (CTF) were detected in the surface fraction using an anti-APP antibody. Expression of Tsp3, Tsp15 and APP was confirmed by immunoblot analysis of total lysates using an anti-myc or APP antibody, respectively. **B)** Quantification of APP surface levels of four independent experiments (n=6) shown as mean values  $\pm$ SD. (\*\*p<0.01 according to ANOVA and Bonferroni's post hoc test).

Using an anti-APP antibody, prominent signals of fl-APP and the APP-CTF were detected in biotinylated (+Biotin) pulldown fractions (Fig. 4.16). Surprisingly, the expression of Tspan3-myc led to a clear increase of the APP-CTF (pulldown, +Biotin), which was not visible in the other samples (Fig. 4.16A). In comparison to mock and Tspan15-myc transfected samples, Tspan3-myc expression also tends to increase the surface level of fl-APP (Fig. 4.16A, B). These results revealed that the overexpression of Tspan3-myc modulates the cell surface expression of APP, in particular that of the APP-CTF. This supports the notion that Tspan3-myc could act as a stabiliser for APP at the cell surface, thereby facilitating  $\alpha$ -secretase cleavage possibly by modulating its endocytosis.

#### 4.1.9.3 Mutation of the tetraspanin-3 endocytic motif modulates the surface level of APP

In accordance with the predominant endosomal localisation of Tspan3 (see section 4.1.8), sequence analysis of Tspan3 revealed the presence of an endosomal sorting signal within its C-terminal cytoplasmic tail (Berditchevski and Odintsova, 2007). This signal consists of the amino acid sequence “tyrosine (Y), glutamic acid (E), leucine (L), leucine (L)” (abbreviated as “YELL”, Fig. 4.17A) and conforms to the consensus sequence of YXXΦ tyrosine-based endocytic sorting motifs, where Φ is a bulky, hydrophobic amino acid (Jadot et al., 1992; Kozik et al., 2010).

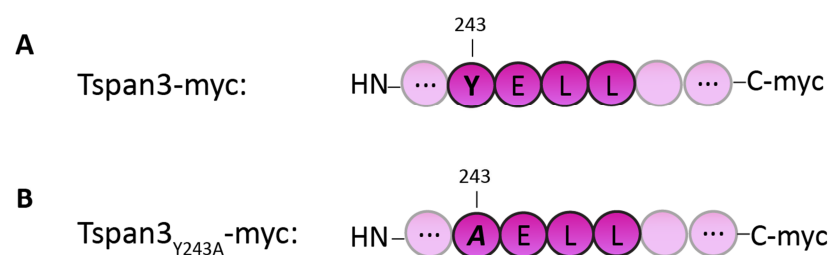


**Fig. 4.17: Tspan3 contains an endocytic sorting motif within its C-terminal tail.**

**A)** Schematic draw showing the sequence of the cytoplasmic C-terminal part of the murine wild-type (wt) Tspan3-myc (Tsp3). Amino acid sequence of the tyrosine-based endocytic sorting motif “Y<sub>243</sub>-E-L-L” is shown in one letter code. **B)** Based on the sequence of wt Tspan3-myc shown in **A)** Tspan3<sub>Y243A</sub>-myc was generated by PCR based mutation of the DNA sequence coding for tyrosine 234 (Y<sub>234</sub>) to alanine (A).

To evaluate whether this endocytic motif is relevant for the function of Tspan3 and its role in ADAM10-mediated APP shedding, the tyrosine at position 243 (Y<sub>243</sub>) of the murine Tspan3-myc expression construct (Fig. 4.17A) was exchanged by an alanine (A), using PCR-based mutagenesis (Fig. 4.17B). The impact of this mutation on the subcellular localisation of Tspan3 was analysed by immunofluorescence.

Either wild-type Tspan3-myc (Tsp3) or the mutated Tspan3<sub>Y243A</sub>-myc (Tsp3<sub>Y243A</sub>) were expressed in HeLa cells and visualised by indirect immunofluorescence staining using an anti-myc antibody. Co-staining of the early endosomal marker EEA1 was performed and cells analysed by confocal microscopy (Fig. 4.18).

Probing for the myc-epitope in Tspan3<sub>Y243A</sub>-myc (Tsp3<sub>Y243A</sub>-myc) transfected cells, revealed prominent fluorescence signals at the cell surface and in intracellular vesicular like structures (Fig. 4.18B). In comparison to that, detection of Tspan3-myc (Tsp3-myc) showed mainly an intracellular and only a weak membrane staining (Fig. 4.18A). Co-staining of the endosomal marker protein EEA1 with Tspan3-myc and Tspan3<sub>Y243A</sub>-myc, respectively, revealed

significantly less co-localisation of EEA1 and Tspan3 in cells expressing Tspan3<sub>Y243A</sub>-myc (Pearson's coefficient=  $0.86 \pm 0.05$ ), compared to cells expressing Tspan3-myc (Pearson's coefficient=  $1.00 \pm 0.03$ ) (Fig. 4.18A, B). However, a large part of Tspan3<sub>Y243A</sub>-myc was still intracellularly found.

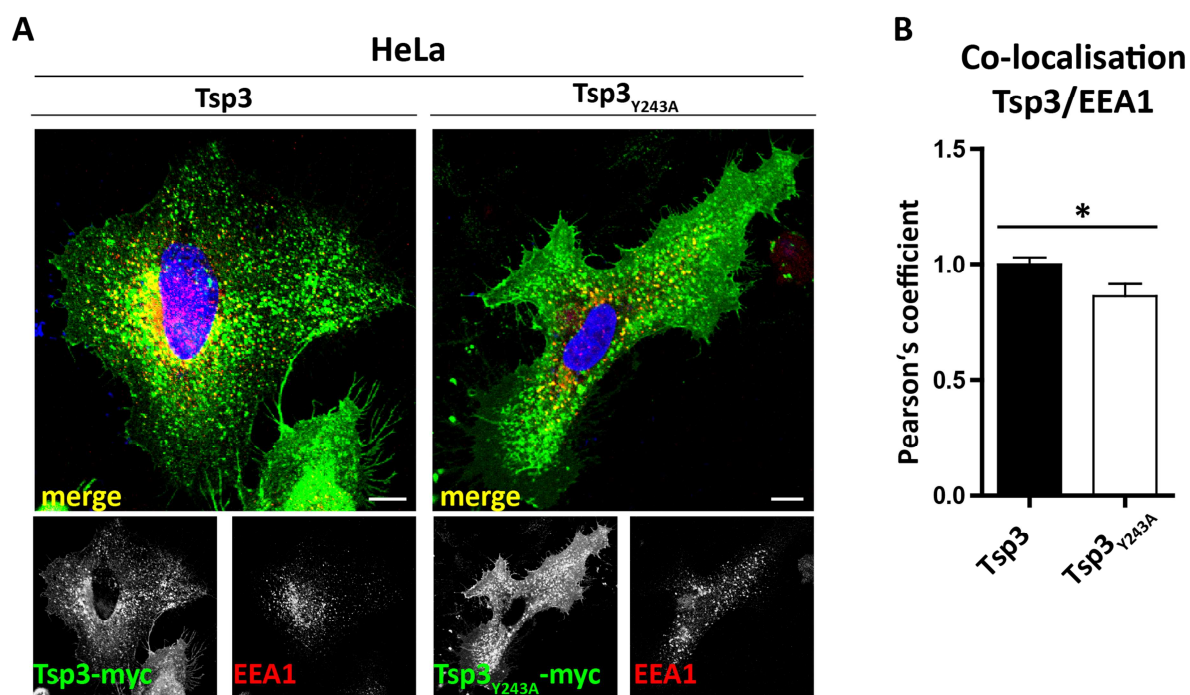


**Fig. 4.18: Comparison of the subcellular localisation of wild-type Tspan3-myc and Tspan3<sub>Y243A</sub>-myc in HeLa cells.**

**A)** HeLa cells transfected with Tspan3-myc (Tsp3-myc) or Tspan3<sub>Y243A</sub>-myc (Tsp3<sub>Y243A</sub>-myc) were analysed by indirect immunofluorescence. Tsp3-myc and Tsp3<sub>Y243A</sub>-myc were visualised with an anti-myc antibody and co-localisation with EEA1 was analysed by confocal microscopy. **B)** Co-localisation of EEA1 with Tsp3-myc and Tsp3<sub>Y243A</sub>-myc was quantified by determination of the Pearson's correlation coefficient (n=12). Statistical significance was tested using Student's t-test (\*p<0.05). EEA1: early endosomal antigen 1.

In an independent approach, the cell surface expression of Tspan3 was analysed by cell surface biotinylation of N2a cells transiently transfected with Tspan3-myc, Tspan3<sub>Y234A</sub>-myc and Tspan15-myc. Mock transfected cells were used as negative control. Prior cell lysis, the cells were treated with biotin (+Biotin) at 4°C to label surface proteins or left untreated (-Biotin). A small amount of the lysate was kept to control for protein expression and the residual lysate was used for precipitation with streptavidin-coupled beads. Subsequently, immunoblotting of precipitates and lysates was performed and Tspan3 expression was analysed (Fig. 4.19).

Staining with an anti-myc antibody showed an increased signal intensity in the biotinylated surface fraction (pulldown, +Biotin) of Tspan3<sub>Y234A</sub>-myc (Tsp3<sub>Y243A</sub>) transfected samples,

compared to Tspan3-myc (Tsp3). Tspan15-myc (Tsp15) was also detected in the pulldown fraction (pulldown, +Biotin) and had a comparable signal intensity as observed for Tspan3<sub>Y234A</sub>-myc. No signals were observed in the mock transfected biotinylated (+Biotin) and untreated (-Biotin) control samples. Only faint background signals were observed after probing the pulldown fraction for GAPDH, validating the pulldown of surface proteins. Detection of myc-tagged proteins in the total lysates confirmed expression of Tspan3-, Tspan3<sub>Y243A</sub>- and Tspan15-myc.

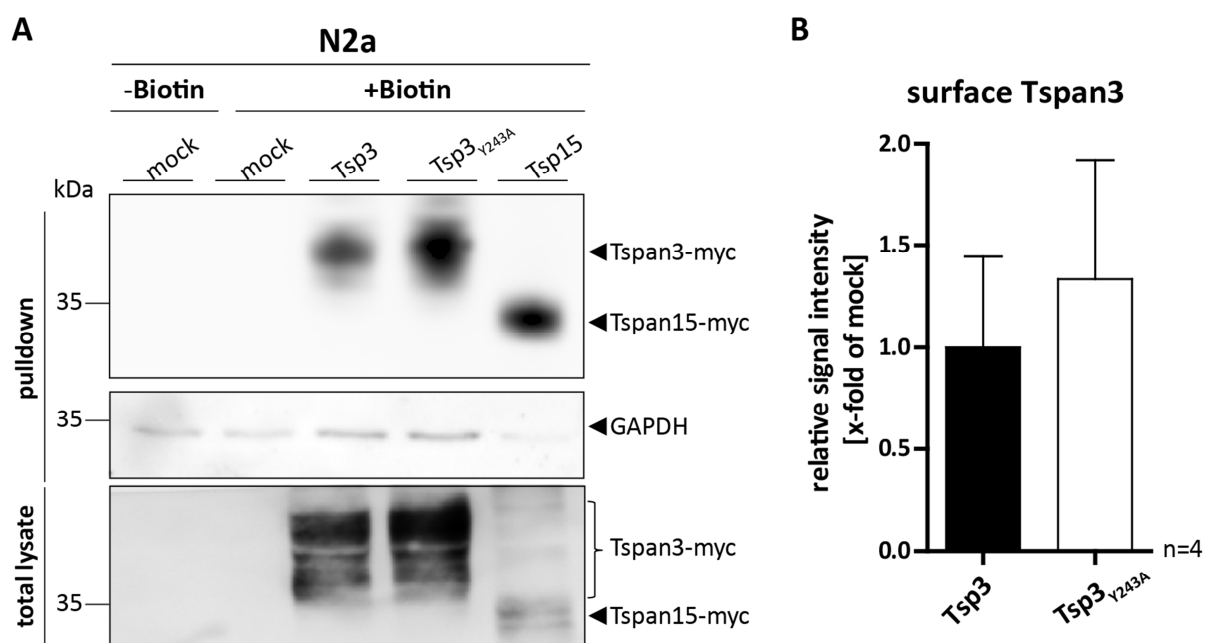


**Fig. 4.19: Mutation of the Tspan3 endocytic motif “YELL” increases its surface expression.**

**A)** N2a cells transiently transfected with Tspan3-myc (Tsp3), Tspan3<sub>Y243A</sub>-myc (Tsp3<sub>Y243A</sub>), Tspan15-myc (Tsp15) and an empty vector as mock control were incubated with Biotin (+Biotin) or left untreated (-Biotin). Precipitation of biotinylated proteins was performed and an immunoblot analysis of Tspan3 expression was conducted. GAPDH staining was used to control unspecific binding of cytosolic proteins. Immunoblot analysis of total lysates confirmed protein expression of Tspan3-, Tspan3<sub>Y243A</sub>- and Tspan15-myc. **B)** Densitometric analysis of Tspan3 cell surface levels in cells expressing Tspan3-myc (Tsp3) and Tspan3<sub>Y243A</sub>-myc (Tsp3<sub>Y243A</sub>) of four independent experiments (n=4). The ratio of surface Tsp3 and Tsp3<sub>Y243A</sub> to respective total Tspan3 in lysates was calculated. Data is shown as mean values ±SD.

Since the previous experiments demonstrated, that mutation of the “YELL” endocytic motif increased the surface presence of Tspan3, it was of interest whether this in turn influences the cell surface expression of APP.

To address this question, APP cell surface levels were analysed by cell surface biotinylation of N2a cells expressing wt Tspan3-myc (Tsp3) or Tsp3<sub>Y243A</sub>-myc (Tsp3<sub>Y243A</sub>). Mock and Tspan15-myc (Tsp15) transfected cells served as controls. After pulldown of biotinylated proteins, total lysates and pulldown fractions were analysed by immunoblot (Fig. 4.20A).

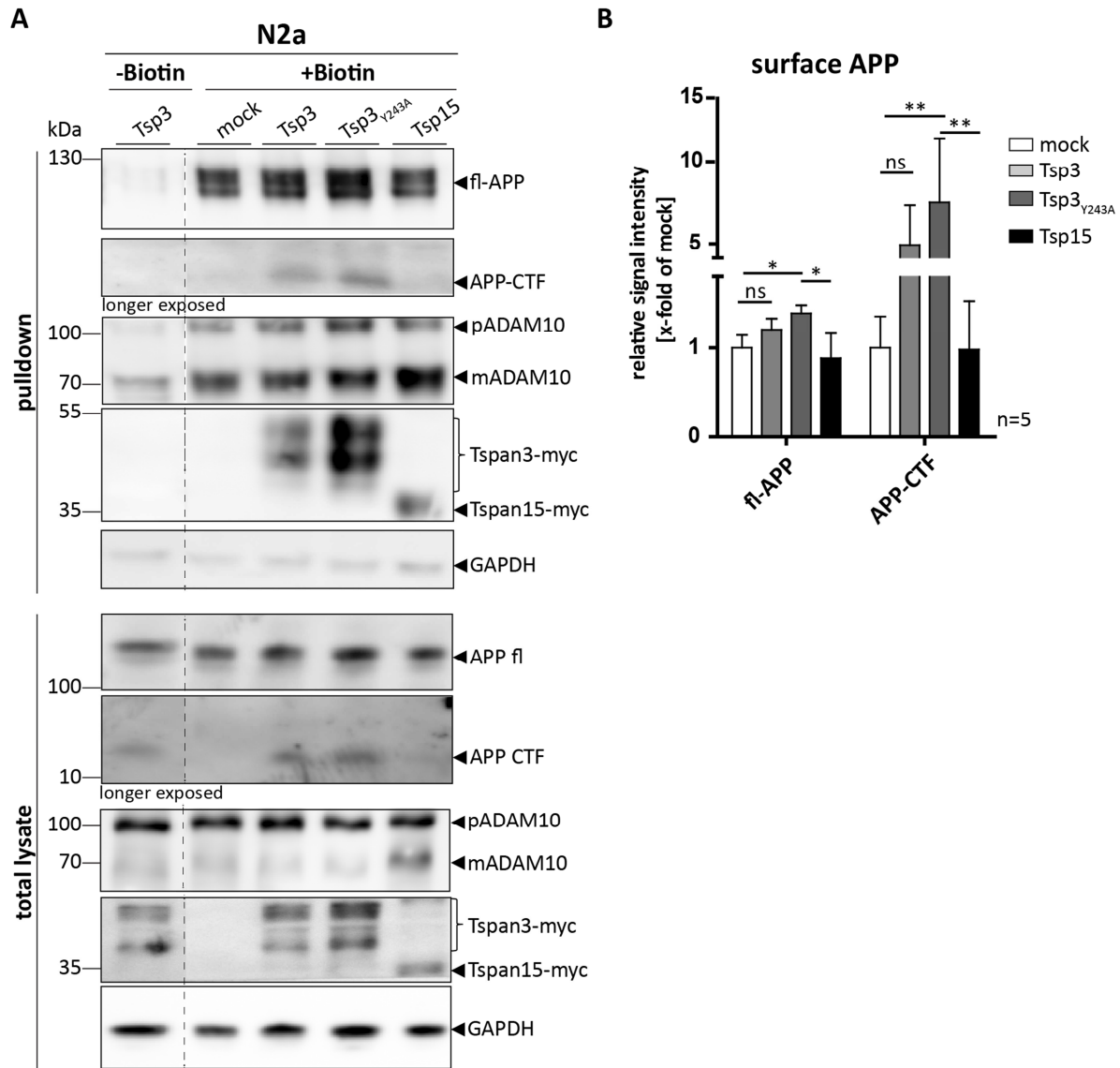


**Fig. 4.20: Expression of Tspan3<sub>Y243A</sub>-myc increases the surface levels of APP and ADAM10.**

**A)** Surface biotinylation of N2a cells expressing Tspan3-myc (Tsp3) or Tsp3<sub>Y243A</sub>-myc (Tsp3<sub>Y243A</sub>). Mock and Tspan15-myc (Tsp15) transfected cells were used as negative controls. Biotinylated (+Biotin) surface proteins were precipitated and non-biotinylated (-Biotin) cells were used to control specificity of the pull-down for biotinylated proteins. Using an anti-myc antibody, surface expression of Tsp3, Tsp3<sub>Y243A</sub> and Tsp15 was observed (+Biotin, pull-down). Surface expression of full length (fl-) APP and the APP-C terminal fragment (CTF) was detected with an anti-APP antibody. Absence of GAPDH signals in the pull-down fraction excluded precipitation of cytosolic proteins. Using the same antibodies, protein expression was confirmed by immunoblot analysis of respective total lysates. **B)** Signal intensity of surface fl-APP and APP-CTF was quantified (n=5 experiments) and analysed by ANOVA's and Bonferroni's multiple comparison test (\*p<0.05, \*\*p<0.01, ns: not significant).

As observed in the previous experiment, the immunoblot analysis of Tspan3 surface levels (pull-down, +Biotin) revealed an increased signal intensity in Tspan3<sub>Y243A</sub>-myc transfected cells, compared to Tspan3-myc (Fig. 4.20A, pull-down, +Biotin). Expression of both Tspan3-myc and Tspan3<sub>Y243A</sub>-myc led to an increased surface expression of the APP-CTF. However, this effect was more pronounced in the Tsp3<sub>Y243A</sub>-myc transfected sample (Fig. 4.20A, pull-down, +Biotin). Additionally, Tspan3<sub>Y243A</sub>-myc expression significantly increased surface expression of fl-APP



compared to the mock control, whereas Tspan3-myc expression had a minor effect. Tspan15-myc expression did not alter the surface expression of fl-APP and the APP-CTF. Detection of ADAM10 using an anti-ADAM10 antibody revealed a slightly increased signal intensity of mature ADAM10 (mADAM10) in the surface fraction of Tspan3<sub>Y243A</sub>-myc expressing cells (Fig. 4.20A, pulldown, +Biotin). As previously observed the expression of Tspan3-myc had no impact on the surface level of mADAM10, compared to mock transfected cells, whereas Tspan15-myc expression clearly increased it (Fig. 4.20A, pulldown, +Biotin). Probing the pulldown fractions (pulldown, ±Biotin) for GAPDH revealed no specific signals. Using the same antibodies, protein expression of the myc-tagged proteins (Tspan3, Tspan3<sub>Y243A</sub>, Tspan15), APP, ADAM10 and GAPDH was confirmed by detection of appropriate signals in total lysates (Fig. 4.20A, total lysate). Overall, the expression of Tspan3<sub>Y243A</sub>-myc further increased the surface level of the APP-CTF, compared to Tspan3-myc and elevated the surface expression of fl-APP and mADAM10. Thus, indicating that Tspan3 might act as a stabiliser for APP and ADAM10 at the cell surface.

These experiments collectively demonstrated that mutation of an endocytic sorting motif within the C-terminal part of Tspan3 increases the cell surface expression of Tspan3 and enhances the Tspan3-mediated increase of the APP-CTF cell surface expression. Furthermore, expression of the endocytic motif mutant Tspan3<sub>Y243A</sub>-myc increased the surface expression of fl-APP and mADAM10.

#### **4.1.10 Downregulation of tetraspanin-3 expression does not affect APP processing**

To this point, the role of Tspan3 in ADAM10-mediated APP processing was only addressed by overexpression experiments. What happens when endogenous Tspan3 expression is downregulated? To answer this question, a siRNA-mediated knockdown of Tspan3 protein expression was performed in human neuroblastoma SH-SY5Y cells by transfection with a Tspan3-specific siRNA (Tsp3 siRNA). Transfection of an unspecific non-targeting control siRNA (ctrl siRNA) was used as negative control. The cells were lysed and ADAM10, Tspan3 and APP expression analysed by immunoblot (Fig. 4.21). Endogenous Tspan3 was detected in control siRNA transfected cells using a self-made C-terminal anti-Tspan3 antibody (Fig. 4.21A). In comparison, Tspan3 siRNA transfected samples showed a clearly reduced signal intensity of Tspan3, indicating successful downregulation of the Tspan3 protein expression. Analysing the APP expression did not reveal significant changes in the signal intensities of fl-APP and the

APP-CTF in Tspan3 siRNA transfected cells (Fig. 4.21A, B). Downregulation of the Tspan3 expression did also not apparently influence the signal intensity of pro- or mature ADAM10, compared to control siRNA transfected cells (Fig. 4.21A, B).

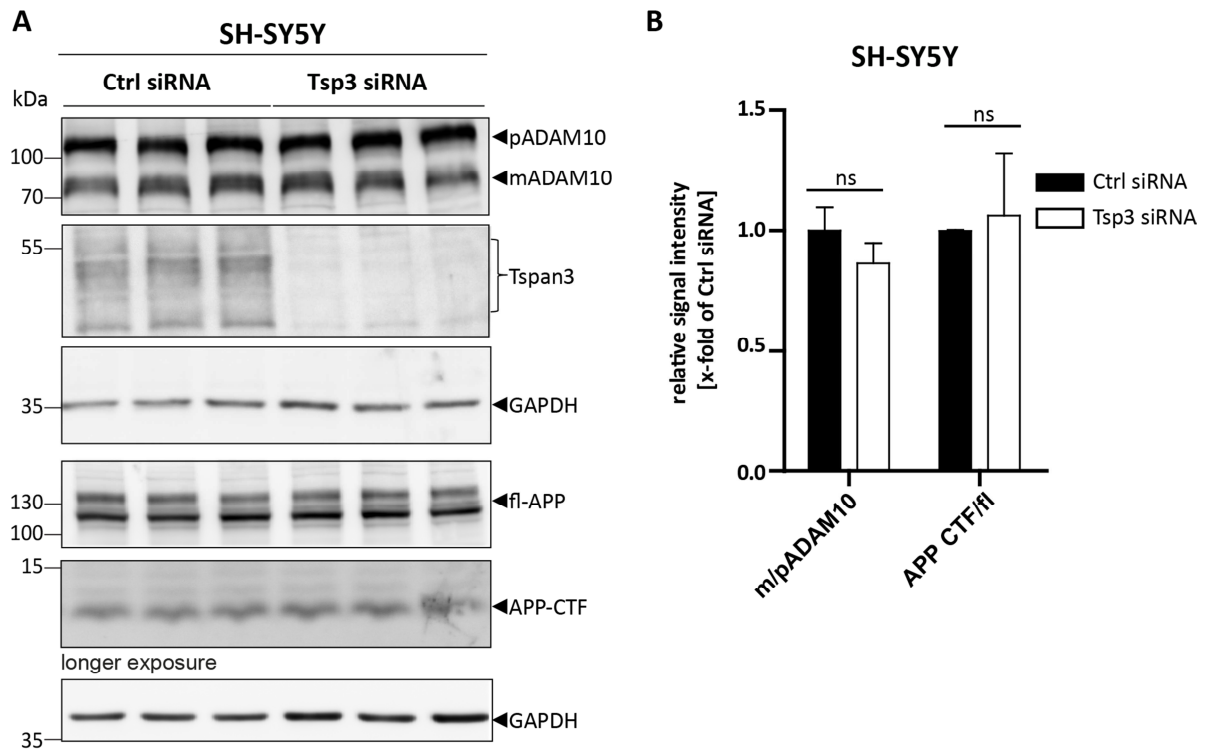


**Fig. 4.21: siRNA-mediated knockdown of Tspan3 has no apparent effect on ADAM10 and APP.**

**A)** Non-targeting control siRNA (Ctrl siRNA) or Tspan3-specific siRNA (Tsp3 siRNA) were transfected in SH-SY5Y cells. The cells were lysed and analysed by immunoblot. Using a specific C-terminal Tspan3 antibody, endogenous Tspan3 expression was detected in Ctrl siRNA transfected cells. Almost no Tspan3 expression was detected in Tsp3 siRNA transfected cells. Detection of pro (p)- and mature (m) ADAM10 and APP (fl: full length, CTF: C-terminal fragment), with respective antibodies, did not reveal differences between Ctrl and Tsp3 siRNA transfected samples. Equal protein loading was verified by GAPDH staining. **B)** Signal intensities of m/pADAM10, APP-CTF/fl were quantified by densitometric analysis. Statistical significance was tested by Student's t-test and revealed no significant differences (ns: not significant).

There is increasing evidence that certain, evolutionary related tetraspanins have redundant functions and could compensate for the loss of each other (Dunn et al., 2010; Fradkin et al., 2002). In order to see whether the lack of an effect on ADAM10 and APP proteolytic processing after downregulation of Tspan3 is due to a compensatory transcriptional upregulation of another tetraspanin, the mRNA levels of Tspan3-related TspanC6 tetraspanins were analysed. Additionally, transcription of Tspan12, which was also shown to regulate ADAM10-dependent APP processing (Xu et al., 2009) and Tspan5 as member of the TspanC8 tetraspanins were assessed.

Total mRNA was isolated from SH-SY5Y cells transfected with Ctrl or Tsp3 siRNA and reversely transcribed in cDNA. Following, mRNA expression of Tspan3, TspanC6 tetraspanins 6, 7, CD63 and Tspan5 and -12 was determined by quantitative-real time PCR (qRT-PCR). Relative mRNA levels were calculated from  $\Delta\text{Ct}$  values (Fig. 4.22).

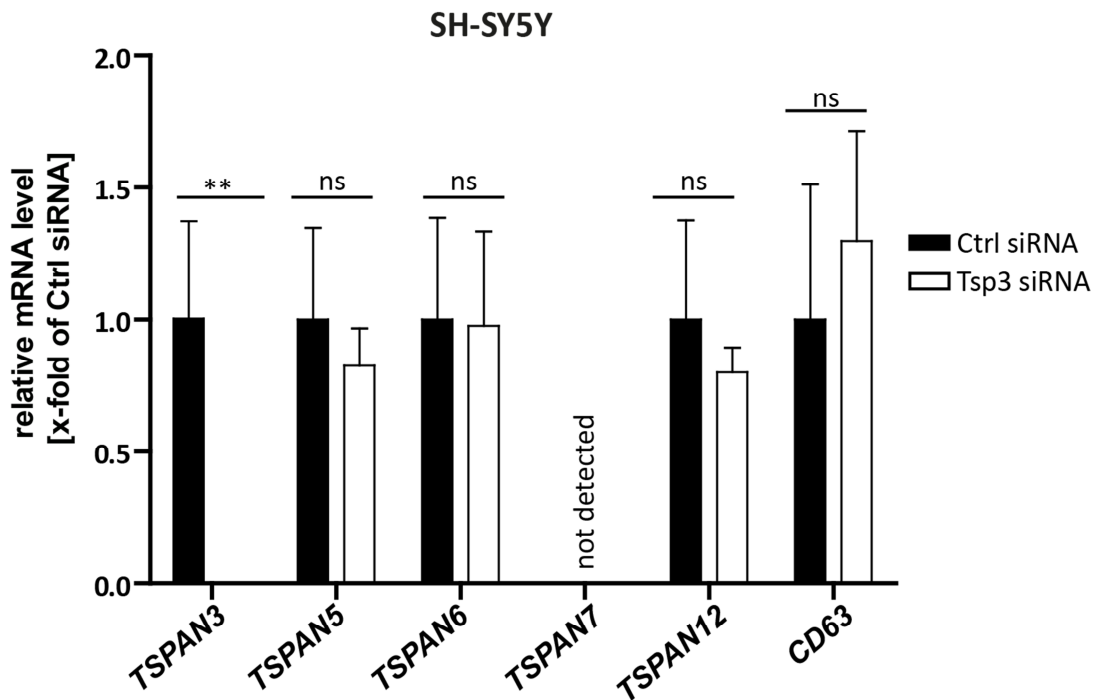


**Fig. 4.22: Downregulation of Tspan3 has no obvious effects on the transcription levels of TspanC6s, Tspan5 and Tspan12.**

SH-SY5Y cells were transfected with control (Ctrl siRNA) or Tspan3 siRNA (Tsp3). Following mRNA isolation and cDNA synthesis, expression of mRNA coding for the tetraspanins-3, -5, -6, -7, -12 and CD63 was measured by qRT-PCR. The relative mRNA level was determined by calculation of  $\Delta\text{Ct}$  values using the housekeeping gene GAPDH as reference. Data is shown as means  $\pm$ SD of  $\Delta\text{Ct}$  values related to Ctrl siRNA transfected samples. Statistical significance was analysed by Student's t-test (\*\* $p < 0.01$ , ns: not-significant).  $\Delta\text{Ct}$  values of Tspan7 were below the detection limit.

The qRT-PCR analysis revealed a significantly decreased *TSPAN3* mRNA level in the Tspan3 siRNA transfected samples (Tsp3 siRNA), compared to control siRNA treated samples (Ctrl siRNA). No significant changes in the transcription levels of *TSPAN5*, *6*, *12* and *CD63* were observed in Tspan3 siRNA transfected samples. The Tspan7 mRNA level was below the detection limit in both, control and Tspan3 siRNA transfected samples. In conclusion, the downregulation of Tspan3 in SH-SY5Y had no obvious effects on ADAM10, APP and did not alter the transcription level of TspanC6 tetraspanins, Tspan12 and Tspan5.

## 4.2 Analysis of the *in vivo* function of tetraspanin-3

The physiological function of Tspan3 is not well studied, yet. Northern Blot analysis of Tspan3 transcripts in mouse and human tissues, revealed Tspan3 expression in multiple organs, where it was predominantly found in the brain (Puls and Wright, 2000; Todd et al., 1998). The knockout of Tspan3 in mice did not show any overt developmental defects, but suggested a role of Tspan3 in the protection of haematopoietic cell function during aging and self-renewal of leukemic stem cells (Kwon et al., 2015).

The previously described, cell culture based experiments, identified Tspan3 as a novel interaction partner of ADAM10 and APP. By modulating ADAM10-dependent APP processing Tspan3 expression increased the generation of the APP- $\alpha$ CTF and reduced liberation of A $\beta$  peptides in HEK293 APP695-swe cells.

Increasing ADAM10  $\alpha$ -secretase activity is discussed as a potential way to reduce the A $\beta$  burden, since it was able to reduce A $\beta$  liberation and amyloid plaque load in an Alzheimer's Disease (AD) mouse model (Postina et al., 2004). Therefore, it was interesting to gain more insight into the physiological function of Tspan3 and its relevance for ADAM10-mediated APP processing and for AD pathology.

### 4.2.1 Tetraspanin-3 is glycosylated and highly expressed in the murine brain

To examine the Tspan3 tissue distribution, different organs were isolated from a wild-type mouse, homogenised and Tspan3 expression was analysed by immunoblot (Fig. 4.23A) using an anti-Tspan3 antibody. Specificity of the anti-Tspan3 antibody was validated by the absence of distinct signals in Tspan3 knockout tissues (see section 4.2.4, Fig. 4.27B).

After immunoblotting, staining with the anti-Tspan3 antibody revealed three signals at around 45 kDa in total brain, cortex, hippocampus and cerebellum samples (Fig. 4.23A). Interestingly in heart, lung, kidney, spleen and intestine Tspan3-specific signals were slightly shifted, towards a molecular weight of about 50 kDa. Additional signals at a molecular weight of about 35 kDa appeared, which possibly correspond to Tspan3 C-terminal fragments (CTFs). The strongest Tspan3 signal was observed in total brain (1.0-fold), cortex (0.9-fold) and hippocampus (0.8-fold) homogenates (Fig. 4.23A, B). Compared to total brain lysate, in the cerebellum (0.6-fold), heart (0.6-fold) and intestine (0.5-fold) Tspan3 signal intensity was clearly decreased (Fig. 4.23A, B). Little Tspan3 expression was observed in lung (0.1-fold), kidney (0.3-fold) and spleen (0.2-fold), whereas hardly any Tspan3 was detected in bone

marrow (Fig. 4.23A, B). In liver, staining for Tspan3 resulted in unspecific signals around 35 kDa (Fig. 4.23A) as evidenced by the occurrence of similar signals in Tspan3-deficient liver homogenates (see 4.2.4, Fig. 4.27B). Additional unspecific signals (\*) were observed in all samples at around 55 kDa, except for bone marrow and intestine (Fig. 4.23A).

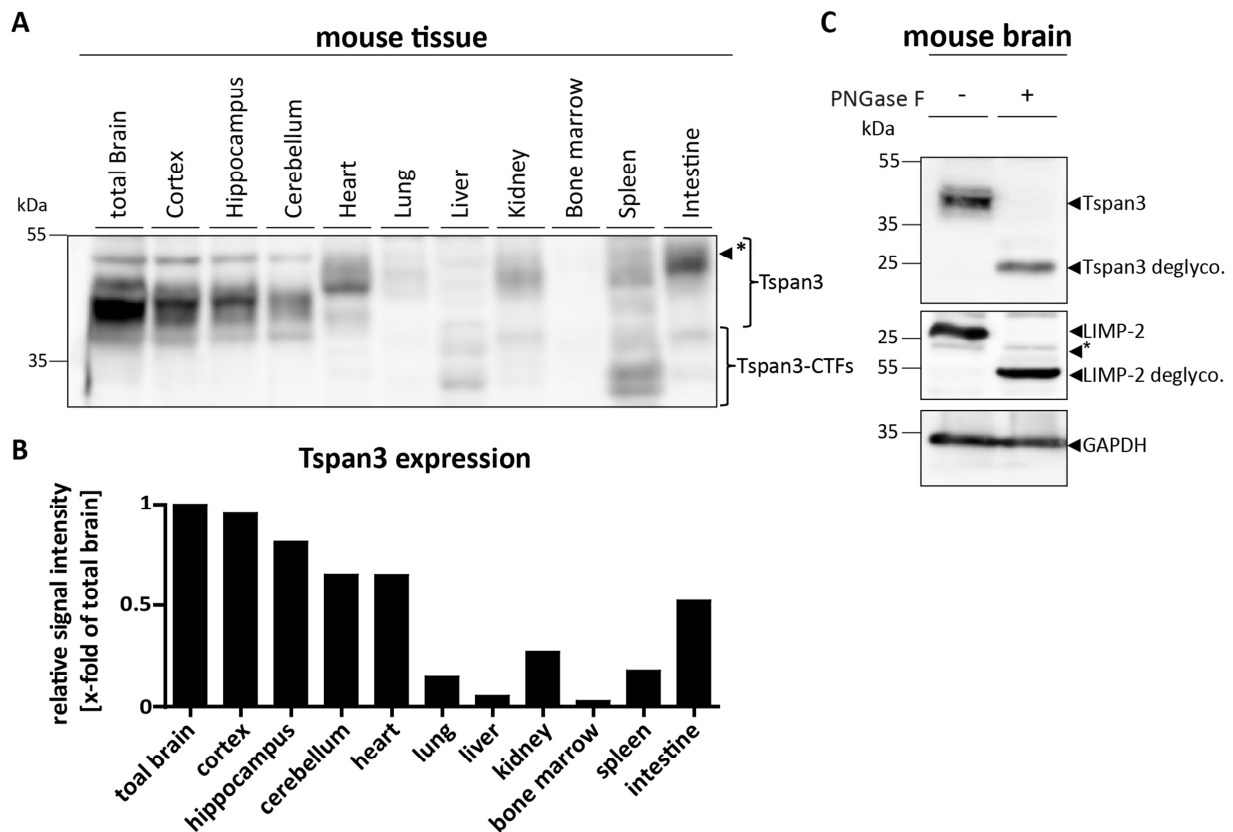


**Fig. 4.23: Tspan3 is a glycosylated protein and is most abundantly expressed in the murine brain.**

**A)** Indicated tissues were isolated from an adult wild-type mouse, homogenized and analysed by immunoblotting. Staining with an anti-Tspan3 antibody revealed Tspan3 expression in all tested tissues, except for bone marrow and liver. The strongest expression was observed in total brain, cortex, hippocampus. **B)** Densitometric analysis of Tspan3 signal intensities. Single values were correlated to the signal intensity of total brain. **C)** Mouse brain was isolated, homogenised and incubated with Peptide N-glycosidase F (PNGase F, "+") or left untreated ("-"). Removal of N-linked glycans, decreased the molecular weight of Tspan3 from 40 kDa ("-") to 25 kDa ("+"). Efficiency of the PNGase F digestion was confirmed by the decreased molecular weight of the lysosomal integral membrane protein, LIMP-2, which is a highly glycosylated lysosomal protein. Probing the immunoblots for GAPDH confirmed equal protein loading in all samples.

Similar to the previously described tissue distribution (Puls and Wright, 2000; Todd et al., 1998), Tspan3 expression was observed in all tissues tested except for liver and bone marrow. The strongest expression was observed in the brain, in particular in the cortical and hippocampal region. Interestingly, the molecular weight of Tspan3 varied between certain tissues.

Since sequence analysis of murine Tspan3 predicted five potential glycosylation sites (Puls and Wright, 2000), it is conceivable that the observed molecular weight differences are due to differential glycosylation of Tspan3.

To elucidate whether Tspan3 is indeed a glycosylated protein, wild-type mouse brain homogenates were prepared and subjected to Peptide N-Glycosidase F (PNGase F) digestion. A sample containing water instead of PNGase F was used as a control. Following digestion at 37°C, homogenates were subjected to SDS-PAGE and immunoblot analysis (Fig. 4.23B).

In the control sample (Fig. 4.23B, “-”) detection of Tspan3 resulted in a strong signal around 45 kDa. After PNGase F treatment (“+”), the Tspan3-specific signal was shifted to around 25 kDa (Tsp3 deglyco.), indicating a reduction of its molecular mass. Likewise, detection of the highly glycosylated lysosomal integral membrane protein 2 (LIMP-2) revealed a reduced molecular weight after PNGase F treatment (Fig. 4.23B, “+”), compared to the untreated sample (“-”), confirming successful PNGase F digestion.

Collectively, these data identified Tspan3 as a glycosylated protein, which is expressed in several tissues, but most abundantly in the murine brain.

#### **4.2.2 Tetraspanin-3 is predominantly expressed in neurons of the murine brain**

In order to analyse where Tspan3 is exactly expressed within the murine brain, Tspan3 expression in mouse brain was analysed by immunohistochemistry.

3 µm thin sagittal sections from the brain of a wild-type mouse were prepared and stained for Tspan3 using an anti-Tspan3 antibody. Tissue sections of Tspan3 knockout (ko) mice (described in section 4.2.3) were used to control specificity of the Tspan3 antibody. Subsequently, Tspan3 localisation was visualised by diaminobenzidine (DAB) staining (Fig. 4.24, I-IV). The DAB staining, revealed Tspan3 expression as a brown-coloured staining in cells of the cortex, hippocampus (CA2/CA3), cerebellum and brainstem of wild-type (wt) sections (Fig. 4.24, I-IV, indicated by black arrows). No staining was observed in the respective Tspan3 knockout sections (Fig. 4.24, I-IV), confirming the specificity of the anti-Tspan3 antibody. It was conspicuous, that Tspan3-positive cells in the wild-type cortex, hippocampus and brainstem presented a cell body with a triangular shape, which is a main feature of pyramidal neurons. In the cerebellum, Tspan3 expression occurred in cells located between the molecular (ML) and the granular layer (GL), where Purkinje cells are typically found (Fig. 4.24, IV).

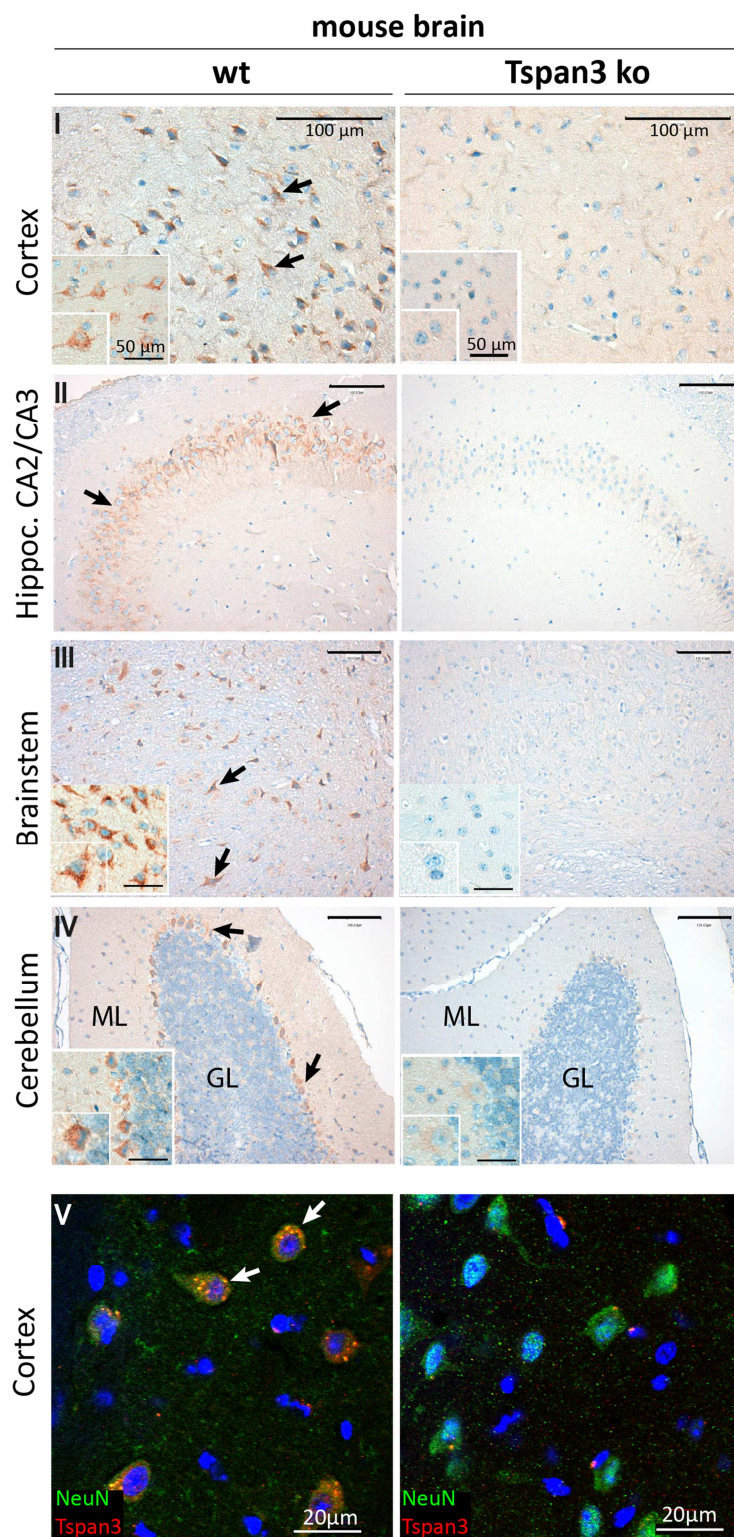


**Fig. 4.24: Tspan3 is expressed in neurons of the murine brain.**

**I-IV:** Diaminobenzidine (DAB) staining of Tspan3 in indicated regions of a wild-type (wt) and Tspan3 knockout (ko) mouse brain (collaboration with *Dr. Hermann Altmeyen* from University Medical Centre Hamburg-Eppendorf). Tspan3 expression was detected in neurons of wt cortex (I), hippocampus (hippoc. CA2/CA3, II), brainstem (III) and in Purkinje cells of the Cerebellum (IV), indicated by black arrows. No Tspan3 was detected in the respective Tspan3 ko samples, confirming specificity of the anti-Tspan3 antibody. Scale bars represent 100  $\mu\text{m}$  in the overview pictures and 50  $\mu\text{m}$  in the insets. **V:** Immunofluorescence staining showing co-localisation of Tspan3 (red) and neuronal nuclei (NeuN, green) in the cortex of the wt mouse brain, indicated by white arrows. No Tspan3 was detected in a comparable region of the Tspan3 ko brain. Scale bars: 20  $\mu\text{m}$ . GL: granular layer, ML: molecular layer.

To further verify the neuronal localisation of Tspan3, indirect immunofluorescence staining of Tspan3 and the neuron-specific nuclear protein NeuN (neuronal nuclei) in wild-type and Tspan3 knockout brain sections was performed (Fig. 4.24, V). Using confocal microscopy, a clear co-localisation (indicated by white arrows) of Tspan3 (red) and NeuN (green) was observed in the cortical region of wild-type (wt) brain sections (Fig. 4.24, V). Absence of a Tspan3-specific signal in the Tspan3 knockout (Tsp3 ko) sample, validated the antibody specificity. Taken together, these results confirmed that Tspan3 is expressed in neurons of the murine brain.

### **4.2.3 Tetraspanin-3 interacts with ADAM10 and APP in mouse brain**

The previous experiments demonstrated a high expression of Tspan3 in neurons of the murine brain, where also ADAM10 and APP are co-expressed (Marcinkiewicz and Seidah, 2000). To investigate whether Tspan3 could have a similar function for ADAM10-mediated APP processing in the murine brain, as indicated by the cell culture-based experiments (see section 4.1), the interaction of Tspan3 with ADAM10 and APP was analysed under endogenous conditions.

Therefore, the brain of a wild-type mouse was prepared and a tissue lysate prepared using stringent detergent conditions. A small amount of the total lysate was kept to control for protein expression. Endogenous Tspan3 was precipitated using a C-terminal anti-Tspan3 antibody and protein G coupled beads. As a negative control, the precipitation was performed with the brain lysate of a Tspan3 knockout mouse (described in 4.2.3). To control for unspecific protein binding to the beads, a sample control containing lysate and beads, but no antibody (bead control), was used. Another sample, containing lysis buffer and antibody should reveal unspecific immunoglobulin signals (antibody control). Immunoprecipitates and total lysates were subjected to immunoblot analysis and expression of Tspan3, ADAM10 and APP was analysed (Fig. 4.25).

After immunoblotting, detection of Tspan3 resulted in a prominent signal in the wild-type (wt) immunoprecipitate (Fig. 4.25, IP Tsp3). No Tspan3 was detected in the knockout (ko) immunoprecipitate, confirming specific precipitation of Tspan3. Co-immunoprecipitation of mature (m) ADAM10, fl-APP and the APP-CTF was observed in the Tspan3 wild-type immunoprecipitate (IP Tsp3), using an anti-ADAM10 and anti-APP antibody. Unspecific signals (\*) in wild-type and knockout immunoprecipitates (IP Tsp3) correspond to the protein G of the



used beads and denatured immunoglobulin fragments, as they were detected in the bead and antibody control (ab ctrl). Immunoblot analysis of total lysates, confirmed the expression of mADAM10 and APP in wild-type and Tspan3 knockout samples. Considerable expression of Tspan3 was detected in the wild-type, but not in knockout brain homogenate. GAPDH staining confirmed equal protein loading.

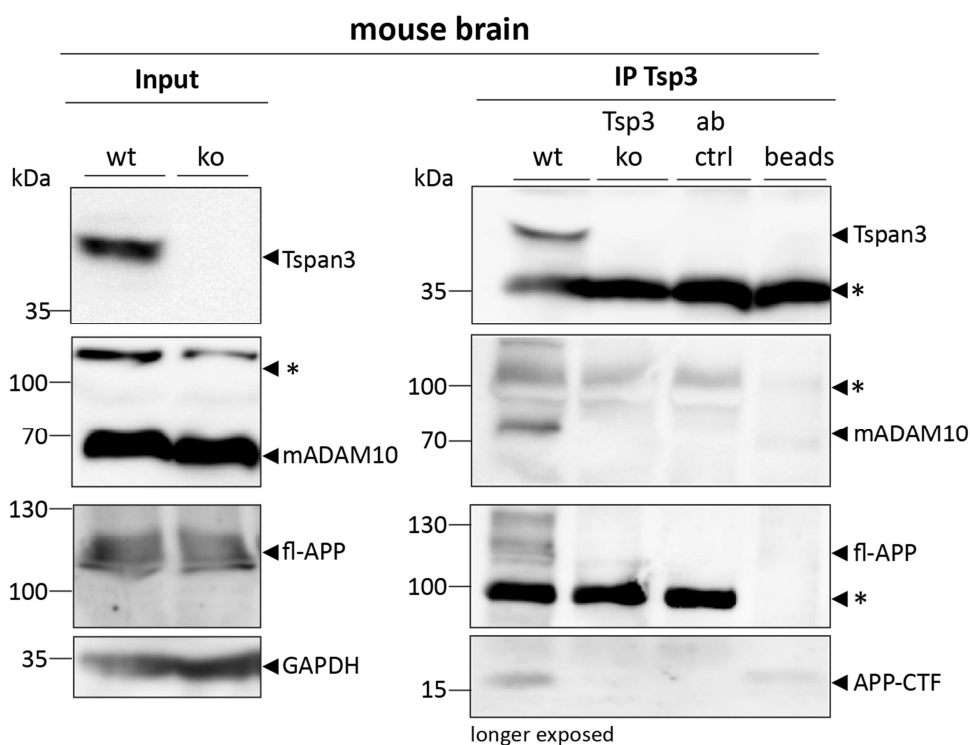


**Fig. 4.25: Tspan3 interacts with ADAM10 and APP under endogenous conditions.**

The brains of a wild-type (wt) and a Tspan3 knockout (ko) mouse were isolated and tissue lysates were prepared in the presence of 0.5 % NP-40. A small amount of the total lysate was kept and Tspan3 precipitated using a C-terminal anti-Tspan3 antibody (IP Tsp3). Immunoprecipitates and total lysates were analysed by immunoblot. Staining with an anti-Tspan3 antibody confirmed precipitation of Tspan3 (IP Tsp3). Co-precipitation of mature (m) ADAM10, full length (fl-) APP and the APP-C-terminal fragment (CTF) was detected with an anti-ADAM10 and an anti-APP antibody, respectively (IP Tsp3). Expression of Tspan3, APP and ADAM10 was assessed in total lysates using the same antibodies. GAPDH staining confirmed equal protein loading in total lysates.

#### 4.2.4 Does tetraspanin-3 deficiency alter ADAM10-mediated shedding?

The finding that Tspan3 interacts with ADAM10 and APP under endogenous conditions prompted the question whether Tspan3 is involved in ADAM10-mediated cleavage events in the murine brain. To address this question the impact of Tspan3-deficiency on ADAM10-mediated cleavage events was analysed using a Tspan3 knockout mouse model.

To achieve a gene-specific knockout, transcription activated-like effector nuclease (TALEN)-mediated genome editing (Sung et al., 2013) was used. The TALEN-mediated knockout strategy aims to introduce a locus-specific premature translational stop codon, which prevents synthesis of a functional gene product. TALENs consist of a sequence specific TAL-effector DNA binding domain fused to an endonuclease, which enables the locus-specific introduction of a double-strand break. Following double-strand break, the DNA is repaired by error-prone repair mechanisms, *e.g.* non-homologous end joining, which produces different insertion or deletion mutations. In this way, frameshift mutations occur and generate a premature translational stop codon, which finally leads to a non-functional gene product and loss of the protein.

For the knockout of *Tspan3*, TALENs were designed to target exon2 of the *Tspan3* gene locus (Fig. 4.26A). To increase the probability of a frameshift mutation, TALEN precursors were injected into zygotes of a founder mice together with a 46-base pair (bp) long, single stranded oligodeoxynucleotide (ssODN), consisting of a *Xba*I restriction site and three stop codons (short X46), (see section 3.6.1). Upon TALEN-directed double-strand break, the ssODN should be incorporated into *Tspan3* exon2 by homology directed repair and cause loss of gene function (Fig. 4.26A). Sequence analysis of genomic DNA obtained from offspring mice revealed a 27-bp insertion mutation (Fig. 4.26B, *Tspan3X46*), which led to a premature translational stop codon in the *Tspan3* exon2 (Fig. 4.26A). Hereafter, the mutated *Tspan3* allele is referred to as *Tspan3X46*.

Further breeding aimed to obtain homozygous *Tspan3X46* mice, which should be deficient for *Tspan3* and wild-type littermates, not carrying the mutation. Heterozygous mice were bred according to the breeding scheme shown in section 3.6.3.

To identify wild-type and potential *Tspan3* knockout mice, genomic DNA was isolated and subjected to PCR. To distinguish between wild-type and *Tspan3X46* mutant alleles a primer pair (forward and reverse), covering the sequence of the *Tspan3* exon2 was used for amplification. The PCR products were analysed by agarose gel electrophoresis and visualised under UV light using ethidium bromide staining (Fig. 4.26C). In the wild-type sample, a PCR amplicon of 326 bp length was detected. Bearing the 27 bp insertion mutation, amplification of the mutant *Tspan3X46* exon2 resulted in a 354 bp PCR product, as observed in the knockout (ko) sample (Fig. 4.26B). Heterozygous mice (+/-) were identified by the occurrence

of a shorter 326 bp and longer 354 bp PCR product, corresponding to the wild-type and the mutant *Tspan3X46* allele.

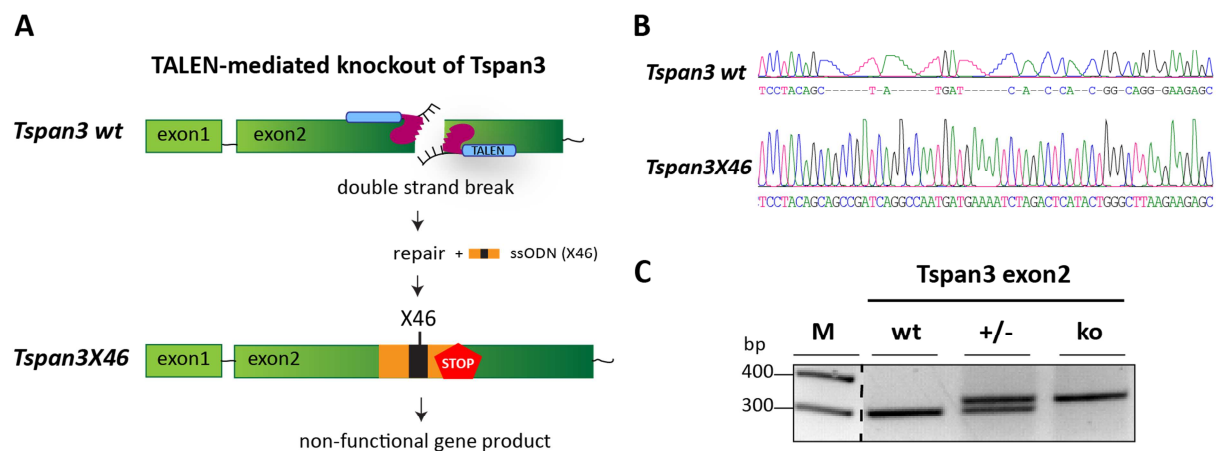


**Fig. 4.26: TALEN-mediated knockout of *Tspan3* in mice.**

**A)** Schematic drawing of the TALEN-mediated *Tspan3* knockout strategy. TALENs were designed to introduce a double-strand break within exon2 of the *Tspan3* gene-locus. Upon TALEN-directed double-strand break, a 46-base pair long, single stranded oligodeoxynucleotide (ssODN), bearing three stop codons and a *Xba*I restriction site (X46) was incorporated by homology directed repair and led to a 27 bp insertion mutation. This mutation led to a premature translational stop codon, which should lead to a disruption of gene function. **B)** Sequencing chromatogram of the TALEN-targeted region of the wild-type and mutated (*Tspan3X46*) *Tspan3* exon2 gene locus. **C)** Agarose gel electrophoresis of PCR products obtained from genomic DNA, isolated from homozygous wildtype (wt), heterozygous (+/-) and *Tspan3* knockout (ko) mice. For the amplification, a primer pair targeting the region around *Tspan3* exon2 was used. The length of amplicons was estimated by comparison to the defined signals of the marker (M).

According to the used breeding scheme, a Mendelian genotype distribution of 25% wild-type, 25% knockout and 50% heterozygous animals was expected. The genotype analysis of mice older than three weeks (Tab. 4.1, total alive) revealed a slightly increased birth rate of wild-type (wt) animals (31%) and a decreased number of heterozygous mice (43%). However, the birth rate of knockout animals (ko) was as expected (26%). Additionally, the postnatal mortality rate was determined. The percentage of total alive to total born mice was calculated and revealed a low mortality rate of 6% within the first three weeks after birth.

**Tab. 4.1: Number of animals and genotype distribution of *Tspan3X46* breeding.**

Animals	total		Genotypes of total alive		
	born	alive*	wt	+/-	ko
Number (n)	368	345	108	149	88
%	100	94	31	43	26

\*after 3 weeks of birth. wt, wild-type; +/-, heterozygous; ko, knockout.

Collectively, TALEN-mediated genome editing led to the introduction of a 27 bp mutation in the *Tspan3* exon2 and the presence of a premature stop codon, indicating that no functional gene product could be synthesised. Furthermore, breeding of heterozygous mice did not reveal any apparent anomalies with regards to Mendelian inheritance and postnatal mortality rate.

To analyse whether the *Tspan3X46* mutation was effective to prevent *Tspan3* expression, different tissues were isolated from a homozygous *Tspan3X46* mouse, which will hereafter be indicated as *Tspan3* knockout (ko). Appropriate tissues, isolated from a wild-type (wt) mouse, were used as a control. Tissue lysates were prepared and *Tspan3* expression assessed by immunoblot analysis (Fig. 4.27).

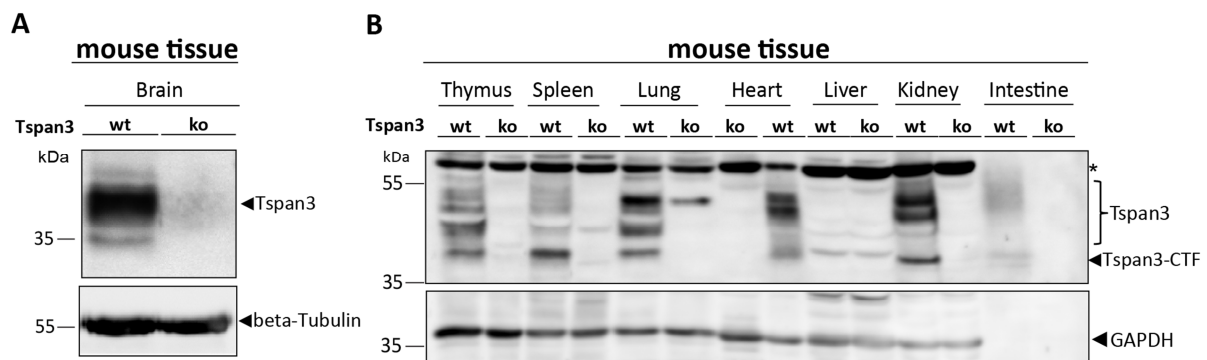


**Fig. 4.27: TALEN-mediated knockout of *Tspan3* was confirmed in several tissues.**

**A, B)** Indicated tissues were isolated from a three-week-old *Tspan3* wild-type (wt) and knockout (ko) mouse. Tissues were homogenised and *Tspan3* expression analysed by immunoblot. Using an anti-*Tspan3* antibody, *Tspan3* expression was detected in the indicated wild-type tissues, except for liver, but not in the respective ko tissues. Beta-tubulin (A) and GAPDH (B) staining was used to control protein loading.

In the wild-type (wt) brain homogenate (Fig. 4.27A), a prominent signal around 45 kDa was detected after staining with a C-terminus specific anti-*Tspan3* antibody. No *Tspan3* signal was observed in the knockout (ko) brain sample (Fig. 4.27A), confirming absence of the *Tspan3* protein. Using the same antibody, a considerable *Tspan3* expression was observed in thymus, spleen, lung, heart, kidney and intestine of the wild-type (wt) animal by prominent signals around 45 to 55 kDa (Fig. 4.27B). In the same samples, additional signals were observed at around 35 kDa, which might correspond to a C-terminal fragment (CTF) of *Tspan3*. *Tspan3*-specific signals were not detected in the respective knockout (ko) tissues. In liver, *Tspan3* expression was neither detected in wild-type, nor in the knockout tissue (Fig. 4.27B). Staining for beta-tubulin (Fig. 4.27A) and GAPDH (Fig. 4.27B) confirmed equal protein loading between matching wild-type and knockout samples. No GAPDH was detected in the intestine samples.

Altogether, these results confirm the successful generation of Tspan3-deficient mice using TALEN-mediated genome editing. As previously reported (Kwon et al., 2015) these mice did not show any overt phenotype.

#### 4.2.4.1 The knockout of tetraspanin-3 has no apparent effect on ADAM10 and APP

Since the generation of Tspan3-deficient mice was successful, the importance of Tspan3 for ADAM10-mediated shedding events was analysed.

Brains from eleven-day-old Tspan3 knockout and wild-type mice were isolated and homogenised. Following, the expression of ADAM10, APP and the cellular prion protein (PrP<sup>C</sup>), another well-described ADAM10 substrate in the brain (Altmeppen et al., 2011), were analysed by immunoblotting (Fig. 4.28A). After immunoblotting (Fig. 4.28A), detection of ADAM10 revealed similar signal intensities of pro-, mature ADAM10 and the ADAM10-C-terminal fragment in wild-type (wt) and Tspan3 knockout (ko) samples (Fig. 4.28A, B). Likewise, equal signal intensities of fl-APP and APP-CTF were observed in Tspan3 knockout and wild-type brains. Using an antibody directed against the full length cellular prion protein (PrP<sup>C</sup>), resulted in three specific signals, which correspond to the di-glycosylated (d, 35 kDa), mono-glycosylated (m, 32 kDa) and unglycosylated (u, 25 kDa) form of PrP<sup>C</sup>. Compared to the wild-type samples, Tspan3-deficiency (Tspan3 ko) had no effect on the signal intensity of none of the PrP<sup>C</sup> forms. Using an anti-Tspan3 antibody, Tspan3 expression was detected in wild-type, but not in the Tspan3 knockout samples. Staining for GAPDH confirmed equal protein loading in all samples. In addition to the immunoblot analysis, the transcription level of ADAM10 was analysed by qRT-PCR. For this purpose, total mRNA was isolated from brains of eleven-day-old wild-type and Tspan3 knockout mice. The mRNA was reversely transcribed into cDNA and ADAM10 transcription analysed by qRT-PCR (Fig. 4.28C).

To determine the relative ADAM10 mRNA level (Fig. 4.28C),  $\Delta C_t$  values were calculated by correlation to GAPDH and normalised to values of the wild-type samples. Similar mRNA levels were observed in the wild-type (wt) and Tspan3 knockout (ko) samples.

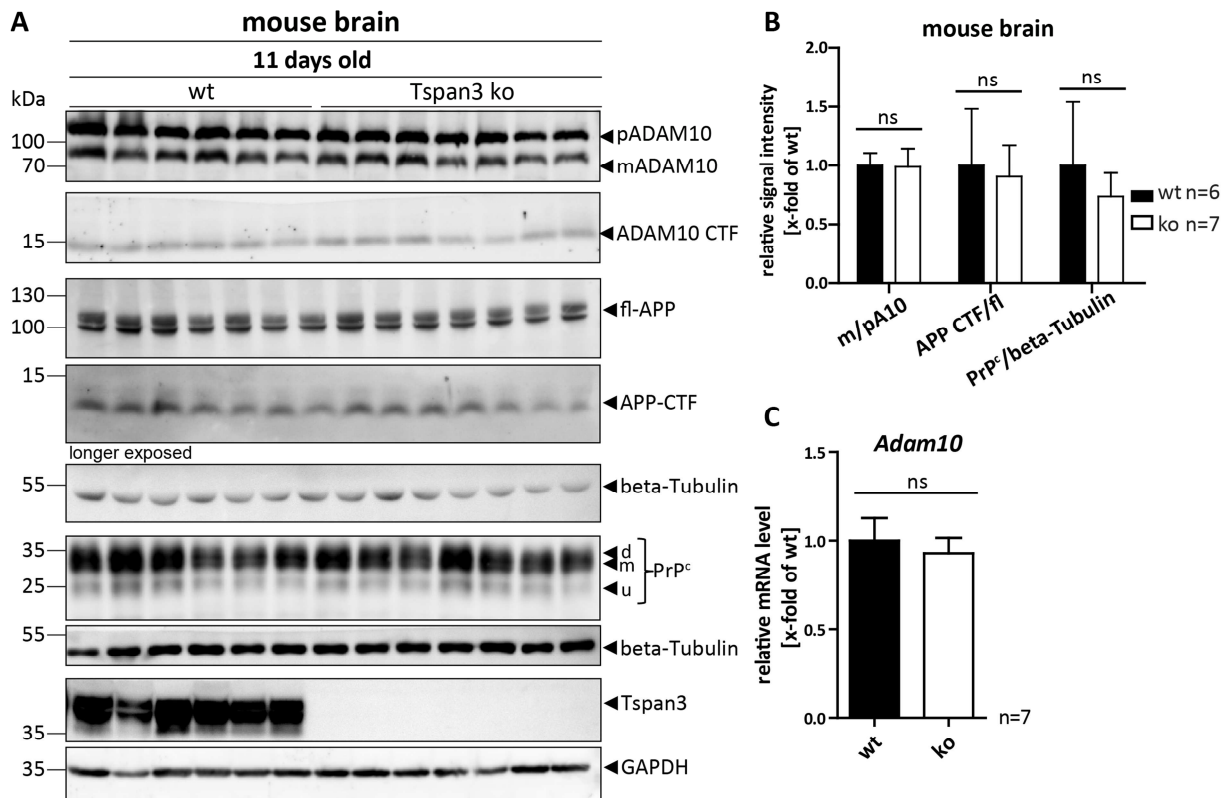


**Fig. 4.28: Loss of Tspan3 has no effect on ADAM10, APP and PrP<sup>c</sup> in eleven-day-old mice.**

**A)** Immunoblot analysis of ADAM10, APP, PrP<sup>c</sup> in the brain of eleven-day-old Tspan3 knockout (ko) and wild-type (wt) mice. Pro- (p) and mature (m) ADAM10, full length (fl-) APP, APP-C-terminal fragment (CTF), were detected with anti-ADAM10 and anti-APP antibodies. Di- (d), mono- (m) and unglycosylated (u) PrP<sup>c</sup> were detected with an anti-PrP<sup>c</sup> antibody (POM1). Tspan3 was detected in wt but not in Tspan3 ko samples. Probing for GAPDH confirmed equal protein loading. **B)** Quantification of m/pADAM10, APP CTF/fl and PrP<sup>c</sup>/beta-tubulin signal intensities. Data are shown as mean values  $\pm$ SD. Student's t-test did not reveal significant differences (ns). **C)** qRT-PCR analysis of the *Adam10* transcription level. Total mRNA was isolated, reverse-transcribed into cDNA. The relative mRNA level was determined by calculation of  $\Delta$ Ct values. Values were normalised to the wt control and are shown as means  $\pm$ SD.

To confirm the finding that loss of Tspan3 does not affect protein levels of ADAM10 and shedding of APP and PrP<sup>c</sup> in older mice, immunoblot analysis of brain homogenates prepared from four-week-old mice was conducted (Fig. 4.29A). Staining with the above mentioned anti-ADAM10, anti-APP and anti-PrP<sup>c</sup> antibodies did not reveal any significant differences in Tspan3 knockout samples compared to wild-type controls (Fig. 4.29A, B). GAPDH and beta-tubulin staining verified equal protein loading. Thereby, confirming the findings observed in eleven-day-old mice (Fig. 4.28).

In conclusion, these data showed that loss of Tspan3 has no apparent effect on the expression of ADAM10 and ADAM10-mediated shedding of APP and PrP<sup>c</sup> in the murine brain.

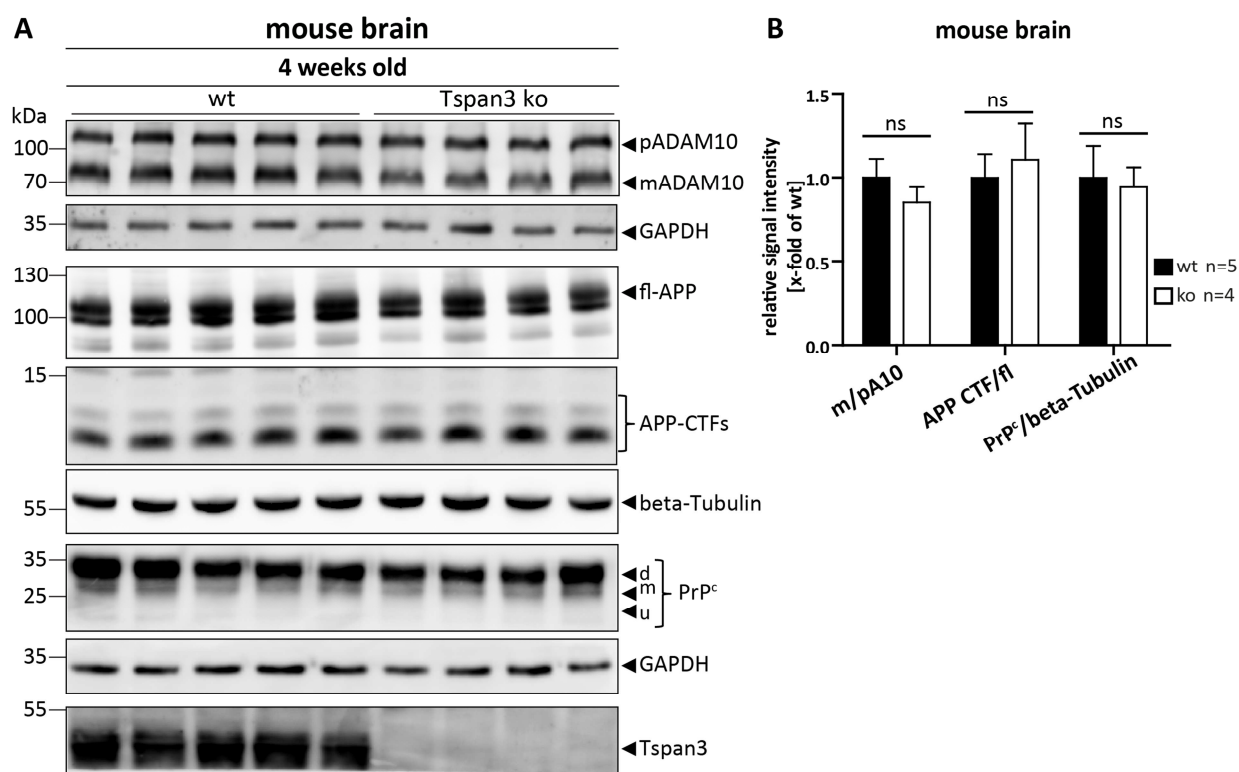


**Fig. 4.29: Knockout of Tspan3 does not affect ADAM10, APP and PrP<sup>c</sup> in four-week-old mice.**

**A** Immunoblot analysis of brain homogenates from four-week-old wild-type and Tspan3 knockout (ko) mice. Mature (m) and the pro-(p) ADAM10, full length (fl)-APP, APP-C-terminal fragments (CTFs) were detected with an anti ADAM10 and anti-APP antibody, respectively. Di- (d), mono- (m) and unglycosylated (u) full length PrP<sup>c</sup> were detected with an anti PrP<sup>c</sup> antibody (POM1). Staining for GAPDH and beta-tubulin confirmed equal protein loading. **B**) Densitometric analysis of ADAM10, APP and PrP<sup>c</sup> signal intensities. Data are shown as mean values  $\pm$ SD of m/p ADAM10, APP CTF/fl and PrP<sup>c</sup>/beta-tubulin signal intensities. Using Student's t-test for statistical analysis, revealed no significant differences between wild type (wt) and Tspan3 knockout (ko) samples (ns).

#### 4.2.4.2 Loss of tetraspanin-3 is possibly compensated by tetraspanin-5 and -7

As observed by the siRNA-mediated knockdown of Tspan3 (see section 4.1.10), the loss of Tspan3 in mouse brains had no obvious effect on the expression of ADAM10 and its proteolytic activity in regards towards APP and PrP<sup>c</sup> shedding, respectively.

In order to examine if, under physiological conditions, loss of Tspan3 might be compensated by other tetraspanins, total mRNA was isolated from brains of eleven-days-old Tspan3 knockout and wild-type mice. cDNA was generated and the transcription levels of Tspan5, Tspan12 and the TspanC6 tetraspanins, Tspan6, Tspan7 and CD63 were analysed by qRT-PCR. After qRT-PCR measurement, the relative mRNA level was determined by the calculation of  $\Delta$ Ct values. For each gene, the  $\Delta$ Ct values of Tspan3 knockout (ko) samples were correlated to the respective wild-type controls, which were set as one (Fig. 4.30). The qRT-PCR-analysis (Fig. 4.30) revealed a clear upregulation of *Tspan7* and *Tspan5* mRNA levels in the brains of

Tspan3-deficient mice (ko). Additionally, significant downregulation of the *Tspan6*, *Cd63*, and *Tspan12* mRNA levels were observed in the Tspan3 knockout (ko) samples.

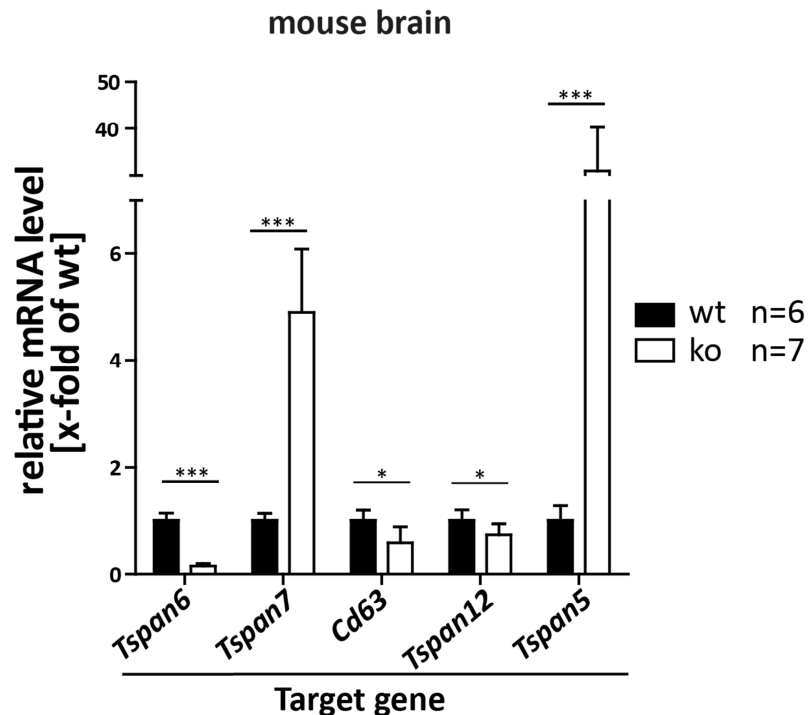


**Fig. 4.30: Tspan3-deficiency increases the transcription level of Tspan5 and Tspan7.**

Total mRNA was isolated from brains of eleven-day-old wild-type (wt) and Tspan3 knockout (ko) mice. mRNA was reverse transcribed into cDNA and the transcription levels of *Tspan6*, *Tspan7*, *Cd63*, *Tspan12* and *Tspan5* analysed by qRT-PCR. The graph shows the relative mRNA level calculated by determination of  $\Delta C_t$  values.  $\Delta C_t$  values of Tspan3 ko samples were related to wt  $\Delta C_t$  values, which were set as one. Bars represent mean values  $\pm$ SD. Statistical significance was tested using Student's t-test (\* $p < 0.05$ , \*\*\* $p < 0.001$ .)

In contrast to cell culture based experiments (see section 4.1.10), knockout of Tspan3 in mice revealed, significant changes in the transcription levels of TspanC6 tetraspanins (*Tspan6*, *Tspan7*, *Cd63*), *Tspan5* and *Tspan12* in the brain. In particular, the transcription of *Tspan7* and *Tspan5* was drastically increased, which indicated that these tetraspanins might be able to compensate for the loss of Tspan3.

#### 4.2.4.3 Overexpression of tetraspanin-7 increases the appearance of the APP-CTF

Tspan3 and Tspan7 are evolutionary related and belong to the subgroup of TspanC6 tetraspanins. To investigate whether Tspan7 has a similar function as Tspan3, its effect on APP proteolytic processing was analysed.

To this end, N2a cells were transfected with Tspan3-myc and a murine C-terminal myc-tagged Tspan7 (Tspan7-myc) expression construct. Cells transfected with an empty vector were used



as negative (mock) control. After cell lysis, generation of APP-CTFs was assessed by immunoblot analysis (Fig. 4.31).

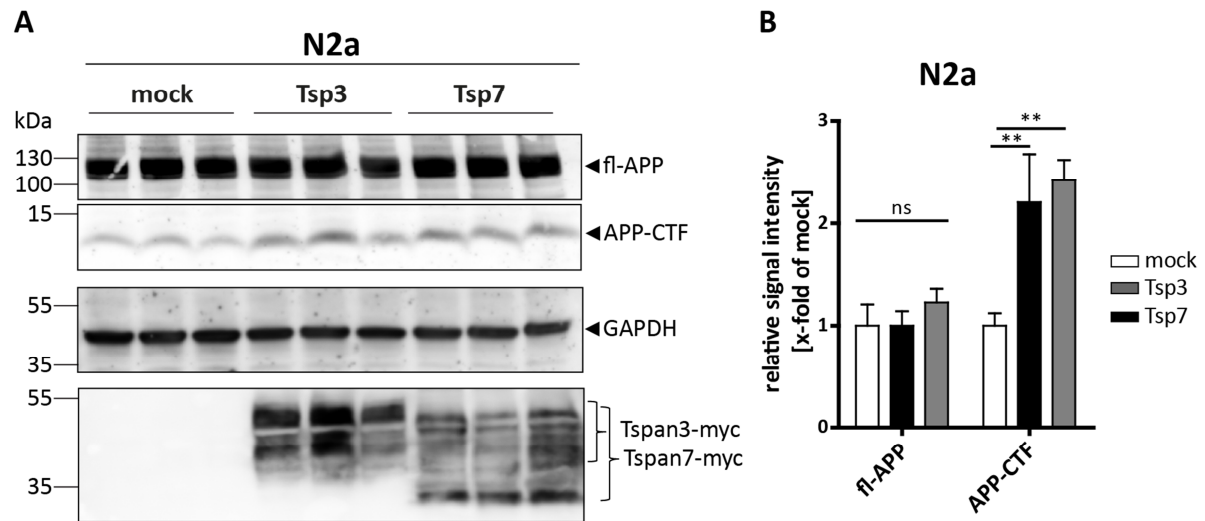


**Fig. 4.31: Expression of Tspan7 mimics the Tspan3-induced effect on APP-CTF generation.**

**A)** Tspan3-myc (Tsp3) and Tspan7-myc (Tsp7) were expressed in N2a cells. Mock transfected cells were used as negative control. The cells were lysed and APP proteolytic processing analysed by immunoblot. Full length (fl-) APP and the APP-C-terminal fragment (CTF) were detected with an anti-APP antibody. Staining with an anti-myc antibody confirmed expression of both Tsp3 and Tsp7. Equal protein loading was validated by detection of GAPDH. **B)** Signal intensities of fl-APP and APP-CTF were quantified by densitometric analysis. Statistical significance was tested using ANOVA followed by Bonferroni's multiple comparison test (\*\* $p < 0.01$ ).

Using an anti-APP antibody fl-APP and the APP-CTF were detected (Fig. 4.31A). As previously observed, Tspan3-myc (Tsp3) expression did not alter the signal intensity of fl-APP, but led to a more than twofold increase of the APP-CTF, as compared to mock transfected cells (Fig. 4.31B). Similar to this, Tspan7-myc (Tsp7) expressing cells increased the signal intensity of the APP-CTF compared to control cells (mock), whereas fl-APP was unaffected. Staining with an anti-myc antibody confirmed successful expression of Tspan3-myc and Tspan7-myc by prominent signals at around 45 kDa (Tsp3) and 40 kDa (Tsp7). Similar signal intensities after GAPDH staining confirmed equal protein loading in all samples.

Taken together, the expression of Tspan7-myc led to an increased appearance of the APP-CTF, which is comparable to the Tspan3-induced increase of the APP-CTF.

#### 4.2.5 Tetraspanin-3 expression is elevated in the brains of Alzheimer's Disease patients

Because Tspan3 expression was predominantly found in the murine brain, where it associated with APP and ADAM10, it was of interest whether Tspan3 expression is modulated with the development of Alzheimer's Disease (AD) in human. To test this, Tspan3 expression was analysed in post-mortem brain samples of AD patients.

Tissue lysates of prefrontal cortex samples of AD patients and age-matched controls (more detailed information provided in section 3.7, Tab. 3.16) were prepared and subjected to immunoblot analysis (Fig. 4.32A).

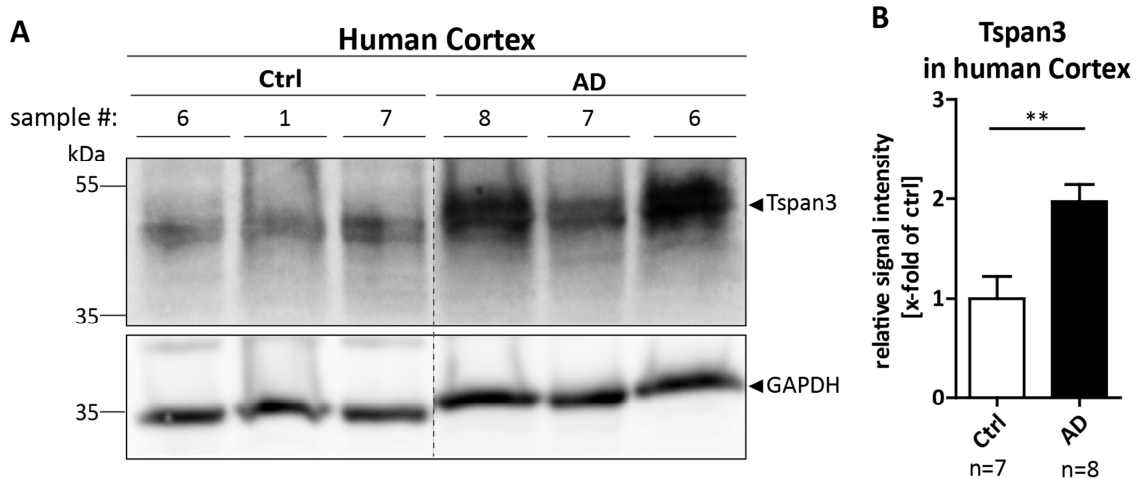


**Fig. 4.32: Tspan3 expression is increased in the prefrontal cortex of AD patients.**

**A)** Representative immunoblot, showing Tspan3 expression in post-mortem prefrontal cortex samples of Alzheimer's disease patients (AD) and healthy controls (Ctrl). Equal protein loading was verified by GAPDH staining. **B)** Quantification of Tspan3 signal intensities in Ctrl (n=7) and AD (n=8) samples. Statistical significance was tested by using Student's t-test (\*\*p<0.01).

Using an anti-Tspan3 antibody, prominent signals at around 45 kDa corresponding to Tspan3 were detected in all samples (Fig. 4.32A). Compared to control samples (Ctrl), Tspan3 expression was clearly increased in the samples of AD patients. Staining for GAPDH confirmed equal protein loading. This finding was further confirmed by the analysis of a higher number of samples, including seven controls (n=7) and eight AD (n=8) specimens (Fig. 4.32B). These data confirmed that Tspan3 expression is increased in the brains of AD patients.

### 4.3 Characterisation of the *in vivo* function of tetraspanin-15

Tspan15 is one of the first TspanC8 tetraspanins, which was identified as a direct interaction partner of ADAM10 (Dornier et al., 2012; Haining et al., 2012; Prox et al., 2012). *In cellulo* experiments revealed Tspan15 as potent regulator of ADAM10 proteolytic activity. Through acceleration of ADAM10's ER exit and stabilisation of its mature form, Tspan15 increased ADAM10 maturation and surface expression. This also enhanced ADAM10-mediated ectodomain shedding of N-cadherin and APP in N2a, HEK293 and Cos7 cells (Prox et al., 2012). In the human osteosarcoma cell line, U2OS-N1, Tspan15 was shown to be a negative regulator of Notch and APP processing, indicating that Tspan15 has cell type specific functions (Jouannet et al., 2015). Moreover, Tspan15 expression modulated the composition of proteins which are associated with ADAM10 at the plasma membrane and influenced its motility (Jouannet et al., 2015).

Despite the increased understanding how Tspan15 regulates ADAM10-mediated shedding, its physiological functions have not been addressed yet. To study the role of Tspan15 for ADAM10-mediated shedding events *in vivo*, a Tspan15 knockout mouse model was generated and analysed.

#### 4.3.1 Generation of tetraspanin-15 knockout mice

To achieve a gene specific knockout of Tspan15, a TALEN-mediated approach was used (Fig. 4.33A). Similar to the previously described knockout strategy for Tspan3, TALENs were designed to target exon2 of the *Tspan15* gene locus (Fig. 4.33A) and microinjected into zygotes of a founder mouse. Sequence analysis (Fig. 4.33B) of genomic DNA obtained from offspring mice revealed a 104 bp deletion mutation in the TALEN-targeted region (*Tspan15* $\Delta$ 104), which led to a premature translational stop codon and was supposed to cause loss of gene function (Fig. 4.33A).

In order to distinguish wild-type and potential Tspan15 knockout mice, the presence of the mutated or wild-type allele was tested. Therefore, genomic DNA was isolated and subjected to PCR. For amplification, a primer pair (forward and reverse) surrounding the sequence of *Tspan15* exon2, was used. Following, PCR products were analysed by agarose gel electrophoresis (Fig. 4.33B). In the wild-type (wt) sample DNA amplification resulted in a 600 bp long PCR product, which corresponds to the wild-type *Tspan15* exon2 (Fig. 4.33B). According to the predicted 104 bp deletion mutation, the knockout (ko) allele was identified

by the presence of a clearly smaller amplicon, at around 500 bp. Heterozygous mice (+/-), bearing one wild-type and one mutated allele were identified by the presence of two amplicons at around 500 bp and 600 bp (Fig. 4.33B).

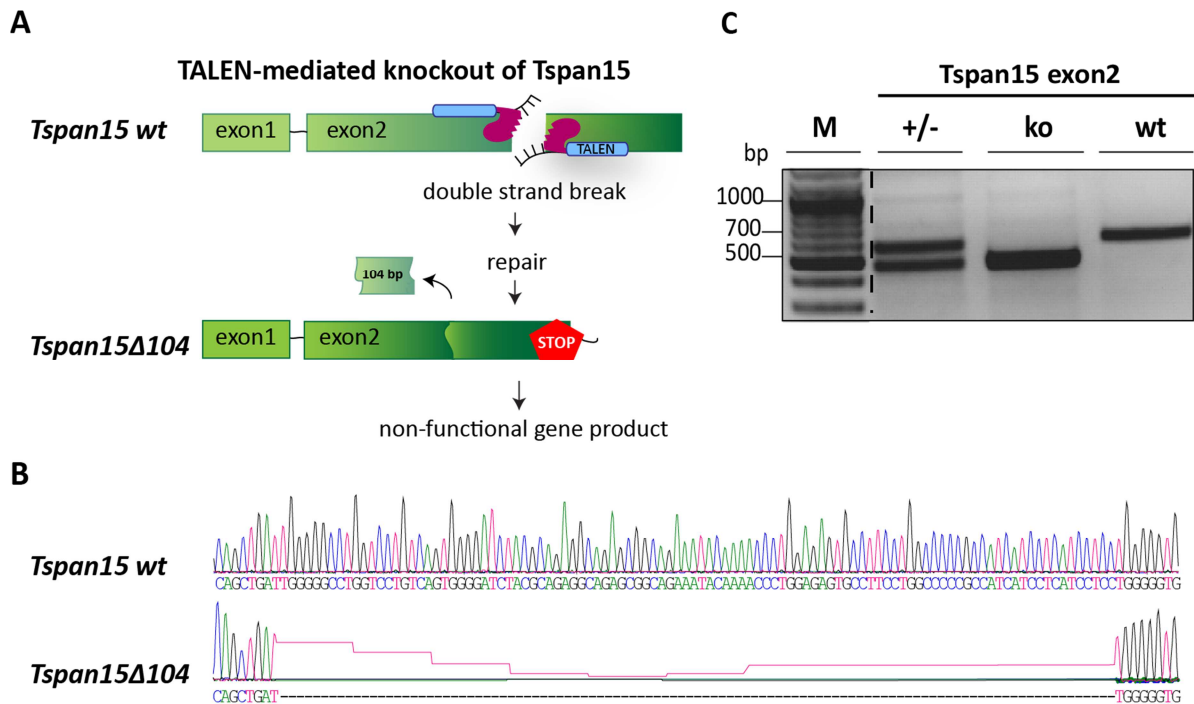


**Fig. 4.33: TALEN-mediated knockout strategy for the generation of *Tspan15*-deficient mice.**

**A)** Schematic drawing showing the transcription-activated like effector nuclease (TALEN)-mediated knockout strategy for the generation of *Tspan15*-deficient mice. TALENs were designed to induce a site-specific double strand break within exon2 of the *Tspan15* gene locus. Subsequent DNA repair led to a 104-base pair (bp) deletion mutation (*Tspan15Δ104*), which generated a premature translational stop codon. **B)** Sequencing chromatogram of the TALEN-targeted region within the wild-type (*Tspan15 wt*) and mutated *Tspan15* exon2 (*Tspan15Δ104*). **C)** Agarose gel electrophoresis of PCR products amplified from genomic DNA of *Tspan15* heterozygous (+/-), knockout (ko) and wild-type mice using a primer pair (forward and reverse) surrounding the sequence of *Tspan15* exon2.

In order to obtain homozygous *Tspan15Δ104* mice, which should be deficient for *Tspan15*, and respective wild-type controls, heterozygous mice were bred (see breeding scheme in section 3.6.3). During breeding, it was conspicuous that an increased number of animals died within the first weeks after birth. To calculate the postnatal mortality rate, the number of born mice and mice, that were still alive three weeks after birth, was determined (Tab. 4.2). Calculation of the percentage of total alive to total born animals revealed an increased mortality rate of 16% within the first three weeks after birth, which could indicate the occurrence of early developmental defects. Genotype analysis (Tab. 4.2, total alive) revealed a Mendelian distribution of wild-type (wt, 24%), heterozygous (+/-, 50%) and knockout (ko, 26%) animals with no obvious anomalies.

Tab. 4.2: Genotype distribution of *Tspan15* $\Delta$ 104 breeding.

Animals	total		Genotypes of total alive		
	born	alive*	wt	+/-	ko
Number (n)	321	272	65	136	70
%	100	84	24	50	26

\*3 weeks after birth. wt, wild-type; +/-, heterozygous; ko, knockout.

To validate that the observed frameshift mutation was efficient to cause loss of the *Tspan15* protein, the expression of *Tspan15* was analysed in different organs of a homozygous *Tspan15* $\Delta$ 104 mouse, which will hereafter be referred to as *Tspan15* knockout mouse. For this purpose, brain, heart, lung, spleen, kidney and liver were isolated from a three-week-old *Tspan15* knockout (ko) mouse. As a positive control, the respective organs from an age matched wild-type mouse were used. *Tspan15* expression was analysed by immunoblotting (Fig. 4.34).

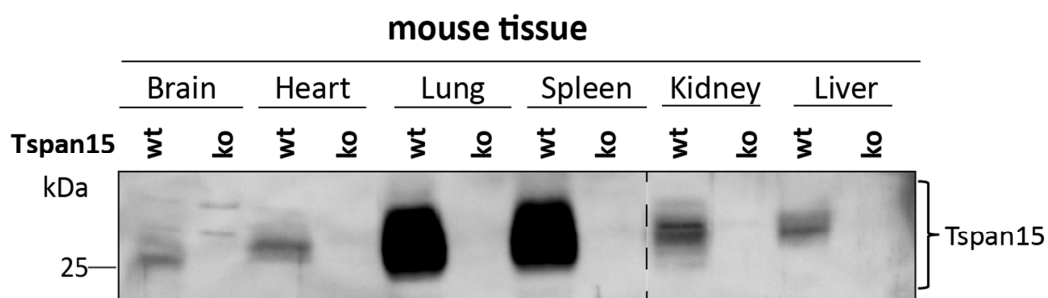


**Fig. 4.34: TALEN-mediated knockout of *Tspan15* was confirmed in all tested tissues.**

Immunoblot analysis of *Tspan15* knockout efficiency in indicated organs. Tissue lysates of a wild-type (wt) and *Tspan15* knockout (ko) mouse were prepared and subjected to immunoblot analysis. Using a C-terminal anti-*Tspan15* antibody, endogenous *Tspan15* was detected in all wild-type tissues. No *Tspan15*-specific signals were observed in the respective knockout samples.

Staining with a C-terminal anti-*Tspan15* antibody (Fig. 4.34), revealed prominent signals at around 28 kDa in the all tested wild-type (wt) tissues, which correspond to endogenous *Tspan15* (Fig. 4.34). No signals were detected in the respective *Tspan15* knockout (ko) samples. Thus, confirming the successful knockout of *Tspan15* in these organs (Fig. 4.34).

In conclusion, the introduction of a 104 bp deletion mutation within the murine *Tspan15* gene locus led to the successful knockout of the *Tspan15* protein. It was noticeable that breeding of *Tspan15* mice led to a slightly increased mortality rate within the first three weeks after birth. However, *Tspan15*-deficient animals showed no apparent developmental defects or an overt phenotype after birth.

### 4.3.2 Tetraspanin-15 is predominantly expressed in lung and intestine

To gain more insight into the physiological role of Tspan15, its distribution in adult mouse tissues was analysed by immunoblot analysis using the above validated and specific anti-Tspan15 antibody. To this end, different organs were isolated from a six-month-old wild-type mouse, homogenised and Tspan15 expression assessed by immunoblot analysis (Fig. 4.35A).

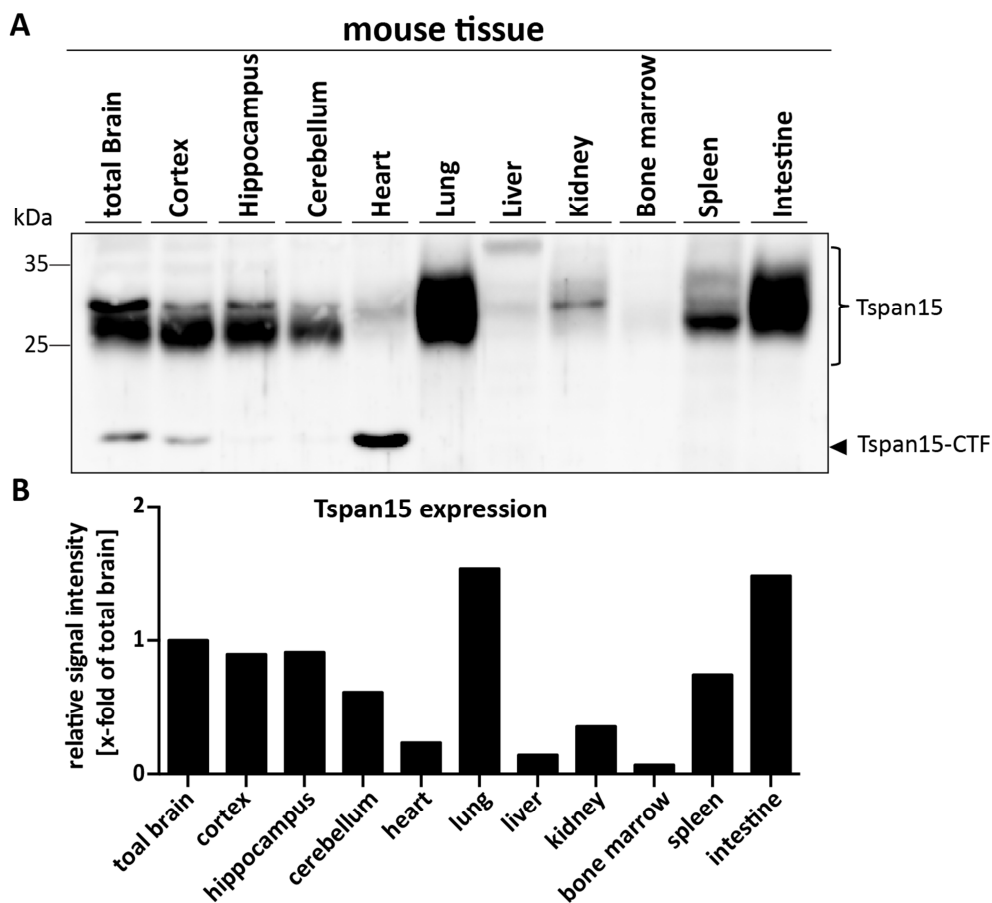


**Fig. 4.35: Expression pattern of Tspan15 in adult mouse tissues.**

**A)** Indicated organs were isolated from a six-month-old wild-type (wt) mouse, homogenised and analysed by immunoblotting. Using a C-terminal anti-Tspan15 antibody, Tspan15 expression was detected in all tissues except for bone marrow. **B)** Quantification of Tspan15 signal intensities. Data are shown as single values, correlated to Tspan15 signal intensity in the total brain sample.

After immunoblotting (Fig. 4.35A), staining with an anti-Tspan15 antibody revealed strong signals at around 28 kDa in all samples. Interestingly, in total brain, cortex and heart samples an additional signal at 10 kDa was observed, which could correspond to a C-terminal fragment (CTF) of Tspan15. The strongest Tspan15 signal intensity was observed in lung (1.5-fold) and intestine (1.5-fold, Fig. 4.35A, B). Also in brain (1.0-fold), cortex (0.9-fold), hippocampus (0.9-fold), cerebellum (0.8-fold) and spleen (0.6-fold) Tspan15 was highly expressed. Minor signal

intensities were observed in heart (0.2-fold), liver (0.1-fold) and kidney (0.3-fold) homogenates and hardly any Tspan15 was detected in bone marrow (0.06-fold) homogenates.

Taken together, Tspan15 showed a broad expression pattern and was predominantly expressed in lung and intestine.

### 4.3.3 Tetraspanin-15 knockout impairs ADAM10 maturation and shedding activity

Since Tspan15 revealed a prominent expression in the brain, where the function of ADAM10 is well-characterized (reviewed in Saftig and Lichtenthaler, 2015), the influence of Tspan15-deficiency in the brain was further analysed.

To study the impact of loss of Tspan15 on ADAM10 maturation and proteolytic activity, brains of three-week-old Tspan15-deficient and wild-type (wt) mice were isolated. Tissue lysates were prepared and the expression of ADAM10, N-cadherin, APP and Tspan15 was analysed by immunoblot (Fig. 4.36A). After staining with an anti-Tspan15 antibody (Fig. 4.36A), prominent signals were observed in the wild-type (wt) samples. No signals were observed in the lysates of Tspan15 knockout (Tspan15 ko) mice, validating the absence of Tspan15. In correlation with the loss of Tspan15, detection of ADAM10 in Tspan15 knockout samples, revealed clearly decreased signal intensities of mature (m) ADAM10, compared to wild-type samples (Fig. 4.36A, C). Comparable signal intensities of pro- (p) ADAM10 were observed in both, wild-type and Tspan15 knockout lysates. APP was detected with a C-terminal anti-APP antibody. Similar signal intensities of full length (fl-) APP and the APP-C-terminal fragment (CTF) were observed in wild-type and Tspan15 knockout samples. Detection of N-cadherin revealed a slightly increased expression of full length N-Cadherin (N-cad. fl) in the brains of Tspan15 knockout mice compared to wild-type samples. Using the same antibody and a longer exposure time, a significant decrease of the ADAM10-generated N-cadherin cleavage product CTF1 (N-cad. CTF1) was observed in the Tspan15 knockout samples (Fig. 4.36A, C). Staining for beta-Tubulin confirmed equal protein loading. These findings demonstrate that the loss of Tspan15 decreased ADAM10 maturation and N-cadherin shedding, whereas proteolytic processing of APP was apparently unaffected.

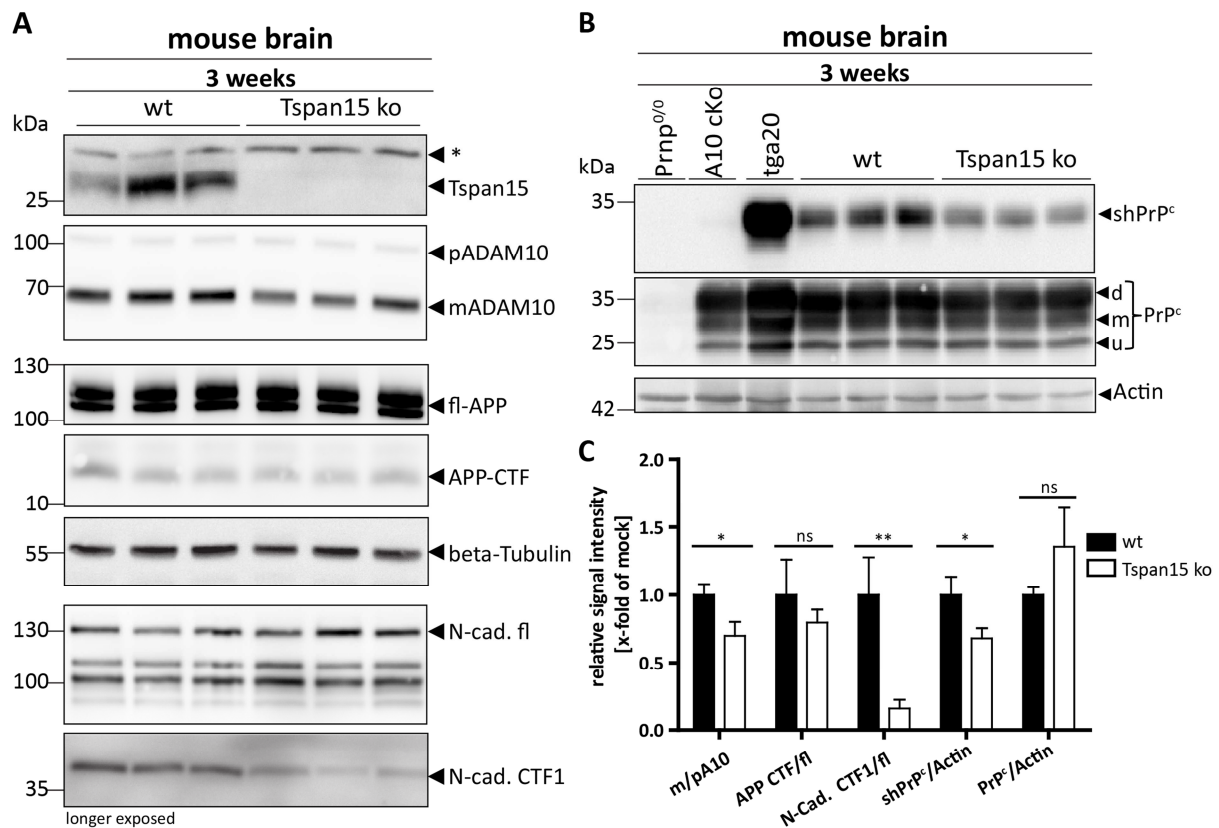


**Fig. 4.36: Knockout of Tspan15 decreases mADAM10 and reduces N-cadherin and PrP<sup>c</sup> shedding.**

**A)** Brain lysates of three-week-old wild-type (wt) and Tspan15 knockout (ko) mice were prepared and analysed by immunoblot. Tspan15-deficiency in Tspan15 ko samples was confirmed by using an anti-Tspan15 antibody. Expression of pro- (p) and mature (m) ADAM10 was observed with an anti-ADAM10 antibody. Using an anti-APP antibody, expression of full length (fl-) APP and the APP-C-terminal fragment (CTF) was detected. Expression of full length N-cadherin (N-cad. fl) and the ADAM10-generated C-terminal fragment CTF1 (N-cad. CTF1) was monitored with an anti-N-cadherin antibody. Beta-tubulin staining was used to control for equal protein loading. \*: unspecific signals. **B)** Mouse brain homogenates were analysed for the proteolytic processing of the cellular prion protein (PrP<sup>c</sup>). As controls, samples from PrP-deficient mice (Prnp<sup>0/0</sup>), conditional ADAM10 knockout mice (A10 cKO) with a postnatal deletion in neurons and PrP<sup>c</sup> overexpressing mice (tga20) were used. The soluble PrP<sup>c</sup> ectodomain, referred to as shed PrP<sup>c</sup> (shPrP<sup>c</sup>), was detected with an N-terminal PrP<sup>c</sup> antibody. Di (d)-, mono- (m) and unglycosylated (u) full length PrP<sup>c</sup> were detected with a C-terminal anti-PrP<sup>c</sup> antibody (POM1). **C)** Quantitative analysis of ADAM10 (m/p), APP (CTF/fl), N-cadherin (CTF1/fl), shPrP<sup>c</sup>/Actin and PrP<sup>c</sup>/Actin signal intensities. Data are shown as mean values  $\pm$ SD. Mean values of wt samples were set as one. Statistical significance was analysed by Student's t-test (\*p<0.05, \*\*p<0.01).

Due to the fact that the neuron-specific knockout of ADAM10 in mice, prevented shedding of the cellular prion protein (PrP<sup>c</sup>) (Altmepfen et al., 2011), it was further of interest, whether the decreased maturation of ADAM10 in Tspan15 knockout mice has a similar effect on PrP<sup>c</sup>-shedding. Hence, in collaboration with *Dr. Hermann Altmepfen* (University Medical Centre, Hamburg-Eppendorf), the appearance of full length PrP<sup>c</sup> and its soluble ectodomain, which is released upon ADAM10 cleavage (named shed PrP<sup>c</sup>), was analysed. Brain homogenates were prepared from three-week-old wild-type and Tspan15 knockout mice. Additionally, brain homogenates of PrP<sup>c</sup> deficient mice (Prnp<sup>0/0</sup>), ADAM10 conditional knockout mice (A10 cKO) and PrP<sup>c</sup> overexpressing mice (tga20) were used as controls. Tissue lysates were subjected to



immunoblotting and expression of full length PrP<sup>c</sup> and shed PrP (shPrP<sup>c</sup>) was analysed (Fig. 4.36B). Using an anti-shPrP<sup>c</sup> antibody, raised against the N-terminus of PrP<sup>c</sup>, shPrP<sup>c</sup> was detected in tga20 homogenates, but not in PrP<sup>c</sup>-deficient and A10 cKO samples, indicating specificity of the antibody (Fig. 4.36B). In comparison to wild-type (wt) homogenates, the shPrP<sup>c</sup> signal intensities were significantly reduced in the brains of Tspan15 knockout (ko) mice (Fig. 4.36B, C). Staining for full length PrP<sup>c</sup>, using a C-terminal anti-PrP<sup>c</sup> antibody, revealed no significant difference of PrP<sup>c</sup> (di-, mono- and unglycosylated) signal intensities in wild-type and Tspan15 knockout brains (Fig. 4.36B, C). In PrP<sup>c</sup> overexpressing mice (tga20), the PrP<sup>c</sup> signal intensity was clearly increased, whereas it was slightly reduced in the ADAM10 conditional knockout (A10 cKo) sample (Fig. 4.36B). These results further show that loss of Tspan15 reduced the shedding of another important ADAM10 substrate, PrP<sup>c</sup>.

To validate these findings in adult mice, immunoblot analysis of ADAM10 maturation, APP, N-cadherin and PrP<sup>c</sup> shedding was performed with brain homogenates of 21-week-old mice (Fig. 4.37A, B). As previously observed, signal intensities of mature ADAM10 were significantly reduced in brains of Tspan15 knockout mice compared to wild-type samples (Fig. 4.37A, C). Staining for N-cadherin revealed significantly reduced signal intensities of N-cadherin CTF1 (N-cad. CTF1) in Tspan15 knockout samples, whereas signal intensities of fl-APP and APP-CTFs were unchanged compared to wild-type samples (Fig. 4.37A, C). Analysis of PrP<sup>c</sup> shedding also revealed a significantly reduced level of shPrP<sup>c</sup> and an increased level of full length PrP<sup>c</sup> (di-, mono- and unglycosylated) in Tspan15 knockout samples compared to wild-type homogenates (Fig. 4.37B, C).

In conclusion, the knockout of Tspan15 in mice decreased the expression of mature ADAM10 and reduced shedding of two prominent ADAM10 substrates, N-cadherin and PrP<sup>c</sup>, in the brains of three-week-old and adult mice. Surprisingly, APP proteolytic processing, as revealed by detection with a C-terminal anti-APP antibody, was not affected in the brains of Tspan15 knockout mice.

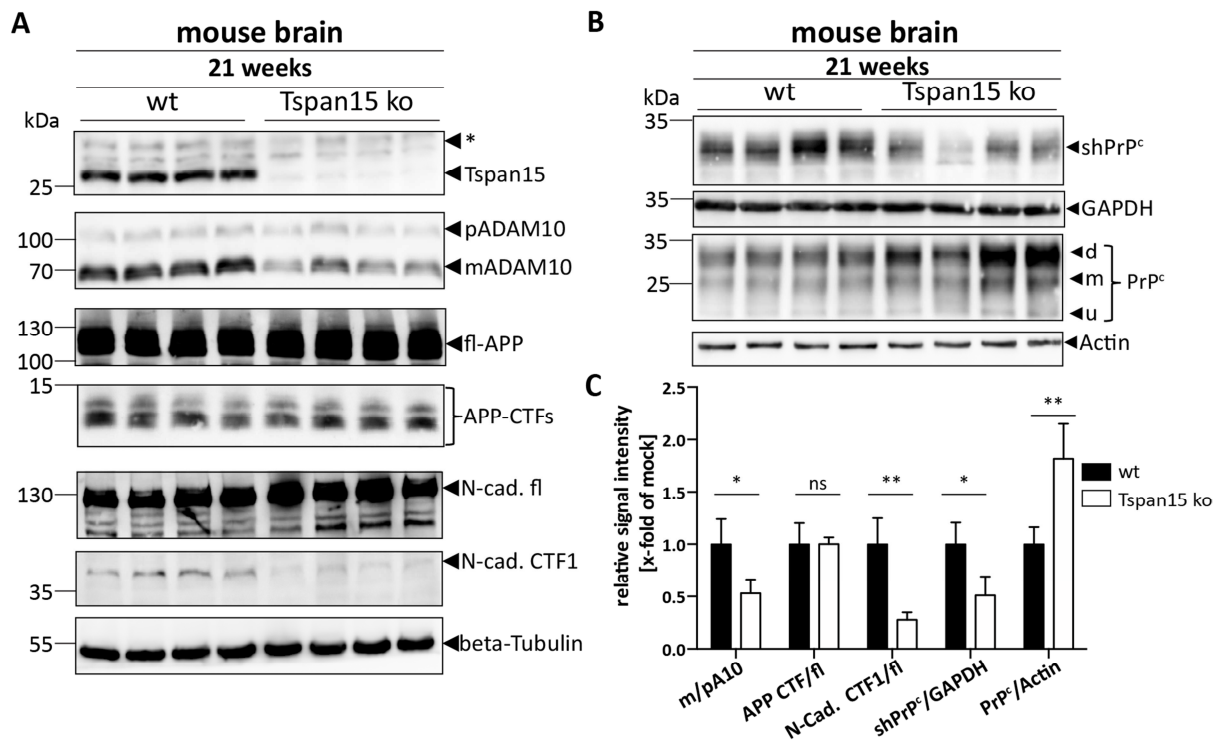


**Fig. 4.37: Loss of Tspan15 in 21-week-old mice reduces ADAM10 maturation, N-cadherin and PrP<sup>c</sup> shedding.**

**A**) Immunoblot analysis of brain homogenates from 21-week-old wild-type (wt) and Tspan15 knockout (ko) mice. Absence of Tspan15 in Tspan15 ko samples was confirmed by staining with an anti-Tspan15 antibody. ADAM10 maturation, APP and N-cadherin (N-cad.) shedding were analysed using anti-ADAM10, anti-APP and anti-N-cadherin antibodies (fl: full length, CTF: C-terminal fragment, p: pro, m: mature). Beta-tubulin staining confirmed equal protein loading. **B**) Analysis of PrP<sup>c</sup> shedding. A N-terminal anti-PrP<sup>c</sup> antibody was used to detect shed PrP<sup>c</sup> (shPrP<sup>c</sup>). Detection of di (d)-, mono- (m) and unglycosylated (u) full length PrP<sup>c</sup> was performed with a C-terminal anti-PrP<sup>c</sup> antibody (POM1). **C**) Densitometric analysis of signal intensities of ADAM10 (m/p), APP (CTF/fl), N-cadherin (CTF1/fl), shPrP<sup>c</sup>/Actin and PrP<sup>c</sup>/Actin. Data are shown as mean values  $\pm$ SD and Student's t-test was performed (\* $p$ <0.05, \*\* $p$ <0.01).

#### 4.3.4 Loss of Tspan15 increases the appearance of perforated postsynaptic densities

The postnatal neuronal depletion of ADAM10 in mice was shown to cause learning deficits and impaired synaptic plasticity, which was associated with morphological changes of the synaptic spine structure (Prox et al., 2012). The ultrastructural analysis of ADAM10-deficient hippocampal neurons revealed enlarged dendritic spines with a shrunken and stubby shape, which was most likely due to reduced shedding of neuronal adhesion molecules like Nectin-1 and N-cadherin (Prox et al., 2012). Similarly, alterations of ADAM10's synaptic localisation and activity increased dendritic spine head width by decreasing N-cadherin shedding (Malinverno et al., 2010).

To investigate whether the reduced presence of mature ADAM10 in Tspan15-deficient mice has a similar effect on the morphology of dendritic spines, an ultrastructural analysis was performed. To this end, in collaboration with *Dr. Michaela Schweizer* (University Medical Centre, Hamburg-Eppendorf) brains of 12-week-old wild type and Tspan15 knockout mice were prepared for electron microscopy and electron micrographs of the hippocampal CA1 region were taken (Fig. 4.38A).

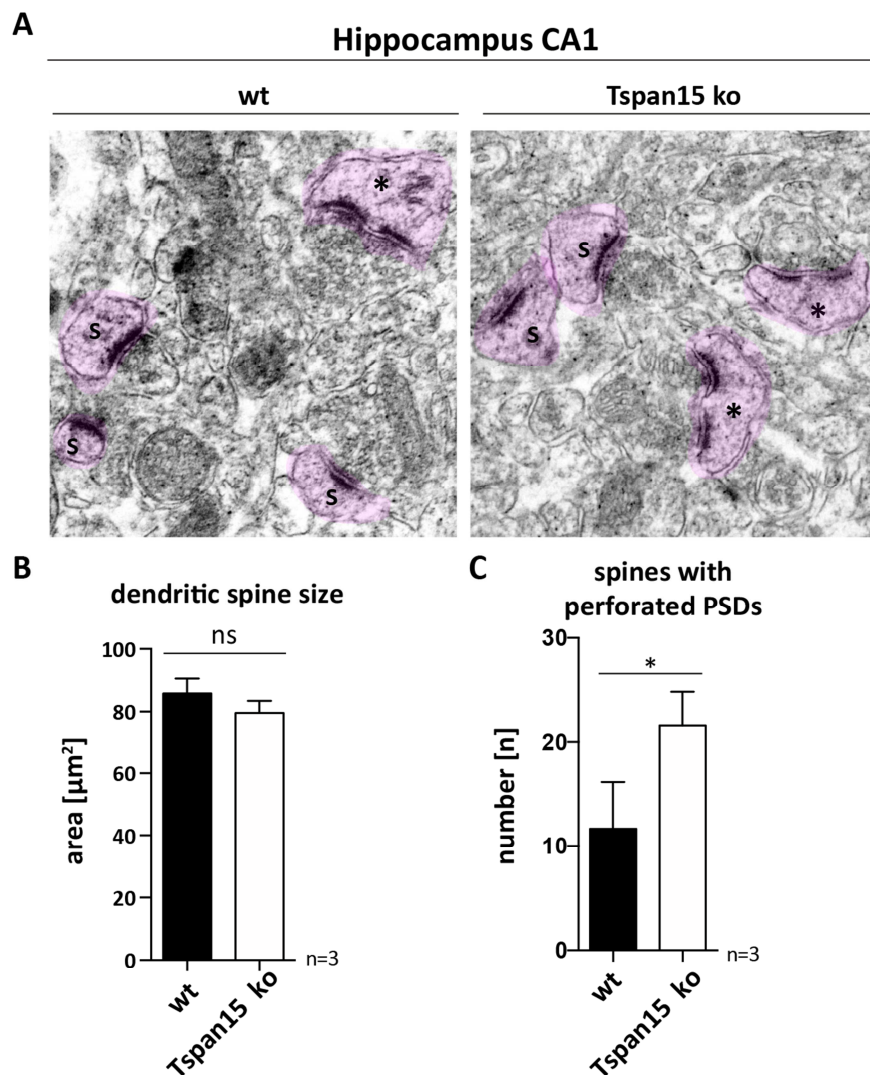


**Fig. 4.38: Tspan15 knockout increases the number of spines with perforated postsynaptic densities (PSDs).**

Representative electron micrographs of the hippocampal CA1 region of wild-type (wt) and Tspan15-deficient mice (Tspan15 ko, collaboration with *Dr. Michaela Schweizer*, University Medical Centre, Hamburg-Eppendorf). Dendritic spines with a continuous (S) and perforated PSD (\*) are highlighted in pink. **B**) Dendritic spine (S) size of 21 electron micrographs per animal (n=3) were measured using ImageJ. Mean values  $\pm$ SD of the measured spine area are shown in  $\mu\text{m}^2$ . **C**) Perforated PSDs (\*) of wild-type (wt) and Tspan15 knockout (ko) animals were counted. Data is shown as mean values  $\pm$ SD. Statistical significance was determined by Student's t-test (\* $p < 0.05$ ).

Analysis of electron micrographs (Fig. 4.38A) revealed spines with a continuous postsynaptic density (S) and spines with a discontinuous or “perforated” (\*) postsynaptic density (PSD).

Using the ImageJ software, spine (S) size was determined (Fig. 4.38A, shown in pink), but revealed no significant difference between Tspan15 knockout and wild-type mice (Fig. 4.38B). It should be noted that perforated spines (\*, Fig. 4.38A) were excluded from spine size measurements. Furthermore, the number of spines with perforated PSDs in wild-type and Tspan15 knockout electron micrographs was counted. This revealed a significantly increased appearance of spines with a perforated PSD in Tspan15 knockout mice, compared to wild-type controls (Fig. 4.38C).

In conclusion, the size of dendritic spines was not affected by the loss of Tspan15, but led to an increased appearance of perforated spines.

## 5 Discussion

ADAM10 has a broad substrate spectrum ranging from different cell adhesion molecules (CAMs), cytokines to the prion protein, APP and the Notch receptor (Kuhn et al., 2016; Reiss and Saftig, 2009). While the function of ADAM10 in physiological and pathological processes is well-described, the mechanisms that control ADAM10 activity in a tissue and substrate-specific manner are still not clear. In this context tetraspanins became interesting candidates involved in ADAM10 regulation. However, the mode of action and the function of tetraspanins in ADAM10-mediated shedding events is still unclear.

### 5.1 Identification of tetraspanin-3 as a novel ADAM10 interaction partner

Tetraspanin-3 (Tspan3) was initially discovered as an ADAM10 interaction partner in yeast. In the course of this work Tspan3 was confirmed as an ADAM10 interaction partner by reciprocal co-immunoprecipitation experiments under overexpression conditions in mammalian cells. ADAM10 was also endogenously co-immunoprecipitated by Tspan3 from murine brain homogenates, which validated their interaction in a physiological context.

In the recent years, several tetraspanins were identified as ADAM10 interaction partners. However, the interaction of most of these tetraspanins, such as CD9, CD63 and CD81 turned out to be of rather indirect nature, which is mediated by tetraspanin-tetraspanin interactions (Dornier et al., 2012). Until now, only members of the TspanC8 tetraspanins were described as direct ADAM10 interaction partners. Interestingly, Tspan3 does not belong to these TspanC8 tetraspanins. By containing only six cysteines within its large extracellular loop, Tspan3 belongs to the subgroup of TspanC6 tetraspanins, which further includes CD63, Tspan6 and Tspan7 (see section 1.4, Fig. 1.6). Since the yeast screen requires a physical interaction of the bait and prey protein to enable growth of yeast clones under selective pressure, the Tspan3-ADAM10 interaction is likely to be of direct nature. This is supported by the fact that all co-immunoprecipitation experiments were performed under stringent detergent conditions using the detergent NP-40. NP-40 preserves direct tetraspanin-protein interactions, whereas indirect tetraspanin-tetraspanin interactions are disrupted (Levy and Shoham, 2005). Therefore, these findings identify Tspan3 as a non-TspanC8 tetraspanin, which directly interacts with ADAM10.

The analysis of Tspan3 protein expression in different mouse tissues revealed a broad tissue distribution of Tspan3. In line with previous studies, which analysed Tspan3 tissue distribution at the mRNA level (Puls and Wright, 2000; Todd et al., 1998; Tokoro et al., 2001), Tspan3 protein expression was detected in several tissues, except for liver and was most abundant in the brain.

To date there is only limited knowledge about the functions of Tspan3. Initially, Tspan3 was discovered as an interaction partner of the oligodendrocyte-specific protein (OSP)/claudin-11 and is therefore also referred to as OSP-associated protein 1 (OAP1). Together with OSP and  $\beta$ 1 integrin, Tspan3 forms a functional complex, which regulates migration and proliferation of oligodendrocyte progenitors (Tiwari-Woodruff et al., 2001). Additionally, Tspan3 regulates neurite outgrowth by acting as a co-receptor for the binding of the neurite outgrowth inhibitor (Nogo)-A- $\Delta$ 20 ligand to its receptor sphingosine-1-phosphate receptor 2 (S1PR2). Tspan3 interacts with the Nogo-A- $\Delta$ 20 ligand and mediates its initial contact with the cell surface. Following Nogo-A- $\Delta$ 20 binding, Tspan3 associates with S1PR2 and mediates ligand-receptor contact. This activates an intracellular signalling cascade, which leads to the inhibition of neurite outgrowth. Moreover, Tspan3 accompanies the receptor-ligand complex through the early endocytic pathway and disassembles from the receptor-ligand complex only at later time-points (Thiede-Stan et al., 2015). Besides these central nervous system-related functions, Tspan3 is also involved in the propagation of acute myelogenous leukaemia (AML) (Kwon et al., 2015). In AML cells, Tspan3 was identified as a target of the mRNA binding protein musashi-2 (Msi2), which is highly upregulated during AML and predicts a poor prognosis for AML patients. In correlation with the increased expression of Msi2, also Tspan3 expression was upregulated in AML cells. It was further demonstrated that Tspan3 promotes AML cell migration in response to the stromal cell-derived factor-1 (SDF1) chemokine by modulating the activation of the C-X-C chemokine receptor 4 (CXCR4). Inversely, Tspan3-deficiency inhibited cancer cell migration (Kwon et al., 2015). Moreover, Tspan3 was detected in neural crest cells during *Xenopus laevis* embryonic development and on resting dendritic cells (DCs), which implicates further functions of Tspan3 in developmental processes and in the immune system (Kashef et al., 2013; Tokoro et al., 2001). The role of Tspan3 as interaction partner of proteases, in particular with metalloproteases of the ADAM family was not yet described. This prompted a more thorough analysis of its role as a protease modulator.

### 5.1.1 Tetraspanin-3 has no apparent effect on ADAM10 maturation and surface trafficking

Transition of the proform of ADAM10 into its mature form is an essential step that determines the activity of ADAM10. This process is located in the *trans*-Golgi network and is mediated by proprotein convertases, which cleave the ADAM10 prodomain. The prodomain also acts as a chaperone, which is required for correct protein folding (Roghani et al., 1999). The importance of the prodomain for ADAM10 functionality is demonstrated by the finding that the point mutations Q170A and R181G, which are located in the ADAM10 prodomain, are associated with the development of late-onset AD (Kim et al., 2009b). By impairing maturation and chaperone function, the expression of these two prodomain mutants decreased ADAM10s  $\alpha$ -secretase activity towards APP and led to an increased A $\beta$  burden in AD mice (Suh et al., 2013).

Furthermore, modulation of ADAM10's surface expression is important to control protease activity. This was for example demonstrated for SAP97, which is an essential regulator of ADAM10 trafficking in neurons. SAP97 binds to the proline rich region within the C-terminal domain of ADAM10 and promotes the transport of ADAM10 from the Golgi outposts to the synaptic membrane (Marcello et al., 2007; Saraceno et al., 2014). As a consequence, the increased surface expression of ADAM10 enhances  $\alpha$ -secretase processing of APP (Marcello et al., 2007). In contrast, disruption of the SAP97/ADAM10 complex by using a cell penetrating Tat peptide fused to the proline rich region of ADAM10, blocked ADAM10 surface trafficking and caused symptoms of sporadic AD in a mouse model (Epis et al., 2010; Marcello et al., 2007).

Interestingly, the potential of most tetraspanins to modulate ADAM10 activity is related to the above described mechanisms, namely ADAM10 maturation and surface trafficking (Dornier et al., 2012; Noy et al., 2016; Prox et al., 2012). In particular, overexpression of TspanC8 tetraspanins Tspan5, Tspan14, Tspan15 and Tspan33, but also Tspan12 promotes ADAM10 maturation and increases the surface presence of ADAM10 (Dornier et al., 2012; Haining et al., 2012; Xu et al., 2009). The mechanism how these tetraspanins modulate ADAM10 maturation and surface trafficking is largely unknown. However, first evidences were provided by the analysis of the Tspan15-ADAM10 interaction (Prox et al., 2012). These studies revealed that the Tspan15-ADAM10 interaction already occurs in the ER. Limiting the ER exit of Tspan15 by adding an ER retention motif to its C-terminus, also enriched ADAM10

localisation in the ER. Moreover, examining ADAM10 maturation over time revealed an accelerated ADAM10 maturation after Tspan15 overexpression. Therefore, it was concluded that Tspan15 promotes ADAM10 maturation and surface trafficking by accelerating the ER exit of ADAM10. It was further speculated that Tspan15 could do so by masking the ADAM10 ER retention motif, which is located in the ADAM10 cytoplasmic C-terminal domain (Prox et al., 2012).

In contrast to Tspan15, the overexpression of Tspan3 had no apparent effect on the appearance of the pro- or the mature form of ADAM10 and did not obviously alter the surface expression of ADAM10. This contradictory finding might be explained by the differential subcellular localisation of Tspan15 and Tspan3. While Tspan15 is mainly found in the ER and at the plasma membrane (Prox et al., 2012), Tspan3 showed only little plasma membrane and almost no ER localisation. On the contrary, a prominent Tspan3 localisation was observed in endosomal and lysosomal compartments. Interestingly, a similar subcellular localisation is described for Tspan3's close relative CD63 (Berditchevski and Odintsova, 2007; Metzelaar et al., 1991). The comparable subcellular distribution could hint to a similar function of Tspan3 and CD63, which is involved in the internalisation and sorting of its partner proteins during endocytosis (van Niel et al., 2011; Takino et al., 2003). The potential role of Tspan3 in endocytic processes will be discussed in section 5.1.4.

These results indicate that, although Tspan3 was identified as another direct interaction partner of ADAM10, its function with regards to accelerated ER-plasma membrane transport of ADAM10 is clearly different from that of Tspan15 and other previously described ADAM10-interacting tetraspanins.

### **5.1.2 The role of tetraspanin-3 in the proteolytic processing of APP**

To further analyse the impact of Tspan3 on ADAM10, the shedding of two ADAM10 substrates, N-cadherin and APP, was analysed. Surprisingly, overexpression of Tspan3 did not alter the generation of ADAM10-mediated N-cadherin cleavage product CTF1, but led to a clear increase of the APP-CTF. In contrast, Tspan15 overexpression increased N-cadherin cleavage, but only mildly affected APP proteolytic processing. This observation is in agreement with previous studies, which revealed that Tspan15 predominantly affects N-cadherin shedding and only affects APP processing in specific cell-types (Jouannet et al., 2015; Noy et al., 2016; Prox et al., 2012).



Interestingly, similar substrate specific functions have also been observed for other members of the TspanC8 tetraspanins (see section 1.4.2, Tab. 1.2). For example, while Tspan5 stimulates Notch shedding and increases CD44 shedding, Tspan33 and Tspan15 do not affect CD44 shedding and reduce Notch shedding. Moreover, Tspan14 is the only TspanC8 member which specifically reduces GPVI shedding in platelets (Jouannet et al., 2015; Noy et al., 2016). Hence, the finding that Tspan3 increases the APP-CTF production, but does not affect N-cadherin processing indicates that its function could be specific to APP. Nevertheless, given the huge substrate spectrum of ADAM10 (Kuhn et al., 2016; Reiss and Saftig, 2009), it is still possible that Tspan3 has an impact on the cleavage of other ADAM10 substrates.

Although, APP is a well-described ADAM10 substrate, APP-CTFs can also be generated by other potential  $\alpha$ -secretases and by the  $\beta$ -secretase BACE1. Since, ADAM10-derived and  $\beta$ -secretase generated APP-CTFs are difficult to distinguish, it was necessary to confirm that the Tspan3-induced increase of the APP-CTF is related to ADAM10. Attenuating ADAM10 activity by inhibitor treatment or siRNA-mediated knockdown diminished the Tspan3-induced increase of the APP-CTF and confirmed that this effect is dependent on ADAM10 activity. Moreover, overexpression of Tspan3 in HEK293 APP-swe cells increased the appearance of APP-C83 CTFs, but not of the  $\beta$ -secretase cleavage product C99, which excluded an influence of Tspan3 on  $\beta$ -secretase-dependent APP processing (Fig. 5.1). In HEK293 APP-wt cells Tspan3 expression not only increased the APP-C83, but also the extracellular counterpart, soluble APP $\alpha$  (sAPP $\alpha$ ), which indicated that the increased appearance of the APP-CTF is not related to an inhibition of the  $\gamma$ -secretase complex. This was further confirmed by analysing the effects of a  $\gamma$ -secretase inhibition on APP-CTF production. While treatment with a  $\gamma$ -secretase inhibitor increased APP-C83, -C89 and -C99 production, Tspan3 expression only increased the APP-C83 cleavage product.

In addition to its promoting effect on APP-C83 production, Tspan3 overexpression also reduced the liberation of A $\beta$  peptides in HEK293 APP-swe cells (Fig. 5.1). This demonstrates that Tspan3 expression not only promotes ADAM10-mediated APP processing, but also shifts APP proteolytic processing from the amyloidogenic to the non-amyloidogenic processing pathway. However, in the same experiment it was conspicuous that Tspan3 expression increased APP-C83, but did not alter sAPP $\alpha$  liberation. This discrepancy can be explained by different findings. First, it was reported that APP-swe is differentially processed and sorted, compared to APP-wt. In polarized Mardin-Darby Canine Kidney (MDCK) cells, soluble APP

species released from APP-wt were mainly found in basolateral compartments and only 10% were sorted to the apical compartment. In contrast, in APP-swe expressing MDCK cells 20% of sAPP species were apically released. Moreover, despite being cleaved in endosomes, the  $\beta$ -secretase cleavage of APP-swe occurs already in the Golgi apparatus (Haass et al., 1995; Lo et al., 1994), which correlates with the detection of sAPP $\beta$  fragments in cell lysates (Lo et al., 1994). Although,  $\alpha$ -secretase cleavage is mainly localised at the plasma membrane, ADAM10 activity was also observed in late secretory compartments (Gutwein, 2002). Therefore, it is conceivable the  $\alpha$ -secretase cleavage of APP-swe also occurs in late secretory compartments, such as the *trans*-Golgi network or secretory vesicles. Similar to sAPP $\beta$ , sAPP $\alpha$  fragments could then be retained intracellularly. This could explain the constant sAPP $\alpha$  levels observed in the cell culture supernatant of HEK293 APP-swe cells. To test this hypothesis, the amount of sAPP $\alpha$  in cell lysates could be analysed.

Another reason for the apparently discrepant finding of increased APP-C83 levels and unaltered sAPP $\alpha$  liberation could be a different stability and/or different degradation kinetics of the APP-swe cleavage products. While the APP-CTFs are further cleaved by the  $\gamma$ -secretase complex and degraded in the lysosome, the fate of sAPP species is different. It was reported that after release from the cell surface, sAPP species are re-internalised into the cell by binding to sortilin and sortilin-related receptor with A-type repeats (SorLA), which target them either to lysosomal degradation or to the paranuclear region, respectively (Gustafsen et al., 2013). It is possible that the Swedish mutation, which is located in the sAPP $\alpha$  domain promotes uptake and degradation of sAPP $\alpha$ , whereas the stability of the APP-C83 fragment is not affected. Hence, at steady state, sAPP $\alpha$  levels could appear to be unaltered, while APP-C83 levels are increased. The third and most likely explanation is based on the finding that ADAM10 not only sheds full length APP, but is also able to cleave or trim APP- $\beta$ CTFs (C89 ,C99) to generate APP-C83 (Kuhn et al., 2010). Since APP-swe is preferentially cleaved by the  $\beta$ -secretase, which leads to increasing amounts of APP-C99, ADAM10 might prefer APP-C99 shedding rather than cleavage of the full length APP-swe. Moreover, the common localisation of APP-C99 and ADAM10 in the Golgi apparatus could promote ADAM10-mediated cleavage of the APP-C99 fragment. Therefore, it is possible that, the increased appearance of APP-C83 in APP-swe overexpressing cells results from increased shedding of APP-C99 fragments and not of full length APP-swe, which ultimately does not alter the level of sAPP $\alpha$ .

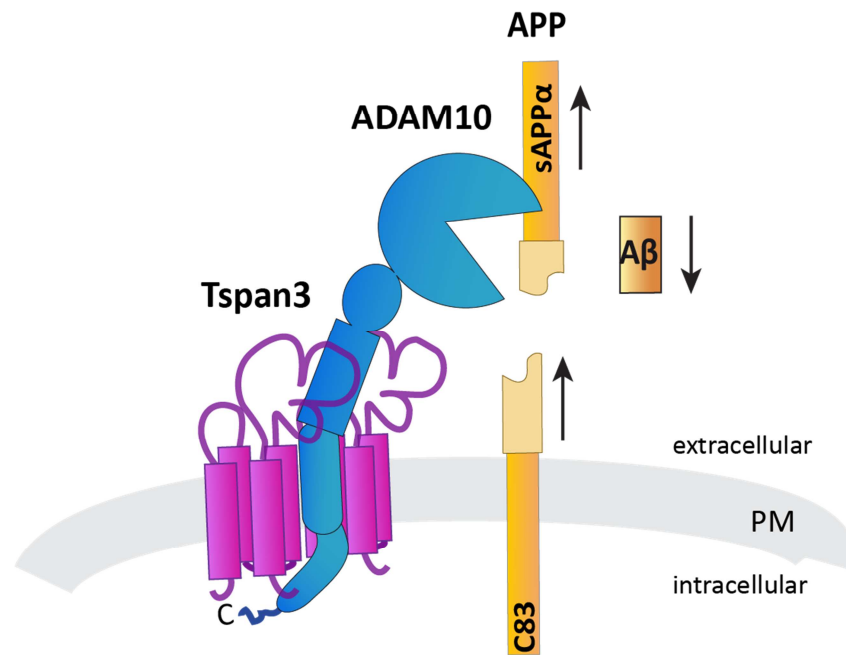


**Fig. 5.1: Tspan3 expression promotes ADAM10-mediated processing of APP.**

Tspan3 expression increases ADAM10-dependent APP processing. This leads to an increased appearance of APP C-terminal fragment (C83) and also increased the level of soluble APP $\alpha$  (sAPP $\alpha$ ). By promoting ADAM10-mediated APP processing, Tspan3 expression reduces the liberation of A $\beta$  peptides and shifts the amyloidogenic to non-amyloidogenic APP processing.

Despite the finding that the Tspan3-induced increase of the APP-CTF is mediated by ADAM10, expression of Tspan3 in ADAM10-deficient HEK293 cells still increased APP-CTF production. It is likely that in these cells other proteases with  $\alpha$ -secretases activity, such as ADAM17 or ADAM9, compensate for the loss of ADAM10. In such a scenario, Tspan3 could contribute to an alternative  $\alpha$ -secretases cleavage event and promote APP processing. Since Tspan3 did not interact with ADAM17 in cell-based co-immunoprecipitation experiments, it is more likely that Tspan3 promotes APP cleavage by modulating ADAM9 activity. Whether Tspan3 interacts with ADAM9 and modulates its activity has to be investigated.

Moreover, the observation that Tspan3 overexpression still increased APP-CTF levels in the absence of ADAM10 could partially be based on an effect of Tspan3 on APP itself. This possibility will be discussed in the next section.

### 5.1.3 Tetraspanin-3 acts as a scaffold for non-amyloidogenic APP processing

While most described tetraspanins, like TspanC8 members and Tspan12 regulate ADAM10-mediated cleavage by promoting its maturation or plasma membrane localisation, Tspan3 did not exert such an effect. However, Tspan3 expression increased ADAM10-mediated APP proteolytic processing.

Tetraspanins are described to take part in multiple interactions (Hemler, 2005). For example, CD9 associates with ADAM10 and ADAM17 (Arduise et al., 2008a; Gutiérrez-López et al., 2011). Interestingly, by interacting with these two proteases, CD9 has opposing effects on the ability of ADAM10 and ADAM17 to cleave their common substrate TNF $\alpha$ . This was demonstrated by treatment with monoclonal anti-CD9 antibodies, which promoted ADAM10-mediated TNF $\alpha$  cleavage, but reduced TNF $\alpha$  release by ADAM17 (Arduise et al., 2008a; Gutiérrez-López et al., 2011). Furthermore, by associating with more than one partner protein at the same time tetraspanins also exert cooperative effects. This was also shown for CD9, which acts as a co-receptor for the diphtheria toxin and increases the sensitivity and affinity of the diphtheria toxin receptor (Cha et al., 2000).

Similarly, Tspan3 is involved in multiple interactions, as part of the OSP/claudin-11/ $\beta$ 1-integrin complex and as mediator for the Nogo-A- $\Delta$ 20 and S1RP2 interaction (Thiede-Stan et al., 2015; Tiwari-Woodruff et al., 2001). Therefore, the question whether Tspan3 in addition to ADAM10, directly interacts with APP came into focus. Co-immunoprecipitation experiments after overexpression of Tspan3 and APP in cells and under endogenous conditions in mouse brain identified APP as another interaction partner of Tspan3. Interestingly, co-localisation of both proteins was observed close to the plasma membrane and in intracellular vesicular structures. This is consistent with subcellular localisation of Tspan3, which is also found close to the plasma membrane and in endosomal and lysosomal compartments. This finding suggests that Tspan3 could not only play a role for APP at the cell surface, where ADAM10 is located, but also in the endocytic pathway of APP. While this part of the discussion will focus on the role of Tspan3 at the plasma membrane, the potential role of Tspan3 for APP in endocytic processes will be addressed in section 5.1.4.

Further experiments aiming to analyse the function of the Tspan3-APP interaction, revealed that overexpression of Tspan3 increases the presence of the APP-CTF at the cell surface. Interestingly, increasing the Tspan3 surface levels by expression of a Tspan3 endocytic motif mutant enhanced the accumulation of the APP-CTF at the plasma membrane. In addition, expression of the mutant Tspan3 also increased the surface levels of full length APP and ADAM10. These findings indicate that Tspan3 could have a stabilising function for its partner proteins at the plasma membrane and possibly modulates their presence at the cell surface.

The trafficking and localisation of APP is an essential step, which determines its proteolytic processing route. As a secreted protein, APP is transported to the cell surface, where it

encounters ADAM10 and is subjected to non-amyloidogenic processing. Additionally, a certain part of full length APP is rapidly internalised from the plasma membrane. This process is mediated by a C-terminal YENPTY endocytic sorting motif, which initiates clathrin dependent endocytosis through binding to the clathrin adaptor protein AP-2 (Perez et al., 1999; Poulsen et al., 2015; Sisodia, 1995). After APP is sorted to early endosomes, one fraction of APP is recycled back to the plasma membrane and another part is subjected to  $\beta$  secretase cleavage and lysosomal degradation (Nordstedt et al., 1993; Sisodia, 1995; Yamazaki et al., 1996). Consistent with the localisation of  $\beta$ - and  $\gamma$ -secretase in endosomes and lysosomes, A $\beta$  was mainly found in these compartments (Haass et al., 1992; Koo and Squazzo, 1994).

Modulating APP localisation by inhibiting APP endocytosis, increased APP surface levels and enhances non-amyloidogenic processing, whereas amyloidogenic A $\beta$  generation is decreased (Carey et al., 2005; Koo and Squazzo, 1994; Perez et al., 1999). The other way around, promoting APP internalisation by upregulation of the endocytic pathway increased amyloidogenic processing and A $\beta$  generation (Grbovic et al., 2003; Haass et al., 1992). Therefore, it is conceivable that Tspan3 promotes ADAM10-dependent APP processing by stabilising APP at the cell surface, which decreases its internalisation and increases the probability of ADAM10 to cleave APP (Fig. 5.2).

Moreover, it is likely that Tspan3 not only stabilises APP, but ADAM10 and APP together in a functional complex (Fig. 5.2). From a mechanistic point of view, it could be speculated that Tspan3 stabilises ADAM10 and APP at the cell surface by a similar mechanism that has been suggested for Tspan15. It was hypothesised that Tspan15 accelerates ADAM10 maturation and trafficking to the cell surface by masking the cytosolic ADAM10 ER retention motif (Prox et al., 2012a). In a similar way, Tspan3 could cover the AP-2 binding site in the C-terminal domain of ADAM10 and APP, which could consequently impair or decelerate their internalisation.

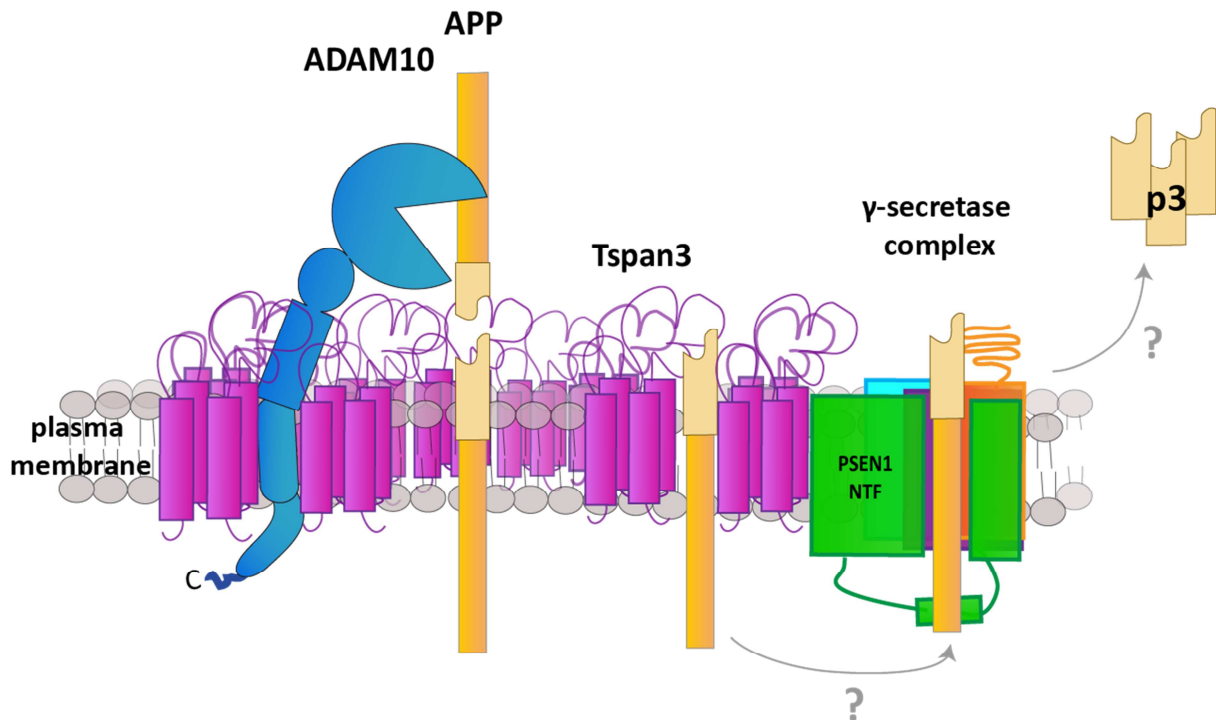


**Fig. 5.2: Tspan3 acts as a scaffold for non-amyloidogenic APP processing.**

Tspan3 interacts with ADAM10, APP and the N-terminal fragment (NTF) of presenilin-1 (PSEN1), which is the catalytic active subunit of the  $\gamma$ -secretase complex. By stabilising them together at the plasma membrane, Tspan3 promotes non-amyloidogenic processing of APP and provides a scaffold for the formation of a multisecretase complex consisting of ADAM10 and the  $\gamma$ -secretase complex. Not clear is whether this promotes  $\gamma$ -secretase-mediated cleavage of the APP-C83 and increases generation of the p3 fragment (labelled with question marks).

The finding that Tspan3 overexpression predominantly increased the surface levels the APP-CTF implicates that Tspan3 not only stabilises full length APP, but also the cleavage product APP-C83. Therefore, Tspan3 could also be involved in the further degradation of APP-C83 by the  $\gamma$ -secretase complex. This idea is supported by the finding that the N-terminal part of presenilin-1, which is the catalytic active subunit of the  $\gamma$ -secretase complex, was also found in Tspan3 immunoprecipitates. This indicates that Tspan3 could also function as a link for the  $\gamma$ -secretase complex and its substrate APP-C83 (Fig. 5.2). It is of interest that ADAM10 and the  $\gamma$ -secretase complex interact with each other to form a multisecretase complex at the plasma membrane (Chen et al., 2015). Tspan12 and Tspan17 are involved in the association of the multisecretase complex and promote ADAM10 activity (Chen et al., 2015). Similarly, Tspan3 acts as a scaffold for its partner proteins. By stabilising ADAM10, APP and the  $\gamma$ -secretase complex together in a functional complex, Tspan3 could promote non-amyloidogenic APP processing (Fig. 5.2). Moreover, it is conceivable that Tspan3 could be a part of the suggested ADAM10- $\gamma$ -secretase multisecretase complex and acts in concert with Tspan12 and Tspan17.

To analyse whether Tspan3 contributes to the formation of such a multisequester complex further co-immunoprecipitation experiments could be performed. Furthermore, analysis of the p3 fragment, which is generated by  $\gamma$ -secretase cleavage of the APP-C83, could give further information about the influence of Tspan3 on  $\gamma$ -secretase activity (Fig. 5.2).

#### 5.1.4 The potential function of tetraspanin-3 in endocytic processes

Endocytosis represents a mechanism to regulate the spatiotemporal presence of surface proteins. By invagination of the plasma membrane and subsequent formation of endocytic vesicles, membrane components are internalised and targeted for degradation to the lysosome or are recycled back to the plasma membrane (reviewed in Huotari and Helenius, 2011).

Besides its localisation at the plasma membrane, Tspan3 was mainly found in endosomal and lysosomal compartments. Consistent with this finding, a tyrosine-based endocytic sorting motif, Y-E-L-L, was identified in the C-terminus and cytoplasmic domain of Tspan3.

Tyrosine-based endocytic sorting motifs of the type Y-X-X- $\phi$ , where X can be any amino acid and  $\phi$  is a bulky hydrophobic amino acid, are linked to binding by adaptor protein-2 (AP-2) followed by clathrin-dependent endocytosis (Bonifacino and Angelica, 1999). Apart from Tspan3 similar sorting motifs were discovered in 12 other tetraspanins, including CD63 Tspan6 and Tspan7, which also belong to the TspanC6 subgroup (Berditchevski and Odintsova, 2007).

Mutation of the Tspan3 endocytic motif increased its surface expression and decreased its co-localisation with the early endosomal marker protein EEA1, indicating that the endocytic motif is indeed relevant for the internalisation of Tspan3 from the plasma membrane. However, a large part of the mutant Tspan3 was still found intracellularly. This can be explained by the finding that tetraspanins also use alternative transport and internalisation routes (Berditchevski and Odintsova, 2007). For example, CD63 typically traffics to the lysosome via the plasma membrane. Additionally, it was also found to be directly transported from the *trans*-Golgi network to the lysosome by interacting with AP-3 complex proteins (Rous et al., 2002). Alternatively, Latishevy et al. reported an AP-independent mechanism, where CD63 internalisation is triggered by interaction with syntenin-1 (Latysheva et al., 2006). Syntenin-1 is a PDZ domain-containing adaptor protein and is associated with the small GTPase ADP ribosylation factor 6 (Arf6), Rab5 and Rab11, which are involved in endocytosis and recycling (Fialka et al., 1999; Lambaerts et al., 2012). Syntenin-1 favours interaction with the last amino

acids of the CD63 endocytic sorting motif (X- $\phi$  amino acids), which indicates that CD63 can either associate with AP-2 or syntenin-1. Therefore, it is suggested that mutation of the tyrosine (Y) of the Y-X-X- $\phi$  motif favours syntenin-1-dependent internalisation of CD63 (Berditchevski and Odintsova, 2007). Interestingly, increased expression of syntenin-1 did not alter the steady-state distribution of CD63, but decreased the rate of endocytosis of CD63 (Latysheva et al., 2006). Similarly, mutation of the Tspan3 endocytic motif could facilitate binding of PDZ domain containing proteins, such as syntenin-1, instead of AP-2 and in turn slows down Tspan3 internalisation. Consequently, this could increase Tspan3 surface levels without completely blocking its endocytosis.

Although expression of the Tspan3 mutant only mildly increased Tspan3 surface expression, it clearly enhanced the surface presence of its partner proteins ADAM10 and APP. This implicated a role of Tspan3 endocytosis for the function of Tspan3 in APP non-amyloidogenic processing. It is noteworthy that the Tspan3-APP co-localisation was also observed in vesicular structures. According to the subcellular distribution of Tspan3, these vesicles are most likely endosomes or lysosomes. Therefore, it is possible that Tspan3 could facilitate endocytosis of its partner proteins, in particular APP. Moreover, Tspan3 could stabilise APP throughout the endocytic pathway, which in turn could also promote its recycling to the plasma membrane. This could also prevent  $\beta$ -secretase-mediated APP processing in endocytic compartments.

The  $\beta$ -secretase BACE1 associates with lipid raft components and its activity can be stimulated by treatment with specific lipid raft resident lipids (Hattori et al., 2006; Kalvodova et al., 2005). In contrast, targeting ADAM10 into lipid rafts by adding a C-terminal GPI-anchor inhibits its activity (Harris et al., 2009). In correlation with these observations,  $\beta$ -secretase processing of APP is considered to take place in lipid rafts, whereas  $\alpha$ -secretase processing of APP is suggested to be mainly localised in non-raft regions (Cordy et al., 2003; Harris et al., 2009; Kojro et al., 2001). Since lipid rafts and TEMs are regarded as two distinct microdomains, Tspan3 might constrain APP in TEMs during endocytosis (Hemler, 2005). This could prevent APP localisation to lipid rafts and consequently decrease  $\beta$ -secretase cleavage. It can also be speculated that by preventing  $\beta$ -secretase cleavage in the endocytic pathway, Tspan3 supports recycling of internalised full length APP back to plasma membrane, which in turn can be subjected to  $\alpha$ -secretase processing.

The membrane remaining APP-C83 still contains the endocytic sorting motif and also undergoes endocytosis. This is supported by the finding that  $\gamma$ -secretase processing of the



APP-C83 not only occurs at the plasma membrane, but also in lysosomal compartments (Chen et al., 2000; Haass et al., 1992). In this context, it is important to note that for the co-localisation studies of APP and Tspan3 performed in this work, a C-terminal APP antibody was used, which detects full length APP and the APP-CTF. Therefore, Tspan3 could also be involved in the endocytic trafficking of the APP-C83 fragment. Similar, to the full length APP, Tspan3 could thereby modulate degradation of the APP-C83. By stabilising the APP-C83 not only at the plasma membrane, but possibly also during endocytosis, Tspan3 could delay transport of the APP-C83 to the lysosome and decrease its degradation. Although there are no evidences yet, the APP-C83 could also be re-transported to the plasma membrane for  $\gamma$ -secretase processing, which could also involve Tspan3.

The close relationship and the comparable subcellular localisation of CD63 and Tspan3 could indicate another role of Tspan3 for APP during endosomal/lysosomal transport. As described in the introduction (see section 1.4.1), CD63 is involved in the formation of ESCRT-independent intraluminal vesicles (ILVs) and modulates sorting of the premelanosome protein (PMEL) into ESCRT-dependent and independent vesicles during melanosome maturation (van Niel et al., 2011). Also APP and its cleavage products are localised in multivesicular bodies (Morel et al., 2013; Takahashi et al., 2002). It was shown that sorting of APP to ILVs by an ESCRT-dependent mechanism is required for its lysosomal degradation (Edgar et al., 2015). Since, a small proportion of APP was still found in ILVs after depletion of the ESCRT0 component Hrs (hepatocyte growth factor-regulated tyrosine kinase substrate), APP could also participate in an ESCRT-independent sorting mechanism. In this regard, it is conceivable that similar to CD63, Tspan3 promotes ESCRT-independent formation of ILVs and modulates sorting of APP. It can be speculated that Tspan3 could thereby specifically target cleavage products, such as the APP-C83, to lysosomal degradation or might be involved in the formation of exosomes, where APP cleavage products have already been observed (Rajendran et al., 2006).

Whether Tspan3 impairs APP endocytosis, lysosomal degradation and is possibly involved in an ESCRT-independent sorting mechanism has to be further elucidated. In this regards determination of the half-life of full length APP and the APP-C83 using pulse-chase experiments and analysis of  $\gamma$ -secretase cleavage product p3 could provide more insight into the role of Tspan3 in APP trafficking and  $\gamma$ -secretase processing. Furthermore, ultrastructural

analysis of ILV formation and localisation of Tspan3, full length APP and the APP-C83 in such structures could provide insight into a potential role of Tspan3 in ESCRT-independent sorting. In lack of a specific ADAM10 antibody for immunofluorescence studies, it was not possible to test if Tspan3 and ADAM10 also endogenously co-localise. However, the finding that mutation of the Tspan3 endocytic motif enhanced ADAM10 surface levels, while expression of wild-type Tspan3 did not, implicates a role of Tspan3 for ADAM10 internalisation.

### **5.1.5 The influence of tetraspanin-3 on the production of ADAM10-CTFs**

In addition to the APP-CTF, overexpression of Tspan3 also increased the presence of two ADAM10-specific C-terminal fragments (CTFs). These CTFs are generated upon shedding of ADAM10 by ADAM9 and ADAM15, but could also be generated through autocatalytic processing by ADAM10 (Fig. 5.3) (Suh et al., 2013; Tousseyn et al., 2009). Which of these proteases is responsible for the generation the ADAM10-CTF1 or CTF2, is not yet clear. It is suggested that this cleavage event could also involve another so far unknown protease (Tousseyn et al., 2009). The ADAM10-CTFs are further processed by the  $\gamma$ -secretase complex, which results in the release of the ADAM10 intracellular domain (ICD). The ADAM10-ICD contains a nuclear localisation sequence in its C-terminus and was found to localise to nuclear speckles (Tousseyn et al., 2009). Therefore, it is assumed that the ADAM10-ICD contributes to gene regulation, but possible targets were not yet identified. On the other hand, the released ectodomain of ADAM10 is proposed to act as a protease in *trans*. This hypothesis is supported by the finding that a truncated ADAM10 construct, mimicking the released soluble ADAM10 ectodomain, was still catalytic active against a synthetic peptide substrate (Parkin and Harris, 2009). On the contrary, the same ADAM10 construct was unable to shed membrane bound APP in cells (Parkin and Harris, 2009). This indicates that release of the ADAM10 ectodomain on the one hand represents a mechanism to rapidly down-regulate ADAM10 activity at the plasma membrane, but may also enable shedding events in *trans*. Since the mechanisms that regulate shedding of ADAM10 are barely understood, the role of Tspan3 for the proteolytic processing of ADAM10 is elusive.

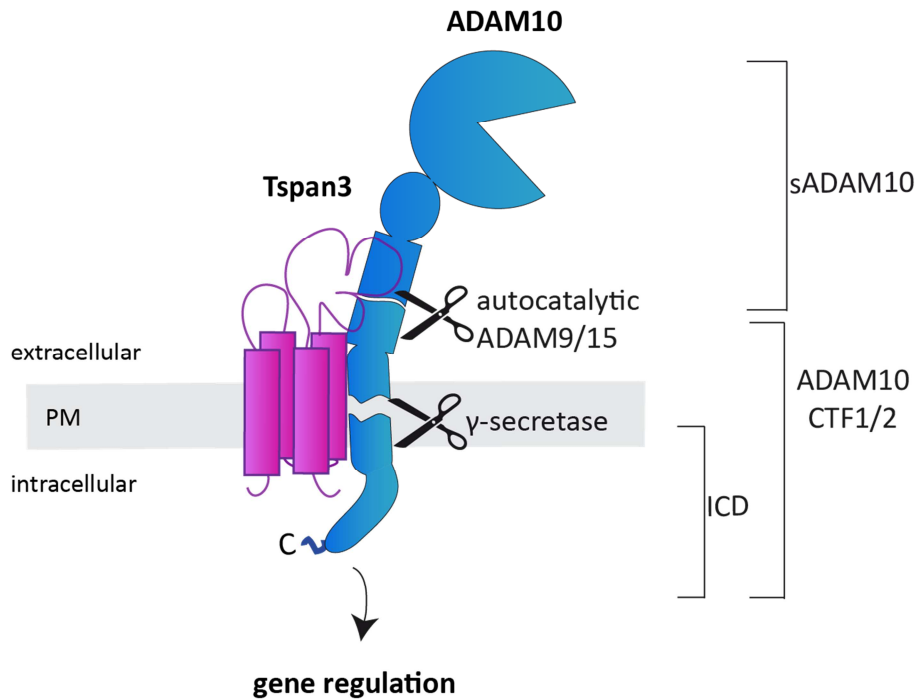


**Fig. 5.3: Generation of ADAM10 C-terminal fragments.**

Shedding of ADAM10 by ADAM9, ADAM15 or autocatalytic cleavage by itself generates ADAM10 C-terminal fragments (CTF) 1 and 2. The CTFs are further processed by the  $\gamma$ -secretase complex. The ADAM10 intracellular domain (ICD) is released and translocate to the nucleus, where it is possibly involved in gene regulation. The soluble ectodomain of ADAM10 (sADAM0) is released. Overexpression of Tspan3 increases the appearance of ADAM10-CTFs.

How could Tspan3 promote shedding of ADAM10? Surprisingly, while overexpression of wild-type Tspan3 did not alter ADAM10 surface levels, expression of the Tspan3 endocytic motif mutant led to an increased surface expression of ADAM10. This finding indicates that Tspan3 plays a role for ADAM10 stabilisation and internalisation. In this context, it was demonstrated that decreased endocytosis of ADAM10 by expression of a dominant-negative dynamin mutant, increased ADAM10 surface levels and ADAM10-CTF production (Carey et al., 2005). Contrary to blocking ADAM10 internalisation, expression of Tspan3 most likely delays ADAM10 internalisation (discussed in section 5.1.3). Similar to its role in APP proteolytic processing, Tspan3 could promote ADAM10-CTF production by stabilising it at the cell surface in a functional complex together with further partner proteins. It is conceivable that Tspan3 could directly contribute to an interaction of ADAM10 with ADAM9 or ADAM15, but this could also involve other yet unidentified proteins. Moreover, the interaction of Tspan3 with a distinct region of ADAM10, may constrain ADAM10 in a distinct conformation, in which it favours autocatalytic cleavage. A similar mechanism was already used to explain the substrate specific functions of different TspanC8 tetraspanins (Noy et al., 2016). Noy et al. demonstrated that members of the TspanC8 tetraspanins interact with different ADAM10

domains and suggest that depending on the TspanC8 tetraspanin, ADAM10 is constrained in a specific conformation, which facilitates substrate cleavage (Noy et al., 2016).

Since the increased appearance of ADAM10-CTFs indicates an enhanced shedding of ADAM10, a reduction of ADAM10 activity at the plasma membrane would have been expected. However, Tspan3 expression promotes ADAM10-mediated APP processing. Therefore, the most likely explanation for the increased appearance of ADAM10-CTFs could be that Tspan3 stabilises ADAM10-CTFs at the plasma membrane. Moreover, the observation that Tspan3 also interacts with the N-terminal part of presenilin-1, implicates that in any of these scenarios Tspan3 could also modulate  $\gamma$ -secretase processing of the ADAM10-CTFs.

Whether Tspan3 affects  $\gamma$ -secretase processing of the ADAM10-CTFs and if this has further functional consequences with regards to the putative gene regulatory function of the ADAM10-ICD has to be further elucidated.

## **5.2 Tetraspanin-3 deficiency is likely compensated by other tetraspanins**

To address the function of Tspan3 *in vivo*, Tspan3 knockout mice were generated using a TALEN-mediated genome editing approach. Immunoblot analysis of different tissues confirmed that the incorporation of a 26 bp insertion mutation into the Tspan3 gene locus was efficient to disrupt Tspan3 protein expression. However, Tspan3-deficient mice did not display an overt phenotype. Surprisingly, analysis of APP proteolytic processing revealed no changes in the levels of full length APP or the APP-CTF. Also, ADAM10 maturation, ADAM10-CTF generation and shedding of the cellular prion protein were unaffected by the loss of Tspan3. This indicates that, despite clear evidences obtained in cell-based systems, Tspan3 is not essential for ADAM10-mediated shedding processes *in vivo*.

Interestingly, the lack of an overt phenotype was described for several tetraspanin knockout mouse models and is most likely due to redundant functions exerted by other tetraspanins. The functional redundancy of tetraspanins was first observed when monoclonal antibodies specific for CD9, CD53, CD81 and CD82, respectively, triggered the same costimulatory effect for T-cell activation (Lagaudrière-Gesbert et al., 1997). Further analysis of tetraspanin functions confirmed these observations for example for Tspan33 and Tspan5, which synergistically regulate Notch activation in cancer cells (Dunn et al., 2010). Therefore, it is

likely that loss of a tetraspanin can be easily compensated by upregulation of other tetraspanins.

Analysis of the transcription level of TspanC6 tetraspanins, Tspan12 and Tspan5 in Tspan3-deficient mice revealed a prominent upregulation of Tspan7 (four-fold) and Tspan5 (30-fold) transcripts. This identified Tspan5 and Tspan7 as likely candidates which compensate for the loss of Tspan3. Tspan7 belongs to the same subgroup as Tspan3, which indicates a functional similarity. In contrast, Tspan5 belongs to the TspanC8 tetraspanins, which have clearly different effects on ADAM10 compared to Tspan3 (discussed in section 5.1.1). The alignment of the murine Tspan3, Tspan5 and Tspan7 amino acid sequences (Fig. 5.4) reveals only a low sequence similarity of Tspan3 and Tspan5 (23%) or Tspan7 (33 %), respectively. Also, in the large extracellular region, which is responsible for the interaction with partner proteins and could indicate similar functions, no striking sequence overlap can be observed (Fig. 5.4, highlighted in yellow). Therefore, it is surprising that these two rather divergent tetraspanins may compensate for the loss of Tspan3. Despite a low homology at the amino acid level, evolutionary coupling analysis based on the crystal structure of CD81, suggested a high conservation of the overall structure of tetraspanins (Zimmerman et al., 2016). In particular, the sequence pattern of the transmembrane region, which forms an intramembrane cavity in the CD81 structure, is tightly conserved among tetraspanins. According to the finding that tetraspanins prefer binding of different partner proteins, the LEL is a more variable region (Zimmerman et al., 2016). Interestingly, for the channel catfish Tspan7 and Tspan3, a structural similarity of the LEL was already predicted (Yeh and Klesius, 2012). Since the amino acid sequence of Tspan3 and Tspan7 is highly conserved among different species (Yeh and Klesius, 2012), it is likely that the structure of the murine Tspan3 and Tspan7 LEL are also similar. Therefore, Tspan3 and Tspan7 might associate with similar partner proteins.

Overexpression of Tspan7 in N2a cells led to a comparable increase of the APP-CTF as observed for Tspan3 overexpression. This indicates a similar function of both tetraspanins for the proteolytic processing of APP. Like Tspan3, Tspan7 is broadly distributed in murine tissues and is mainly expressed in the brain (Hosokawa et al., 1999). Interestingly, Tspan7 contains an endocytic sorting motif within its C-terminus, which is similar to the Y-E-L-L motif in the sequence of Tspan3 (Fig. 5.4, highlighted in green). It is conceivable that Tspan7 has a comparable subcellular localisation as observed for Tspan3 and is also involved in endocytic processes. Although, the potential role of Tspan7 in ADAM10-mediated shedding processes is

unknown, it is upregulated (1.5-fold) in ADAM10-deficient neurons (Kuhn et al., 2016). Therefore, Tspan7 may be regarded as a likely candidate to compensate for the function of Tspan3 as a regulator of ADAM10-mediated APP processing in Tspan3-deficient mice.

```

Tspan5      MSGKHYKGPEVSCCIKYFIFGFNVIWFVLGITFLGIGLWAWNEKGVLSNISSITDLGGFD
Tspan3      -----MGQCGITSSKTVLVFLNLI FWGAAGILCYVGAYVFITYDDY--DHFFEDVYTLF
Tspan7      MASRRMETKPVITCLKTLIIYSFVFWITGVILLAVGVWGKLTGLTY--ISLIAENSTNA
              . * . . . . : : * : . : :
              . * . . . . : : * : . : :

Tspan5      PVWLFLVVGVMFILGFAGCIGALRENTFLLKFFSVFLGIIFLELTAGVLA FVFKDWIK
Tspan3      PAVVI IAVGALLFI IGLIGCCATIRESRCGLATFVFILLVVFTEVVVVVLGYVYRAKVE
Tspan7      P-YVLIGTGT TIVVFLFGCFATCRGSPWMLKLYAMFLSLVFLAELVAGISGFVFRHEIK
              * : : . * : : : * : : * . * : : * : : * : : : : :

Tspan5      DQLYFFINNNIRAYRDD--IDLQNLIDFTQEYWQCCGAFGADDWNLNIYFNCTDSNASRE
Tspan3      NEVDRSIQKVYKTYNGTNSDAASRAIDYVQRQLHCCGIHNYSDWENTDWFKETK-----
Tspan7      DTFLRITYTDAMQTYNGN--DERSRAVDHVQRSLSCCGVQNYTNWSTSPYFLEH-----
              : . . : : * . . . . : : * . . * . * . * . : * . . : *

Tspan5      RCGVPFSCCTKDP AEDVINTQCGYDARQKPEVDQQI VIYTKGCV PQFEKWLQDNL TIVAG
Tspan3      NQSVPLSCCRETAKSCNGS-----L-A-----NPSDLAEGCEALVVKKLQEI LMHV I W
Tspan7      --GIPPSCCMNETDCNPQD-----L-HNLTVAATKVNQKGCYDLVTSFMETNMGI IAG
              : * * * : . : : * * . . : : : :

Tspan5      IFIGIAL LQIFGICLAQNLVSDIEAVRA-----SW-
Tspan3      AALFAFAAIQLLGM L CACIVLCRRSRDPAYELLITGGTYA
Tspan7      VAFGIAFSQLIGMLLACCLS-RFITANQYEMV-----
              : : * * : : * :

```

**Fig. 5.4: Sequence alignment of the murine amino acid sequences of Tspan3, Tspan5 and Tspan7.**

Sequence alignment of Tspan3, Tspan5 and Tspan7 was performed with ClustalOmega. Sequence similarity between Tspan3 and Tspan5 is 23% and 33% between Tspan3 and Tspan7. Sequence of the large extracellular region is highlighted in yellow. Endocytic sorting motifs are highlighted in green. Conserved (\*), conservative (:) and semi-conservative (.) residues are labelled.

In contrast to Tspan7, Tspan5 has been described as a regulator of ADAM10 maturation and surface trafficking. Tspan5 overexpression has no impact on APP processing in the human osteosarcoma cell line U2OS-N1, but positively regulates Notch activity and CD44 shedding in U2OS-N1 cells and in human prostate cancer cells PC3, respectively (Dornier et al., 2012; Jouannet et al., 2015; Zhou et al., 2014).

Since, Tspan3 acts as a stabiliser for ADAM10 at the cell surface, it can be speculated that in the absence of Tspan3 ADAM10 internalisation may be enhanced. In such a scenario, upregulation of Tspan5 could compensate for the reduced ADAM10 surface levels by promoting ADAM10 maturation and surface trafficking. By promoting APP processing on the one hand and assisting ADAM10 surface trafficking and maturation on the other hand, Tspan7 and Tspan5 could act in concert to compensate for the loss of Tspan3 in mice. With regards to Tspan15, whose influence on APP proteolytic processing is dependent on the cellular system,

it is conceivable that Tspan5 promotes APP proteolytic processing in other cellular systems (Jouannet et al., 2015; Prox et al., 2012). Moreover, Tspan5 could also compensate a yet unknown function of Tspan3, which is probably related to CD44 and Notch receptor shedding. Similar to Tspan3-deficient mice, siRNA-mediated knockdown of Tspan3 in SH-SY5Y cells did not alter ADAM10 levels and APP-CTF generation. Surprisingly, in these cells transcription of TspanC6 tetraspanins, Tspan12 and Tspan5 were unchanged. It should be noted that in these cells no Tspan7 transcripts could be detected. Therefore, it is likely that in these cells other tetraspanins compensate for the lack of Tspan3.

### 5.3 Tetraspanin-3 in Alzheimer's Disease

Analysis of the Tspan3 tissue distribution in mice revealed a high expression level in the brain. Using immunohistochemical staining methods, Tspan3 could be detected in neurons of the cortex, the hippocampus, the cerebellum and the brainstem. The cortex and the hippocampus are regions, which are associated with memory, learning and general cognitive functions (Frith and Dolan, 1996; Wallenstein et al., 1998). In correlation with memory loss and impaired cognitive functions observed in AD patients, the cortex and the hippocampus are the brain regions that are mainly affected by the AD pathology. In early stages of AD, amyloid plaques and neurofibrillary tangles are first observed in the cortex and the hippocampus (Braak and Braak, 1991; Thal et al., 2002). The loss of neurons is most pronounced in these the two brain regions and occurs already at early disease stages (Sabuncu, 2011). In later stages of AD pathology, also other regions, such as the thalamus, the cerebellum and the brainstem become affected by amyloid plaques and neurofibrillary tangle formation (Braak and Braak, 1991; Thal et al., 2002).

The finding that Tspan3 promoted non-amyloidogenic APP processing in cell-based experiments raised the question whether Tspan3 expression is somehow associated with the molecular pathology described in AD. Surprisingly, in post-mortem brain samples of AD patients, Tspan3 expression was significantly increased in comparison to control samples. This could indicate a correlation between AD pathology and Tspan3 protein expression. However, this result should be validated, since only a small number of samples (seven controls versus eight AD samples) were analysed. Despite an overall increase of Tspan3 expression in AD samples, the Tspan3 expression varied between individual samples. This variability could be

related to the different disease stages of the AD patients (see section 3.7, Tab. 3.16). Additionally, also other individual differences, such as gender and age, could influence Tspan3 expression. Since Tspan3 is mainly localised in endosomes and lysosomes the increased appearance of Tspan3 could even be a side effect of the disturbed endocytic/lysosomal system observed in AD (Cataldo et al., 1995, 1997, 1996). Besides an increased number of lysosomes and an increased synthesis of acid hydrolases, pyramidal neurons of AD brains show enlarged endosomes. This is further accompanied by an enhanced presence of cathepsin B and D in early endosomes. Both cathepsins are involved in the lysosomal degradation of A $\beta$  peptides (Dreyer et al., 1994; Evin et al., 1995; Hamazaki, 1996; Mueller-Steiner et al., 2006). It is likely that the increased endocytic activity causes an enrichment of Tspan3 in endosomes, which is enhanced by the presence of enlarged endosomes and consequently results in increased Tspan3 expression. However, Tspan3 could also contribute to the early steps in the pathologic processes by stabilisation of APP through the early endocytic pathway. While loss of Tspan3 may not contribute to the development of AD due to compensatory mechanisms by other tetraspanins, Tspan3 mutations that impair its binding to APP and APP trafficking could be a factor modulating AD pathogenesis.

#### **5.4 Characterisation of the physiological function of tetraspanin-15**

Tspan15 is a potent regulator of ADAM10 maturation, trafficking to the cell surface and substrate cleavage. Since Tspan15 promotes the ER exit of ADAM10, it was assumed that Tspan15 accelerates ADAM10 maturation and surface trafficking by masking an ER retention motif within the C-terminal domain of ADAM10. Tspan15 overexpression promoted N-cadherin cleavage in several cell lines (Noy et al., 2016; Prox et al., 2012). In addition, Tspan15 was identified as a negative regulator of Notch activity and depending on the cell type Tspan15 expression reduced or promoted APP proteolytic processing (see section 1.4.2, Tab. 1.2) (Haining et al., 2012; Jouannet et al., 2015; Prox et al., 2012)

Although, TspanC8 tetraspanins have a similar effect on ADAM10 maturation and trafficking, the ability of Tspan15 to promote N-cadherin cleavage is a unique feature among the TspanC8 tetraspanins. It is supposed that by interacting with different regions of ADAM10, TspanC8 tetraspanins constrain ADAM10 in distinct conformations, where it prefers cleavage of specific substrates (Noy et al., 2016). Since Tspan15 is the only TspanC8 tetraspanin that



interacts with the membrane proximal stalk region of ADAM10 (Noy et al., 2016), it is likely that Tspan15 stabilises ADAM10 in a conformation, which is favourable for N-cadherin shedding. Further analysis aiming to understand the substrate specific functions of TspanC8 tetraspanins revealed that Tspan15 influences the membrane environment of ADAM10 (Jouannet et al., 2015). This became evident by quantitative mass spectrometric analysis of the composition of ADAM10-associated membrane proteins after Tspan5 and Tspan15 expression, respectively (Jouannet et al., 2015). While expression of Tspan5 in U2OS-N1 cells promoted the association of ADAM10 with classical components of the tetraspanin web, like integrins and CD9, Tspan15 expression reduced these interactions (Jouannet et al., 2015). Additionally, Tspan15 expression directed ADAM10 to different plasma membrane localisations, compared to Tspan5 and increased the motility of ADAM10 molecules (Jouannet et al., 2015). These findings further indicate that Tspan15 modulates ADAM10 cleavage events by directing it to specific membrane compartments.

Despite an increasing understanding of the functions of Tspan15 and other TspanC8 tetraspanins for ADAM10 activity and substrate cleavage, their physiological relevance is not well-characterised. To date Tspan33-deficient mice were the only available TspanC8 knockout mouse model. These mice displayed splenomegaly and developed anaemia during aging, which indicated an impaired erythropoiesis (Heikens et al., 2007). Analysis of Tspan33-deficient erythrocytes, revealed decreased surface levels of ADAM10 (Haining et al., 2012). However, whether the reduced ADAM10 levels are the cause for the phenotype of Tspan33-deficient mice has not been addressed yet.

#### **5.4.1 Loss of tetraspanin-15 affects ADAM10 substrates in the brain**

To analyse the importance of Tspan15 for the function of ADAM10 *in vivo*, Tspan15 knockout mice were generated by TALEN-mediated genome editing. Sequence and immunoblot analysis confirmed the successful introduction of a frameshift mutation within the Tspan15 exon2, which abolished Tspan15 protein expression in all tested tissues. Tspan15-deficient mice did not display an overt phenotype and the appearance of genotypes after heterozygous breeding was according to the expected Mendelian distribution. Nevertheless, 16 % of the born animals died within the first three weeks. Albeit, it is not clear if these mice were only Tspan15-deficient mice, this may indicate a slightly increased rate of postnatal lethality. Interestingly, a similar phenomenon was described for the postnatal disruption of ADAM10 in neurons and is

most likely due to an impaired Notch signalling (Prox et al., 2013). Thus, the increased postnatal lethality of Tspan15-deficient mice could also indicate a disturbed Notch signalling. In contrast to the knockout of ADAM10, which reduced Notch signalling, it is likely that Tspan15-deficiency increases Notch signalling rather than reducing it. This hypothesis is based on the finding that in cell-based experiments overexpression of Tspan15 decreased ligand-induced Notch signalling, whereas Tspan15 downregulation increased Notch activity (Haining et al., 2012).

Given the fact that TspanC8 tetraspanins (except for Tspan10 and Tspan17) have redundant functions in regards to ADAM10 maturation and trafficking (Dornier et al., 2012; Haining et al., 2012; Jouannet et al., 2015), it is surprising that the analysis of Tspan15-deficient brains revealed a decreased level of mature ADAM10. This finding highlights the important role of Tspan15 for ADAM10 maturation *in vivo* and further implicates that loss of Tspan15 is not or only partially compensated by another tetraspanin. However, the observation that loss of Tspan15 did not completely abolish ADAM10 maturation demonstrates that not only Tspan15 but also other mechanisms control ADAM10 maturation. In addition to the decreased level of mature ADAM10, also N-cadherin and PrP<sup>c</sup> shedding were decreased in Tspan15-deficient mice. This confirms that also *in vivo* Tspan15 is an important regulator for ADAM10-mediated substrate shedding.

ADAM10-mediated N-cadherin shedding is essential for cell adhesion and has important functions in the activation of  $\beta$ -catenin signalling (Reiss et al., 2005). As a neuronal adhesion molecule N-cadherin is associated with synaptic adhesion, spine morphology and plasticity (Mendez et al., 2010; Togashi et al., 2002; Xie et al., 2008). The conditional knockout (cKO) of ADAM10 reduced N-cadherin shedding and caused severe developmental defects in the cortex, learning deficits, impaired network formation and led to changes in dendritic spine morphology (Jorissen et al., 2010; Prox et al., 2013). Although, loss of Tspan15 had no apparent effect on the size of dendritic spines, the increased appearance of perforated spines indicates an influence of Tspan15-deficiency on dendritic spine morphology. It is possible that the increased appearance of perforated spines is related to the reduced N-cadherin shedding observed in Tspan15-deficient mice. However, given the large number of ADAM10 substrates in the CNS (see section 1.1.4, Tab. 1.1), this could also be related to an impaired shedding of other synaptic adhesion molecules. The detailed outcome of this analysis will be described and discussed in the next section (see section 5.4.2).

In addition to its function in cell adhesion, N-cadherin is directly linked to intracellular  $\beta$ -catenin and functions in  $\beta$ -catenin signalling. ADAM10-mediated N-cadherin shedding is a prerequisite for  $\gamma$ -secretase cleavage, which enables redistribution of  $\beta$ -catenin into the nucleus. In the nucleus  $\beta$ -catenin is involved in the activation of downstream target genes, such as cyclin D1, c-myc and c-jun, which are involved in cell proliferation and survival (Brown et al., 1998; He et al., 1998; Mann et al., 1999; Shtutman et al., 1999). In addition to Notch signalling, impaired  $\beta$ -catenin signalling likely contributes to the severe developmental defects and the overall phenotype of ADAM10 cKO mice (Jorissen et al., 2010; Prox et al., 2013). It is conceivable that the reduced N-cadherin shedding in Tspan15 knockout mice also impairs  $\beta$ -catenin signalling. These changes might be of a subtle nature, since Tspan15-deficiency reduces N-cadherin shedding, but does not completely abolish it. In this context it is also interesting to note that Tspan5, another member of the TspanC8 tetraspanins, was found as a downstream target of  $\beta$ -catenin signalling in a microarray screen of colorectal cancer cells (van de Wetering et al., 2002). Therefore, the reduced N-cadherin shedding in Tspan15 knockout mice could also modulate the transcription of other TspanC8 members. In turn this could lead to changes of the tetraspanin composition in certain tissues and impair the formation of TEMs.

Whether loss of Tspan15 has an effect on  $\beta$ -catenin signalling has to be further elucidated. Since the effect of Tspan15 on N-cadherin is so far unique among TspanC8 tetraspanins, it could also be interesting to analyse whether Tspan15, similar to Tspan3 promotes association of ADAM10 with its substrates N-cadherin. This could be addressed by additional co-immunoprecipitation experiments.

Surprisingly, in addition to N-cadherin, loss of Tspan15 also reduced shedding of the cellular prion protein (PrP<sup>C</sup>). This identifies PrP<sup>C</sup> as another ADAM10 substrate that is regulated by Tspan15 expression. Interestingly, Tspan15 is not the first tetraspanin, which is associated with PrP<sup>C</sup>-biology. In erythroblast, PrP<sup>C</sup> co-localises with CD81 at the plasma membrane and intracellularly with CD63 (Griffiths et al., 2007). This finding is surprising since, as a GPI-anchored protein PrP<sup>C</sup> is assumed to be mainly localised in lipid rafts, whereas tetraspanins are present in tetraspanin-enriched microdomains (TEMs), which are a clearly different type of microdomain (Hemler, 2005; Taylor and Hooper, 2017). However, the association of PrP<sup>C</sup> with tetraspanins could provide a likely explanation for the apparent discrepancy that ADAM10 is the main responsible protease in PrP<sup>C</sup> shedding, but is inactive in lipid rafts

(Altmepfen et al., 2011; Harris et al., 2009). By associating with tetraspanins, PrP<sup>c</sup> could be directed into TEMs, where ADAM10 is present and active (Dornier et al., 2012; Haining et al., 2012). Besides targeting PrP<sup>c</sup> to TEMs, tetraspanins could also promote the formation of a functional ADAM10-PrP<sup>c</sup> complex, which facilitates PrP<sup>c</sup> shedding. Moreover, the co-localisation of PrP<sup>c</sup> with CD63, which is involved in endocytic processes, indicates a further role of tetraspanins in the internalisation of PrP<sup>c</sup>. Despite co-localisation of CD81 and CD63 with PrP<sup>c</sup>, a direct interaction could not be demonstrated (Griffiths et al., 2007). The interaction of CD81 and CD63 with PrP<sup>c</sup> is therefore likely to be of an indirect nature. Similarly, CD81 is an indirect interaction partner of ADAM10 (Arduise et al., 2008a; Dornier et al., 2012). Therefore, it is conceivable that CD81 acts as a linker, which connects ADAM10 and PrP<sup>c</sup> with other tetraspanins. As a direct interaction partner of ADAM10, Tspan15 could be involved in mediating this indirect interaction. Moreover, since the interaction of Tspan15 with ADAM10 substrates is not yet analysed, it is also possible that Tspan15 mediates ADAM10-PrP<sup>c</sup> association by a direct interaction with PrP<sup>c</sup>.

The physiological function of PrP<sup>c</sup> is not well-understood yet. It is proposed to function in neurogenesis and differentiation of neuronal precursor cells, maintenance of myelin and in the immune system (Bremer et al., 2010; Isaacs et al., 2006; Steele et al., 2006). Its role in neurodegenerative diseases is well documented (reviewed in Aguzzi and Calella, 2009; Soto and Satani, 2011). By conversion into the misfolded pathologic form, scrapie PrP (PrP<sup>Sc</sup>), the prion protein is the main causative of prion diseases such as Creutzfeldt-Jakob disease and kuru in human (Collinge, 2001). This was confirmed by the analysis of PrP<sup>c</sup>-deficient mice, which are resistant to prion infection (Büeler et al., 1993). ADAM10 was identified as the main sheddase of PrP<sup>c</sup>, which releases a GPI-anchorless form of PrP<sup>c</sup> (Altmepfen et al., 2011). This was confirmed by the CamKII $\alpha$ -Cre-driven deletion of ADAM10 in neurons, which reduced PrP<sup>c</sup> shedding and resulted in an accumulation of the full length PrP<sup>c</sup> in the early secretory pathway (Altmepfen et al., 2011). Interestingly, after prion infection, the same mice showed an increased conversion of PrP<sup>c</sup> into PrP<sup>Sc</sup>, but simultaneously displayed a reduced pathology and prion spreading (Altmepfen et al., 2015). It is likely that the knockout of Tspan15 could have a similar effect in prion disease.

The observation that TspanC8 tetraspanins mediate substrate specificity by holding ADAM10 in a specific conformation, which favours cleavage of specific substrates, implicates that their function could also depend on a specific conformation of the ADAM10 substrate. In this

context, it is interesting to note, that the conversion of PrP<sup>C</sup> into PrP<sup>Sc</sup> is based on a conformational change. While the structure of PrP<sup>C</sup> has a high  $\alpha$ -helix content and only little  $\beta$ -sheets, PrP<sup>Sc</sup> contains mainly  $\beta$ -sheets and less  $\alpha$ -helices (Cohen et al., 1993). Therefore, it is conceivable that Tspan15 could also play a different role in prion disease possibly by favouring ADAM10-mediated shedding of either of PrP<sup>C</sup> or PrP<sup>Sc</sup>.

In contrast to N-cadherin and PrP<sup>C</sup>, APP proteolytic processing was not affected by the loss of Tspan15 in the brain. This is in line with previous cell-based findings, which revealed that Tspan15 has only a minor role in APP processing and that its ability to promote APP shedding is cell-type dependent (Jouannet et al., 2015; Prox et al., 2012). In addition to its expression in brain, Tspan15 was highly expressed in lung and intestine. Since APP is also ubiquitously expressed, Tspan15 could play a role for APP processing in these tissues (Tanzi et al., 1987). APP exists in three major isoforms, which are generated by alternative splicing (Sandbrink et al., 1996). The two longer isoforms APP<sub>751</sub> and APP<sub>770</sub> contain a Kunitz-type protease inhibitor (KPI) domain and the latter of them an additional Ox-2 antigen domain. The shorter APP<sub>695</sub> isoform lacks both domains (Sandbrink et al., 1996). While APP<sub>751</sub> and APP<sub>770</sub> are widely expressed, APP<sub>695</sub> is mainly present in the brain (Tanaka et al., 1989). It is conceivable that Tspan15 could preferentially promote ADAM10-mediated shedding of the longer APP isoforms APP<sub>751</sub> and APP<sub>770</sub>.

Taken together, loss of function studies identified Tspan15 as an important regulator of ADAM10 maturation and shedding activity *in vivo*. The lack of an overt phenotype implicates that Tspan15-deficiency causes only subtle alterations of the physiological function of ADAM10. Besides N-cadherin, PrP<sup>C</sup> was identified as a novel ADAM10 substrate that is influenced by Tspan15 expression. How Tspan15 regulates ADAM10 activity *in vivo* and whether further substrates are affected by the loss of Tspan15 will be interesting questions for future experiments. Moreover, it will be worthwhile to perform a more detailed analysis of the role of Tspan15 in PrP<sup>C</sup> shedding and its importance in pathological processes, such as prion and Alzheimer's Disease.

#### 5.4.2 The role of tetraspanin-15 in dendritic spine morphology

ADAM10 is localised at the postsynaptic membrane of excitatory synapses (Gardoni et al., 2012; Malinverno et al., 2010; Marcello et al., 2013). By cleaving neuronal adhesion molecules such as N-cadherin, ADAM10 regulates the formation of novel synaptic contacts and is

involved in synaptic plasticity and network formation (Malinverno et al., 2010; Marcello et al., 2007; Prox et al., 2013). ADAM10 is also directly associated with two major mechanisms of synaptic plasticity, long-term potentiation (LTP) and long-term depression (LTD). While LTP is a process that strengthens synaptic signal transmission, LTD reduces synaptic signal transmission. Interestingly, induction of LTD promotes trafficking of ADAM10 to the postsynaptic membrane and increases its activity (Marcello et al., 2013), whereas LTP induces endocytosis of ADAM10 (Marcello et al., 2013). These findings might reflect the fact that during LTD synaptic contacts are loosened, which requires an enhanced shedding of adhesion molecules, whereas during LTP reduced shedding of adhesion molecules strengthens synaptic contacts. Mice deficient for ADAM10 in neurons showed a reduced ability to respond to LTP, which correlated with a decreased shedding of the adhesion molecules N-cadherin and Nectin-1 (Prox et al., 2013). In particular, N-cadherin was identified to play a pivotal role in spine size and synaptic remodelling not only by promoting synaptic contacts, but also by regulating the number of AMPA receptors at synaptic membranes (Saglietti et al., 2007; Tai et al., 2008). AMPA receptors are activated by glutamate and are key elements in fast excitatory signal transmission and increased AMPA receptor activity is also associated with LTP (reviewed in Brecht and Nicoll, 2003; Shepherd and Huganir, 2007). Interestingly, it was demonstrated that inhibition of ADAM10 increases AMPA receptor number and functions by decreasing N-cadherin shedding (Malinverno et al., 2010). Additionally, reduced N-cadherin shedding also led to an increase of dendritic spine size (Malinverno et al., 2010). Similarly, ADAM10-deficient hippocampal neurons showed an increased spine size and a stubby-like structure (Prox et al., 2013). Therefore, it appears that the impaired spine size and morphology in ADAM10 cKO mice is related to an impaired N-cadherin shedding. However, also other neuronal adhesion molecules, such as NCAM and Nectin-1, are decreased in ADAM10-deficient neurons (Kuhn et al., 2016; Prox et al., 2013) and are likely to contribute the synaptic phenotype of these mice.

Although, Tspan15 knockout mice showed a clear reduction in mature ADAM10 and N-cadherin cleavage, the dendritic spine size of hippocampal CA1 neurons was unaffected. It was noteworthy that in Tspan15 knockout mice the number of perforated spines was almost doubled compared to wild-type animals. Perforated spines are characterized by a widened spine head and two segmented post-synaptic densities (PSDs) (Fig. 5.5). They represent a specific form of dendritic spines, which occurs as an intermediate stage during LTP-induced

remodelling of synaptic structures. The perforated spine splits into two new spines, which are connected to the same presynaptic terminal (Fig. 5.5). In turn, this leads to an enhancement of synaptic signal transmission. Accordingly, an increased appearance of perforated spines and an increase of the dendritic spine density is related to LTP induction (Dhanrajan et al., 2004; Trommald et al., 1996). Thus, the increased appearance of perforated spines in Tspan15 knockout mice could indicate changes in LTP.

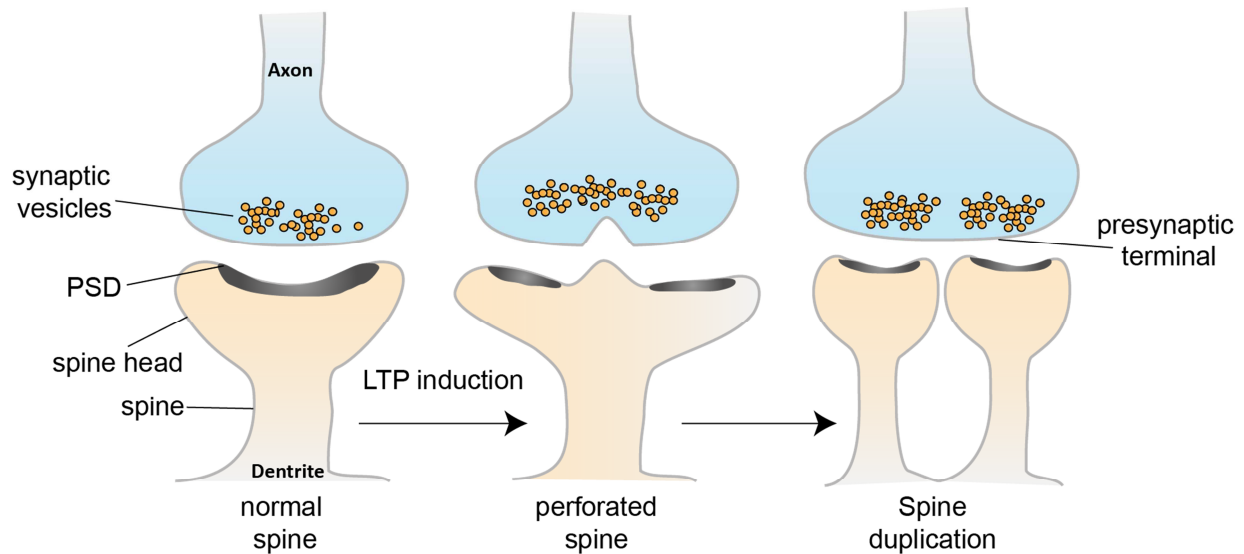


**Fig. 5.5: Remodelling of dendritic spine morphology after LTP induction.**

Schematic drawing showing the remodelling of dendritic spines during long-term potentiation (LTP). Normal spines (left) contain a continuous post-synaptic density (PSD). LTP induces formation of dendritic spines with a discontinuous or perforated PSD (middle). The perforated spine further splits into two spines, which branch from the same dendrite (right). This results in an increased number of spines, which contact the same presynaptic terminal. Redrawn and modified from (Hering and Sheng, 2001).

Whether loss of Tspan15 contributes to LTP by reducing ADAM10 maturation and shedding of N-cadherin or probably impairs LTP by retaining perforated spines in an intermediate stage, which blocks spine duplication, is yet not clear. However, in both scenarios, it is likely that an impaired ability to remove or form novel synaptic contacts impairs synaptic plasticity and network formation. Similar to ADAM10 cKO mice, this could lead to learning deficits and behavioural changes. Since the phenotype of Tspan15 knockout mice is relatively mild, compared to ADAM10 cKO mice, this requires further analysis, like LTP measurements, behavioural and memory tests. In this context it will also be interesting to investigate whether loss of Tspan15 alters shedding of other neuronal adhesion molecules such as NCAM, Nectin-1 and  $\gamma$ -protocadherin C3 (Kuhn et al., 2016; Saftig and Lichtenthaler, 2015)

## 5.5 Tetraspanin-3 and -15 as potential therapeutic targets

The therapeutic potential of tetraspanins was already demonstrated by different studies using monoclonal antibodies (mAbs), soluble recombinant large extracellular loops (sLEL) of tetraspanins and siRNA to modulate the tetraspanin functions. Application of monoclonal antibodies (mAbs) directed against CD81 reduced the inflammatory neurological injuries in a multiple sclerosis mouse model (Dijkstra et al., 2008). Even prophylactic injection of CD81 antibodies had therapeutic potential and prevented hepatitis C virus (HCV) infection of mice (Meuleman et al., 2008). Manipulation of CD9 functions by application of anti-CD9 mAbs reduced tumour progression in mice and is proposed as a novel therapeutic target for gastric cancer in human (Murayama et al., 2015; Nakamoto et al., 2009). The mAbs most likely inhibit tetraspanin functions by disruption of lateral association with their partner proteins. However, also stimulating effects of mAbs have been reported. For example, mAbs against CD151 reduced metastasis of tumour cells by increasing cell adhesion. The therapeutic potential of tetraspanin mAbs is demonstrated by the humanized anti-CD37 IgG fusion protein, which is known as Otlertuzumab or TRU-016. Otlertuzumab has modest clinical activity as therapeutic drug for the treatment of chronic lymphocytic leukaemia (Byrd et al., 2014; Robak et al., 2009). The application of Otlertuzumab in combination with an already established chemotherapeutic drug was recently tested in a phase II clinical trial and improved the therapeutic efficiency (Robak et al., 2017). Similar to mAbs, sLELs are promising tools to modulate tetraspanin functions in pathophysiological events. CD81 sLELs reduced HCV infectivity and CD9, CD81, CC63 and CD151 sLELs prevented HIV-1 entry into macrophages (Flint et al., 2006; Ho et al., 2006). Moreover, RNAi mediated knockdown of CD81 and treatment with CD81 mAbs in cells reduced  $\gamma$ -secretase activity and A $\beta$  liberation, which suggests a beneficial role in the context of AD.

Can Tspan3 and Tspan15 be regarded as therapeutic targets? Liberation and deposition of A $\beta$  peptides are a main cause for pathology in AD (Hardy and Selkoe, 2002). Diminishing A $\beta$  deposition and production is a promising approach for the treatment of AD (Citron, 2010; Hardy and Selkoe, 2002). In course of this work, Tspan3 was identified as a modulator of APP non-amyloidogenic processing. By promoting ADAM10-mediated APP processing Tspan3 reduced the liberation of A $\beta$  peptides. Therefore, increasing ADAM10-mediated APP processing by accelerating Tspan3 expression could be an interesting approach for the treatment of AD. Besides decreasing A $\beta$  liberation, Tspan3 overexpression also increased



sAPP $\alpha$  secretion. sAPP $\alpha$  has potential neurotrophic and neuroprotective functions (Chasseigneaux and Allinquant, 2012; Goodman and Mattson, 1994; Mattson et al., 1993). Increasing its liberation by stimulating ADAM10 activity could counteract neurotoxic processes and decrease neurodegeneration in AD.

The potential of promoting ADAM10 activity as a therapeutic approach in AD was previously reported. Upregulation of ADAM10 expression had beneficial effects in an AD mouse model and increased sAPP $\alpha$  levels, while reducing A $\beta$  deposition (Postina et al., 2004). Furthermore, a recent study demonstrated that treatment of AD patients with the synthetic retinoic acid derivative *acitretin*, stimulates ADAM10 activity and increases sAPP $\alpha$  levels (Endres et al., 2014). Nevertheless, it has to be considered that ADAM10 has a broad substrate spectrum and is associated with multiple physiological functions (Kuhn et al., 2016; Reiss and Saftig, 2009; Saftig and Lichtenthaler, 2015; Weber and Saftig, 2012). While upregulation of ADAM10 in AD has beneficial effects, increased ADAM10 activity is associated with cancer progression, metastasis and inflammation (Crawford et al., 2009; Gavert et al., 2007; Kohutec et al., 2009; Lendeckel et al., 2005). Therefore, increasing the overall activity of ADAM10 could cause adverse effects, which are for example related to an increased shedding of other substrates, such as cytokines and adhesion molecules. In this context, Tspan3 could be an advantageous therapeutic target for ADAM10 stimulation. The results of the present study indicate that Tspan3 specifically increases ADAM10 activity towards APP, without affecting its general activity by increasing maturation or surface expression. Hence, stimulating Tspan3 functions with agonistic mAbs or transcriptional upregulation could increase ADAM10-mediated APP processing, without affecting its activity towards other substrates. Despite these beneficial effects, Tspan3 has to be regarded carefully as a therapeutic target. Besides APP and N-cadherin the impact of Tspan3 overexpression on other ADAM10 substrates such as Notch, TNF $\alpha$ , EGF and other cell surface proteins has not yet been investigated. It cannot be excluded that an increased expression of Tspan3 affects these substrates.

Moreover, Tspan3 also interacts with the  $\gamma$ -secretase complex and possibly alters its activity. Although, inhibition of  $\gamma$ -secretase activity was a promising therapeutic target in AD, due to its pivotal role in the liberation of A $\beta$  peptides, most approaches led to severe adverse effects, such as development of skin cancer and gastrointestinal infections (Doody et al., 2013). These unwanted effects are most likely related to an impaired processing of other  $\gamma$ -secretase substrates, such as Notch (Haapasalo and Kovacs, 2011). Although Tspan3 overexpression had

no apparent inhibitory effect on the  $\gamma$ -secretase complex, it could contribute to disadvantageous effects by increasing  $\gamma$ -secretase activity. In such a scenario Tspan3 could possibly enhance Notch activity, which is also associated with human disorders such as T-cell lymphoblastic leukaemia, lung and breast cancer (summarised in Andersson and Lendahl, 2014).

In contrast to Tspan3, Tspan15 is a less suitable therapeutic target for the treatment of AD. Although, Tspan15 promotes ADAM10 activity by increasing maturation, it seems to play only a minor role ADAM10-mediated APP proteolytic processing as evidenced by an unaltered APP processing in Tspan15-deficient brains. Nevertheless, enhanced expression of Tspan15 could still have a beneficial effect in AD.

The finding that loss of Tspan15 reduces PrP<sup>C</sup> shedding in the brain, implicates that an enhanced Tspan15 expression could have the opposite effect and increases PrP<sup>C</sup> shedding. Membrane bound PrP<sup>C</sup> acts as a receptor for A $\beta$  and promotes neurotoxicity by intracellular activation of the tyrosine kinase Fyn (Laurén et al., 2009; Um et al., 2012). By reducing the amount of membrane bound PrP<sup>C</sup> receptors that can bind to A $\beta$  peptides, upregulation of Tspan15 expression could prevent neurotoxic signalling. However, Tspan15 expression also promotes N-cadherin shedding (Jouannet et al., 2015; Noy et al., 2016; Prox et al., 2012). Based on its important role as adhesion and signalling molecule, enhanced N-cadherin shedding is associated with cancer cell migration and activation of intracellular signalling pathways leading to metastasis (Kohutek et al., 2009; Suyama et al., 2002). By stimulating Tspan15 expression severe disadvantageous effects related to an increased N-cadherin shedding could occur, which would probably dominate its potential beneficial effects in AD. However, in the context of N-cadherin as a mediator of cancer progression and metastasis, downregulation of Tspan15, using siRNA, mAbs or sLELs is an interesting therapeutic option for the treatment of different kinds of cancers. For example, enhanced N-cadherin shedding promotes glioblastoma cell migration and invasiveness (Kohutek et al., 2009). Reducing N-cadherin shedding by decreasing Tspan15 expression could reduce metastasis and cancer cell spreading. In this context, it is also noteworthy that Tspan15-deficient mice do not display severe defects, indicating that such an approach could have rather low adverse effects. Besides cancer, Tspan15 is also a potential target for prion disease. However, due to the dual role of ADAM10 activity in prion disease, in this case it is not clear whether an up- or a downregulation of Tspan15 expression would be of therapeutic benefit.

Although, Tspan15-deficiency leads to rather subtle alterations, the higher degree of postnatal lethality and the changes in dendritic spine structure indicate an important role of Tspan15 in physiological processes. Therefore, modulation of Tspan15 expression may also have yet unidentified disadvantageous effects and the therapeutic potential of Tspan15 has to be considered carefully.

Taken together Tspan3 and Tspan15 are potential targets for the regulation of ADAM10 activity in pathophysiological events such as AD, prion disease and cancer. However, only little is known about their physiological function and their role in the regulation of ADAM10-mediated shedding processes. Functional redundancy with other tetraspanins may not only hamper the therapeutic efficiency of possible drugs, but also may cause unwanted effects. Therefore, further experimentation is necessary to reveal the full therapeutic potential of Tspan3 and Tspan15.

## 5.6 Conclusions and Outlook

In the present work Tspan3 was identified as a novel ADAM10 interaction partner. Expression of Tspan3 increases ADAM10-mediated APP processing, but has no impact on N-cadherin shedding. By interacting with ADAM10, APP and the  $\gamma$ -secretase complex Tspan3 groups its partner proteins into a functional complex at the plasma membrane and promotes non-amyloidogenic APP processing. In addition, Tspan3 seems to stabilise its partner proteins at the cell surface and modulates their internalisation. The analysis of Tspan3 knockout mice did not reveal an overt phenotype, which can be explained by the previously reported observations of functional redundancy between different tetraspanins. Tspan7 and Tspan5 were identified as likely candidates for the compensation of Tspan3-related functions.

This study revealed a novel mechanism how a specific tetraspanin modulates ADAM10-mediated shedding processes, without affecting ADAM10 maturation or surface trafficking. This, together with the ability of Tspan3 to reduce A $\beta$  liberation, makes it an interesting target for the therapeutic modulation of ADAM10 activity in AD. However, further studies are necessary to understand the role of Tspan3 in AD and in modulating the shedding of other substrates. In this regard, it will also be important to analyse the role of Tspan5 and Tspan7 and their functional redundancy with Tspan3 in more detail. Further open questions are how Tspan3 modulates endocytic processes of its partner proteins and whether Tspan3 influences  $\gamma$ -secretase activity.

In an independent approach, the *in vivo* function of Tspan15 was analysed using a Tspan15 knockout mouse model. The generation of mature ADAM10 was clearly reduced. Loss of Tspan15 led to a significant reduction of N-cadherin and PrP<sup>C</sup> shedding in the brain. Moreover, knockout of Tspan15 led to morphological changes of dendritic spines, which implicates a possible role in LTP and synaptic signal transmission.

Altogether the analysis of Tspan15 knockout mice confirmed the important role of Tspan15 as regulator of ADAM10 *in vivo*. Since this study focused on the role of Tspan15 in the brain, for future experiments it will be interesting to analyse the function of Tspan15 in other tissues as well. In addition, more detailed analysis how Tspan15 influences N-cadherin and PrP<sup>C</sup> shedding should be performed.

Moreover, to unravel the therapeutic potential of Tspan15, but also of Tspan3, further studies should address the role of these two tetraspanins in disease models, such as for prion disease and AD. It would be worthwhile to characterise the Tspan3 and Tspan15 promoter region to identify possible targets for therapeutic drugs that could modulate Tspan15 or Tspan3 expression.

## 6 References

- Abraham, C.R., Selkoe, D.J., and Potter, H.** (1988). Immunochemical identification of the serine protease inhibitor  $\alpha$ 1-antichymotrypsin in the brain amyloid deposits of Alzheimer's disease. *Cell* 52, 487–501.
- Aguzzi, A., and Calella, A.M.** (2009). Prions: protein aggregation and infectious diseases. *Physiol Rev* 89, 1105–1152.
- Ahmad, M., Takino, T., Miyamori, H., Yoshizaki, T., Furukawa, M., and Sato, H.** (2006). Cleavage of amyloid-beta precursor protein (APP) by membrane-type matrix metalloproteinases. *J Biochem* 139, 517–526.
- Altmeyden, H.C., Prox, J., Puig, B., Kluth, M. a, Bernreuther, C., Thurm, D., Jorissen, E., Petrowitz, B., Bartsch, U., De Strooper, B., et al.** (2011). Lack of a-disintegrin-and-metalloproteinase ADAM10 leads to intracellular accumulation and loss of shedding of the cellular prion protein in vivo. *Mol Neurodegener* 6, 36.
- Altmeyden, H.C., Prox, J., Krasemann, S., Puig, B., Kruszewski, K., Dohler, F., Bernreuther, C., Hoxha, A., Linsenmeier, L., Sikorska, B., et al.** (2015). The sheddase ADAM10 is a potent modulator of prion disease. *Elife* 4, 1–28.
- Alzheimer Association** (2016). 2016 Alzheimer's Disease Facts and Figures. *Alzheimer's Dement* 2016 12, 1–80.
- Amour, A., Knight, C.G., Webster, A., Slocombe, P.M., Stephens, P.E., Knäuper, V., Docherty, A.J.P., and Murphy, G.** (2000). The in vitro activity of ADAM-10 is inhibited by TIMP-1 and TIMP-3. *FEBS Lett* 473, 275–279.
- Anders, A., Gilbert, S., Garten, W., Postina, R., and Fahrenholz, F.** (2001). Regulation of the  $\alpha$ -secretase ADAM10 by its prodomain and proprotein convertases. *FASEB J* 15, 1837–1839.
- Andersson, E.R., and Lendahl, U.** (2014). Therapeutic modulation of Notch signalling — are we there yet? *Nat Publ Gr* 13, 357–378.
- Arduise, C., Abache, T., Li, L., Billard, M., Chabanon, A., Ludwig, A., Mauduit, P., Boucheix, C., Rubinstein, E., and Le Naour, F.** (2008a). Tetraspanins regulate ADAM10-mediated cleavage of TNF-alpha and epidermal growth factor. *J Immunol* 181, 7002–7013.
- Arduise, C., Abache, T., Li, L., Billard, M., Chabanon, A., Ludwig, A., Mauduit, P., Boucheix, C., Rubinstein, E., and Naour, F. Le** (2008b). Tetraspanins Regulate ADAM10-Mediated Cleavage of TNF- $\alpha$  and Epidermal Growth Factor. *J Immunol* 181, 7002–7013.
- Aydin, D., Weyer, S.W., and Müller, U.C.** (2012). Functions of the APP gene family in the nervous system: Insights from mouse models. *Exp Brain Res* 217, 423–434.
- Bang, M.L., and Owczarek, S.** (2013). A matter of balance: Role of neurexin and neuroligin at the synapse. *Neurochem Res* 38, 1174–1189.

- Bascom, R.A., Manara, S., Collins, L., Molday, R.S., Kalnins, V.I., and McInnes, R.R.** (1992). Cloning of the CDNA for a novel photoreceptor membrane protein (rom-1) identifies a disk rim protein family implicated in human retinopathies. Neuron 8, 1171–1184.
- Bassani, S., and Cingolani, L. a** (2012). Tetraspanins: Interactions and interplay with integrins. Int J Biochem Cell Biol 44, 703–708.
- Bassani, S., Cingolani, L.A., Valnegri, P., Folci, A., Zapata, J., Gianfelice, A., Sala, C., Goda, Y., and Passafaro, M.** (2012). The X-Linked Intellectual Disability Protein TSPAN7 Regulates Excitatory Synapse Development and AMPAR Trafficking. Neuron 73, 1143–1158.
- Berditchevski, F., and Odintsova, E.** (2007). Tetraspanins as regulators of protein trafficking. Traffic 8, 89–96.
- Berditchevski, F., Odintsova, E., Sawada, S., and Gilbert, E.** (2002). Expression of the palmitoylation-deficient CD151 weakens the association of  $\alpha 3\beta 1$  integrin with the tetraspanin-enriched microdomains and affects integrin-dependent signaling. J Biol Chem 277, 36991–37000.
- Biedler, J.L., Roffler-Tarlov, S., Schachner, M., and Freedman, L.S.** (1978). Multiple neurotransmitter synthesis by human neuroblastoma cell lines and clones. Cancer Res 38, 3751–3757.
- Bienstock, R.J., and Carl Barrett, J.** (2001). KAI1, a prostate metastasis suppressor: Prediction of solvated structure and interactions with binding partners; integrins, cadherins, and cell-surface receptor proteins. Mol Carcinog 32, 139–153.
- Biname, F., Sakry, D., Dimou, L., Jolivel, V., and Trotter, J.** (2013). NG2 regulates directional migration of oligodendrocyte precursor cells via Rho GTPases and polarity complex proteins. J Neurosci 33, 10858–10874.
- Bloch, L., Sineschekova, O., Reichenbach, D., Reiss, K., Saftig, P., Kuro-o, M., and Kaether, C.** (2009). Klotho is a substrate for  $\alpha$ -,  $\beta$ - and  $\gamma$ -secretase. FEBS Lett 583, 3221–3224.
- Bode, W., Gomis-Rüth, F.X., and Stöckler, W.** (1993). Astacins, serralyins, snake venom and matrix metalloproteinases exhibit identical zinc-binding environments (HEXXHXXGXXH and Met-turn) and topologies and should be grouped into a common family, the “metzincins.” FEBS Lett 331, 134–140.
- Boland, B., Smith, D. a, Mooney, D., Jung, S.S., Walsh, D.M., and Platt, F.M.** (2010). Macroautophagy is not directly involved in the metabolism of amyloid precursor protein. J Biol Chem 285, 37415–37426.
- Bonifacino, J.S., and Angelica, E.C.D.** (1999). molecular bases for the recognition of tyrosin-based Sorting Signals. J Cell Biol 145, 923–926.
- Boucheix, C., and Rubinstein, E.** (2001). Tetraspanins. Cell Mol Life Sci 58, 1189–1205.
- Braak, H., and Braak, E.** (1991). Neuropathological staging of Alzheimer-related changes. Acta Neuropathol 82, 239–259.

- Bredt, D.S., and Nicoll, R.A.** (2003). AMPA receptor trafficking at excitatory synapses. *Neuron* *40*, 361–379.
- Bremer, J., Baumann, F., Tiberi, C., Wessig, C., Fischer, H., Schwarz, P., Steele, A.D., Toyka, K. V., Nave, K.-A., Weis, J., et al.** (2010). Axonal prion protein is required for peripheral myelin maintenance. *Nat Neurosci* *13*, 310–318.
- Brenneman, L.H., Moss, M.L., and Maness, P.F.** (2014). EphrinA/EphA-induced ectodomain shedding of neural cell adhesion molecule regulates growth cone repulsion through ADAM10 metalloprotease. *J Neurochem* *128*, 267–279.
- Brookmeyer, R., Corrada, M.M., Curriero, F.C., and Kawas, C.** (2002). Survival following a diagnosis of Alzheimer disease. *Arch Neurol* *59*, 1764–1767.
- Brookmeyer, R., Johnson, E., Ziegler-Graham, K., and Arrighi, H.M.** (2007). Forecasting the global burden of Alzheimer’s disease. *Alzheimer’s Dement* *3*, 186–191.
- Brown, J.R., Nigh, E., Lee, R.J., Ye, H., Thompson, M.A., Saudou, F., Pestell, R.G., and Greenberg, M.E.** (1998). Fos family members induce cell cycle entry by activating cyclin D1. *Mol Cell Biol* *18*, 5609–5619.
- Büeler, H., Aguzzi, A., Sailer, A., Greiner, R.A., Autenried, P., Aguet, M., and Weissmann, C.** (1993). Mice devoid of PrP are resistant to scrapie. *Cell* *73*, 1339–1347.
- Buxbaum, J.D., Liu, K.N., Luo, Y., Slack, J.L., Stocking, K.L., Peschon, J.J., Johnson, R.S., Castner, B.J., Cerretti, D.P., and Black, R.A.** (1998). Evidence that tumor necrosis factor alpha converting enzyme is involved in regulated alpha-secretase cleavage of the Alzheimer amyloid protein precursor. *J Biol Chem* *273*, 27765–27767.
- Byrd, J.C., Pagel, J.M., Awan, F.T., Forero, A., Flinn, I.W., Deauna-Limayo, D.P., Spurgeon, S.E., Andritsos, L.A., Gopal, A.K., Leonard, J.P., et al.** (2014). A phase 1 study evaluating the safety and tolerability of otlertuzumab, an anti-CD37 mono-specific ADAPTIR therapeutic protein in chronic lymphocytic leukemia. *Blood* *123*, 1302–1308.
- Caescu, C.I., Jeschke, G.R., and Turk, B.E.** (2009). Active-site determinants of substrate recognition by the metalloproteinases TACE and ADAM10. *Biochem J* *424*, 79–88.
- Cai, H., Wang, Y., McCarthy, D., Wen, H., Borchelt, D.R., Price, D.L., and Wong, P.C.** (2001). BACE1 is the major beta-secretase for generation of Abeta peptides by neurons. *Nat Neurosci* *4*, 233–234.
- Carey, R.M., Balcz, B. a, Lopez-Coviella, I., and Slack, B.E.** (2005). Inhibition of dynamin-dependent endocytosis increases shedding of the amyloid precursor protein ectodomain and reduces generation of amyloid beta protein. *BMC Cell Biol* *6*, 30.
- Carloni, V., Mazzocca, A., and Ravichandran, K.S.** (2004). Tetraspanin CD81 is linked to ERK/MAPKinase signaling by Shc in liver tumor cells. *Oncogene* *23*, 1566–1574.

- Cataldo, A.M., Barnett, J.L., Berman, S.A., Li, J., Quarless, S., Bursztajn, S., Lipka, C., and Nixon, R.A.** (1995). Gene expression and cellular content of cathepsin D in Alzheimer's disease brain: Evidence for early up-regulation of the endosomal-lysosomal system. Neuron *14*, 671–680.
- Cataldo, A.M., Barnett, J.L., Pieroni, C., and Nixon, R.A.** (1997). Increased Neuronal Endocytosis and Protease Delivery to Early Endosomes In Sporadic Alzheimers-Disease - Neuropathologic Evidence For a Mechanism Of Increased  $\beta$ -Amyloidogenesis. J Neurosci *17*, 6142–6151.
- Cataldo, a M., Hamilton, D.J., Barnett, J.L., Paskevich, P. a, and Nixon, R. a** (1996). Properties of the endosomal-lysosomal system in the human central nervous system: disturbances mark most neurons in populations at risk to degenerate in Alzheimer's disease. J Neurosci *16*, 186–199.
- Cha, J.H., Brooke, J.S., Ivey, K.N., and Eidels, L.** (2000). Cell surface monkey CD9 antigen is a coreceptor that increases diphtheria toxin sensitivity and diphtheria toxin receptor affinity. J Biol Chem *275*, 6901–6907.
- Charrin, S., Manié, S., Oualid, M., Billard, M., Boucheix, C., and Rubinstein, E.** (2002). Differential stability of tetraspanin/tetraspanin interactions: role of palmitoylation. FEBS Lett *516*, 139–144.
- Charrin, S., Manié, S., Thiele, C., Billard, M., Gerlier, D., Boucheix, C., and Rubinstein, E.** (2003). A physical and functional link between cholesterol and tetraspanins. Eur J Immunol *33*, 2479–2489.
- Charrin, S., le Naour, F., Silvie, O., Milhiet, P.-E., Boucheix, C., and Rubinstein, E.** (2009). Lateral organization of membrane proteins: tetraspanins spin their web. Biochem J *420*, 133–154.
- Charrin, S., Jouannet, S., Boucheix, C., and Rubinstein, E.** (2014). Tetraspanins at a glance. J Cell Sci *127*, 3641–3648.
- Chasseigneaux, S., and Allinquant, B.** (2012). Functions of A $\beta$ , sAPP $\alpha$  and sAPP $\beta$ : Similarities and differences. J Neurochem.
- Chen, A.C., Kim, S., Shepardson, N., Patel, S., Hong, S., and Selkoe, D.J.** (2015). Physical and functional interaction between the  $\alpha$ - and  $\gamma$ -secretases: A new model of regulated intramembrane proteolysis. J Cell Biol *211*, 1157–1176.
- Chen, C.-D., Podvin, S., Gillespie, E., Leeman, S.E., and Abraham, C.R.** (2007). Insulin stimulates the cleavage and release of the extracellular domain of Klotho by ADAM10 and ADAM17. Proc Natl Acad Sci U S A *104*, 19796–19801.
- Chen, C.-D., Sloane, J.A., Li, H., Aytan, N., Giannaris, E.L., Zeldich, E., Hinman, J.D., Dedeoglu, A., Rosene, D.L., Bansal, R., et al.** (2013). The antiaging protein Klotho enhances oligodendrocyte maturation and myelination of the CNS. J Neurosci *33*, 1927–1939.



- Chen, F., Yang, D.S., Petanceska, S., Yang, A., Tandon, A., Yu, G., Rozmahel, R., Ghiso, J., Nishimura, M., Zhang, D.M., et al.** (2000). Carboxyl-terminal fragments of alzheimer  $\beta$ -amyloid precursor protein accumulate in restricted and unpredicted intracellular compartments in presenilin 1-deficient cells. *J Biol Chem* *275*, 36794–36802.
- Chow, V.W., Mattson, M.P., Wong, P.C., and Gleichmann, M.** (2010). An overview of APP processing enzymes and products. *Neuromolecular Med* *12*, 1–12.
- Choy, R.W.-Y., Cheng, Z., and Schekman, R.** (2012). Amyloid precursor protein (APP) traffics from the cell surface via endosomes for amyloid  $\beta$  ( $A\beta$ ) production in the trans-Golgi network. *Proc Natl Acad Sci U S A* *109*, E2077-82.
- Cissé, M.A., Sunyach, C., Lefranc-Jullien, S., Postina, R., Vincent, B., and Checler, F.** (2005). The disintegrin ADAM9 indirectly contributes to the physiological processing of cellular prion by modulating ADAM10 activity. *J Biol Chem* *280*, 40624–40631.
- Citron, M.** (2010). Alzheimer's disease: strategies for disease modification. *Nat Rev Drug Discov* *9*, 387–398.
- Citron, M., Oltersdorf, T., Haass, C., McConlogue, L., Hung, a Y., Seubert, P., Vigo-Pelfrey, C., Lieberburg, I., and Selkoe, D.J.** (1992). Mutation of the beta-amyloid precursor protein in familial Alzheimer's disease increases beta-protein production. *Nature* *360*, 672–674.
- Cohen, F.E., Fletterick, R.J., Serban, A., Gasset, M., Baldwin, M., Mehlhorn, I., Nguyen, J., Huang, Z., Pan, K.M., and Groth, D.** (1993). Conversion of alpha-helices into beta-sheets features in the formation of the scrapie prion proteins. *Proc Natl Acad Sci U S A* *90*, 10962–10966.
- Collinge, J.** (2001). Prion diseases of humans and animals: their causes and molecular basis. *Annu Rev Neurosci* *24*, 519–550.
- Corder, E.H., Saunders, a M., Strittmatter, W.J., Schmechel, D.E., Gaskell, P.C., Small, G.W., Roses, a D., Haines, J.L., and Pericak-Vance, M. a** (1993). Gene dose of apolipoprotein E type 4 allele and the risk of Alzheimer's disease in late onset families. *Science* *261*, 921–923.
- Cordy, J.M., Hussain, I., Dingwall, C., Hooper, N.M., and Turner, A.J.** (2003). Exclusively targeting  $\beta$ -secretase to lipid rafts by GPI-anchor addition up-regulates  $\beta$ -site processing of the amyloid precursor protein. *Proc Natl Acad Sci U S A* *100*, 11735–11740.
- Crawford, H., Dempsey, P., Brown, G., Adam, L., and Moss, M.** (2009). ADAM10 as a Therapeutic Target for Cancer and Inflammation. *Curr Pharm Des* *15*, 2288–2299.
- Crew, V.K., Burton, N., Kagan, A., Green, C.A., Levene, C., Flinter, F., Brady, R.L., Daniels, G., and Anstee, D.J.** (2004). CD151, the first member of the tetraspanin (TM4) superfamily detected on erythrocytes, is essential for the correct assembly of human basement membranes in kidney and skin. *Blood* *104*, 2217–2223.
- Dawkins, E., and Small, D.H.** (2014). Insights into the physiological function of the  $\beta$ -amyloid precursor protein: Beyond Alzheimer's disease. *J Neurochem* *129*, 756–769.

- De, S.B., Annaert, W., Cupers, P., Saftig, P., Craessaerts, K., Mumm, J.S., Schroeter, E.H., Schrijvers, V., Wolfe, M.S., Ray, W.J., et al.** (1999). A presenilin-1-dependent gamma-secretase-like protease mediates release of Notch intracellular domain. *Nature* **398**, 518–522.
- Dhanrajan, T.M., Lynch, M.A., Kelly, A., Popov, V.I., Rusakov, D.A., and Stewart, M.G.** (2004). Expression of long-term potentiation in aged rats involves perforated synapses but dendritic spine branching results from high-frequency stimulation alone. *Hippocampus* **14**, 255–264.
- Dijkstra, S., Kooij, G., Verbeek, R., van der Pol, S.M.A., Amor, S., Geisert, E.E., Dijkstra, C.D., van Noort, J.M., and Vries, H.E. de** (2008). Targeting the tetraspanin CD81 blocks monocyte transmigration and ameliorates EAE. *Neurobiol Dis* **31**, 413–421.
- Doody, R.S., Raman, R., Farlow, M., Iwatsubo, T., Vellas, B., Joffe, S., Kieburtz, K., He, F., Sun, X., Thomas, R.G., et al.** (2013). A phase 3 trial of semagacestat for treatment of Alzheimer's disease. *N Engl J Med* **369**, 341–350.
- Dornier, E., Coumailleau, F., Ottavi, J.-F., Moretti, J., Boucheix, C., Mauduit, P., Schweisguth, F., and Rubinstein, E.** (2012). TspanC8 tetraspanins regulate ADAM10/Kuzbanian trafficking and promote Notch activation in flies and mammals. *J Cell Biol* **199**, 481–496.
- Dreyer, R.N., Bausch, K.M., Fracasso, P., Hammond, L.J., Wunderlich, D., Wirak, D.O., Davis, G., Brini, C.M., Buckholz, T.M., Konig, G., et al.** (1994). Processing of the Pre-beta-amyloid Protein by Cathepsin d is Enhanced by a Familial Alzheimer's Disease Mutation. *Eur J Biochem* **224**, 265–271.
- Dunn, C.D., Sulis, M.L., Ferrando, A. a, and Greenwald, I.** (2010). A conserved tetraspanin subfamily promotes Notch signaling in *Caenorhabditis elegans* and in human cells. *Proc Natl Acad Sci U S A* **107**, 5907–5912.
- Düsterhöft, S., Jung, S., Hung, C.W., Tholey, A., Sönnichsen, F.D., Grötzinger, J., and Lorenzen, I.** (2013). Membrane-proximal domain of a disintegrin and metalloprotease-17 represents the putative molecular switch of its shedding activity operated by protein-disulfide isomerase. *J Am Chem Soc* **135**, 5776–5781.
- Ebsen, H., Lettau, M., Kabelitz, D., and Janssen, O.** (2014). Identification of SH3 Domain Proteins Interacting with the Cytoplasmic Tail of the A Disintegrin and Metalloprotease 10 (ADAM10). *PLoS One* **9**, e102899.
- Edgar, J.R., Willen, K., Gouras, G.K., and Futter, C.E.** (2015). ESCRTs regulate amyloid precursor protein sorting in multivesicular bodies and intracellular amyloid-accumulation. *J Cell Sci* **128**, 2520–2528.
- Endres, K., Postina, R., Schroeder, A., Mueller, U., and Fahrenholz, F.** (2005). Shedding of the amyloid precursor protein-like protein APLP2 by disintegrin-metalloproteinases: Retinoic acid-induced upregulation of substrate and proteinase ADAM10 during neuronal cell differentiation. *FEBS J* **272**, 5808–5820.

- Endres, K., Fahrenholz, F., Lotz, J., Hiemke, C., Teipel, S., Lieb, K., Tuscher, O., and Fellgiebel, A. (2014). Increased CSF APPs- levels in patients with Alzheimer disease treated with acitretin. *Neurology* 83, 1930–1935.
- Epis, R., Marcello, E., Gardoni, F., Vastagh, C., Malinverno, M., Balducci, C., Colombo, A., Borroni, B., Vara, H., Dell’Agli, M., et al. (2010). Blocking ADAM10 synaptic trafficking generates a model of sporadic Alzheimer’s disease. *Brain* 133, 3323–3335.
- Escrevente, C., Morais, V. a, Keller, S., Soares, C.M., Altevogt, P., and Costa, J. (2008). Functional role of N-glycosylation from ADAM10 in processing, localization and activity of the enzyme. *Biochim Biophys Acta* 1780, 905–913.
- Evin, G., Cappai, R., Li, Q.X., Culvenor, J.G., Small, D.H., Beyreuther, K., and Masters, C.L. (1995). Candidate gamma-secretases in the generation of the carboxyl terminus of the Alzheimer’s disease beta A4 amyloid: possible involvement of cathepsin D. *Biochemistry* 34, 14185–14192.
- Felsenstein, K.M., Hunihan, L.W., and Roberts, S.B. (1994). Altered cleavage and secretion of a recombinant  $\beta$ -APP bearing the Swedish familial Alzheimer’s disease mutation. *Nat Genet* 6, 251–256.
- Fialka, I., Steinlein, P., Ahorn, H., Böck, G., Burbelo, P.D., Haberfellner, M., Lottspeich, F., Paiha, K., Pasquali, C., and Huber, L.A. (1999). Identification of syntenin as a protein of the apical early endocytic compartment in Madin-Darby canine kidney cells. *J Biol Chem* 274, 26233–26239.
- Flint, M., von Hahn, T., Zhang, J., Farquhar, M., Jones, C.T., Balfe, P., Rice, C.M., and McKeating, J.A. (2006). Diverse CD81 proteins support hepatitis C virus infection. *J Virol* 80, 11331–11342.
- Fradkin, L.G., Kamphorst, J.T., DiAntonio, A., Goodman, C.S., and Noordermeer, J.N. (2002). Genomewide analysis of the Drosophila tetraspanins reveals a subset with similar function in the formation of the embryonic synapse. *Proc Natl Acad Sci* 99, 13663–13668.
- Frith, C., and Dolan, R. (1996). The role of the prefrontal cortex in higher cognitive functions. In *Cognitive Brain Research*, pp. 175–181.
- Fryer, J.D., DeMattos, R.B., McCormick, L.M., O’Dell, M.A., Spinner, M.L., Bales, K.R., Paul, S.M., Sullivan, P.M., Parsadanian, M., Bu, G., et al. (2005). The low density lipoprotein receptor regulates the level of central nervous system human and murine apolipoprotein E but does not modify amyloid plaque pathology in PDAPP mice. *J Biol Chem* 280, 25754–25759.
- Fujinaga, M., Cherney, M.M., Oyama, H., Oda, K., and James, M.N.G. (2004). The molecular structure and catalytic mechanism of a novel carboxyl peptidase from *Scytalidium lignicolum*. *Proc Natl Acad Sci* 101, 3364–3369.
- Gardoni, F., Saraceno, C., Malinverno, M., Marcello, E., Verpelli, C., Sala, C., and Di Luca, M. (2012). The neuropeptide PACAP38 induces dendritic spine remodeling through ADAM10-N-cadherin signaling pathway. *J Cell Sci* 125, 1401–1406.

- Garrett, A.M., and Weiner, J.A.** (2009). Control of CNS Synapse Development by - Protocadherin-Mediated Astrocyte-Neuron Contact. J Neurosci 29, 11723–11731.
- Garrett, A.M., Schreiner, D., Lobas, M.A., and Weiner, J.A.** (2012).  $\gamma$ -Protocadherins Control Cortical Dendrite Arborization by Regulating the Activity of a FAK/PKC/MARCKS Signaling Pathway. Neuron 74, 269–276.
- Gavert, N., Sheffer, M., Raveh, S., Spaderna, S., Shtutman, M., Brabletz, T., Barany, F., Paty, P., Notterman, D., Domany, E., et al.** (2007). Expression of L1-CAM and ADAM10 in human colon cancer cells induces metastasis. Cancer Res 67, 7703–7712.
- Gomis-Rüth, F.X.** (2003). Structural aspects of the metzincin clan of metalloendopeptidases. Mol Biotechnol 24, 157–202.
- Goodman, Y., and Mattson, M.P.** (1994). Secreted forms of  $\beta$ -amyloid precursor protein protect hippocampal neurons against amyloid  $\beta$ -peptide-induced oxidative injury. Exp Neurol 128, 1–12.
- Gordon, W.R., Arnett, K.L., and Blacklow, S.C.** (2009). The molecular logic of Notch signaling: a structural and biochemical perspective. J Cell Sci 121, 3109–3119.
- Grbovic, O.M., Mathews, P.M., Jiang, Y., Schmidt, S.D., Dinakar, R., Summers-Terio, N.B., Ceresa, B.P., Nixon, R.A., and Cataldo, A.M.** (2003). Rab5-stimulated up-regulation of the endocytic pathway increases intracellular beta-cleaved amyloid precursor protein carboxyl-terminal fragment levels and A $\beta$  production. J Biol Chem 278, 31261–31268.
- Griffiths, R.E., Heesom, K.J., and Anstee, D.J.** (2007). Normal prion protein trafficking in cultured human erythroblasts. Blood 110, 4518–4525.
- Gunther, W., Luchow, A., Cluzeaud, F., Vandewalle, A., and Jentsch, T.J.** (1998). ClC-5, the chloride channel mutated in Dent's disease, colocalizes with the proton pump in endocytotically active kidney cells. Proc Natl Acad Sci 95, 8075–8080.
- Gustafsen, C., Glerup, S., Pallesen, L.T., Olsen, D., Andersen, O.M., Nykjaer, A., Madsen, P., and Petersen, C.M.** (2013). Sortilin and SorLA Display Distinct Roles in Processing and Trafficking of Amyloid Precursor Protein. J Neurosci 33, 64–71.
- Gutiérrez-López, M.D., Gilsanz, A., Yáñez-Mó, M., Ovalle, S., Lafuente, E.M., Domínguez, C., Monk, P.N., González-Alvaro, I., Sánchez-Madrid, F., and Cabañas, C.** (2011). The sheddase activity of ADAM17/TACE is regulated by the tetraspanin CD9. Cell Mol Life Sci 68, 3275–3292.
- Gutwein, P.** (2002). ADAM10-mediated cleavage of L1 adhesion molecule at the cell surface and in released membrane vesicles. FASEB J 17, 292–294.
- H. Hook, V.Y., Toneff, T., Aaron, W., Yasothornsrikul, S., Bunday, R., and Reisine, T.** (2002).  $\beta$ -Amyloid peptide in regulated secretory vesicles of chromaffin cells: evidence for multiple cysteine proteolytic activities in distinct pathways for  $\beta$ -secretase activity in chromaffin vesicles. J Neurochem 81, 237–256.

- Haapasalo, A., and Kovacs, D.M.** (2011). The many substrates of presenilin/ $\gamma$ -secretase. J Alzheimer's Dis 25, 3–28.
- Haass, C., Koo, E.H., Mellon, a, Hung, a Y., and Selkoe, D.J.** (1992). Targeting of cell-surface beta-amyloid precursor protein to lysosomes: alternative processing into amyloid-bearing fragments. Nature 357, 500–503.
- Haass, C., Hung, A.Y., Schlossmacher, M.G., Teplow, D.B., and Selkoe, D.J.** (1993). beta-Amyloid peptide and a 3-kDa fragment are derived by distinct cellular mechanisms. J Biol Chem 268, 3021–3024.
- Haass, C., Lemere, C.A., Capell, A., Citron, M., Seubert, P., Schenk, D., Lannfelt, L., and Selkoe, D.J.** (1995). The Swedish mutation causes early-onset Alzheimer's disease by  $\beta$ -secretase cleavage within the secretory pathway. Nat Med 1, 1291–1296.
- Haass, C., Kaether, C., Thinakaran, G., and Sisodia, S.** (2012). Trafficking and proteolytic processing of APP. Cold Spring Harb Perspect Med 2, a006270.
- Haining, E.J., Yang, J., Bailey, R.L., Khan, K., Collier, R., Tsai, S., Watson, S.P., Frampton, J., Garcia, P., and Tomlinson, M.G.** (2012). The TspanC8 subgroup of tetraspanins interacts with a disintegrin and metalloprotease 10 (ADAM10) and regulates its maturation and cell surface expression. J Biol Chem 287, 39753–39765.
- Hamazaki, H.** (1996). Cathepsin D is involved in the clearance of Alzheimer's  $\beta$ -amyloid protein. FEBS Lett 396, 139–142.
- Hardy, J., and Selkoe, D.J.** (2002). The amyloid hypothesis of Alzheimer's disease: progress and problems on the road to therapeutics. Science 297, 353–356.
- Harris, B., Pereira, I., and Parkin, E.** (2009). Targeting ADAM10 to lipid rafts in neuroblastoma SH-SY5Y cells impairs amyloidogenic processing of the amyloid precursor protein. Brain Res 1296, 203–215.
- Hartmann, D., de Strooper, B., Serneels, L., Craessaerts, K., Herreman, A., Annaert, W., Umans, L., Lübke, T., Lena Illert, A., von Figura, K., et al.** (2002). The disintegrin/metalloprotease ADAM 10 is essential for Notch signalling but not for alpha-secretase activity in fibroblasts. Hum Mol Genet 11, 2615–2624.
- Hattori, C., Asai, M., Onishi, H., Sasagawa, N., Hashimoto, Y., Saido, T.C., Maruyama, K., Mizutani, S., and Ishiura, S.** (2006). BACE1 interacts with lipid raft proteins. J Neurosci Res 84, 912–917.
- Hattori, M., Osterfield, M., and Flanagan, J.G.** (2000). Regulated cleavage of a contact-mediated axon repellent. Science (80-) 289, 1360–1365.
- He, T.C., Sparks, A.B., Rago, C., Hermeking, H., Zawel, L., da Costa, L.T., Morin, P.J., Vogelstein, B., Kinzler, K.W., Groden, J., et al.** (1998). Identification of c-MYC as a target of the APC pathway. Science 281, 1509–1512.

- Heikens, M.J., Cao, T.M., Morita, C., DeHart, S.L., and Tsai, S.** (2007). Penumbra encodes a novel tetraspanin that is highly expressed in erythroid progenitors and promotes effective erythropoiesis. Blood 109.
- Hemler, M.E.** (2003). Tetraspanin Proteins Mediate Cellular Penetration, Invasion, and Fusion Events and Define a Novel Type of Membrane Microdomain. Annu Rev Cell Dev Biol 19, 397–422.
- Hemler, M.E.** (2005). Tetraspanin functions and associated microdomains. Nat Rev Mol Cell Biol 6, 801–811.
- Hering, H., and Sheng, M.** (2001). Dendritic Spines: Structure, Dynamics and Regulation. Nat Rev Neurosci 2, 880–888.
- Hitoshi, S.** (2002). Notch pathway molecules are essential for the maintenance, but not the generation, of mammalian neural stem cells. Genes Dev 16, 846–858.
- Ho, S.-H., Martin, F., Higginbottom, A., Partridge, L.J., Parthasarathy, V., Moseley, G.W., Lopez, P., Cheng-Mayer, C., and Monk, P.N.** (2006). Recombinant Extracellular Domains of Tetraspanin Proteins Are Potent Inhibitors of the Infection of Macrophages by Human Immunodeficiency Virus Type 1. J Virol 80, 6487–6496.
- Hoettecke, N., Ludwig, A., Foro, S., and Schmidt, B.** (2010). Improved Synthesis of ADAM10 Inhibitor GI254023X. Neurodegener Dis 7, 232–238.
- Hortsch, M.** (1996). The L1 Family of Neural Cell Adhesion Molecules: Old Proteins Performing New Tricks. Neuron 17, 587–593.
- Hosokawa, Y., Ueyama, E., Morikawa, Y., Maeda, Y., Seto, M., and Senba, E.** (1999). Molecular cloning of a cDNA encoding mouse A15, a member of the transmembrane 4 superfamily, and its preferential expression in brain neurons. Neurosci Res 35, 281–290.
- von Hoven, G., Rivas, A.J., Neukirch, C., Klein, S., Hamm, C., Qin, Q., Meyenburg, M., Fuser, S., Saftig, P., Hellmann, N., et al.** (2016). Dissecting the role of ADAM10 as a mediator of Staphylococcus aureus -toxin action. Biochem J 473, 1929–1940.
- Howard, L., Lu, X., Mitchell, S., Griffiths, S., and Glynn, P.** (1996). Molecular cloning of MADM: a catalytically active mammalian disintegrin–metalloprotease expressed in various cell types. 50, 45–50.
- Howard, L., Maciewicz, R.A., and Blobel, C.P.** (2000). Cloning and characterization of ADAM28: evidence for autocatalytic pro-domain removal and for cell surface localization of mature ADAM28. Biochem J 348, 21.
- Huang, S., Yuan, S., Dong, M., Su, J., Yu, C., Shen, Y., Xie, X., Yu, Y., Yu, X., Chen, S., et al.** (2005). The phylogenetic analysis of tetraspanins projects the evolution of cell–cell interactions from unicellular to multicellular organisms. Genomics 86, 674–684.
- Hubbard, B.M., and Anderson, J.M.** (1981). A quantitative study of cerebral atrophy in old age and senile dementia. J Neurol Sci 50, 135–145.

- Huotari, J., and Helenius, A. (2011). Endosome maturation. *EMBO J* 30, 3481–3500.
- Hussain, I., Powell, D., Howlett, D.R., Tew, D.G., Meek, T.D., Chapman, C., Gloger, I.S., Murphy, K.E., Southan, C.D., Ryan, D.M., et al. (1999). Identification of a Novel Aspartic Protease (Asp 2) as  $\beta$ -Secretase. *Mol Cell Neurosci* 14, 419–427.
- Imayoshi, I., Sakamoto, M., Yamaguchi, M., Mori, K., and Kageyama, R. (2010). Essential Roles of Notch Signaling in Maintenance of Neural Stem Cells in Developing and Adult Brains. *J Neurosci* 30, 3489–3498.
- Inoshima, I., Inoshima, N., Wilke, G.A., Powers, M.E., Frank, K.M., Wang, Y., and Bubeck Wardenburg, J. (2011). A Staphylococcus aureus pore-forming toxin subverts the activity of ADAM10 to cause lethal infection in mice. *Nat Med* 17, 1310–1314.
- Isaacs, J.D., Jackson, G.S., and Altmann, D.M. (2006). The role of the cellular prion protein in the immune system. *Clin Exp Immunol* 146, 1–8.
- Jadot, M., Canfield, W.M., Gregory, W., and Kornfeld, S. (1992). Characterization of the signal for rapid internalization of the bovine mannose 6-phosphate/insulin-like growth factor-II receptor. *J Biol Chem* 267, 11069–11077.
- Janes, P.W., Saha, N., Barton, W. a, Kolev, M. V, Wimmer-Kleikamp, S.H., Nievergall, E., Blobel, C.P., Himanen, J.-P., Lackmann, M., and Nikolov, D.B. (2005). Adam Meets Eph: An ADAM Substrate Recognition Module Acts as a Molecular Switch for Ephrin Cleavage In trans. *Cell* 123, 291–304.
- Jarriault, S., Le Bail, O., Hirsinger, E., Pourquié, O., Logeat, F., Strong, C.F., Brou, C., Seidah, N.G., and Israël, A. (1998). Delta-1 Activation of Notch-1 Signaling Results in HES-1 Transactivation. *Mol Cell Biol* 18, 7423–7431.
- Jorissen, E., Prox, J., Bernreuther, C., Weber, S., Schwanbeck, R., Serneels, L., Snellinx, A., Craessaerts, K., Thathiah, A., Tesseur, I., et al. (2010). The Disintegrin/Metalloproteinase ADAM10 Is Essential for the Establishment of the Brain Cortex. *J Neurosci* 30, 4833–4844.
- Jouannet, S., Saint-pol, J., and Fernandez, L. (2015). TspanC8 tetraspanins differentially regulate the cleavage of ADAM10 substrates , Notch activation and ADAM10 membrane compartmentalization. *Cell Mol Life Sci* 73, 1895–1915.
- Kagan, A., Feld, S., Chemke, J., and Bar-Khayim, Y. (1988). Occurrence of Hereditary Nephritis, Pretibial Epidermolysis bullosa and Beta-Thalassemia minor in Two Siblings with End-Stage Renal Disease. *Nephron* 49, 331–332.
- Kajiwara, K., Berson, E.L., and Dryja, T.P. (1994). Digenic retinitis pigmentosa due to mutations at the unlinked peripherin/RDS and ROM1 loci. *Science* 264, 1604–1608.
- Kalvodova, L., Kahya, N., Schwille, P., Eehalt, R., Verkade, P., Drechsel, D., and Simons, K. (2005). Lipids as modulators of proteolytic activity of BACE: Involvement of cholesterol, glycosphingolipids, and anionic phospholipids in vitro. *J Biol Chem* 280, 36815–36823.

- Kärkkäinen, I., Rybnikova, E., Pelto-Huikko, M., and Huovila, A.-P.J.** (2000). Metalloprotease-Disintegrin (ADAM) Genes Are Widely and Differentially Expressed in the Adult CNS. Mol Cell Neurosci *15*, 547–560.
- Kashef, J., Diana, T., Oelgeschläger, M., and Nazarenko, I.** (2013). Expression of the tetraspanin family members Tspan3, Tspan4, Tspan5 and Tspan7 during *Xenopus laevis* embryonic development. Gene Expr Patterns *13*, 1–11.
- Kasperek, P., Krausova, M., Haneckova, R., Kriz, V., Zbodakova, O., Korinek, V., and Sedlacek, R.** (2014). Efficient gene targeting of the Rosa26 locus in mouse zygotes using TALE nucleases. FEBS Lett *588*, 3982–3988.
- Katsouri, L., and Georgopoulos, S.** (2011). Lack of LDL Receptor Enhances Amyloid Deposition and Decreases Glial Response in an Alzheimer's Disease Mouse Model. PLoS One *6*, e21880.
- Kim, J., Castellano, J.M., Jiang, H., Basak, J.M., Parsadanian, M., Pham, V., Mason, S.M., Paul, S.M., and Holtzman, D.M.** (2009a). Overexpression of Low-Density Lipoprotein Receptor in the Brain Markedly Inhibits Amyloid Deposition and Increases Extracellular A $\beta$  Clearance. Neuron *64*, 632–644.
- Kim, J., Lilliehook, C., Dudak, A., Prox, J., Saftig, P., Federoff, H.J., and Lim, S.T.** (2010). Activity-dependent alpha-cleavage of nectin-1 is mediated by a disintegrin and metalloprotease 10 (ADAM10). J Biol Chem *285*, 22919–22926.
- Kim, M., Suh, J., Romano, D., Truong, M.H., Mullin, K., Hooli, B., Norton, D., Tesco, G., Elliott, K., Wagner, S.L., et al.** (2009b). Potential late-onset Alzheimer's disease-associated mutations in the ADAM10 gene attenuate alpha-secretase activity. Hum Mol Genet *18*, 3987–3996.
- Kitadokoro, K.** (2001). CD81 extracellular domain 3D structure: insight into the tetraspanin superfamily structural motifs. EMBO J *20*, 12–18.
- Ko, K.S., Arora, P.D., and McCulloch, C.A.G.** (2001). Cadherins Mediate Intercellular Mechanical Signaling in Fibroblasts by Activation of Stretch-sensitive Calcium-permeable Channels. J Biol Chem *276*, 35967–35977.
- Kohl, S., Christ-Adler, M., Apfelstedt-Sylla, E., Kellner, U., Eckstein, A., Zrenner, E., and Wissinger, B.** (1997). RDS/peripherin gene mutations are frequent causes of central retinal dystrophies. J Med Genet *34*, 620–626.
- Kohutek, Z. a, DiPierro, C.G., Redpath, G.T., and Hussaini, I.M.** (2009). ADAM-10-Mediated N-Cadherin Cleavage Is Protein Kinase C- Dependent and Promotes Glioblastoma Cell Migration. J Neurosci *29*, 4605–4615.
- Koike, H., Tomioka, S., Sorimachi, H., Saido, T.C., Maruyama, K., Okoyama, A., Fujisawa-Sehara, A., Ohno, S., Suzuki, K., and Ishiura, S.** (1999). Membrane-anchored metalloprotease MDC9 has an  $\alpha$ -secretase activity responsible for processing the amyloid precursor protein. Biochem J *343*, 371–375.



- Kojro, E., Gimpl, G., Lammich, S., Marz, W., and Fahrenholz, F.** (2001). Low cholesterol stimulates the nonamyloidogenic pathway by its effect on the alpha -secretase ADAM 10. Proc Natl Acad Sci U S A *98*, 5815–5820.
- Kojro, E., Fuger, P., Prinzen, C., Kanarek, A.M., Rat, D., Endres, K., Fahrenholz, F., and Postina, R.** (2010). Statins and the squalene synthase inhibitor zaragozic acid stimulate the non-amyloidogenic pathway of amyloid-beta protein precursor processing by suppression of cholesterol synthesis. J Alzheimers Dis *20*, 1215–1231.
- Koo, E.H., and Squazzo, S.L.** (1994). Evidence that production and release of amyloid beta-protein involves the endocytic pathway. J Biol Chem *269*, 17386–17389.
- Kozik, P., Francis, R.W., Seaman, M.N.J., and Robinson, M.S.** (2010). A Screen for Endocytic Motifs. Traffic *11*, 843–855.
- Kuhn, P., Colombo, A.V., Schusser, B., Drey Mueller, D., Wetzels, S., Schepers, U., Herber, J., Ludwig, A., Kremmer, E., Montag, D., et al.** (2016). Systematic substrate identification indicates a central role for the metalloprotease ADAM10 in axon targeting and synapse function. Elife *5*, x.
- Kuhn, P.-H., Wang, H., Dislich, B., Colombo, A., Zeitschel, U., Ellwart, J.W., Kremmer, E., Rossner, S., and Lichtenthaler, S.F.** (2010). ADAM10 is the physiologically relevant, constitutive alpha-secretase of the amyloid precursor protein in primary neurons. EMBO J *29*, 3020–3032.
- Kuro-o, M., Matsumura, Y., Aizawa, H., Kawaguchi, H., Suga, T., Utsugi, T., Ohyama, Y., Kurabayashi, M., Kaname, T., Kume, E., et al.** (1997). Mutation of the mouse klotho gene leads to a syndrome resembling ageing. Nature *390*, 45–51.
- Kwon, H.Y., Bajaj, J., Ito, T., Blevins, A., Konuma, T., Weeks, J., Lytle, N.K., Koechlein, C.S., Rizzieri, D., Chuah, C., et al.** (2015). Tetraspanin 3 Is Required for the Development and Propagation of Acute Myelogenous Leukemia. Cell Stem Cell *17*, 152–164.
- Laemmli, U.K.** (1970). Cleavage of Structural Proteins during the Assembly of the Head of Bacteriophage T4. Nature *227*, 680–685.
- Lagaudriere-Gesbert, C., Naour, F. Le, Lebel-Binay, S., Billard, M., Lemichez, E., Boquet, P., Boucheix, C., Conjeaud, H., and Rubinstein, E.** (1997). Functional Analysis of Four Tetraspans, CD9, CD53, CD81, and CD82, Suggests a Common Role in Costimulation, Cell Adhesion, and Migration: Only CD9 Upregulates HB-EGF Activity. Cell Immunol *182*, 105–112.
- Lambaerts, K., Van Dyck, S., Mortier, E., Ivarsson, Y., Degeest, G., Luyten, A., Vermeiren, E., Peers, B., David, G., and Zimmermann, P.** (2012). Syntenin, a syndecan adaptor and an Arf6 phosphatidylinositol 4,5-bisphosphate effector, is essential for epiboly and gastrulation cell movements in zebrafish. J Cell Sci *125*, 1129–1140.

- Lammich, S., Kojro, E., Postina, R., Gilbert, S., Pfeiffer, R., Jasionowski, M., Haass, C., and Fahrenholz, F.** (1999). Constitutive and regulated alpha-secretase cleavage of Alzheimer's amyloid precursor protein by a disintegrin metalloprotease. Proc Natl Acad Sci U S A *96*, 3922–3927.
- Lashley, T., Revesz, T., Plant, G., Bandopadhyay, R., Lees, A.J., Frangione, B., Wood, N.W., de Silva, R., Ghiso, J., Rostagno, A., et al.** (2008). Expression of BRI2 mRNA and protein in normal human brain and familial British dementia: its relevance to the pathogenesis of disease. Neuropathol Appl Neurobiol *34*, 492–505.
- Latysheva, N., Muratov, G., Rajesh, S., Padgett, M., Hotchin, N.A., Overduin, M., and Berditchevski, F.** (2006). Syntenin-1 Is a New Component of Tetraspanin-Enriched Microdomains: Mechanisms and Consequences of the Interaction of Syntenin-1 with CD63. Mol Cell Biol *26*, 7707–7718.
- Laurén, J., Gimbel, D.A., Nygaard, H.B., Gilbert, J.W., and Strittmatter, S.M.** (2009). Cellular prion protein mediates impairment of synaptic plasticity by amyloid-beta oligomers. Nature *457*, 1128–1132.
- Lendeckel, U., Kohl, J., Arndt, M., Carl-McGrath, S., Donat, H., and Röcken, C.** (2005). Increased expression of ADAM family members in human breast cancer and breast cancer cell lines. J Cancer Res Clin Oncol *131*, 41–48.
- Levy, S., and Shoham, T.** (2005). The tetraspanin web modulates immune-signalling complexes. Nat Rev Immunol *5*, 136–148.
- Litterst, C., Georgakopoulos, A., Shioi, J., Ghersi, E., Wisniewski, T., Wang, R., Ludwig, A., and Robakis, N.K.** (2007). Ligand binding and calcium influx induce distinct ectodomain/gamma-secretase-processing pathways of EphB2 receptor. J Biol Chem *282*, 16155–16163.
- Lo, A.C., Haass, C., Wagner, S.L., Teplow, D.B., and Sisodia, S.S.** (1994). Metabolism of the "Swedish" amyloid precursor protein variant in Madin-Darby canine kidney cells. J Biol Chem *269*, 30966–30973.
- López-Otín, C., and Bond, J.S.** (2008). Proteases: Multifunctional enzymes in life and disease. J Biol Chem *283*, 30433–30437.
- López-Otín, C., and Matrisian, L.M.** (2007). Emerging roles of proteases in tumour suppression. Nat Rev Cancer *7*, 800–808.
- Lopez-Perez, E., Seidah, N.G., and Checler, F.** (1999). Proprotein convertase activity contributes to the processing of the Alzheimer's  $\beta$ -amyloid precursor protein in human cells: Evidence for a role of the prohormone convertase PC7 in the constitutive  $\alpha$ -secretase pathway. J Neurochem *73*, 2056–2062.
- Lorenzen, I., Trad, A., and Grötzinger, J.** (2011). Multimerisation of A disintegrin and metalloprotease protein-17 (ADAM17) is mediated by its EGF-like domain. Biochem Biophys Res Commun *415*, 330–336.

- Lorenzen, I., Lokau, J., Düsterhöft, S., Trad, A., Garbers, C., Scheller, J., Rose-John, S., and Grötzinger, J. (2012). The membrane-proximal domain of A Disintegrin and Metalloprotease 17 (ADAM17) is responsible for recognition of the interleukin-6 receptor and interleukin-1 receptor II. FEBS Lett 586, 1093–1100.
- Lum, L., Reid, M.S., and Blobel, C.P. (1998). Intracellular maturation of the mouse metalloprotease disintegrin MDC15. J Biol Chem 273, 26236–26247.
- Luo, Y., Bolon, B., Kahn, S., Bennett, B.D., Babu-Khan, S., Denis, P., Fan, W., Kha, H., Zhang, J., Gong, Y., et al. (2001). Mice deficient in BACE1, the Alzheimer's  $\beta$ -secretase, have normal phenotype and abolished  $\beta$ -amyloid generation. Nat Neurosci 4, 231–232.
- Lyons, A., Lynch, A.M., Downer, E.J., Hanley, R., O'Sullivan, J.B., Smith, A., and Lynch, M.A. (2009). Fractalkine-induced activation of the phosphatidylinositol-3 kinase pathway attenuates microglial activation *in vivo* and *in vitro*. J Neurochem 110, 1547–1556.
- Malinverno, M., Carta, M., Epis, R., Marcello, E., Verpelli, C., Cattabeni, F., Sala, C., Mülle, C., Di Luca, M., and Gardoni, F. (2010). Synaptic localization and activity of ADAM10 regulate excitatory synapses through N-cadherin cleavage. J Neurosci 30, 16343–16355.
- Maness, P.F., and Schachner, M. (2007). Neural recognition molecules of the immunoglobulin superfamily: signaling transducers of axon guidance and neuronal migration. Nat Neurosci 10, 19–26.
- Mann, B., Gelos, M., Siedow, A., Hanski, M.L., Gratchev, A., Ilyas, M., Bodmer, W.F., Moyer, M.P., Riecken, E.O., Buhr, H.J., et al. (1999). Target genes of beta-catenin-T cell-factor/lymphoid-enhancer-factor signaling in human colorectal carcinomas. Proc Natl Acad Sci U S A 96, 1603–1608.
- Marcello, E., Gardoni, F., Mauceri, D., Romorini, S., Jeromin, A., Epis, R., Borroni, B., Cattabeni, F., Sala, C., Padovani, A., et al. (2007). Synapse-Associated Protein-97 Mediates -Secretase ADAM10 Trafficking and Promotes Its Activity. J Neurosci 27, 1682–1691.
- Marcello, E., Gardoni, F., Di Luca, M., and Pérez-Otan, I. (2010). An arginine stretch limits ADAM10 exit from the endoplasmic reticulum. J Biol Chem 285, 10376–10384.
- Marcello, E., Saraceno, C., Musardo, S., Vara, H., De La Fuente, A.G., Pelucchi, S., Di Marino, D., Borroni, B., Tramontano, A., Pérez-Otaño, I., et al. (2013). Endocytosis of synaptic ADAM10 in neuronal plasticity and Alzheimer's disease. J Clin Invest 123, 2523–2538.
- Marcinkiewicz, M., and Seidah, N.G. (2000). Coordinated expression of  $\beta$ -amyloid precursor protein and the putative  $\beta$ -secretase BACE and  $\alpha$ -secretase ADAM10 in mouse and human brain. J Neurochem 75, 2133–2143.
- Maretzky, T., Schulte, M., Ludwig, A., Rose-John, S., Blobel, C., Hartmann, D., Altevogt, P., Saftig, P., and Reiss, K. (2005). L1 is sequentially processed by two differently activated metalloproteases and presenilin/gamma-secretase and regulates neural cell adhesion, cell migration, and neurite outgrowth. Mol Cell Biol 25, 9040–9053.

- Martin, L., Fluhrer, R., Reiss, K., Kremmer, E., Saftig, P., and Haass, C.** (2008). Regulated intramembrane proteolysis of Bri2 (Itm2b) by ADAM10 and SPPL2a/SPPL2b. *J Biol Chem* 283, 1644–1652.
- Mattila, P.K., Feest, C., Depoil, D., Treanor, B., Montaner, B., Otipoby, K.L., Carter, R., Justement, L.B., Bruckbauer, A., and Batista, F.D.** (2013). The Actin and Tetraspanin Networks Organize Receptor Nanoclusters to Regulate B Cell Receptor-Mediated Signaling. *Immunity* 38, 461–474.
- Mattson, M.P., Cheng, B., Culwell, A.R., Esch, F.S., Lieberburg, I., and Rydel, R.E.** (1993). Evidence for excitoprotective and intraneuronal calcium-regulating roles for secreted forms of the  $\beta$ -amyloid precursor protein. *Neuron* 10, 243–254.
- McGeer, P.L., and McGeer, E.G.** (2007). NSAIDs and Alzheimer disease: Epidemiological, animal model and clinical studies. *Neurobiol Aging* 28, 639–647.
- Mendez, P., Roo, M. De, Poglia, L., Klauser, P., and Muller, D.** (2010). N-cadherin mediates plasticity-induced long-term spine stabilization. *J Cell Biol* 189, 589–600.
- Metzelaar, M.J., Wijngaard, P.L.J., Peters, P.J., Sixma, J.J., Nieuwenhuis, H.K., and Clevers, H.C.** (1991). CD63 antigen: A novel lysosomal membrane glycoprotein, cloned by a screening procedure for intracellular antigens in eukaryotic cells. *J Biol Chem* 266, 3239–3245.
- Meuleman, P., Hesselgesser, J., Paulson, M., Vanwolleghem, T., Desombere, I., Reiser, H., and Leroux-Roels, G.** (2008). Anti-CD81 antibodies can prevent a hepatitis C virus infection in vivo. *Hepatology* 48, 1761–1768.
- Mizoguchi, A., Nakanishi, H., Kimura, K., Matsubara, K., Ozaki-Kuroda, K., Katata, T., Honda, T., Kiyohara, Y., Heo, K., Higashi, M., et al.** (2002). Nectin: an adhesion molecule involved in formation of synapses. *J Cell Biol* 156, 555–565.
- Morel, E., Chamoun, Z., Lasiacka, Z.M., Chan, R.B., Williamson, R.L., Vetanovetz, C., Dall’Armi, C., Simoes, S., Point Du Jour, K.S., McCabe, B.D., et al.** (2013). Phosphatidylinositol-3-phosphate regulates sorting and processing of amyloid precursor protein through the endosomal system. *Nat Commun* 4, 2250.
- Morganti, J.M., Nash, K.R., Grimmig, B.A., Ranjit, S., Small, B., Bickford, P.C., and Gemma, C.** (2012). The Soluble Isoform of CX3CL1 Is Necessary for Neuroprotection in a Mouse Model of Parkinson’s Disease. *J Neurosci* 32, 14592–14601.
- Moss, M.L., Bomar, M., Liu, Q., Sage, H., Dempsey, P., Lenhart, P.M., Gillispie, P.A., Stoeck, A., Wildeboer, D., Bartsch, J.W., et al.** (2007). The ADAM10 prodomain is a specific inhibitor of ADAM10 proteolytic activity and inhibits cellular shedding events. *J Biol Chem* 282, 35712–35721.
- Mueller-Stainer, S., Zhou, Y., Arai, H., Roberson, E.D., Sun, B., Chen, J., Wang, X., Yu, G., Esposito, L., Mucke, L., et al.** (2006). Anti-amyloidogenic and Neuroprotective Functions of Cathepsin B: Implications for Alzheimer’s Disease. *Neuron* 51, 703–714.

- Mullan, M., Crawford, F., Axelman, K., Houlden, H., Lilius, L., Winblad, B., and Lannfelt, L.** (1992). A pathogenic mutation for probable Alzheimer's disease in the APP gene at the N-terminus of beta-amyloid. *Nat Genet* *1*, 345–347.
- Munro, K.M., Nash, A., Pignoni, M., Lichtenthaler, S.F., and Gunnensen, J.M.** (2016). Functions of the Alzheimer's Disease Protease BACE1 at the Synapse in the Central Nervous System. *J Mol Neurosci* *60*, 305–315.
- Murayama, Y., Oritani, K., and Tsutsui, S.** (2015). Novel CD9-targeted therapies in gastric cancer. *World J Gastroenterol* *21*, 3206–3213.
- Nakamoto, T., Murayama, Y., Oritani, K., Boucheix, C., Rubinstein, E., Nishida, M., Katsube, F., Watabe, K., Kiso, S., Tsutsui, S., et al.** (2009). A novel therapeutic strategy with anti-CD9 antibody in gastric cancers. *J Gastroenterol* *44*, 889–896.
- Naus, S., Reipschläger, S., Wildeboer, D., Lichtenthaler, S.F., Mitterreiter, S., Guan, Z., Moss, M.L., and Bartsch, J.W.** (2006). Identification of candidate substrates for ectodomain shedding by the metalloprotease-disintegrin ADAM8. *Biol Chem* *387*, 337–346.
- Neumann, S., Schöbel, S., Jäger, S., Trautwein, A., Haass, C., Pietrzik, C.U., and Lichtenthaler, S.F.** (2006). Amyloid precursor-like protein 1 influences endocytosis and proteolytic processing of the amyloid precursor protein. *J Biol Chem* *281*, 7583–7594.
- van Niel, G.** (2006). Exosomes: A Common Pathway for a Specialized Function. *J Biochem* *140*, 13–21.
- van Niel, G., Charrin, S., Simoes, S., Romao, M., Rochin, L., Saftig, P., Marks, M.S., Rubinstein, E., and Raposo, G.** (2011). The Tetraspanin CD63 Regulates ESCRT-Independent and -Dependent Endosomal Sorting during Melanogenesis. *Dev Cell* *21*, 708–721.
- Nishiuchi, R., Sanzen, N., Nada, S., Sumida, Y., Wada, Y., Okada, M., Takagi, J., Hasegawa, H., and Sekiguchi, K.** (2005). Potentiation of the ligand-binding activity of integrin alpha3beta1 via association with tetraspanin CD151. *Proc Natl Acad Sci U S A* *102*, 1939–1944.
- Nordstedt, C., Caporaso, G.L., Thyberg, J., Gandy, S.E., and Greengard, P.** (1993). Identification of the Alzheimer  $\beta$ /A4 amyloid precursor protein in clathrin-coated vesicles purified from PC12 cells. *J Biol Chem* *268*, 608–612.
- Noy, P.J., Yang, J., Reyat, J.S., Matthews, A.L., Charlton, A.E., Furnston, J., Rogers, D.A., Rainger, G.E., and Tomlinson, M.G.** (2016). TspanC8 Tetraspanins and A Disintegrin and Metalloprotease 10 (ADAM10) Interact Via Their Extracellular Regions: Evidence For Distinct Binding Mechanisms For Different TspanC8s. *J Biol Chem* *291*, 3145–3157.
- O'Brien, R.J., and Wong, P.C.** (2011). Amyloid precursor protein processing and Alzheimer's disease. *Annu Rev Neurosci* *34*, 185–204.

- Odintsova, E., Butters, T.D., Monti, E., Sprong, H., van Meer, G., and Berditchevski, F.** (2006). Gangliosides play an important role in the organization of CD82-enriched microdomains. Biochem J *400*, 315–325.
- Ohno, M., Chang, L., Tseng, W., Oakley, H., Citron, M., Klein, W.L., Vassar, R., and Disterhoft, J.F.** (2006). Temporal memory deficits in Alzheimer's mouse models: Rescue by genetic deletion of BACE1. Eur J Neurosci *23*, 251–260.
- Ohno, M., Cole, S.L., Yasvoina, M., Zhao, J., Citron, M., Berry, R., Disterhoft, J.F., and Vassar, R.** (2007). BACE1 gene deletion prevents neuron loss and memory deficits in 5XFAD APP/PS1 transgenic mice. Neurobiol Dis *26*, 134–145.
- Ohtsuka, T., Ishibashi, M., Rald Gradwohl, G., Nakanishi, S., Guillemot, F.O., and Kageyama, R.** (1999). Hes1 and Hes5 as Notch effectors in mammalian neuronal differentiation. EMBO J *18*, 2196–2207.
- Olmsted, J.B., Carlson, K., Klebe, R., Ruddle, F., and Rosenbaum, J.** (1970). Isolation of microtubule protein from cultured mouse neuroblastoma cells. Proc Natl Acad Sci U S A *65*, 129–136.
- Olsen, E.A., Weed, W.W., Meyer, C.J., and Cobo, L.M.** (1989). A double-blind, placebo-controlled trial of acitretin for the treatment of psoriasis. J Am Acad Dermatol *21*, 681–686.
- Ortman, J.M., Velkof, V.A., and Hogan, H.** (2014). An Aging Nation: The Older Population in the United States, current population reports.
- Parkin, E., and Harris, B.** (2009). A disintegrin and metalloproteinase (ADAM)-mediated ectodomain shedding of ADAM10. J Neurochem *108*, 1464–1479.
- Parvathy, S., Hussain, I., Karran, E.H., Turner, A.J., and Hooper, N.M.** (1999). Cleavage of Alzheimer's Amyloid Precursor Protein by  $\alpha$ -Secretase Occurs at the Surface of Neuronal Cells. Biochemistry *38*, 9728–9734.
- Paudel, S., Kim, Y.-H., Huh, M.-I., Kim, S.-J., Chang, Y., Park, Y.J., Lee, K.W., and Jung, J.-C.** (2013). ADAM10 mediates N-cadherin ectodomain shedding during retinal ganglion cell differentiation in primary cultured retinal cells from the developing chick retina. J Cell Biochem *114*, 942–954.
- Perez, R.G., Soriano, S., Hayes, J.D., Ostaszewski, B., Xia, W., Selkoe, D.J., Chen, X., Stokin, G.B., and Koo, E.H.** (1999). Mutagenesis identifies new signals for beta-amyloid precursor protein endocytosis, turnover, and the generation of secreted fragments, including Abeta42. J Biol Chem *274*, 18851–18856.
- Pols, M.S., and Klumperman, J.** (2009). Trafficking and function of the tetraspanin CD63. Exp Cell Res *315*, 1584–1592.

- Postina, R., Schroeder, A., Dewachter, I., Bohl, J., Schmitt, U., Kojro, E., Prinzen, C., Endres, K., Hiemke, C., Blessing, M., et al. (2004). A disintegrin-metalloproteinase prevents amyloid plaque formation and hippocampal defects in an Alzheimer disease mouse model. *J Clin Invest* *113*, 1456–1464.
- Poulsen, E., Larsen, A., Zollo, A., Jørgensen, A., Sanggaard, K., Enghild, J., and Matrone, C. (2015). New Insights to Clathrin and Adaptor Protein 2 for the Design and Development of Therapeutic Strategies. *Int J Mol Sci* *16*, 29446–29453.
- Prinzen, C., Müller, U., Endres, K., Fahrenholz, F., and Postina, R. (2005). Genomic structure and functional characterization of the human ADAM10 promoter. *FASEB J* *19*, 1522–1524.
- Prox, J., Willenbrock, M., Weber, S., Lehmann, T., Schmidt-Arras, D., Schwanbeck, R., Saftig, P., and Schwake, M. (2012). Tetraspanin15 regulates cellular trafficking and activity of the ectodomain sheddase ADAM10. *Cell Mol Life Sci* *69*, 2919–2932.
- Prox, J., Bernreuther, C., Altmepfen, H., Grendel, J., Glatzel, M., D’Hooge, R., Stroobants, S., Ahmed, T., Balschun, D., Willem, M., et al. (2013). Postnatal Disruption of the Disintegrin/Metalloproteinase ADAM10 in Brain Causes Epileptic Seizures, Learning Deficits, Altered Spine Morphology, and Defective Synaptic Functions. *J Neurosci* *33*, 12915–12928.
- Puente, X.S., and Lo, C. (2004). A Genomic Analysis of Rat Proteases and Protease Inhibitors. *Genome Res* *14*, 609–622.
- Puls, K.L., and Wright, M.D. (2000). The molecular characterisation of mouse tspan-3. *DNA Seq* *11*, 271–275.
- Radice, G.L., Rayburn, H., Matsunami, H., Knudsen, K.A., Takeichi, M., and Hynes, R.O. (1997). Developmental defects in mouse embryos lacking N-cadherin. *Dev Biol* *181*, 64–78.
- Rajendran, L., Honsho, M., Zahn, T.R., Keller, P., Geiger, K.D., Verkade, P., and Simons, K. (2006). Alzheimer’s disease beta-amyloid peptides are released in association with exosomes. *Proc Natl Acad Sci* *103*, 11172–11177.
- Rawlings, N.D., and Barrett, A.J. (1995). Evolutionary families of Peptidases. *Methods Enzymol* *248*, 183–228.
- Reinhardt, S., Schuck, F., Grosgen, S., Riemenschneider, M., Hartmann, T., Postina, R., Grimm, M., and Endres, K. (2014). Unfolded protein response signaling by transcription factor XBP-1 regulates ADAM10 and is affected in Alzheimer’s disease. *FASEB J* *28*, 978–997.
- Reiss, K., and Saftig, P. (2009). The “A Disintegrin And Metalloprotease” (ADAM) family of sheddases: Physiological and cellular functions. *Semin Cell Dev Biol* *20*, 126–137.

- Reiss, K., Maretzky, T., Ludwig, A., Tousseyn, T., de Strooper, B., Hartmann, D., and Saftig, P.** (2005). ADAM10 cleavage of N-cadherin and regulation of cell-cell adhesion and beta-catenin nuclear signalling. *EMBO J* 24, 742–752.
- Reiss, K., Maretzky, T., Haas, I.G., Schulte, M., Ludwig, A., Frank, M., and Saftig, P.** (2006). Regulated ADAM10-dependent ectodomain shedding of gamma-protocadherin C3 modulates cell-cell adhesion. *J Biol Chem* 281, 21735–21744.
- Riethmueller, S., Ehlers, J.C., Lokau, J., Düsterhöft, S., Knittler, K., Dombrowsky, G., Grötzinger, J., Rabe, B., Rose-John, S., and Garbers, C.** (2016). Cleavage Site Localization Differentially Controls Interleukin-6 Receptor Proteolysis by ADAM10 and ADAM17. *Sci Rep* 6, 25550.
- Rikimaru, A., Komori, K., Sakamoto, T., Ichise, H., Yoshida, N., Yana, I., and Seiki, M.** (2007). Establishment of an MT4-MMP-deficient mouse strain representing an efficient tracking system for MT4-MMP/MMP-17 expression in vivo using  $\beta$ -galactosidase. *Genes to Cells* 12, 1091–1100.
- Robak, T., Robak, P., and Smolewski, P.** (2009). TRU-016, a humanized anti-CD37 IgG fusion protein for the potential treatment of B-cell malignancies. *Curr Opin Investig Drugs* 10, 1383–1390.
- Robak, T., Hellmann, A., Kloczko, J., Loscertales, J., Lech-Maranda, E., Pagel, J.M., Mato, A., Byrd, J.C., Awan, F.T., Hebart, H., et al.** (2017). Randomized phase 2 study of otlertuzumab and bendamustine versus bendamustine in patients with relapsed chronic lymphocytic leukaemia. *Br J Haematol* 176, 618–628.
- Roghani, M., Becherer, J.D., Moss, M.L., Atherton, R.E., Erdjument-Bromage, H., Arribas, J., Blackburn, R.K., Weskamp, G., Tempst, P., and Blobel, C.P.** (1999). Metalloprotease-disintegrin MDC9: Intracellular maturation and catalytic activity. *J Biol Chem* 274, 3531–3540.
- Rous, B.A., Reaves, B.J., Ihrke, G., Briggs, J.A.G., Gray, S.R., Stephens, D.J., Banting, G., and Luzio, J.P.** (2002). Role of Adaptor Complex AP-3 in Targeting Wild-Type and Mutated CD63 to Lysosomes. *Mol Biol Cell* 13, 1071–1082.
- Rovelet-Lecrux, A., Hannequin, D., Raux, G., Meur, N. Le, Laquerrière, A., Vital, A., Dumanchin, C., Feuillette, S., Brice, A., Vercelletto, M., et al.** (2006). APP locus duplication causes autosomal dominant early-onset Alzheimer disease with cerebral amyloid angiopathy. *Nat Genet* 38, 24–26.
- Rubinstein, E., Naour, F. Le, Lagaudrière-Gesbert, C., Billard, M., Conjeaud, H., and Boucheix, C.** (1996). CD9, CD63, CD81, and CD82 are components of a surface tetraspan network connected to HLA-DR and VLA integrins. *Eur J Immunol* 26, 2657–2665.
- Sabuncu, M.R.** (2011). The Dynamics of Cortical and Hippocampal Atrophy in Alzheimer Disease. *Arch Neurol* 68, 1040.
- Saftig, P., and Lichtenthaler, S.F.** (2015). The alpha secretase ADAM10: A metalloprotease with multiple functions in the brain. *Prog Neurobiol* 135, 1–20.



- Saftig, P., and Reiss, K.** (2011). The “A Disintegrin And Metalloproteases” ADAM10 and ADAM17: Novel drug targets with therapeutic potential? *Eur J Cell Biol* *90*, 527–535.
- Saglietti, L., Dequidt, C., Kamieniarz, K., Rousset, M.-C., Valnegri, P., Thoumine, O., Beretta, F., Fagni, L., Choquet, D., Sala, C., et al.** (2007). Extracellular Interactions between GluR2 and N-Cadherin in Spine Regulation. *Neuron* *54*, 461–477.
- Sakry, D., Neitz, A., Singh, J., Frischknecht, R., Marongiu, D., Binamé, F., Perera, S.S., Endres, K., Lutz, B., Radyushkin, K., et al.** (2014). Oligodendrocyte Precursor Cells Modulate the Neuronal Network by Activity-Dependent Ectodomain Cleavage of Glial NG2. *PLoS Biol* *12*, e1001993.
- Sandbrink, R., Masters, C.L., and Beyreuther, K.** (1996). APP Gene Family Alternative Splicing Generates Functionally Related Isoforms. *Ann N Y Acad Sci* *777*, 281–287.
- Sanger, F., Nicklen, S., and Coulson, a R.** (1977). DNA sequencing with chain-terminating inhibitors. *Proc Natl Acad Sci* *74*, 5463–5467.
- Saraceno, C., Marcello, E., Di Marino, D., Borroni, B., Claeysen, S., Perroy, J., Padovani, A., Tramontano, A., Gardoni, F., and Di Luca, M.** (2014). SAP97-mediated ADAM10 trafficking from Golgi outposts depends on PKC phosphorylation. *Cell Death Dis* *5*, e1547.
- Scheuner, D., Eckman, C., Jensen, M., Song, X., Citron, M., Suzuki, N., Bird, T.D., Hardy, J., Hutton, M., Kukull, W., et al.** (1996). Secreted amyloid beta-protein similar to that in the senile plaques of Alzheimer’s disease is increased in vivo by the presenilin 1 and 2 and APP mutations linked to familial Alzheimer’s disease. *Nat Med* *2*, 864–870.
- Schlomann, U., Wildeboer, D., Webster, A., Antropova, O., Zeuschner, D., Knight, C.G., Docherty, A.J.P., Lambert, M., Skelton, L., Jockusch, H., et al.** (2002). The Metalloprotease Disintegrin ADAM8: Processing by autocatalysis is required for proteolytic activity and cell adhesion. *J Biol Chem* *277*, 48210–48219.
- Schöbel, S., Neumann, S., Seed, B., and Lichtenthaler, S.F.** (2006). Expression cloning screen for modifiers of amyloid precursor protein shedding. *Int J Dev Neurosci* *24*, 141–148.
- Schroder, J., Lullmann-Rauch, R., Himmerkus, N., Pleines, I., Nieswandt, B., Orinska, Z., Koch-Nolte, F., Schroder, B., Bleich, M., and Saftig, P.** (2009). Deficiency of the Tetraspanin CD63 Associated with Kidney Pathology but Normal Lysosomal Function. *Mol Cell Biol* *29*, 1083–1094.
- Schroeter, E.H., Kisslinger, J.A., and Kopan, R.** (1998). Notch-1 signalling requires ligand-induced proteolytic release of intracellular domain. *Nature* *393*, 382–386.
- Seals, D.F., and Courtneidge, S. a** (2003). The ADAMs family of metalloproteases: Multidomain proteins with multiple functions. *Genes Dev* *17*, 7–30.
- Seemüller, E., Lupas, a, Stock, D., Löwe, J., Huber, R., and Baumeister, W.** (1995). Proteasome from *Thermoplasma acidophilum*: a threonine protease. *Science* *268*, 579–582.

- Seigneuret, M., Delaguillaumie, A., Lagaudrière-Gesbert, C., and Conjeaud, H.** (2001). Structure of the tetraspanin main extracellular domain: A partially conserved fold with a structurally variable domain insertion. *J Biol Chem* 276, 40055–40064.
- Seipold, L., Damme, M., Prox, J., Rabe, B., Kasperek, P., Sedlacek, R., Altmeppen, H., Willem, M., Boland, B., Glatzel, M., et al.** (2017). Tetraspanin 3: A central endocytic membrane component regulating the expression of ADAM10, presenilin and the amyloid precursor protein. *Biochim Biophys Acta - Mol Cell Res* 1864, 217–230.
- Shepherd, J.D., and Huganir, R.L.** (2007). The Cell Biology of Synaptic Plasticity: AMPA Receptor Trafficking. *Annu Rev Cell Dev Biol* 23, 613–643.
- Shtutman, M., Zhurinsky, J., Simcha, I., Albanese, C., D'Amico, M., Pestell, R., and Ben-Ze'ev, A.** (1999). The cyclin D1 gene is a target of the  $\beta$ -catenin/LEF-1 pathway. *Proc Natl Acad Sci* 96, 5522–5527.
- Shukla, D., Scanlan, P.M., Tiwari, V., Sheth, V., Clement, C., Guzman-Hartman, G., Dermody, T.S., and Valyi-Nagy, T.** (2006). Expression of Nectin-1 in Normal and Herpes Simplex Virus Type 1-Infected Murine Brain. *Appl Immunohistochem Mol Morphol* 14, 341–347.
- Sinha, S., Anderson, J.P., Barbour, R., Basi, G.S., Caccavello, R., Davis, D., Doan, M., Dovey, H.F., Frigon, N., Hong, J., et al.** (1999). Purification and cloning of amyloid precursor protein beta-secretase from human brain. *Nature* 402, 537–540.
- Sisodia, S.S.** (1995). Characterization of Sorting Signals in the beta-Amyloid Precursor Protein Cytoplasmic Domain. *J Biol Chem* 270, 3565–3573.
- Slack, B.E., Ma, L.K., and Seah, C.C.** (2001). Constitutive shedding of the amyloid precursor protein ectodomain is up-regulated by tumour necrosis factor- $\alpha$  converting enzyme. *Biochem J* 357, 787–794.
- Smith, K.M., Gaultier, A., Cousin, H., Alfandari, D., White, J.M., and DeSimone, D.W.** (2002). The cysteine-rich domain regulates ADAM protease function in vivo. *J Cell Biol* 159, 893–902.
- Van Soest, S., Westerveld, A., De Jong, P.T.V.M., Bleeker-Wagemakers, E.M., and Bergen, A.A.B.** (1999). Retinitis pigmentosa: Defined from a molecular point of view. *Surv Ophthalmol* 43, 321–334.
- Soto, C., and Satani, N.** (2011). The intricate mechanisms of neurodegeneration in prion diseases. *Trends Mol Med* 17, 14–24.
- Srichai, M.B., Colleta, H., Gewin, L., Matrisian, L., Abel, T.W., Koshikawa, N., Seiki, M., Pozzi, A., Harris, R.C., and Zent, R.** (2011). Membrane-Type 4 Matrix Metalloproteinase (MT4-MMP) Modulates Water Homeostasis in Mice. *PLoS One* 6, e17099.
- Steele, A.D., Emsley, J.G., Ozdinler, P.H., Lindquist, S., and Macklis, J.D.** (2006). Prion protein (PrPc) positively regulates neural precursor proliferation during developmental and adult mammalian neurogenesis. *Proc Natl Acad Sci* 103, 3416–3421.

- Stöcker, W., and Bode, W.** (1995). Structural features of a superfamily of zinc-endopeptidases: the metzincins. Curr Opin Struct Biol 5, 383–390.
- Südhof, T.C.** (2008). Neuroligins and neuexins link synaptic function to cognitive disease. Nature 455, 903–911.
- Sue Lee, C., and Koo, J.** (2005). A review of acitretin, a systemic retinoid for the treatment of psoriasis. Expert Opin Pharmacother 6, 1725–1734.
- Suh, J., Choi, S.H., Romano, D.M., Gannon, M. a, Lesinski, A.N., Kim, D.Y., and Tanzi, R.E.** (2013). ADAM10 missense mutations potentiate  $\beta$ -amyloid accumulation by impairing prodomain chaperone function. Neuron 80, 385–401.
- Sung, Y.H., Baek, I.-J., Kim, D.H., Jeon, J., Lee, J., Lee, K., Jeong, D., Kim, J.-S., and Lee, H.-W.** (2013). Knockout mice created by TALEN-mediated gene targeting. Nat Biotechnol 31, 23–24.
- Suyama, K., Shapiro, I., Guttman, M., and Hazan, R.B.** (2002). A signaling pathway leading to metastasis is controlled by N-cadherin and the FGF receptor. Cancer Cell 2, 301–314.
- Suzuki, K., Hayashi, Y., Nakahara, S., Kumazaki, H., Prox, J., Horiuchi, K., Zeng, M., Tanimura, S., Nishiyama, Y., Osawa, S., et al.** (2012). Activity-Dependent Proteolytic Cleavage of Neuroligin-1. Neuron 76, 410–422.
- Tai, C.Y., Kim, S.A., and Schuman, E.M.** (2008). Cadherins and synaptic plasticity. Curr Opin Cell Biol 20, 567–575.
- Takagi, S., Fujikawa, K., Imai, T., Fukuhara, N., Fukudome, K., Minegishi, M., Tsuchiya, S., Konno, T., Hinuma, Y., and Yoshie, O.** (1995). Identification of a highly specific surface marker of T-cell acute lymphoblastic leukemia and neuroblastoma as a new member of the transmembrane 4 superfamily. Int J Cancer 61, 706–715.
- Takahashi, R.H., Milner, T.A., Li, F., Nam, E.E., Edgar, M.A., Yamaguchi, H., Beal, M.F., Xu, H., Greengard, P., and Gouras, G.K.** (2002). Intraneuronal Alzheimer A $\beta$ 42 Accumulates in Multivesicular Bodies and Is Associated with Synaptic Pathology. Am J Pathol 161, 1869–1879.
- Takeda, S.** (2009). Three-dimensional domain architecture of the ADAM family proteinases. Semin Cell Dev Biol 20, 146–152.
- Takeda, S., Igarashi, T., Mori, H., and Araki, S.** (2006). Crystal structures of VAP1 reveal ADAMs' MDC domain architecture and its unique C-shaped scaffold. EMBO J 25, 2388–2396.
- Takino, T., Miyamori, H., Kawaguchi, N., Uekita, T., Seiki, M., and Sato, H.** (2003). Tetraspanin CD63 promotes targeting and lysosomal proteolysis of membrane-type 1 matrix metalloproteinase. Biochem Biophys Res Commun 304, 160–166.

- Tanaka, S., Shiojiri, S., Takahashi, Y., Kitaguchi, N., Ito, H., Kameyama, M., Kimura, J., Nakamura, S., and Ueda, K.** (1989). Tissue-specific expression of three types of  $\beta$ -protein precursor mRNA: Enhancement of protease inhibitor-harboring types in Alzheimer's disease brain. Biochem Biophys Res Commun *165*, 1406–1414.
- Tanzi, R., Gusella, J., Watkins, P., Bruns, G., St George-Hyslop, P., Van Keuren, M., Patterson, D., Pagan, S., Kurnit, D., and Neve, R.** (1987). Amyloid beta protein gene: cDNA, mRNA distribution, and genetic linkage near the Alzheimer locus. Science (80-) *235*, 880–884.
- Taylor, D.R., and Hooper, N.M.** (2017). Molecular Membrane Biology The prion protein and lipid rafts (Review) The prion protein and lipid rafts (Review).
- Taylor, D.R., Parkin, E.T., Cocklin, S.L., Ault, J.R., Aschcroft, A.E., Turner, A.J., and Hooper, N.M.** (2009). Role of ADAMs in the ectodomain shedding and conformational conversion of the prion protein. J Biol Chem *284*, 22590–22600.
- van Tetering, G., van Diest, P., Verlaan, I., van der Wall, E., Kopan, R., and Vooijs, M.** (2009). Metalloprotease ADAM10 is required for Notch1 site 2 cleavage. J Biol Chem *284*, 31018–31027.
- Thal, D.R., Rüb, U., Orantes, M., and Braak, H.** (2002). Phases of A beta-deposition in the human brain and its relevance for the development of AD. Neurology *58*, 1791–1800.
- Thiede-Stan, N.K., Tews, B., Albrecht, D., Ristic, Z., Ewers, H., and Schwab, M.E.** (2015). Tetraspanin-3 is an organizer of the multi-subunit Nogo-A signaling complex. J Cell Sci *128*, 3583–3596.
- Tippmann, F., Hundt, J., Schneider, A., Endres, K., and Fahrenholz, F.** (2009). Up-regulation of the  $\alpha$ -secretase ADAM10 by retinoic acid receptors and acitretin. FASEB J *23*, 1643–1654.
- Tiwari-Woodruff, S.K., Buznikov, a G., Vu, T.Q., Micevych, P.E., Chen, K., Kornblum, H.I., and Bronstein, J.M.** (2001). OSP/claudin-11 forms a complex with a novel member of the tetraspanin super family and beta1 integrin and regulates proliferation and migration of oligodendrocytes. J Cell Biol *153*, 295–305.
- Todd, S.C., Doctor, V.S., and Levy, S.** (1998). Sequences and expression of six new members of the tetraspanin/TM4SF family. Biochim Biophys Acta *1399*, 101–104.
- Togashi, H., Abe, K., Mizoguchi, A., Takaoka, K., Chisaka, O., and Takeichi, M.** (2002). Cadherin regulates dendritic spine morphogenesis. Neuron *35*, 77–89.
- Tokoro, Y., Shibuya, K., Osawa, M., Tahara-Hanaoka, S., Iwama, A., Kitamura, T., Nakauchi, H., and Shibuya, A.** (2001). Molecular Cloning and Characterization of Mouse Tspan-3, a Novel Member of the Tetraspanin Superfamily, Expressed on Resting Dendritic Cells. Biochem Biophys Res Commun *288*, 178–183.
- Tousseyn, T., Thathiah, A., Jorissen, E., Raemaekers, T., Konietzko, U., Reiss, K., Maes, E., Snellinx, A., Serneels, L., Nyabi, O., et al.** (2009). ADAM10, the Rate-limiting Protease of Regulated Intramembrane Proteolysis of Notch and Other Proteins, Is Processed by ADAMS-9, ADAMS-15, and the -Secretase. J Biol Chem *284*, 11738–11747.

- Trad, A., Hedemann, N., Shomali, M., Pawlak, V., Grötzinger, J., and Lorenzen, I.** (2011). Development of sandwich ELISA for detection and quantification of human and murine a disintegrin and metalloproteinase17. *J Immunol Methods* 371, 91–96.
- Trommald, M., Hulleberg, G., and Andersen, P.** (1996). Long-term potentiation is associated with new excitatory spine synapses on rat dentate granule cells. *Learn Mem* 3, 218–228.
- Tsai, Y.C., and Weissman, A.M.** (2011). Dissecting the diverse functions of the metastasis suppressor CD82/KAI1. *FEBS Lett* 585, 3166–3173.
- Tucher, J., Linke, D., Koudelka, T., Cassidy, L., Tredup, C., Wichert, R., Pietrzik, C., Becker-Pauly, C., and Tholey, A.** (2014). LC-MS based cleavage site profiling of the proteases ADAM10 and ADAM17 using proteome-derived peptide libraries. *J Proteome Res* 13, 2205–2214.
- Turk, B.** (2006). Targeting proteases: successes, failures and future prospects. *Nat Rev Drug Discov* 5, 785–799.
- Um, J.W., Nygaard, H.B., Heiss, J.K., Kostylev, M.A., Stagi, M., Vortmeyer, A., Wisniewski, T., Gunther, E.C., and Strittmatter, S.M.** (2012). Alzheimer amyloid-beta oligomer bound to postsynaptic prion protein activates Fyn to impair neurons. *Nat Neurosci* 15, 1227–1235.
- Vassar, R.** (1999). Beta-Secretase Cleavage of Alzheimer’s Amyloid Precursor Protein by the Transmembrane Aspartic Protease BACE. *Science* (80-) 286, 735–741.
- Vences-Catalán, F., Kuo, C.-C., Sagi, Y., Chen, H., Kela-Madar, N., van Zelm, M.C., van Dongen, J.J.M., and Levy, S.** (2015). A mutation in the human tetraspanin CD81 gene is expressed as a truncated protein but does not enable CD19 maturation and cell surface expression. *J Clin Immunol* 35, 254–263.
- Vidal, R., Frangione, B., Rostagno, A., Mead, S., Revesz, T., Plant, G., and Ghiso, J.** (1999). A stop-codon mutation in the BRI gene associated with familial British dementia. *Nature* 399, 776–781.
- Vidal, R., Revesz, T., Rostagno, A., Kim, E., Holton, J.L., Bek, T., Bojsen-Moller, M., Braendgaard, H., Plant, G., Ghiso, J., et al.** (2000). A decamer duplication in the 3’ region of the BRI gene originates an amyloid peptide that is associated with dementia in a Danish kindred. *Proc Natl Acad Sci U S A* 97, 4920–4925.
- Vincent, B., Paitel, E., Saftig, P., Frobert, Y., Hartmann, D., De Strooper, B., Grassi, J., Lopez-Perez, E., and Checler, F.** (2001). The Disintegrins ADAM10 and TACE Contribute to the Constitutive and Phorbol Ester-regulated Normal Cleavage of the Cellular Prion Protein. *J Biol Chem* 276, 37743–37746.
- Wallenstein, G. V., Eichenbaum, H., and Hasselmo, M.E.** (1998). The hippocampus as an associator of discontinuous events. *Trends Neurosci* 21, 317–323.
- Wang, H.-X., Li, Q., Sharma, C., Knoblich, K., and Hemler, M.E.** (2011). Tetraspanin protein contributions to cancer. *Biochem Soc Trans* 39, 547–552.

- Wang, X., Weiner, J.A., Levi, S., Craig, A.M., Bradley, A., and Sanes, J.R.** (2002). Gamma protocadherins are required for survival of spinal interneurons. *Neuron* 36, 843–854.
- Weber, S., and Saftig, P.** (2012). Ectodomain shedding and ADAMs in development. *Development* 139, 3693–3709.
- Weskamp, G., Cai, H., Brodie, T.A., Higashiyama, S., Manova, K., Ludwig, T., and Blobel, C.P.** (2002). Mice lacking the metalloprotease-disintegrin MDC9 (ADAM9) have no evident major abnormalities during development or adult life. *Mol Cell Biol* 22, 1537–1544.
- van de Wetering, M., Sancho, E., Verweij, C., de Lau, W., Oving, I., Hurlstone, A., van der Horn, K., Batlle, E., Coudreuse, D., Haramis, A.-P., et al.** (2002). The  $\beta$ -Catenin/TCF-4 Complex Imposes a Crypt Progenitor Phenotype on Colorectal Cancer Cells. *Cell* 111, 241–250.
- White, J.M.** (2003). ADAMs: Modulators of cell-cell and cell-matrix interactions. *Curr Opin Cell Biol* 15, 598–606.
- Wilke, G.A., and Wardenburg, J.B.** (2010). Role of a disintegrin and metalloprotease 10 in Staphylococcus aureus -hemolysin-mediated cellular injury. *Proc Natl Acad Sci* 107, 13473–13478.
- Willem, M., Tahirovic, S., Busche, M.A., Ovsepian, S. V., Chafai, M., Kootar, S., Hornburg, D., Evans, L.D.B., Moore, S., Daria, A., et al.** (2015).  $\eta$ -Secretase processing of APP inhibits neuronal activity in the hippocampus. *Nature* 526, 443–447.
- Wolfe, M.S.** (2008). Inhibition and modulation of gamma-secretase for Alzheimer's disease. *Neurotherapeutics* 5, 391–398.
- Wolfsberg, T.G., Straight, P.D., Gerena, R.L., Huovila, A.-P.J., Primakoff, P., Myles, D.G., and White, J.M.** (1995). ADAM, a Widely Distributed and Developmentally Regulated Gene Family Encoding Membrane Proteins with A Disintegrin And Metalloprotease Domain. *Dev Biol* 169, 378–383.
- Xie, Z., Photowala, H., Cahill, M.E., Srivastava, D.P., Woolfrey, K.M., Shum, C.Y., Huganir, R.L., and Penzes, P.** (2008). Coordination of synaptic adhesion with dendritic spine remodeling by AF-6 and kalirin-7. *J Neurosci* 28, 6079–6091.
- Xu, D., Sharma, C., and Hemler, M.E.** (2009). Tetraspanin12 regulates ADAM10-dependent cleavage of amyloid precursor protein. *FASEB J* 23, 3674–3681.
- Yamazaki, T., Koo, E.H., and Selkoe, D.J.** (1996). Trafficking of cell-surface amyloid beta-protein precursor. II. Endocytosis, recycling and lysosomal targeting detected by immunolocalization. *J Cell Sci* 109 ( Pt 5), 999–1008.
- Yan, R., Bienkowski, M.J., Shuck, M.E., Miao, H., Tory, M.C., Pauley, a M., Brashier, J.R., Stratman, N.C., Mathews, W.R., Buhl, a E., et al.** (1999). Membrane-anchored aspartyl protease with Alzheimer's disease beta-secretase activity. *Nature* 402, 533–537.
- Yáñez-Mó, M., Sánchez-Madrid, F., and Cabañas, C.** (2011). Membrane proteases and tetraspanins: Figure 1. *Biochem Soc Trans* 39, 541–546.

- Yang, X.** (2002). Palmitoylation of Tetraspanin Proteins: Modulation of CD151 Lateral Interactions, Subcellular Distribution, and Integrin-dependent Cell Morphology. Mol Biol Cell *13*, 767–781.
- Yauch, R.L.** (2000). Direct Extracellular Contact between Integrin alpha 3beta 1 and TM4SF Protein CD151. J Biol Chem *275*, 9230–9238.
- Yeh, H.-Y., and Klesius, P.H.** (2012). Channel catfish, *Ictalurus punctatus* (Rafinesque), tetraspanin membrane protein family: identification, characterization and phylogenetic analysis of tetraspanin 3 and tetraspanin 7 (CD231) transcripts. Fish Physiol Biochem *38*, 1553–1563.
- Younkin, S.G.** (1998). The role of A $\beta$ 42 in Alzheimer's disease. J Physiol *92*, 289–292.
- Van Zelm, M.C., Smet, J., Adams, B., Mascart, F., Schandené, L., Janssen, F., Ferster, A., Kuo, C.C., Levy, S., Van Dongen, J.J.M., et al.** (2010). CD81 gene defect in humans disrupts CD19 complex formation and leads to antibody deficiency. J Clin Invest *120*, 1265–1274.
- Zemni, R., Bienvenu, T., Vinet, M.C., Sefiani, A., Carrié, A., Billuart, P., McDonnell, N., Couvert, P., Francis, F., Chafey, P., et al.** (2000). A new gene involved in X-linked mental retardation identified by analysis of an X;2 balanced translocation. Nat Genet *24*, 167–170.
- Zhang, Z., Song, M., Liu, X., Su Kang, S., Duong, D.M., Seyfried, N.T., Cao, X., Cheng, L., Sun, Y.E., Ping Yu, S., et al.** (2015). Delta-secretase cleaves amyloid precursor protein and regulates the pathogenesis in Alzheimer's disease. Nat Commun *6*, 8762.
- Zhou, J., Fujiwara, T., Ye, S., Li, X., and Zhao, H.** (2014). Downregulation of Notch Modulators, Tetraspanin 5 and 10, Inhibits Osteoclastogenesis in Vitro. Calcif Tissue Int *95*, 209–217.
- Zhu, X.-C., Tan, L., Wang, H.-F., Jiang, T., Cao, L., Wang, C., Wang, J., Tan, C.-C., Meng, X.-F., and Yu, J.-T.** (2015). Rate of early onset Alzheimer's disease: a systematic review and meta-analysis. Ann Transl Med *3*, 38.
- Zimmerman, B., Kelly, B., McMillan, B.J., Seegar, T.C.M., Dror, R.O., Kruse, A.C., and Blacklow, S.C.** (2016). Crystal Structure of a Full-Length Human Tetraspanin Reveals a Cholesterol-Binding Pocket. Cell *167*, 1041–1051.e11.





## 7 List of Figures and Tables

### List of figures

Fig. 1.1: Structure of A Disintegrin and Metalloproteases (ADAMs).....	3
Fig. 1.2: ADAM10 maturation and ectodomain shedding.....	5
Fig. 1.3: Processing of the amyloid precursor protein. ....	12
Fig. 1.4: Regulation of ADAM10. ....	16
Fig. 1.5: The structure of tetraspanins. ....	18
Fig. 1.6: Phylogenetic tree of the 33 human tetraspanins. ....	19
Fig. 3.1: Breeding strategy for Tspan3 and Tspan15 knockout .....	52
Fig. 4.1: Identification of Tspan3 as an ADAM10 interaction partner in a split-ubiquitin yeast two hybrid screen.....	56
Fig. 4.2: Transiently expressed Tspan3 interacts with ADAM10 but not with ADAM17 in HeLa cells..	58
Fig. 4.3: Tspan3 overexpression does not affect ADAM10 maturation. ....	60
Fig. 4.4: Analysis of the cell surface expression of ADAM10 using cell surface biotinylation.....	61
Fig. 4.5: FACS analysis of ADAM10 cell surface levels.....	62
Fig. 4.6: Tspan3 expression increases the APP-CTF, but has no effect on N-cadherin shedding.....	63
Fig. 4.7: Inhibition of ADAM10 counteracts the Tspan3-induced increase of the APP-CTF.....	65
Fig. 4.8: siRNA-mediated ADAM10 knockdown diminishes the Tspan3 induced increase of the APP-CTF.....	66
Fig. 4.9: Analysis of APP processing in ADAM10- and ADAM17-deficient HEK293 cells.....	67
Fig. 4.10: Expression of Tspan3 in HEK293 APP-wt cells increases APP-CTF and sAPP $\alpha$ levels. ....	68
Fig. 4.11: Tspan3 increases the appearance of the APP fragment C83 and reduces A $\beta$ -levels. ....	69
Fig. 4.12: Tspan3 expression does not inhibit $\gamma$ -secretase activity. ....	70
Fig. 4.13: Tspan3 is mainly localised in endosomal compartments. ....	72
Fig. 4.14: Tspan3 co-localises with endogenous and overexpressed APP in HeLa cells.....	73
Fig. 4.15: Tspan3-myc interacts with APP and presenilin-1. ....	75
Fig. 4.16: Overexpression of Tspan3 increases the surface levels of fl-APP and the APP-CTF.....	76
Fig. 4.17: Tspan3 contains an endocytic sorting motif within its C-terminal tail. ....	77
Fig. 4.18: Comparison of the subcellular localisation of wild-type Tspan3-myc and Tspan3 <sub>Y243A</sub> -myc in HeLa cells. ....	78
Fig. 4.19: Mutation of the Tspan3 endocytic motif “YELL” increases its surface expression.....	79
Fig. 4.20: Expression of Tspan3 <sub>Y243A</sub> -myc increases the surface levels of APP and ADAM10.....	80
Fig. 4.21: siRNA-mediated knockdown of Tspan3 has no apparent effect on ADAM10 and APP. ....	82

Fig. 4.22: Downregulation of Tspan3 has no obvious effects on the transcription levels of TspanC6s, Tspan5 and Tspan12. ....	83
Fig. 4.23: Tspan3 is a glycosylated protein and is most abundantly expressed in the murine brain. ....	85
Fig. 4.24: Tspan3 is expressed in neurons of the murine brain. ....	87
Fig. 4.25: Tspan3 interacts with ADAM10 and APP under endogenous conditions. ....	89
Fig. 4.26: TALEN-mediated knockout of Tspan3 in mice. ....	91
Fig. 4.27: TALEN-mediated knockout of Tspan3 was confirmed in several tissues. ....	92
Fig. 4.28: Loss of Tspan3 has no effect on ADAM10, APP and PrP <sup>c</sup> in eleven-day-old mice. ....	94
Fig. 4.29: Knockout of Tspan3 does not affect ADAM10, APP and PrP <sup>c</sup> in four-week-old mice. ....	95
Fig. 4.30: Tspan3-deficiency increases the transcription level of Tspan5 and Tspan7. ....	96
Fig. 4.31: Expression of Tspan7 mimics the Tspan3-induced effect on APP-CTF generation. ....	97
Fig. 4.32: Tspan3 expression is increased in the prefrontal cortex of AD patients. ....	98
Fig. 4.33: TALEN-mediated knockout strategy for the generation of Tspan15-deficient mice. ....	100
Fig. 4.34: TALEN-mediated knockout of Tspan15 was confirmed in all tested tissues. ....	101
Fig. 4.35: Expression pattern of Tspan15 in adult mouse tissues. ....	102
Fig. 4.36: Knockout of Tspan15 decreases mADAM10 and reduces N-cadherin and PrP <sup>c</sup> shedding. .	104
Fig. 4.37: Loss of Tspan15 in 21-week-old mice reduces ADAM10 maturation, N-cadherin and PrP <sup>c</sup> shedding. ....	106
Fig. 4.38: Tspan15 knockout increases the number of spines with perforated postsynaptic densities (PSDs). ....	107
Fig. 5.1: Tspan3 expression promotes ADAM10-mediated processing of APP. ....	115
Fig. 5.2: Tspan3 acts as a scaffold for non-amyloidogenic APP processing. ....	118
Fig. 5.3: Generation of ADAM10 C-terminal fragments. ....	123
Fig. 5.4: Sequence alignment of the murine amino acid sequences of Tspan3, Tspan5 and Tspan7. ....	126
Fig. 5.5: Remodelling of dendritic spine morphology after LTP induction. ....	135

## List of tables

Tab. 1.1: List of selected ADAM10 substrates and their function in the CNS. ....	8
Tab. 1.2: Diverse effects of TspanC8 tetraspanins on ADAM10-mediated substrate cleavage. ....	23
Tab. 3.1: List of primary antibodies. ....	27
Tab. 3.2: List of secondary antibodies. ....	28
Tab. 3.3: Oligonucleotides used for genotyping, mutagenesis PCR and sequencing. ....	29
Tab. 3.4: Oligonucleotides and hydrolysis probes (UPL, Roche) used for qRT-PCR. ....	30
Tab. 3.5: List of used siRNAs. ....	31
Tab. 3.6: List of plasmids and expression constructs. ....	31

---

Tab. 3.7: List of used cell lines and bacteria strains .....	32
Tab. 3.8: List of transgenic mouse lines .....	32
Tab. 3.9: List of frequently used buffers and solutions.....	32
Tab. 3.10: Pipetting scheme for mutagenesis PCR.....	35
Tab. 3.11: Program for mutagenesis PCR.....	35
Tab. 3.12: Composition of SDS gels.....	46
Tab. 3.13: List of TALEN target sequences .....	51
Tab. 3.14: Pipetting scheme for genotyping PCR.....	53
Tab. 3.15: Genotyping PCR program .....	53
Tab. 3.16: Clinical characteristics of AD patients .....	54
Tab. 3.17: Characteristics of control subjects .....	54
Tab. 4.1: Number of animals and genotype distribution of Tspan3X46 breeding .....	91
Tab. 4.2:Genotype distribution of Tspan15 $\Delta$ 104 breeding.....	101



## 8 Declaration

Herewith I declare that, apart from the supervisor's guidance, I have prepared the present thesis on my own and according to the Rules of Good Scientific Practice of the German Research Foundation. Concepts and ideas that were taken from other sources are indicated as such.

This thesis has not been submitted partially or wholly as part of a doctoral degree to another examining body.

Parts of this Work have been published in the following articles:

**Seipold, L.**, Damme, M., Prox, J., Rabe, B., Kasperek, P., Sedlacek, R., Altmeyden, H., Willem, M., Boland, B., Glatzel, M, Saftig, P. (2017) *Tetraspanin 3: A central endocytic membrane component regulating the expression of ADAM10, presenilin and the amyloid precursor protein*. Biochimica et Biophysica Acta (BBA) - Molecular Cell Research 1864, 217-230.

**Seipold, L.** and Saftig, P. (2016) *The Emerging Role of Tetraspanins in the Proteolytic Processing of the Amyloid Precursor Protein*. Frontiers in Molecular Neuroscience 9,149.

Kiel, February 2017

Lisa Seipold



## 9 Curriculum Vitae

Lisa Seipold  
Steinstraße 10  
24118 Kiel

Born: 4<sup>th</sup> of November 1986  
Nationality: German

### Education

- |                  |   |
|------------------|---|
| Since April 2013 | <b>PhD studies</b> as a member of the SFB877 `Proteolysis as Regulatory Event in Pathophysiology` in the working group of Prof. Paul Saftig, Biochemical Institute, University of Kiel<br><br>Title: <i>The role of tetraspanins in the regulation of the A Disintegrin and the Metalloprotease 10 (ADAM10)</i> |
| 04/2012-11/2012  | <b>Master thesis</b> in the working group of Prof. Paul Saftig, Biochemical Institute, University of Kiel<br><br>Title: <i>Regulation und Modulation der regulierten Membranproteolyse durch Tetraspanin-3</i>  |
| 10/2010-04/2012  | <b>Master studies</b> in Biochemistry, University of Kiel   |
| 04/2010-06/2010  | <b>Bachelor thesis</b> in the working group of Prof. Jürgen Scheller, Biochemical Institute, University of Kiel<br><br>Title: <i>Untersuchungen zum Shedding des Transmembranproteins CD27</i>  |
| 04/2008-04/2010  | <b>Bachelor studies</b> in Biochemistry, University of Kiel   |
| 10/2006-04/2008  | <b>Diploma studies</b> in Chemistry, University of Kiel   |
| 08/1999-06/2006  | <b>Abitur</b><br><i>Gymnasium am Kattenberge Buchholz in der Nordheide</i>  |





## 10 Publications and scientific participations

### Publications:

**Seipold, L.**, Damme, M., Prox, J., Rabe, B., Kasperek, P., Sedlacek, R., Altmeyen, H., Willem, M., Boland, B., Glatzel, M, Saftig, P. (2017) *Tetraspanin 3: A central endocytic membrane component regulating the expression of ADAM10, presenilin and the amyloid precursor protein*. Biochimica et Biophysica Acta (BBA) - Molecular Cell Research 1864, 217-230.

**Seipold, L**, Saftig P. (2016) *The emerging role of tetraspanins in the Proteolytic Processing of the Amyloid Precursor Protein*. Frontiers in Molecular Neuroscience 9, 149.

### Scientific participations:

- |         |   |
|---------|---|
| 09/2016 | 2 <sup>nd</sup> International Symposium: Protease World in Health and Disease, Kiel, Germany (poster presentation)  |
| 09/2015 | IRTG Summer School on <i>Proteases and Pathophysiology</i> , Kiel, Germany (poster presentation)  |
| 10/2014 | Workshop: Current Trends in Biomedicine: <i>Proteases at work: Cues for Understanding Neural Development and Degeneration</i> Baeza, Spain (oral and poster presentation) |
| 06/2014 | 6 <sup>th</sup> European Conference on Tetraspanins, Lille, France (oral and poster presentation)   |



## 11 Acknowledgement

An dieser Stelle möchte ich mich bei all denjenigen bedanken, die mich in den letzten 4 Jahren unterstützt und bei der Entstehung dieser Arbeit begleitet haben.

Allen voran danke ich Herrn Prof. Paul Saftig, für die Möglichkeit diese Promotion in seiner Arbeitsgruppe durchführen zu können. Vielen Dank für die wissenschaftliche Betreuung, die konstruktiven Diskussionen und Ratschläge im Auf und Ab der Tetraspanin-Welt.

Herrn Prof. Beitz danke ich für die Bereitschaft das Zweitgutachten für diese Arbeit zu verfassen.

Des Weiteren möchte ich mich bei Johannes Prox bedanken, der mir das Forschungsgebiet der Tetraspanine nahegebracht hat. Darüber hinaus danke ich Markus Damme für die erheiternden und konstruktiven Gespräche.

Bei Herrn Prof. Markus Glatzel und Hermann Altmeppen möchte ich mich sehr für die angenehme Zusammenarbeit und für die Bereitstellung der humanen Patientenproben bedanken. Außerdem danke ich Michaela Schweizer für die elektronenmikroskopischen Aufnahmen und Barry Boland für den Einblick in die Vielfalt der APP-C-terminalen Fragmente.

Bei dem gesamten Team des Victor-Hensen-Hauses und im Besonderen bei Yvonne Rose, möchte ich mich für die kompetente Pflege und Betreuung der Tiere bedanken.

Mein Dank gilt auch allen Mitarbeitern der Arbeitsgruppe Saftig, für die schöne Arbeitsatmosphäre, die große Hilfsbereitschaft und die tolle Zusammenarbeit. Vor allem, meinem lieben „ADAM10 Anti-Buddy“ Sebastian danke ich für die Hilfe, den Zuspruch und unsere großartigen Nach-16-Uhr-Gespräche. Auch Sandra und Sönke möchte ich für die lustige und schöne Zeit bei uns im Technobunker 105 danken. Was wäre der Laboralltag bloß ohne unsere musikalischen Ausflüge, die Glühwein-Eskalation, das Bananentelefon und die Cocktailbar gewesen?! Vielen Dank für eine unvergessliche Zeit!

Ganz besonders danke ich auch meinen Freunden, für die vielen tollen Erlebnisse, Ablenkungen und den Rückhalt während dieser Zeit. Kiel-Hamburg-Berlin-Kiel.

Abschließend möchte ich mich von ganzem Herzen bei meinem Freund Basti und meinen Eltern bedanken. Besonders du lieber Basti, hast mir in der letzten Zeit immer den Rücken freigehalten und mich unglaublich unterstützt. Danke, dass ihr immer für mich da seid, für euer Vertrauen und eure Liebe.